THE USE AND SPECTROSCOPIC PROPERTIES OF ZINQUIN, A ZINC(II) SPECIFIC FLUOROPHORE

KYM M. HENDRICKSON, B.Sc.(Hons)

DEPARTMENT OF CHEMISTRY.

THE UNIVERSITY OF ADELAIDE,

SOUTH AUSTRALIA,

AUSTRALIA.

A Thesis Submitted for the Degree of

Doctor of Philosophy

in

The University of Adelaide

(Faculty of Science)

JANUARY, 1999

Emendations and Comments.

Chapter 2. In answer to a query from a referee concerning the origin of thesis material in Chapter 2, it is here formally asserted that all of the spectral and equilibrium measurements were made by the author. Where referenced, other data from the literature is incorporated in the discussion. The synthesis of Zinquin-A was carried out by Dr. M. Kimber.

p. 23. Because the magnitude of measured fluorescence is instrument dependent, fluorescence is usually referred to as relative fluorescence as is the pratice adopted in this thesis.

p. 141, 146 and Appendix B. Gaussian curves are bilaterally symmetric in energy and therefore in spectral frequencey. The Gaussian analyses were carried out on this basis through program BANDAL which outputs the analyses in terms of wavelength as shown in the spectral analyses plots in this thesis.

p. 153. In Figures 4.23 and 4.24, the right-hand structure has been rotated 90^{o} about a vertical axis in the plane of the page and passing through the Zn centre by comparison with the left-hand structure.

p. 163. Amberlite HRC-120 strong cation exchange resin in the H^{+} form was used.

Elsewhere in the thesis, typographical corrections have been made by hand.

CONTENTS

ABSTRACT

Zinc(II) has an important role in biochemical and nutritional processes. More than 300 enzymes contain Zn^{2+} as an essential component either for structural purposes or for catalytic activity. Much of this intracellular Zn^{2+} is strongly complexed, but there are readily exchangeable pools of less strongly bound Zn^{2+} which are important in a range of processes associated with cell growth. Intracellular Zn^{2+} which is amenable to ligand substitution provides a route for detection through binding ligands which fluoresce upon coordination. The proposed mechanism of action of such a prototype fluorescent ligand capable of detecting intracellular Zn^{2+} down to nanomolar concentration, ethyl-[2-methyl-8-*p*-toluene-sulphonamido-6-quinolyloxy]acetate (Zinquin-E) and its hydrolysis product, 2-methyl-8-*p*-toluenesulphonamido-6-quinolyloxyacetic acid (Zinquin-A), is shown below :

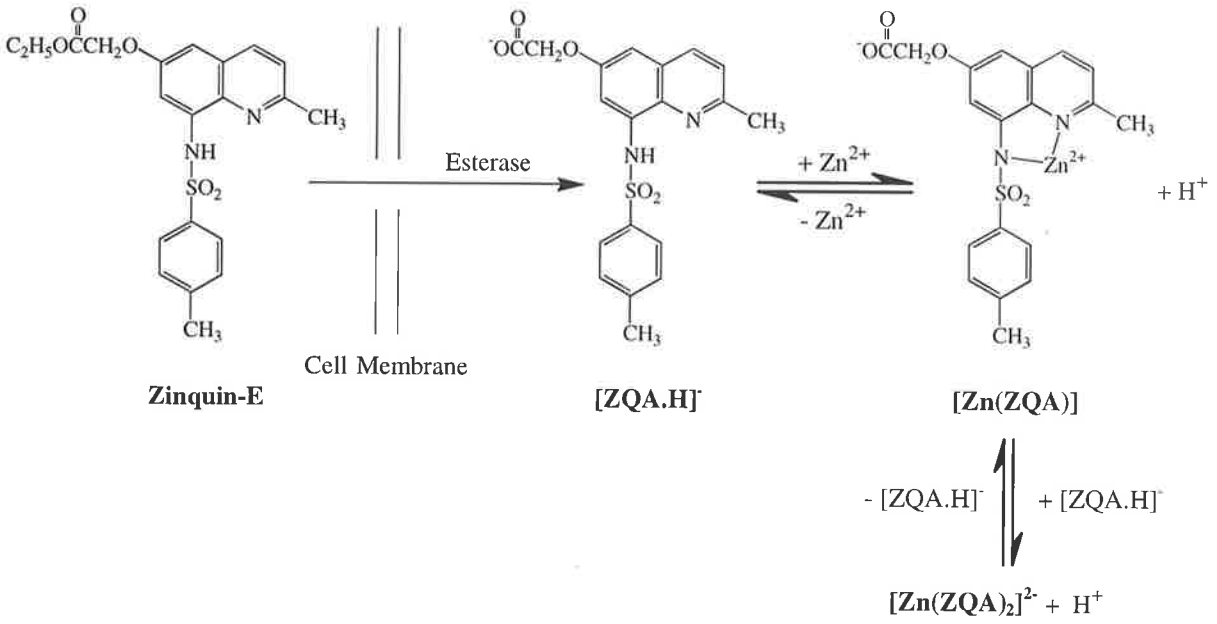

The nature of the Zn^{2+} that Zinquin-A binds to in the cell is uncertain, but it is probable that some of this available Zn^{2+} is partially bound by proteins. This has been modelled using various nitrogen and oxygen donor chelates to form ternary complexes of the type [Zn(L)ZQA], where L = 1,4,7,10-tetraazacyclododecane (cyclen), 1,4,8,11-tetraaza-cyclotetradecane (cyclam), 1,4,7-triazacyclononane (tacn), 1,5,9-triazacyclododecane (tacdo), 2,2′,2″-triaminotriethylamine (tren), nitrilotriacetic acid (NTA^{3-}), Triethanolamine (TEA).

The complexation and spectroscopic properties of these ternary complexes, free Zinquin-A and the Zn^{2+} complexes of Zinquin-A are discussed. Force field molecular modelling was utilised to study these ternary complexes further in the hope of finding a connection between the amount of fluorescence observed and their structure.

The fluorescence of Zinquin-A complexed to Zn^{2+} and as a free ligand are also compared to that of several other sulphonamide ligands in their complexed and free states to obtain an insight into the effect of ligand structure on the fluorescence observed. Finally, examples of the use of Zinquin-E as an intracellular Zn^{2+} probe are given with a discussion of the problems involved with its use and the implications the ternary complexes studied indicate.

DECLARATION

This work contains no material which has been accepted for the award of any other degree or diploma in any university or other tertiary institution and, to the best of my knowledge and belief, contains no material previously published or written by another person, except where due reference has been made in the text.

I give consent to this copy of my thesis, when deposited within the University of Adelaide Barr Smith Library, being available for loan and photocopying.

SIGNED : .... DATE : 19.1.99

Kym Hendrickson

ABBREVIATIONS

a	percent of adventitious Zn^{2+} in the Zinquin-A solid
A	absorbance
AA	atomic absorption
Adv. Zn^{2+}	adventitious Zn^{2+}
Adventitious Zn^{2+}	Zn^{2+} arising from background impurity
AIDS	acquired immune deficiency syndrome
b	concentration of adventitious Zn^{2+} in the buffer (mol dm^{-3})
β	cumulative stability constant
BCQ.H	8-(benzenecarbonamido)quinoline
BHK	baby hamster kidney cells
BSQ.H	8-(benzesulphonamido)quinoline
χ^2	chi squared
CLL	chronic-lymphocytic-leukaemia cells
C-Terminal	carboxylic acid end of a protein
Cyclam	1,4,8,11 - tetraazacyclotetradecane
Cyclen	1,4,7,10 - tetraazacyclododecane
Cysteine S	cysteine thiolate sulphur
DMSO	dimethyl sulphoxide
DNA	deoxyribonucleic acid
E	electrode potential (volts)
E_0	standard electrode potential (volts)
EDTA	ethylenediaminetetraacetic acid
EGTA	ethylenebis(oxyethylenenitrilo)tetraacetic acid
e.m.f.	electromotive force
ESFF	extended systematic force field
ε_X	molar absorbance of species X (dm^3 mol^{-1} cm^{-1})
Ex λ	excitation wavelength
EZn	enzyme and its active site Zn^{2+}
F	Faraday's constant (Coulombs mol^{-1})
Glu	glutamic acid residue
H_3BO_3	boric acid
HBSS	Hank's Balanced Salt Solution

$HClO_4$	perchloric acid
HCO_3^-	carbonic acid
HEPES	*N*-[2-Hydroxyethyl]piperazine-*N*′-[2-ethanesulphonic acid]
His	histidyl residue
HIV	human immunodeficiency virus
HPLC	high performance liquid chromatography
I	ionic strength
K	stability constant
K^*	stability constant of the excited state
K_a	acid dissociation constant
KHphthalate	potassium hydrogen phthalate
K_w	equilibrium constant for the self ionisation of water
l	cell path length (cm)
L	unspecified ligand
LHS	left hand side
LMCT	ligand to metal charge transfer
log	logarithm (base 10)
M^+	monovalent metal ion
M^{2+}	divalent metal ion
M^{3+}	trivalent metal ion
$MClO_4$	metal perchlorate
MM-TSQ.H	6-methoxy-2-methyl-8-(*p*-toluenesulphonamido)-quinoline
MOH	metal hydroxide
MSO_4	metal sulphate
MSQ-H	8-(methanesulphonamido)quinoline
M-TSQ	6-methoxy-8-(*p*-toluenesulphonamido)quinoline
n	*n*-bonding orbital
$NaHCO_3$	sodium hydrogen carbonate
NaOH	sodium hydroxide
NaPIPES	sodium piperazine-*N*,*N*′-bis(2-ethane-sulphonate)
nm	nanometres
$NO^{\cdot}$	nitric oxide radical
$NTA.H_3$	nitrilotriacetic acid
N-Terminal	amine end of a protein
π	pi-bonding orbital
π^*	pi-antibonding orbital

P_2O_5	phosphorous pentoxide
PBS	Dulbecco's phosphate buffered saline
pH	$-\log[H^+]$
pK_a	$-\log(K_a)$
pK_w	$-\log(K_w)$
Pyrithione	sodium 1-hydroxy pyridine-2-thione
p-TSQ.H	8-(*p*-toluenesulphonamido)quinoline
QSB.H	8-quinolinesulphonamido)benzene
R	gas constant (J K^{-1} mol^{-1})
RHS	right hand side
RNA	ribonucleic acid
T	temperature (Kelvin)
Tacdo	1,5,9 - triazacyclododecane
Tacn	1,4,7 - triazacyclononane
TEA	triethanolamine
Tren	tris(2-aminoethyl)amine
UV	ultraviolet
UV-Vis	ultraviolet-visible
[X]	concentration of species X (mol dm^{-3})
Zinc(II)	Zn^{2+}
Zinquin-A	2-methyl-8-*p*-toluenesulphonamido-6-quinolyloxy acetic acid
Zinquin-E	ethyl-[2-methyl-8-*p*-toluenesulphonamido-6-quinolyloxy] acetate
ZQA.H_2	Zinquin-A

ACKNOWLEDGMENTS

I would sincerely like to thank my supervisor, Professor S. F. Lincoln, whose encouragement, guidance, and most importantly patience helped me through the years of my PhD. His keen interest in my work and future was much appreciated.

In addition, I wish to thank Peter Zalewski who guided me through the cellular studies I carried out at The Queen Elizabeth Hospital, Geraldine Murphy and Carolyn Haskard who started me on the fluorescence techniques and Tom Kurucsev for all his help with the spectroscopic and programming aspects of this study.

Thanks also to all those who provided me with compounds over the years, especially Marc Kimber who provided me with all the Zinquin-A and Zinquin-E that I needed.

I would also like to thank my colleagues for their friendship, assistance and support, especially, Paul Low, Lee West, Mel Sandow, and the rest of the SFL group.

Special thanks to Mum and Dad for their invaluable support and encouragement, and for trying to keep me motivated and away from a career in child care.

Finally, I wish to thank Jeremy for his unwavering support, for proof reading my thesis again and again, for trying to de-stress me and for calmly doing the housework, cooking and shopping while I panicked.

I couldn't do it alone,

Thankyou,

CHAPTER 1

INTRODUCTION

1.1 : The Role of Zinc(II) in the Body

1.1.1 : The Biochemical Role of Zinc(II)

Zinc is one of several trace elements known to be essential for human health and is the second most abundant transition metal ion in humans and other mammals after $Fe^{2+/3+}$.[1-6] It exists in the body as Zn^{2+} and is found at some concentration in all organs, tissues, fluids and secretions. Bone and hair have very high Zn^{2+} concentrations, as do reproductive cells, however, just over half of the Zn^{2+} in the body is found in skeletal muscle due to its large bulk. The majority of Zn^{2+} is intracellular, with the concentration in extracellular fluids, such as blood plasma, being relatively low.[7] Within cells, the Zn^{2+} is not distributed evenly, producing regions of high and low Zn^{2+} concentration. The location and distribution of Zn^{2+} varies between cell types and its concentration ranges from less than or equal to 10^{-9} mol dm^{-3} in the cytoplasm to greater than 10^{-3} mol dm^{-3} in some vesicles[7] (see Chapter 3 for definitions of some cellular structures). Much of this Zn^{2+} is tightly coordinated to proteins and enzymes with varying Zn^{2+} affinities, however, there is also evidence of readily exchangeable 'pools' of 'free' or labile intracellular Zn^{2+}.[7] The location and concentration of Zn^{2+} in cells changes during their life cycle as well as in response to various stimuli. For example, Zn^{2+} is released from tightly coordinated sites as a cell undergoes apoptosis (gene directed cell death)[8,9] or when it is treated with nitric oxide.[10]

Zinc(II) is involved in many biological and biochemical processes within the body, more than any other trace element in the periodic table.[7] Zinc(II) is important in many processes associated with cell activation and growth which include neurotransmission,[11,12] apoptosis,[13,14] signal transduction[15] and gene expression,[16,17] although the mechanism of its involvement, in many cases, is still unknown. Certain hormones, including testosterone, thymulin and prolactin, have also been found to be Zn^{2+} dependent, with Zn^{2+} prolonging the biological activity of these hormones.[5] Zinc(II) has also been identified as necessary for wound healing and tissue repair[18,19] and is used by membranes to maintain structure and function.[20]

One of the reasons Zn^{2+} is so prevalent in living cells and tissues is that almost 300 enzymes are known to be regulated by it.[21] Zinc(II) is found in stoichiometric amounts in many metalloenzymes, including carbonic anhydrase,[22-24] alcohol dehydrogenase,[25,26] carboxypeptidase A[27-29] DNA and RNA polymerases,[30,31] aminopeptidase,[32,33] alkaline phosphatases,[34,35] β-lactamase[36] and thermolysin[37-39], with the activity of each being dependent upon the presence of Zn^{2+}. Some enzymes and proteins, such as zinc fingers, insulin[40] and metallothionein,[41-45] appear to use Zn^{2+} to maintain a particular conformation or molecular structure. Zinc(II) is the only trace element known to be utilised by metalloenzymes from all of the six differing types of enzyme categories established by the International Union of Biochemistry (oxidoreductase, transferase, hydrolase, lyase, isomerase and ligase) with enzymes in the hydrolase group being the most abundant.[4] Some of these Zn^{2+} containing, biologically important molecules are discussed in greater detail below.

It is thought that the wide use of Zn^{2+} in biologically significant molecules evolved from its unique chemical properties. Zinc(II) is a strong Lewis acid and therefore causes substantial polarisation of bonds in ligands that are coordinated to it.[46] The most notable example of this is the increased polarisation of the O-H bonds in H_2O coordinated to Zn^{2+}. This leads to the ready deprotonation of $[Zn(H_2O)_6]^{2+}$ to form $[Zn(H_2O)_5OH]^+$ with a $pK_a = 9$, with even lower pK_as observed for some water molecules coordinated to Zn^{2+} in enzymes.[47] Hence the mechanisms of Zn^{2+} enzymes often involve the attack of nucleophiles, such as OH^-, RO^- and H^-, at electrophilic centres such as the partially positive carbons of carbonyl functions. Another important property to consider is the easy conversion between the large range of coordination numbers (usually 4, 5 or 6) and different coordination geometries (tetrahedral, trigonal bipyramidal, octahedral and many other deformed geometries) that Zn^{2+} exhibits[41] (This characteristic of Zn^{2+} arises from its d^{10} electronic configuration and the consequent absence of stereochemical constraints arising from ligand field effects). Hence Zn^{2+} is flexible with respect to the number of ligands coordinated to it, allowing substrates to both coordinate and leave with ease. A wide range of substrates and protein coordination sites are utilised by Zn^{2+} enzymes due to the ability of Zn^{2+} to readily form complexes in the cell with ligands containing nitrogen, oxygen and sulphur donor atoms. Finally, unlike $Fe^{2+/3+}$ and $Cu^{+/2+}$, Zn^{2+} is inert to redox reactions.[41] This feature has two major benefits. Firstly, the use of Zn^{2+} in DNA protein binding to form zinc fingers and other Zn^{2+} bound tertiary protein structures provides cross-links and structures that are stable under reducing conditions, unlike the disulphide cross-links formed by cysteine units.[48] Secondly, Zn^{2+} enzymes can be utilised for processes where oxidation reactions must be avoided, including those involving the easily oxidised amino acids; tryptophan, tyrosine and cysteine.[6]

Many studies have been carried out on Zn^{2+} containing enzymes, including the determination of their crystal structures by X-ray diffraction. Most of the Zn^{2+} in the catalytic sites of enzymes has been found to be coordinated by three protein ligands, often histidine, glutamic acid, aspartic acid or cysteine. The fourth coordination site is usually occupied by a water or hydroxyl ligand, often forming a tetrahedral or deformed tetrahedral geometry.[2,4] For many Zn^{2+} enzymes, the spacing of the protein ligands is strikingly systematic. The first two ligands are often separated by a 'short spacer' consisting of 1 to 3 amino acids. These ligands are separated from the third by a 'long spacer' of between approximately 20 and 120 amino acids. This structure allows both strength and flexibility, with the short spacer forming a strong, bidentate complex with the Zn^{2+}, and the large spacer contributing flexibility to the coordination sphere. The water molecule is activated either by ionisation, polarisation or placement near to substrates.[2,4] As previously mentioned, Zn^{2+} can also play a structural role in proteins and enzymes. In this case, there is often no water ligand and the Zn^{2+} is usually strongly coordinated by 4 or more protein ligands.[4,7] Three Zn^{2+} containing, biologically important molecules are discussed below as examples of the structures and different roles of these enzymes and proteins.

Carbonic Anhydrase II

Carbonic anhydrase is found in both animals and plants and catalyses the reversible hydration of carbon dioxide as shown in Equation 1.1. In animals, one of its physiological roles is the fast hydration of CO_2 in various tissues and dehydration of HCO_3^- in the lungs. As with many other enzymes, there are several different structural forms, or isozymes, of carbonic anhydrase. Although the tertiary structure differs between them, it is thought that the active site structure and catalytic role remains the same. However the catalytic activity does vary with isozyme type.[23] Human carbonic anhydrase II is a particularly efficient catalyst and with a rate constant of 1.4×10^6 s^{-1} for CO_2 hydration, it is one of the fastest enzymes known.[23] The mechanism for the hydration appears to involve the addition of OH^- from the active site Zn^{2+} to CO_2. It has been suggested that the rate determining step is in fact the deprotonation of the Zn^{2+} coordinated water, rather than the formation of the O-C bond in HCO_3^-.[23] A representation of the mechanism for the catalytic cycle is shown in Equations 1.2 and 1.3, where the enzyme and its active site Zn^{2+} are represented by 'EZn'.

$$CO_2 + H_2O \rightleftharpoons HCO_3^- + H^+ \qquad (1.1)$$

$$EZn(OH^-) + CO_2 \rightleftharpoons EZn(OH^-)CO_2 \rightleftharpoons EZn(HCO_3^-) \rightleftharpoons EZn(H_2O) + HCO_3^- \quad (1.2)$$

$$EZn(H_2O) \rightleftharpoons EZn(OH^-) + H^+ \quad (1.3)$$

The crystal structure of human carbonic anhydrase II has been known since 1972.[22] The enzyme, which has a molecular mass of around 30 000 and approximately 258 amino acid residues, is roughly ellipsoidal with an active site situated in a deep crevice leading into the centre of the molecule. The Zn^{2+} is located almost at the bottom of this crevice and is coordinated by three histidyl residues from the β-sheet region of the structure. The Zn^{2+} also has a fourth ligand which is either H_2O or OH^-, as suggested in Equations 1.2 and 1.3, resulting in a distorted tetrahedral coordination geometry about the Zn^{2+}. The active site region is lined with several polar groups, such as other histidyl residues, and also contains several water molecules which are hydrogen bonded both to these, and to each other. All or some of these water molecules may be expelled upon substrate binding.[22] One of the histidyl residues in the active site region, which is linked to Zn^{2+} via hydrogen bonding water, appears to act as a proton shuttle, assisting the deprotonation of the Zn^{2+} coordinated water molecule (Equation 1.3).[23] A schematic diagram of the active site Zn^{2+} and the ligands attached to it is shown in Figure 1.1 below.

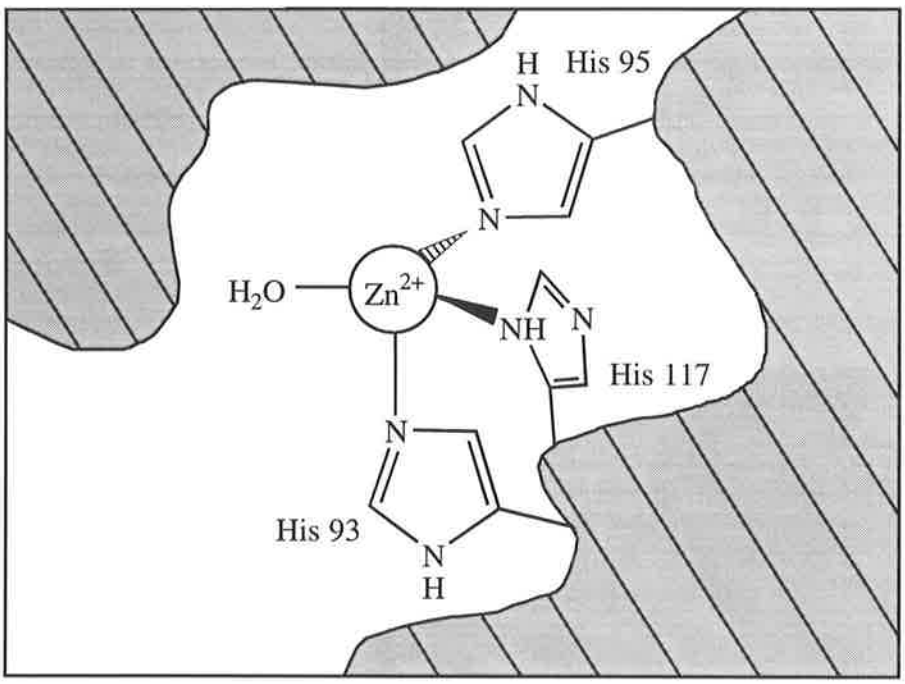

Figure 1.1 : A schematic representation of the active site of human carbonic anhydrase II. The shaded area represents the rest of the enzyme.

Carboxypeptidase A

Carboxypeptidase A consists of a single polypeptide chain of 307 amino acids, with a molecular weight of 34 472 and an active site Zn^{2+} which is necessary for catalytic activity.[27] It is synthesised in the mammalian pancreas as procarboxypeptidase A, which is an inactive precursor. This precursor is then converted to the active enzyme in the intestinal tract by trypsin mediated peptide cleavage. Carboxypeptidase A specifically catalyses the hydrolysis of esters and peptides which contain a branched aliphatic side chain or aromatic group in an L-configuration and have a free carboxylic acid group in the terminal residue.[49] The catalytic mechanism has been extensively studied and has been identified as a multi-point, cooperative process involving three separate regions of the enzyme. Different regions are used for binding the hydrophobic side chain of the substrate, bond cleavage and substrate recognition.[50] As for carbonic anhydrase, the mechanism involves the ionisation of a water molecule coordinated to the Zn^{2+}. The resulting hydroxyl is thought to attack the C-terminal peptide carbonyl group of the substrate, either directly or via an acyl enzyme intermediate, formed from the reaction of a glutamic acid residue (Glu 270) with the substrate.[50]

The active site Zn^{2+} is bound by 3 amino acid residues; two histidyl residues and one glutamic acid residue, as shown schematically in Figure 1.2 below. There is also a water or hydroxyl ligand coordinated to the Zn^{2+}, forming what has been described as a distorted tetrahedral geometry. The substrate also coordinates to this Zn^{2+} by its C-terminal peptide carbonyl group, without displacing the water or hydroxyl ligand.[27,50]

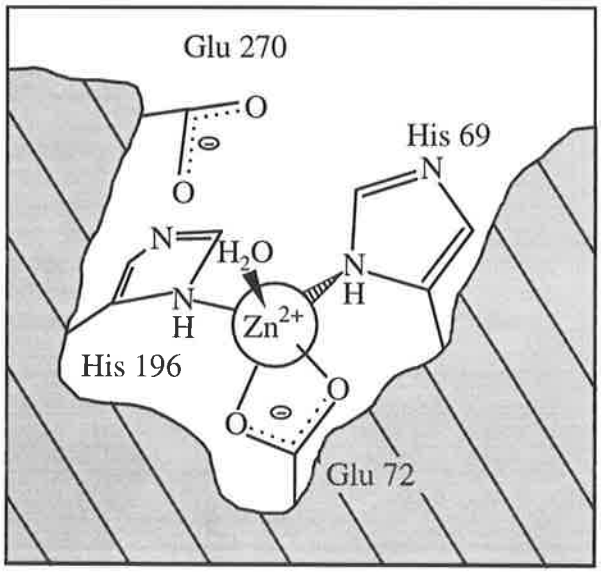

Figure 1.2 : A schematic representation of the active site of carboxypeptidase A. The shaded area represents the rest of the enzyme.

Metallothionein

Unlike the two Zn^{2+} containing molecules discussed so far, metallothionein is not an enzyme. In fact, its fundamental role in the body has remained elusive, although it is clear that it has an important role in the physiology of essential trace elements and in the detoxification of heavy metals. Metallothionein is composed of 61 amino acid residues and has a low molecular weight of approximately 7 000. It can coordinate to many metals other than Zn^{2+}, including Cu^{2+} and Cd^{2+} which are both coordinated more strongly than Zn^{2+}. Up to seven Zn^{2+} can bind to metallothionein at once, in two separate domains. The Zn^{2+} can be removed by proteins and enzymes with a stronger affinity for Zn^{2+} such as carbonic anhydrase, hence it has been postulated that one role of metallothionein may be to regulate the activity of some metalloenzymes. Another possible role may be to transport Zn^{2+} to other parts of the body where it is needed. The highest concentrations of metallothionein in the body are found in the liver, kidney, intestine and pancreas.[45]

Each Zn^{2+} in metallothionein is coordinated by four cysteine thiolate sulphurs in a tetrahedral arrangement. Both terminal and bridging thiolates are observed in both domains. The roughly spherical N-terminal and C-terminal domains contain four and three metal ions, respectively. The environment about the Zn^{2+} is shown schematically in Figure 1.3 for each domain.[51]

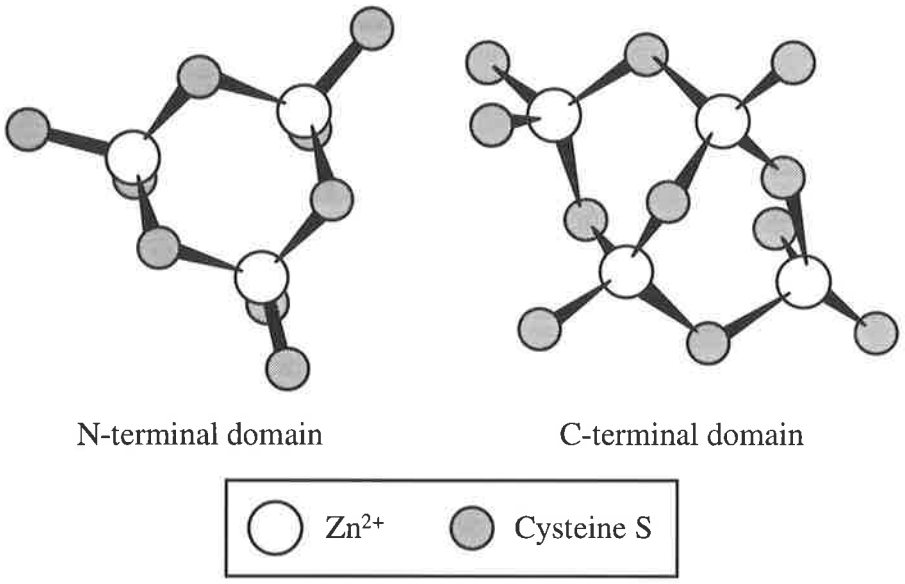

Figure 1.3 : The approximate structure of the two metal clusters found in metallothionein. Metals other than Zn^{2+} are often found in these clusters. The surrounding protein has been omitted for clarity.[51]

1.1.2 : Clinical Aspects of Zinc(II)

With Zn^{2+} so widely required by the body, it is of no surprise to learn that a depletion or deficiency of this essential trace element can contribute to many clinical manifestations. Although iron and iodine have been known to be essential to man for a long period of time, it has only been within the past 30 years that the important role of Zn^{2+} has been identified and surprisingly, Zn^{2+} deficiency was more readily diagnosed in animals than in humans as late as the 1960's and early 1970's, possibly due to its non-specific and protean symptoms. Zinc(II) deficiency can occur either from a lack of Zn^{2+} in the diet, as a symptom of a disease or as a side effect of some medical treatments. A wide range of symptoms may be associated with Zn^{2+} deficiency, including growth retardation,[52] poor appetite (anorexia),[12] altered mental state,[7] taste/smell dysfunction, dermatitis and skin lesions, alopecia (hair loss), defective dark adaptation, immunodeficiency,[53,54] impaired wound healing and gastrointestinal distress and / or diarrhoea[55]. Insufficient Zn^{2+} may also cause retarded primary and secondary sexual development in juvenile males[56] as well as infertility in adult males and the delayed onset of menstruation or amenorrhoea in females.[5] Three of the more frequent manifestations of Zn^{2+} deficiency are alopecia, retarded sexual development and parakeratosis (dry, rough skin lesions) which often occur together. Remarkable recoveries from these conditions can be obtained simply by supplementing the diet with Zn^{2+} in the form of sulphate, gluconate or acetate salts.[7,56,57]

Sufficient intake of dietary Zn^{2+} is especially important during pregnancy and lactation.[7] As a developing embryo receives all of its Zn^{2+} from the mother via the placenta, it is important that the mother receives enough dietary Zn^{2+} both for herself and for the embryo to allow correct development to occur. A Zn^{2+} deficiency can result in still births, low birth weight infants, anomalies of the central nervous system[58] or deformities in the unborn child such as a cleft palate or malformed limbs. Zinc(II) is supplied to infants in breast milk and therefore Zn^{2+} deficiency in the mother is readily passed on to the child during lactation, leading to the child developing some or all of the characteristic symptoms mentioned above.[5]

The occurrence of severe Zn^{2+} deficiency from insufficient dietary Zn^{2+} is not common in the developed world, as foods that contain dietary Zn^{2+} are plentiful and are included in most diets. One exception is a strict vegetarian diet as there are much higher Zn^{2+} concentrations in meat and seafood than in most vegetables. In developing countries, however, Zn^{2+} deficiency has been identified as a greater problem due to wide spread malnutrition and predominantly vegetarian diets consisting mainly of cereal proteins. Nevertheless, with processed foods, fats, oils, sugar and alcoholic beverages having low Zn^{2+} content, as the diets of developed countries move towards convenient or 'fast' foods, the occurrence of Zn^{2+} deficiency in mild forms may become more prevalent. The amount of Zn^{2+} found in foodstuffs is extremely variable and depends on the type of animal, variety of plant, location of production and the part of the animal or plant eaten. Dietary Zn^{2+} is found in highest concentration in oysters, followed by lean red meats and cheese. Dark chicken meat, wholemeal wheat, lentils and other legumes also provide moderate concentrations of Zn^{2+}. Lower concentrations are found in green leafy vegetables, fruits, potatoes, yam, fish, white chicken meat and fatty foods. Although cows milk has only a moderate Zn^{2+} concentration, it is an important source of dietary Zn^{2+} for children.[7]

Apart from dietary Zn^{2+} deficiency, there are many other clinical conditions and diseases associated with a low Zn^{2+} concentration in the body. Some examples include sickle cell anemia,[59] chronic inflammatory bowel disease, hepatic disease, diabetes,[60] porphyria, dermatitis, acute lymphoblastic leukaemia[7] and other cancers,[61] severe burns,[7] and acute myocardial infarction.[62] It is therefore of little surprise that many therapeutic uses for Zn^{2+} have been developed, including treatments for the diseases and conditions listed above. Other therapeutic uses, many still in the developmental stage, include the use of Zn^{2+}-containing ointments for dermatological conditions and Zn^{2+} supplements to speed wound healing as well as treatments for disorders such as acne, genital herpes,[63] leprosy, schizophrenia, gastric ulcers, rheumatoid arthritis, cutaneous ulcers, impaired taste and smell acuity, impotence and infertility.[7] Even studies on the common cold have shown that zinc gluconate[64,65] or zinc acetate[66] lozenges can reduce the severity and duration of a cold if used from the outset.[67,68] Zinc(II) has also been shown to inhibit dental plaque growth[69] and help alleviate hay fever symptoms[70]. The use of Zn^{2+} against AIDS and HIV[71,72] and some cancers[73] has also been studied, as has the role of Zn^{2+} in Alzheimer's disease.[74,75]

High Zn^{2+} concentrations in erythrocytes characterise some diseases and conditions, such as multiple sclerosis, bone metastases, Duchenne muscular dystrophy, uremia[5] and even some of the above-mentioned conditions when the Zn^{2+} concentration is measured from a different location in the body (for example, erythrocyte Zn^{2+} as compared with plasma Zn^{2+} levels). This may be due to a redistribution of the Zn^{2+} in the body caused by the disease or condition. Interestingly, in one case study, a patient exhibited higher than normal serum, dermal and epidermal Zn^{2+} concentrations, yet had the clinical symptoms typical of Zn^{2+} deficiency. After treatment with Zn^{2+}, the symptoms totally disappeared, only to resurface upon discontinuation of the treatment.[76] Hence Zn^{2+} concentrations in tissue and fluid samples are not yet a definitive diagnostic tool in detecting Zn^{2+} deficiency.

Despite the elevation of Zn^{2+} concentrations associated with some diseases and conditions, Zn^{2+} is not thought to be teratogenic, mutagenic or carcinogenic.[5] However, in high doses, it has been found to produce side effects such as nausea, vomiting, gastrointestinal distress, anaemia and bleeding gastric ulcers. Cases of Zn^{2+} toxicity, with similar symptoms, are rare and involve either industrial accidents, such as inhalation of large quantities of zinc oxide dust, or massive intakes of Zn^{2+} orally.[5] Deaths due to excess Zn^{2+} are not common, however one woman died five days after ingesting 28g of zinc sulphate[77] and a schizophrenic patient died after swallowing 461 post-1981 pennies which consisted primarily of zinc.[78] It is thought that the toxicity of Zn^{2+} may arise from the competition between it and Cu^{2+} for various binding sites in the body, especially in the gut and blood transport proteins, and this is supported by the effectiveness of treating Zn^{2+} toxicity with Cu^{2+} supplements in some cases.[5]

The role of Zn^{2+} in many of the diseases and conditions mentioned here is not well understood. Development of a detection method for Zn^{2+} which indicates the location of Zn^{2+} in tissue or cells may be of immense benefit in the understanding of these diseases, and the general role of Zn^{2+} in the body.

1.2 : Measuring Metal Ion Concentrations in Cells and Tissue

1.2.1: Past Methods of Measurement

Atomic absorption spectrophotometry has been widely used for intracellular and extracellular Zn^{2+} detection in the past and is still used today.[79] Although this is a very convenient method for extracellular Zn^{2+} quantification such as serum Zn^{2+} levels, it has the major disadvantage of providing only an average Zn^{2+} concentration for cells and tissue. Due to the necessary destruction of the cells and tissue prior to measurement, no information is provided on the subcellular distribution of Zn^{2+} or the relative concentrations of tightly coordinated and loosely coordinated Zn^{2+}.

Before atomic absorption spectrophotometry became routine in 1955, Zn^{2+} analysis was achieved primarily using various colourimetric methods with agents such as diphenylthiocarbazone and its analogues.[5] Back titration methods, with Zn^{2+} chelators such as ethylenediaminetetraacetic acid, potentiometric stripping analysis,[80] affinity chromatography with immobilised metallothionein,[81] HPLC combined with inductively coupled plasma-mass spectrometry,[82] inductively coupled plasma atomic emission spectrophotometry[83] and flow injection analysis coupled to optical techniques[84] have also been used. As with atomic absorption spectrophotometry, these methods are designed for fluid samples or require the homogenisation of the sample cells and tissue before measurement.

One method which has been developed to indicate the position as well as the concentration of Zn^{2+} is the use of the stable radioactive isotope, $^{65}Zn^{2+}$. This method has been mainly used to study Zn^{2+} absorption and the distribution of Zn^{2+} within the body by studying patients after ingestion of the isotope.[5,85] This method detects only the exchangeable Zn^{2+} pool, as Zn^{2+} that is tightly coordinated is unlikely to exchange with the $^{65}Zn^{2+}$. Although this method works well, and does little harm to the subject, the large quantities of $^{65}Zn^{2+}$ and specialised equipment required means that this method is not the most practical for the study of intracellular Zn^{2+} distribution.

Although all of the methods listed above have been used for Zn^{2+} detection in the past, their ability to quantify and locate intracellular Zn^{2+} is limited. Hence a method of Zn^{2+} detection which can reliably indicate the quantity and position of Zn^{2+} in biological samples, even when only small concentrations are present, could prove to be of great benefit in solving some of the many biochemical questions involving Zn^{2+}.

1.2.2 : Metal Ion Concentration Measurement Using Fluorescent Probes

One method of Zn^{2+} detection that can theoretically indicate both concentration and location of Zn^{2+} in biological samples is fluorescence spectroscopy. This involves the introduction, into the cell, of a ligand, or 'probe' which selectively forms a fluorescent complex with a particular metal ion, with the resulting fluorescence observed giving, in the ideal case, the concentration and location of that metal ion within the cell. Over the past decade several fluorescent probes of this nature, including Quin-2, Indo-1, Fura-2 and Fura-3, have been developed for the measurement of intracellular and extracellular Ca^{2+},[86-88] allowing the detection of low Ca^{2+} concentrations in biological samples. Much effort has been expended in developing similarly operating intracellular fluorescent probes for Zn^{2+} and other metal ions such as Pb^{2+} and Al^{3+}.

In designing a potential fluorophore to be used as a specific probe for a metal ion such as Zn^{2+}, several factors need to be considered. Firstly, the ligand must bind specifically to Zn^{2+} rather than other biologically relevant cations such as Mg^{2+}, Ca^{2+}, Na^{+} and K^{+}. That is, the stability constant for the Zn^{2+} complex must be significantly greater than the stability constants for the complexes formed with Mg^{2+}, Ca^{2+}, Na^{+} and K^{+}. This can be accomplished by selecting a ligand with nitrogen donor atoms rather than oxygen donor atoms. Since the competitor metal ions are hard acids according to Pearson's hard and soft acids and bases concept[89,90] they are expected to exhibit a preference for hard oxygen donor atoms, whereas Zn^{2+} which is borderline between a hard and soft acid would be expected to preferentially bind to the softer nitrogen donor atoms. A further advantage of using nitrogen donor atoms for a probe of this type is that it is known that many of the Zn^{2+} enzymes possess nitrogen donor atoms in their active sites as discussed in Section 1.1.

Secondly, the probe must not bind too strongly to Zn^{2+} as this could destroy the cell or cause a redistribution of Zn^{2+} within it. Thus it may be most beneficial if the Zn^{2+} specific probe can only measure the intracellular free or loosely coordinated Zn^{2+} concentration rather than the total Zn^{2+} concentration. This would also allow the study of the release of Zn^{2+} from strongly coordinated sites under certain stimuli and may also allow the study of living cells and organisms.

Thirdly, the probe must be fluorescent, if only weakly. For fluorescence to be likely, absorption must occur at a wavelength long enough to ensure that chemical dissociation does not occur, as absorption to an unstable state is very unlikely to lead to fluorescence. Usually significant fluorescence is observed with molecules which have delocalised electrons such as those incorporating aromatic entities or other extended conjugated systems. Increased conjugation tends to shift the first absorption maximum ($\pi \rightarrow \pi^*$) to longer wavelengths and therefore increases the probability of fluorescence over decomposition.

Although in some cases the amount of a metal present in a sample may be deduced from the amount of quenching observed, it is far more accurate and informative if complexation results in an increase in fluorescence. Hence the ligand should be designed not only to bind specifically to Zn^{2+} over other biologically relevant cations but also to fluoresce strongly when bound to it. Unlike other transition metal ions, Zn^{2+} does not have vacant *d* orbitals which facilitate quenching. Therefore a $[Zn(ligand)]^{2+}$ complex would show fluorescence if the ligand has the properties mentioned above. Generally fluorescence intensity will increase upon complexation, as discussed later (Section 2.3), due to the increased rigidity induced by the interaction with Zn^{2+}.

Fourthly, a ligand which is very sensitive to even small concentrations of Zn^{2+} would be an advantage. Hence, a ligand which affords a large quantum yield (that is, it fluoresces brightly upon complexing a small amount of Zn^{2+}) would be ideal. A large quantum yield would also prevent the loading of large quantities of the probe into the living cell and therefore limit any possible toxic effects. Another advantage would be to have a ligand which fluoresces at a different wavelength than its Zn^{2+} complex, so the fluorescence collected at a given wavelength can be attributed to the complex alone.

Finally, a non-disruptive loading procedure of the Zn^{2+} specific probe into the cell is required. Hence the probe must be able to readily permeate the hydrophobic lipid bilayer of the cellular membrane. This can be achieved by using an uncharged ligand with a significant proportion of hydrophobic regions which should therefore be able to traverse the hydrophobic lipid bilayer and enter the cell. It would also be advantageous if once inside the cell, the probe was unable to exit the cell. One way to achieve this is to include an ester functional group in the probe. Esterases in the cytoplasm of the cell may then hydrolyse the ester group, creating a membrane-impermeant carboxylate form. The trapped hydrolysed ligand is then able to coordinate to the accessible Zn^{2+} within the cell. It would also be preferable if the rate of complexation of intracellular Zn^{2+} was rapid.

One of the first ligands discovered which met some of the above criteria was the chelator 8-hydroxyquinoline (Figure 1.4). It is known to produce fluorescent complexes with the biologically relevant cations Zn^{2+}, Ca^{2+} and Mg^{2+}.[91] However, due to its much greater stability constant with Zn^{2+} (10^8), it is expected to preferentially bind Zn^{2+} in the presence of Mg^{2+} (10^4) or Ca^{2+} (10^3).[92] Mahanand and Houck[93] showed that even with a large excess concentration of Mg^{2+} and Ca^{2+}, only Zn^{2+} formed a fluorescent complex with 8-hydroxyquinoline at pH 8.0. This ligand was first used as a fluorescent probe for detecting intracellular Zn^{2+} by Smith *et al* in 1969.[94] Since then numerous derivatives of quinoline have been prepared and tested for possible use as fluorescent probes.[12,95,96] The most promising ligand out of this group was 6-methoxy-8-(*p*-toluenesulphonamido)quinoline (M-TSQ) (Figure 1.4),[96] which has been used as a fluorescent histochemical probe for Zn^{2+} in several different tissue samples including sections of the brain, where it is thought to bind to only a minor fraction of the non-metalloenzyme and non-metalloprotein Zn^{2+}.[12]

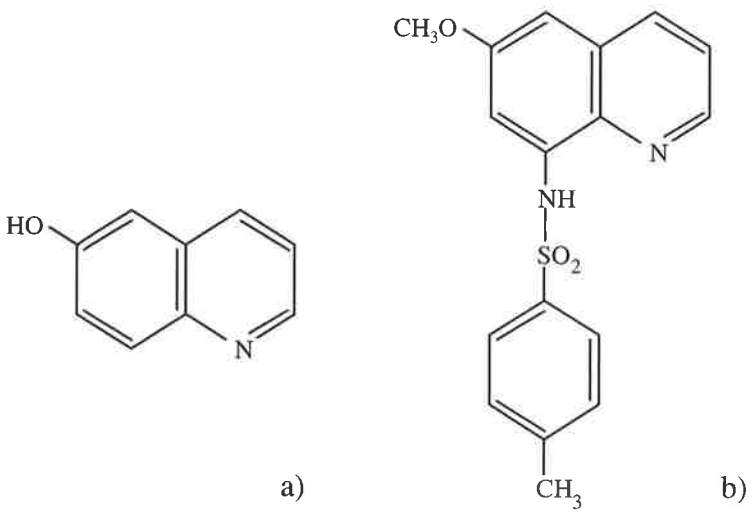

Figure 1.4 : a) 8-hydroxyquinoline and b) 6-methoxy-8-(*p*-toluenesulphonamido)quinoline.

Unfortunately, its use as a successful intracellular probe is limited by its poor cellular retention, however, like other sulphonamidoquinolines, it shows strong metal chelating properties.[97,98] Hence it has been modified by adding an ester functional group to ensure the fluorescent probe is retained within the cell. This resulted in the sulphonamidoquinoline ligand, ethyl-[2-methyl-8-*p*-toluenesulphonamido-6-quinolyloxy] acetate, Zinquin-E, which is discussed in detail, along with its hydrolysis product, 2-methyl-8-*p*-toluenesulphonamido-6-quinolyloxy acetic acid, Zinquin-A, in the following chapters.

1.3 : References

1. W. Kaim and B. Schwederski, "*Bioinorganic Chemistry: Inorganic Elements in the Chemistry of Life*", Wiley, Chichester, 1994.

2. B. L. Vallee and D. S. Auld, *Acc. Chem. Res.*, **26**, 543, 1993.

3. J. J. R. Fausto da Silva and R. J. P. Williams, "*The Biological Chemistry of the Elements*", Oxford University Press, Oxford, 1992.

4. B. L. Vallee and D. S. Auld, *Proc. Natl. Acad. Sci. USA*, **87**, 220, 1990.

5. S. C. Cunnane, "*Zinc: Clinical and Biochemical Significance*", CRC Press, Florida, 1988.

6. R. J. P. Williams, *Polyhedron*, **6**, 61, 1987.

7. "Zinc in Human Biology", C. F. Mills, *Ed.*, Springer-Verlag, London, 1989.

8. P. D. Zalewski, I. J. Forbes R. F. Seamark, R. Borlinghaus, W. H. Betts, S. F. Lincoln and A. D. Ward, *Chem. Biol.*, **1**, 153, 1994.

9. P. D. Zalewski, I. J. Forbes and W. H. Betts, *Biochem. J.*, **296 (2)**, 403, 1993.

10. D. Berendji, V. Kolbbachofen, K. L. Meyer, O. Grapenthin, H. Weber, V. Wahn and K. D. Kroncke, *FEBS Lett.*, **405 (1)**, 37, 1997.

11. X. Xie and T. J. Smart, *Nature*, **349**, 521, 1991.

12. C. J. Frederickson, *Int. Rev. Neurobiol.*, **31**, 145, 1989.

13. P. D. Zalewski, I. J. Forbes and C. Giannakis, *Biochem. Inter.*, **24**, 1093, 1991.

14. S. J. Martin, G. Mazdai, J. J. Strain, T. G. Cotter and B. M. Hannigan, *Clin. Exp. Immunol.*, **83**, 338, 1991.

15. F. Grummt., C. Weinmann-Dorsch, J. Schneider-Schaulies and A. Lux, *Exp. Cell Res.*, **163**, 191, 1986.

16. D. E. Epner and H. R. Herschman, *J. Cell. Physiol.*, **148**, 68, 1991.

17. R. J. Cousins and L. M. Lee-Ambrose, *J. Nutr.*, **122**, 56, 1992.

18. W. J. Pories, E. G. Mansour, F. R. Plecha, A. Flynn and W. H. Strain in "*Trace Elements in Human Health and Disease*", A. S. Prasad, *Ed.*, Academic Press, New York, 1976.

19. A. M. van Rij and W. J. Pories in "*Zinc in the Environment*", J. O. Nriagu, *Ed.*, Pt II, John Wiley and Sons, New York, 1980.

20. W. J. Bettger and B. L. O'Dell, *Life Sci.*, **28**, 1425, 1981.

21. B. L. Vallee and D. S. Auld in "*Methods in Protein Sequence Analysis*", H. Jornvall, J. -O. Hoog, A. -M. Gustavsson, *Eds.*, Birkhäuser Verlag, Basel, 1991.

22. A. Liljas, K. K. Kannan, P.-C. Bergstén, I. Waara, K. Fridborg, B. Strandberg, U. Carlbom, L. Järup, S. Lövgren and M. Petef, *Nature New Biology*, **235**, 131, 1972.

23. D. N. Silverman and S. Lindskog, *Acc. Chem. Res.*, **21**, 30, 1988.

24. A. E. Eriksson, T. A. Jones and A. Liljas, *Proteins*, **4**, 274, 1988.

25. Y. Pocker in "*Metal Ions in Biological Systems*", H. Sigel, *Ed.*, **25**, Marcel Deckker, New York, 1989.

26. H. Eklund, A. Jones and G. Schneider in "*Zinc Enzymes*", I. Bertini, C. Luchinat, M. Maret and M. Zeppezauer, *Eds.*, Birkhäuser, Boston, MA, 1986.

27. D. W. Christianson and W. N. Lipscomb, *Acc. Chem. Res.*, **22**, 62, 1989.

28. S. Mangani and P. Orioli, *Inorg. Chem.*, **31**, 365, 1992.

29. D. S. Auld, J. F. Riordan and B. L. Vallee in "*Metal Ions in Biological Systems*", H. Sigel, *Ed.*, **25**, Marcel Deckker, New York, 1989.

30. C. F. Springgate, A. S. Mildvan, R. Abrahamson and J. L. Engle, *J. Biol. Chem.*, **248**, 5987, 1973.

31. F. Y-H. Wu in "*Zinc Enzymes*", I. Bertini, C. Luchinat, M. Maret and M. Zeppezauer, *Eds.*, Birkhäuser, Boston, MA, 1986.

32. S. K. Burley, P. R. David, A. Taylor and W. N. Lipscomb, *Proc. Natl. Acad. Sci. USA*, **87**, 6878, 1990.

33. K. H. Röhm in "*Zinc Enzymes*", I. Bertini, C. Luchinat, M. Maret and M. Zeppezauer, *Eds.*, Birkhäuser, Boston, MA, 1986.

34. E. E. Kim and H. W. Wyckoff, *J. Mol. Biol.*, **218**, 449, 1991.

35. J. E. Butler-Ransohoff, D. A. Kendall and E. T. Kaiser in "*Metal Ions in Biological Systems*", H. Sigel, *Ed.*, **Vol. 25**, Marcel Deckker, New York, 1989.

36. R. B. Davies and E. P. Abraham, *Biochem. J.*, **143**, 129, 1974.

37. B. W. Matthews, J. N. Jansonius, P. M. Colman, B. P. Schoenborn and D. Dupourque, *Nature New Biology*, **238**, 37, 1972.

38. B. W. Matthews, *Acc. Chem. Res.*, **21**, 33, 1988.

39. A. Fontana, G. Fassina, C. Vita, D. Dalzoppo, M. Zamai and M. Zambonin in "*Zinc Enzymes*", I. Bertini, C. Luchinat, M. Maret and M. Zeppezauer, *Eds.*, Birkhäuser, Boston, MA, 1986.

40. H-P. Roth and M. Kirrchgessner, *Biol. Trace Elem. Res.*, **3**, 13, 1981.

41. R. J. P. Williams, *Endeavour (New Ser.)*, **8**, 65, 1984.

42. R. D. Palmiter, *Toxicol. Appl. Pharmacol.*, **135**, 139, 1995.

43. M. Ebadi, P. L. Iversen, R. Hao, D. R. Cerutis, P. Rojas, H. K. Happe, L. C. Murrin and R. F. Pfeiffer, *Neurochem. Int.*, **27**, 1, 1995.

44. S. Saito and Y. Kojima, *Res. Comm. in Molec. Pathol. Pharmacol.*, **89**, 365, 1995.

45. P. Coyle, J. C. Philcox and A. M. Rofe, *Clin. Biochem. Rev.*, **14**, 118, 1993.

46. E. Ochiai, *J. Chem. Educ.*, **65**, 943, 1988.

47. E. Kimura and T. Koike, *Comm. Inorg. Chem.*, **11**, 285, 1991.

48. H. R. Mahler and E. H. Cordes, "*Biological Chemistry*", New York, Harper and Row, 1969.

49. K. Hofman and M. Bergmann, *J. Biol. Chem.*, **134**, 225, 1940.

50. M. W. Makinen, G. B. Wells and S-O. Kang, *Adv. Inorg. Biochem.*, **6**, 1, 1984.

51. W. F. Furey, A. H. Robbins, L. L. Clancy, D. R. Winge, B. C. Wang and C. D. Stout in "*Metallothionein II*", J. H. R. Kagi and Y. Kojima, *Eds.*, Experientia Supplementum, **52**, Birkhauser Verlag, Basel, 1987.

52. L. H. Allen, *Eur. J. Clin. Nutr.*, **48** (suppl 1), S 75, 1994.

53. W. R. Beisel, *Am. J. Clin. Nutr.*, **35** (suppl), 417, 1982.

54. M. H. N. Golden and B. E. Golden, *Nutr. Res.*, **5** (suppl 1), S 700, 1985.

55. S. Sazawal, R. E. Black, M. K. Bhan, N. Bhandari, A. Sinha and S. Jalla, *N. Engl. J. Med.*, **333**, 839, 1995.

56. A. S. Prasad in "*Trace Elements in Human Health and Disease*", A. S. Prasad, *Ed.*, Academic Press, New York, 1976.

57. W. G. Klingberg, A. S. Prasad and D. Oberleas in "*Trace Elements in Human Health and Disease*", A. S. Prasad, *Ed.*, Academic Press, New York, 1976.

58. N. Akar, *Arch. Dis. Child.*, **78** (**3**), 288, 1998.

59. G. J. Brewer, A. S. Prasad, F. J. Oelshlegel (Jr.), E. B. Schoomaker, J. Ortega and D. Oberleas in "*Trace Elements in Human Health and Disease*", A. S. Prasad, *Ed.*, Academic Press, New York, 1976.

60. A. B. Chausmer, *J. Am. Coll. Nutr.*, **17** (**2**), 109, 1998.

61. A. S. Prasad, F. W. J. Beck, T. D. Doerr, F. H. Shamsa, H. S. Penny, S. C. Marks, J. Kaplan, O. Kucuk and R. H. Mathog, *J. Am. Coll. Nutr.*, **17** (**5**), 409, 1998.

62. R. D. Lindeman, A. A. Yunice and D. J. Baxter, in "*Trace Elements in Human Health and Disease*", A. S. Prasad, *Ed.*, Academic Press, New York, 1976.

63. G. A. Eby and W. W. Halcomb, *Med. Hypotheses*, **17**, 157, 1985.

64. G. A. Eby, D. R. Davis and W. W. Halcomb, *Antimicrob. Agents Chem. Other*, **25**, 20, 1984.

65. B. S. Mossad, M. L. Macmillan, S. V. Medendorp and P. Mason, *Ann. Intern. Med.*, **125**, 81, 1996.

66. G. A. Eby, *J. Pharmacy Technology*, **11**, 110, 1995.

67. M. L. Garland, K. O. Hagmeyer, *Annals of Pharmacotherapy*, **32 (1)**, 63, 1998.

68. S. L. Gorbach, *Infectious Diseases in Clinical Practice*, **7 (3)**, 120, 1998.

69. G. J. Harrop, C. A. Saxton and J. S. Best, *J. Peridontal Res.*, **18**, 634, 1983.

70. L. D. Bailey and C. Shields, *Br. Med. J.*, 808, 1937.

71. W. Sergio, *Med. Hypotheses*, **26**, 251, 1988.

72. E. Mocchegiani, S. Veccia, F. Ancarani, G. Scalise, N. Fabris, *International Journal of Immunopharmacology*, **17 (9)**, 719, 1995.

73. R. E. Patterson, E. White, A. R. Kristal, M. L. Neuhouser and J. D. Potter, *Cancer Causes and Control*, **8 (5)**, 786, 1997.

74. M. P. Cuajungco and G. J. Lees, *Brain Res. Rev.*, **23 (3)**, 219, 1997.

75. P. C. Nachev and A. J. Larner, *Trace Elements in Medicine*, **13 (2)**, 55, 1996.

76. M. Garretts and M. Molokhia, *J. Pediatr.*, **91**, 492, 1977.

77. G. A. B. Cowan, *Br. Med. J.*, **I**, 451, 1947.

78. D. R. Bennett, C. J. Baird, K. M. Chan, P. F. Crookes, C. G. Bremmer, M. M. Gottlieb and W. Y. Naritoku, *Am. J. Forensic Med. Pathol.*, **18 (2)**, 148, 1997.

79. H. Johnson and H. Sauberlich in "*Clinical, Biochemical and Nutritional Aspects of Trace Elements*", A. Prasad, *Ed.*, Alan R. Liss Inc., New York, **6**, 1982.

80. D. M. Taylor, J. A. Liyanage, D. R. Williams and K. G. Harding, *Applied Radiation and Isotopes*, **49**, 677, 1998.

81. P. F. Zhang and J. C. Allen, *Biol. Trace Elem. Res.*, **50 (2)**, 135, 1995.

82. E. Coni, A. Alimonti, A. Bocca, F. Latorre, E. Menghetti, E. Miraglia and S. Caroli, *Trace Elements in Medicine*, **13 (1)**, 26, 1996.

83. M. T. Rajan, K. S. J. Rao, B. M. Mamatha, R. V. Rao, P. Shanmugavelu, R. B. Menon and M. V. Pavithran, *J. of the Neurological Sciences*, **146 (2)**, 153, 1997.

84. J. L. Burguera and M. Burguera, *J. Trace Elements and Electrolytes in Health and Disease*, **7 (1)**, 9, 1993.

85. N. F. Krebs, L. V. Miller, V. L. Naake, S. Lei, J. E. Westcott, P. V. Fennessey and K. M. Hambidge, *J. Nutr. Biochem.*, **6 (6)**, 292, 1995.

86. R. Y. Tsien, T. Possan and T. J. Rink, *J. Cell Biol.*, **94**, 325, 1982.

87. G. Grynkiewicz, M. Poenie and R. Y. Tsien, *J. Biol. Chem.*, **260**, 3440, 1985.

88. M. Wahl, M. J. Lucherini and E. Gruenstein, *Cell Calcium*, **11**, 487, 1990.

89. R. G. Pearson, *J. Am. Chem. Soc.*, **85**, 3533, 1963.

90. R. G. Pearson, *Coord. Chem. Rev.*, **100**, 403, 1990.

91. D. Schacter, *J. Lab. Clin. Med.*, **54**, 763, 1959.

92. S. Watanabe, W. Frantz and D. Trottier, *Anal. Biochem.*, **5**, 345, 1963.

93. D. Mahanand and J. C. Houck, *Clin. Chem.*, **14**, 6, 1968.

94. G. L. Smith, R. A. Jenkins and J. F. Gough, *J. Histochem. Cytochem.*, **17**, 749, 1969.

95. C. J. Frederickson, E. J. Kasarkis, D. Ringo and R. E. Frederickson, *J. Neurosci. Method*, **20**, 91, 1987.

96. D. D. Savage, C. Y. Montano and E. J. Kasarskis, *Brain Res.*, **496**, 257, 1989.

97. J. H. Billman and R. Chernin, *Anal. Chem.*, **34**, 408, 1962.

98. H. Nakamura, T. Yoshida, M. Todoko, K. Ueno and M. Takagi, *Bull. Chem. Soc. Jpn.*, **57**, 2839, 1984.

CHAPTER 2

PROPERTIES OF FREE AND ZINC(II) BOUND ZINQUIN-A

2.1 : An Introduction to Zinquin-A

One fluorophore that satisfies many of the requirements for a good intracellular probe as mentioned in Section 1.2.2 is Zinquin (Figure 2.1).[1] This ligand has been successfully used in several intracellular studies to date,[2-12] with more work awaiting publication (see Chapter 3). Zinquin is supplied as the ester, ethyl-[2-methyl-8-*p*-toluenesulphonamido-6-quinolyloxy] acetate, or Zinquin-E (Figure 2.1). It is this compound that cells and tissue are incubated with in order to visualise Zn^{2+} by fluorescence. As Zinquin-E is uncharged, it is able to freely traverse the lipophilic cellular membrane and enter the cell, as required for an intracellular probe. It is thought that once inside the cell, the esterases present in the cytosol hydrolyse the ester portion of the probe, leading to the formation of the carboxylic acid, 2-methyl-8-*p*-toluenesulphonamido-6-quinolyloxyacetic acid, or Zinquin-A (Figure 2.1). As shown in the scheme below (Figure 2.2), Zinquin-A exists as a negatively charged ion at physiological pH, $[ZQA.H]^-$, and is therefore trapped in the cell due to its charged state which prevents it from passing back through the lipophilic cellular membrane. A similar ester hydrolysis appears to prevent the leakage of the Ca^{2+}-selective fluorophores Quin-2[13] and Fura-2[14] from cells. As will be discussed later in this chapter (Section 2.3), the trapped $[ZQA.H]^-$ is not appreciably fluorescent, however it can bind to the Zn^{2+} present in the cell, forming highly fluorescent complexes of the form [Zn(ZQA)] and $[Zn(ZQA)_2]^{2-}$. Hence, regions in the cell containing high or low concentrations of Zn^{2+} can be identified by observing the pattern of Zinquin-A fluorescence in a Zinquin-E incubated cell. Changes in the amount of Zn^{2+} available to bind to Zinquin-A under the influence of different biochemical stimuli can also be monitored.

Zinquin-A, rather than Zinquin-E, is likely to produce the fluorescence observed in cells due to the proposed metabolism of Zinquin-E shown in Figure 2.2. Therefore it is the binding and spectroscopic properties of Zinquin-A that are of most interest and have been studied in detail here.

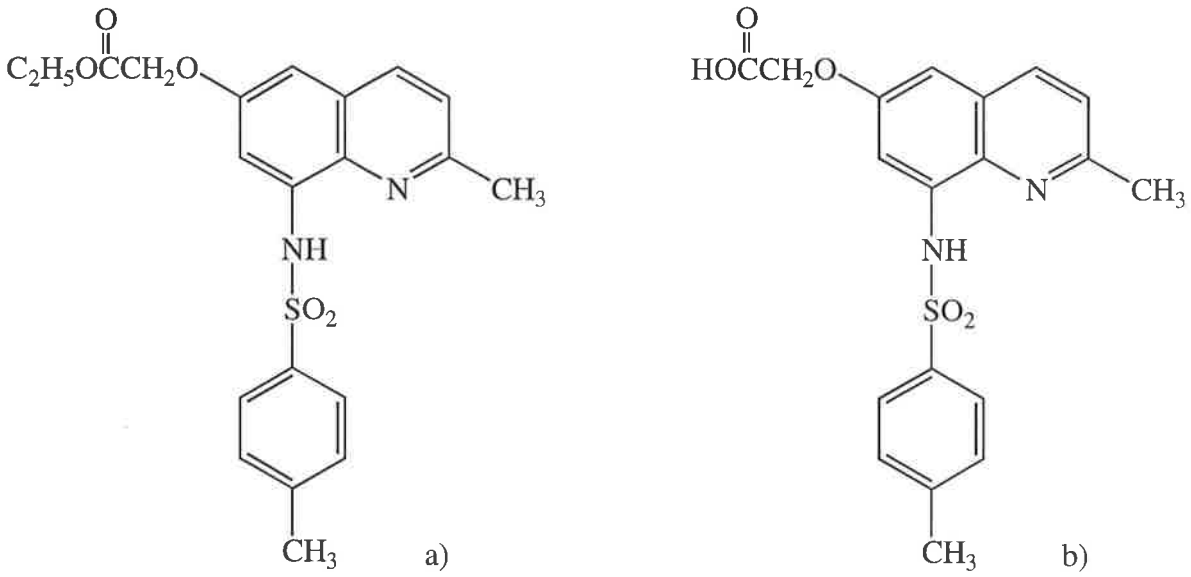

Figure 2.1 : a) Zinquin-E, ethyl-[2-methyl-8-*p*-toluenesulphonamido-6-quinolyloxy]acetate

b) Zinquin-A, 2-methyl-8-*p*-toluenesulphonamido-6-quinolyloxyacetic acid, ($ZQA.H_2$)

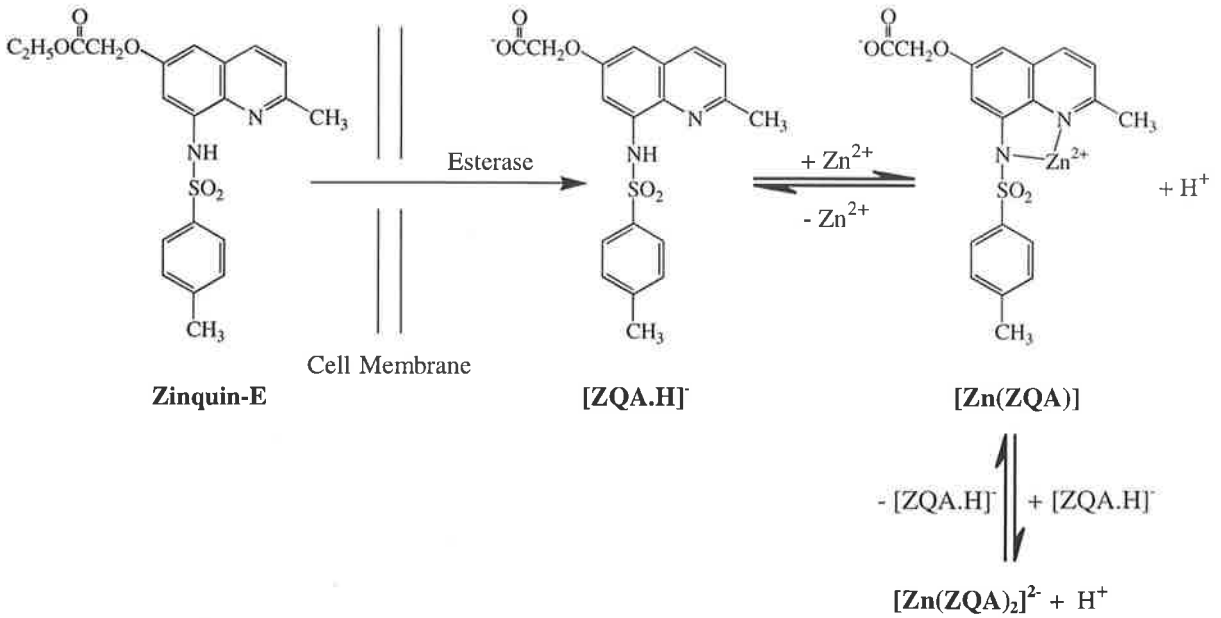

Figure 2.2 : The proposed metabolism of Zinquin-E to Zinquin-A by living cells.

As mentioned in Section 1.2.2, to be an effective probe for Zn^{2+}, Zinquin-A should selectively complex and fluoresce with Zn^{2+} rather than other biologically relevant cations such as Ca^{2+} and Mg^{2+}. It has been shown that although Zinquin-A forms strong complexes with Zn^{2+}, it does not bind selectively to Zn^{2+}, forming stable complexes with Co^{2+}, Ni^{2+}, Cu^{2+} and Cd^{2+} in addition to Zn^{2+}, as can be seen from the cumulative stability constants listed in Table 2.1 below. However, [Ca(ZQA)] and [Mg(ZQA)] species were not detected, suggesting that Zinquin-A binds weakly to these cations and the log β describing the formation of such complexes are below 2.[15] Smaller biologically relevant cations, such as Na^+ and K^+ are unlikely to form stable complexes with Zinquin-A due to their small size and preference for ligands with oxygen donors rather than nitrogen donors. The equations for the complexes referred to in Table 2.1 are shown below.

$$n\,ZQA^{2-} + M^{2+} \overset{\beta_n}{\rightleftharpoons} [M(ZQA)_n]^{(2n-2)-} \qquad (2.1)$$

$$\beta_n = \frac{[M(ZQA)_n^{(2n-2)-}]}{[M^{2+}][ZQA^{2-}]^n} \qquad (2.2)$$

Metal (M)	M.ZQA	$[M(ZQA)_2]^{2-}$	$[M(ZQA)_3]^{4-}$
	$\log \beta_1$	$\log \beta_2$	$\log \beta_3$
Co^{2+}	8.12 ± 0.20	17.06 ± 0.11	25.56 ± 0.11
Ni^{2+}	< 8	15.73 ± 0.03	
Cu^{2+}	11.96 ± 0.02	21.40 ± 0.03	
Zn^{2+}	9.65 ± 0.02	19.11 ± 0.06	
Cd^{2+}	8.44 ± 0.50	15.38 ± 0.40	
Mg^{2+}	< 2		
Ca^{2+}	< 2		

Table 2.1 : Literature values[15] for the complexation of various cations by Zinquin-A in 50% aqueous ethanol at 298.2 K and I = 0.10 ($NaClO_4$).

The acid dissociation constants, pK_as, of protonated Zinquin-A were also determined under the same conditions. Three pK_as were observed for the fully protonated ligand, $[ZQA.H_3]^+$, giving pK_{a1} = 10.01 ± 0.02, pK_{a2} = 3.72 ± 0.03 and pK_{a3} = 1.87 ± 0.10 where K_{an} (n = 1, 2 or 3) is described in Equations 2.3 and 2.4 below. For Zinquin-A, pK_{a1} has been assigned to the sulphonamide proton, pK_{a2} to the carboxylic acid and pK_{a3} to the quinolinium proton.

$$[ZQA.H_n]^{(n-2)+} \overset{K_{an}}{\rightleftharpoons} [ZQA.H_{(n-1)}]^{(n-3)+} + H^+ \quad (2.3)$$

$$K_{an} = \frac{[ZQA.H_{(n-1)}^{(n-3)+}][H^+]}{[ZQA.H_n^{(n-2)+}]} \quad (2.4)$$

The poor selectivity of Zinquin-A for Zn^{2+} does not effect its use as an intracellular fluorescent probe as it has been found that only the Zn^{2+} and Cd^{2+} Zinquin-A complexes fluoresce strongly. All the remaining metals listed in Figure 2.3 did not increase the relative fluorescence above background levels except for Ag^+ which had a lesser effect on the fluorescence than Cd^{2+} and Zn^{2+}. As healthy cells do not contain appreciable amounts of Cd^{2+} or Ag^+, it is possible to assign all the fluorescence observed in a Zinquin-E incubated cell to Zn^{2+} bound to Zinquin-A. Figure 2.3 shows the relative fluorescence intensity obtained for solutions containing 1×10^{-5} mol dm^{-3} cation and 1×10^{-5} mol dm^{-3} Zinquin-A in Hank's Balanced Salt Solution (HBSS) at pH 7.4 (2.0×10^{-2} mol dm^{-3} HEPES buffer) and 310.2 K, which mimics the cellular environment to some extent. Excitation and emission wavelengths of 364 nm (slit width 5 nm) and 485 nm (slit width 10 nm), respectively, were used.[16]

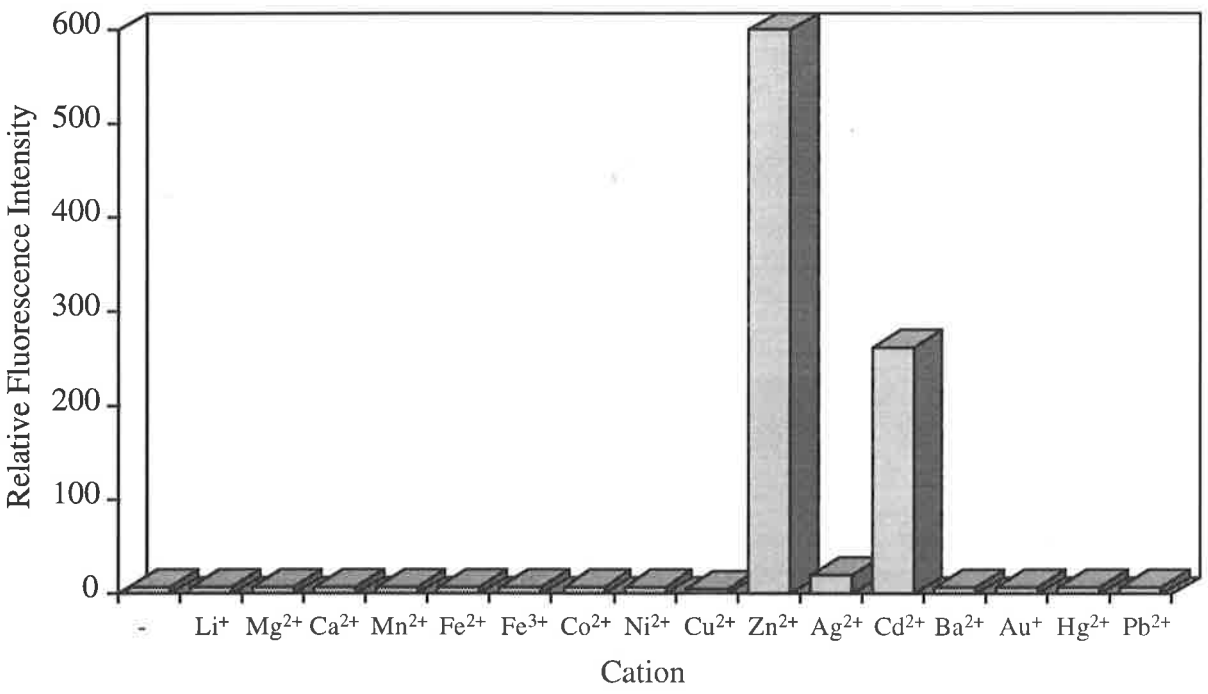

Figure 2.3 : Fluorescence intensity at 485 nm obtained for various cations (1×10^{-5} mol dm^{-3}) with Zinquin-A (1×10^{-5} mol dm^{-3}) in HBBS at pH 7.4 (2×10^{-3} mol dm^{-3} HEPES), T = 310.2 K, slits = 5 and 10 nm, Ex λ = 364 nm.[16]

The selectivity towards Zn^{2+} and Cd^{2+} illustrated in Figure 2.3 can be attributed to quenching of fluorescence in the Co^{2+}, Ni^{2+} and Cu^{2+} complexes due to the presence of paramagnetic metal ions, unlike Zn^{2+} and Cd^{2+} which have a d^{10} configuration and are therefore diamagnetic. This occurs because the rate of intersystem crossing from an excited singlet state to an excited triplet state of Zinquin-A is increased by the unpaired electrons of paramagnetic metal ions[17] and no fluorescence is observed from this triplet state (see Appendix A for an overview of spectroscopy theory). It is possible that as Zinquin-A forms strong complexes with Co^{2+}, Ni^{2+} and Cu^{2+}, they could compete with Zn^{2+} for Zinquin-A in the cell and lower the fluorescence observed, however, these metal ions are of substantially lower concentration than Zn^{2+} in healthy cells[18] and should therefore not appreciably effect the observed fluorescence. The other ions studied do not form appreciably strong complexes with Zinquin-A, as mentioned previously, and so no change in the Zinquin-A fluorescence would be expected upon their addition.

Hence it has been shown that the properties of Zinquin-E and Zinquin-A match the criteria required for a successful intracellular probe (Section 1.2.2).

2.2 : The Adventitious Zinc(II) Problem

Due to the great sensitivity of Zinquin-A to small amounts of Zn^{2+}, care must be taken to account for any traces of Zn^{2+} present as an impurity in even analytical grade reagents when studying it *in vitro*, as opposed to *in vivo*. Early studies of the fluorescence of Zinquin-A with Zn^{2+} showed a significant fluorescence for solutions containing no added Zn^{2+}.[15] This can be seen in Figure 2.4 which shows the fluorescence of 5×10^{-6} mol dm^{-3} Zinquin-A with added Zn^{2+} concentrations increasing from zero to 1×10^{-4} mol dm^{-3} in 50% aqueous ethanol buffered at pH 6.6 and I = 0.1 with 0.1 mol dm^{-3} NaPIPES as described in Section 5.1.5. However, when a strong Zn^{2+} chelating ligand, such as EDTA (ethylenediaminetetraacetic acid) or EGTA (ethylenebis(oxyethylenenitrilo)tetraacetic acid), was added, fluorescence was no longer observed for Zinquin-A in the absence of added Zn^{2+}. This suggests that the fluorescence initially observed was due to Zn^{2+} present as an impurity in the sample, or 'Adventitious Zn^{2+}'. Adventitious Zn^{2+} from varied sources was identified as a problem of Zn^{2+} detection in biological samples as early as 1959[19] and Prasad (1993) has outlined the meticulous steps required to obtain accurate determinations of Zn^{2+} in various samples.[20]

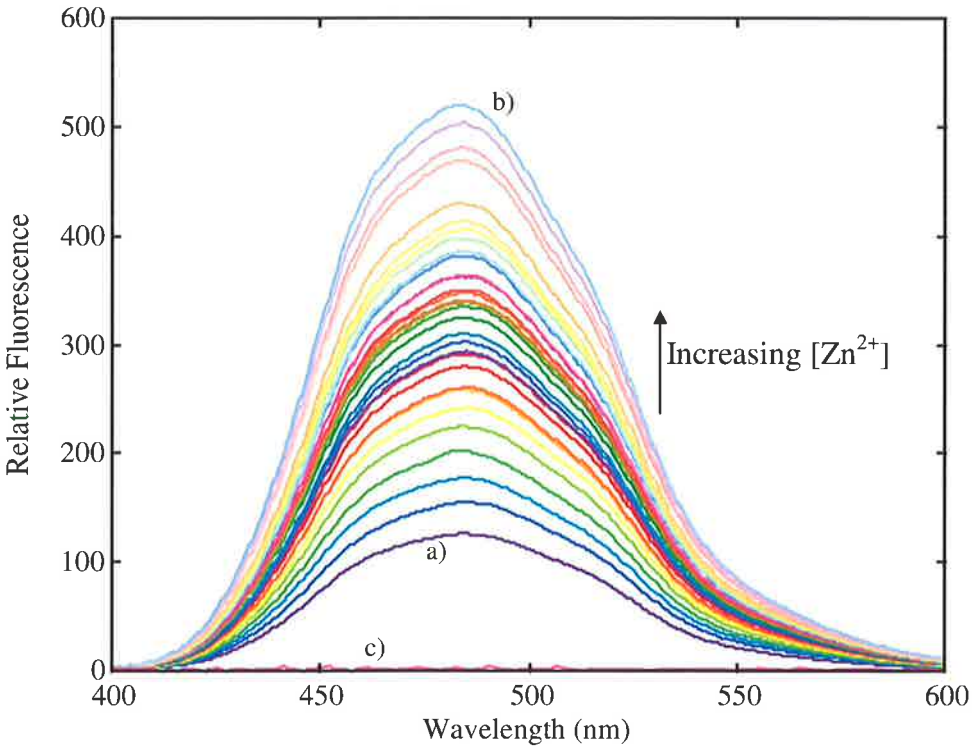

Figure 2.4 : Fluorescence spectra for Zinquin-A (5×10^{-6} mol dm^{-3}) with increasing concentrations of $ZnSO_4$ (0 to 1×10^{-4} mol dm^{-3}) measured in 50% aqueous ethanol, pH 6.6 and $I = 0.1$ (0.1 mol dm^{-3} NaPIPES), $T = 298.2$ K, slits = 5 nm and Ex λ = 358 nm. a) No added Zn^{2+}, b) 1×10^{-4} mol dm^{-3} Zn^{2+} and c) No added Zn^{2+} with 1×10^{-5} mol dm^{-3} EGTA.

Time was spent in trying to eliminate adventitious Zn^{2+} from fluorescence samples before measurement, but although the concentration of this impurity was reduced in some instances, it was not always possible to totally remove it. The reason for this lies in the ubiquitous nature of Zn^{2+} arising from its necessary presence in biological systems (see Section 1.1) and the ability of Zn^{2+} to bind to surfaces such as glass and plastic. Procedures such as adding EDTA to the detergent before washing glassware, pre-washing disposable micropipette tips and general careful laboratory practice helped to lower the amount of adventitious Zn^{2+} present, and prevent large variations in adventitious Zn^{2+} concentration between solutions. Adventitious Zn^{2+} in the buffer was minimised by making large volumes of bulk solutions and adjusting the pH of these solutions with the minimum amount of $HClO_4$ in the shortest time possible to avoid contamination. Attempts to purify the buffer further were unsuccessful in removing adventitious Zn^{2+}.

If the low level of adventitious Zn^{2+} can not be removed, three options remain;

(a) Quantify the adventitious Zn^{2+} present and add this concentration into all calculations,
(b) Quantify the adventitious Zn^{2+} present and add the same concentration of EDTA to counter it,
(c) Use high Zn^{2+} concentrations so the small contribution of adventitious Zn^{2+} causes only a small percentage error and can therefore be ignored.

All three have been used, to some extent, in this work in conjunction with the use of excess EDTA to remove adventitious Zn^{2+} in all solutions where no Zn^{2+} was required. Four different methods for the quantification of adventitious Zn^{2+}, with varying degrees of ease and accuracy, were explored as described in Sections 2.2.1 to 2.2.5 below. Atomic absorption spectroscopy was also attempted, however the low concentration of adventitious Zn^{2+} present was below the detection limit of the equipment available.

2.2.1 : Zinquin-A Fluorescence Titration Fitting

In principle, the fluorescence titration shown in Figure 2.4 above can be fitted to values for the stability constants of [Zn(ZQA)] and $[Zn(ZQA)_2]^{2-}$ using the MATLAB program, SPECFIT[21] as the amount of fluorescence observed is the sum of the fluorescence due to each species present, which is in turn proportional to the concentration of that species. Hence, using a non-linear least squares minimisation, concentrations of [Zn(ZQA)] and $[Zn(ZQA)_2]^{2-}$ can be determined for each spectrum measured and subsequently K_1 and K_2 can be calculated if the total concentrations of Zn^{2+} and Zinquin-A are known. However, in this case the total concentration of Zn^{2+} in each solution is not known due to the adventitious Zn^{2+} present, but values for the stability constants *are* known[15] (see Section 2.1). Therefore SPECFIT was modified to keep the values of K_1 and K_2 constant while the concentration of adventitious Zn^{2+} was fitted to the data. This method assumed that the amount of adventitious Zn^{2+} was the same for all of the solutions measured and that it is valid to use stability constants determined from potentiometric titrations in conjunction with fluorescence results.

When determining stability constants from fluorescence spectra, it is important to keep in mind the equilibria that exist in solution after excitation. It is possible for the excited free ligand, ([ZQA.H]$^-$)*, to be in equilibrium with the excited bound ligand, [Zn(ZQA)]*, as is depicted in Figure 2.5 below. A similar scheme exists for $[Zn(ZQA)_2]^{2-}$.

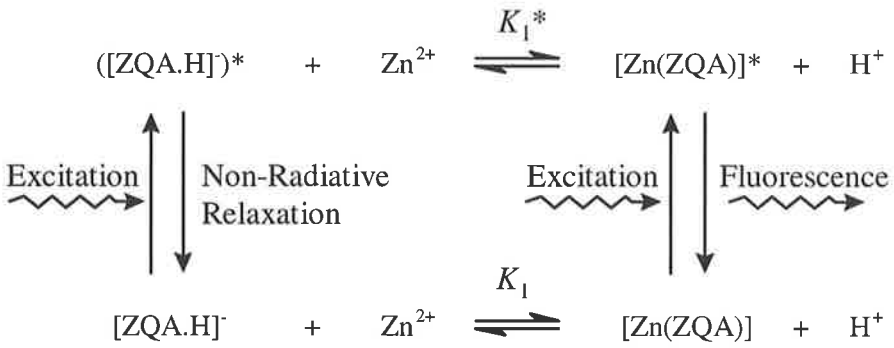

Figure 2.5 : Equilibria present in a fluorescing solution of [Zn(ZQA)].

If this excited state equilibrium does exist, the two extreme cases would be;

1. The excited state equilibrium re-equilibrates very **rapidly** compared with the time it takes for relaxation.

2. The excited state equilibrium re-equilibrates very **slowly** compared with the time it takes for relaxation.

If the first option occurs, after excitation, the concentrations of ([ZQA.H]$^-$)* and [Zn(ZQA)]* rapidly re-equilibrate to the equilibrium concentrations described by the constant K_1* before relaxation can occur. Thus when relaxation does occur, the concentration of [Zn(ZQA)]* is no longer directly proportional to the equilibrium concentration of [Zn(ZQA)] described by K_1 and K_1* would be determined rather than K_1.

For the second option, after excitation, the concentrations of ([ZQA.H]$^-$)* and [Zn(ZQA)]* remain fixed and relaxation occurs before re-equilibration due to the slow rate of equilibration of the excited state. This means that the concentration of [Zn(ZQA)]* remains proportional to the concentration of [Zn(ZQA)] and K_1 would be determined, rather than K_1*.

If the rate of equilibration of the excited state equilibrium lies between these two extremes, fluorescence will occur before the excited state equilibrium has had time to fully re-equilibrate and the concentration of [Zn(ZQA)]* observed will not be proportional to the equilibrium concentration of [Zn(ZQA)] described by K_1, nor will it be the equilibrium concentration of [Zn(ZQA)]* described by K_1*. Therefore the stability constant determined will be neither K_1 nor K_1*.

In the case of Zinquin-A fluorescence, it appears that the first option does not occur. Firstly, it is suggested in Section 2.3 that the absence of fluorescence observed for $[ZQA.H]^-$ is due to rapid non-radiative relaxation after excitation of the fairly flexible unbound Zinquin-A molecule. If this is so, whenever a [Zn(ZQA)]* molecule re-equilibrates to Zn^{2+} and $([ZQA.H]^-)$*, the newly formed $([ZQA.H]^-)$* would rapidly relax to the ground state without emitting any fluorescence. Then by Le Chatelier's Principle, more [Zn(ZQA)]* would be converted into Zn^{2+} and $([ZQA.H]^-)$* to try and attain the equilibrium concentration prescribed by K_1*. As the equilibration rate is rapid for the first option, all the [Zn(ZQA)]* would be rapidly converted into $([ZQA.H]^-)$* which would then show no fluorescence before relaxing to the ground state. Hence no, or very little fluorescence would be observed. As can be seen in Figure 2.4, this is not the case, ruling out option 1 in the case of Zinquin-A.

The second option would result in the determination of a stability constant which represents the ground state equilibrium. This value would therefore agree with values determined by other ground state methods such as ultraviolet-visible spectroscopy and potentiometric titrations. As is evident in Section 2.3, the results obtained from fluorescence agree reasonably with those from titration data, indicating option 2 occurs to some extent. Using this reasoning, it is valid to use the stability constants determined by potentiometric titrations in 50% aqueous ethanol[15] to determine the concentration of adventitious Zn^{2+} in fluorescence solutions in this case.

Using this method, the concentration of adventitious Zn^{2+} in the solutions used to obtain the spectra in Figure 2.4 was determined to be $(1.03 \pm 0.01) \times 10^{-6}$ mol dm^{-3}. The fit for this result is shown in Figure 2.6. Fitting for the stability constants and the concentration of adventitious Zn^{2+} simultaneously did not produce sensible results. This was possibly a result of the greater uncertainty in allowing two unrelated sets of constants to be refined simultaneously. This method was attempted for the fluorescence spectra determined with the more sensitive luminescence spectrophotometer (Sections 2.3 and 2.4), however due to the smaller number of spectra (6 compared with 32) the concentration of adventitious Zn^{2+} could not be successfully fitted to the data. Adventitious Zn^{2+} concentrations determined by Zinquin-A ultraviolet titration methods were used for these spectra instead (Section 2.2.3).

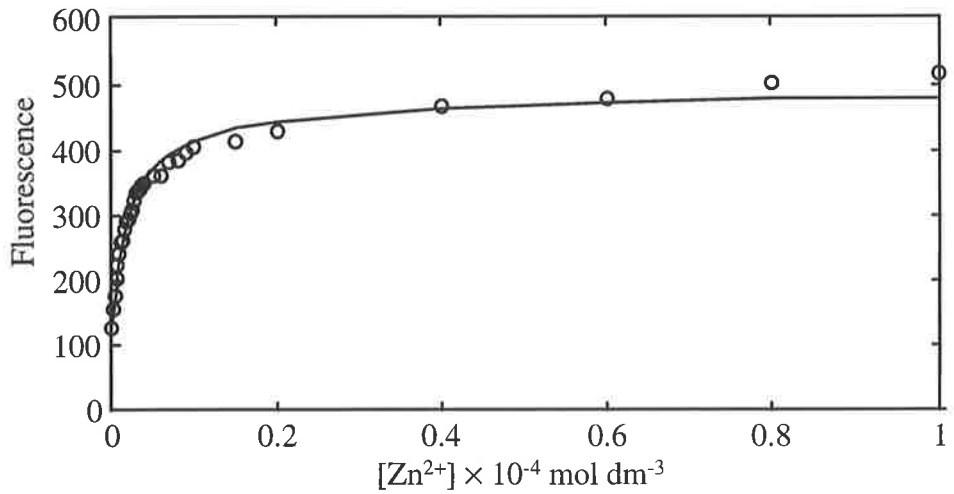

Figure 2.6 : The fit for adventitious Zn^{2+} at 486 nm obtained using all the spectra in Figure 2.4 in the wavelength region 430 to 540 nm.

2.2.2 : EDTA Fluorescence Titration

As mentioned previously, the addition of EDTA, which is a strong Zn^{2+} binder,[22] to solutions containing adventitious Zn^{2+} quenches all the fluorescence due to Zinquin-A binding to Zn^{2+} by preferentially complexing it. Therefore it is reasonable to assume that the minimum concentration of EDTA required to remove all the residual fluorescence due to adventitious Zn^{2+} corresponds to the concentration of adventitious Zn^{2+} present. Hence the fluorescence of solutions with a constant concentration of Zinquin-A (approximately 5×10^{-6} mol dm^{-3}) and increasing concentrations of EDTA were measured for each buffer system used, as described in Section 5.1.2.1. The maximum fluorescence for each spectrum was then plotted against EDTA concentration giving the minimum amount of EDTA required to complex all the adventitious Zn^{2+} (the x-intercept), and therefore the adventitious Zn^{2+} concentration.

Similar results were obtained for both the 25% and 50% aqueous ethanol buffers used, with concentrations of adventitious Zn^{2+} of 4.95×10^{-7} and 7.89×10^{-7} mol dm^{-3}, respectively. The plot of maximum fluorescence intensity against EDTA concentration for 0.1 mol dm^{-3} NaPIPES adjusted to pH 6.6 in 50% aqueous ethanol is shown in Figure 2.7 below and a similar plot was obtained for 1.00×10^{-3} mol dm^{-3} NaPIPES, 0.1 mol dm^{-3} $NaClO_4$ adjusted to pH 6.6 in 25% aqueous ethanol.

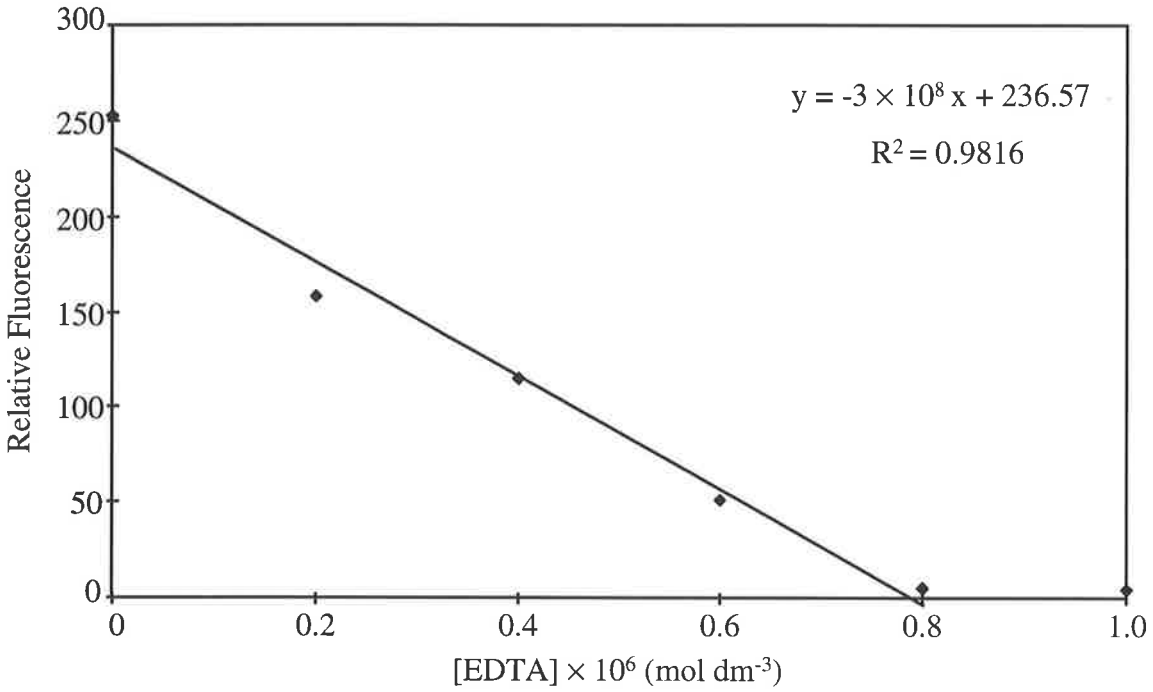

Figure 2.7 : Plot of fluorescence intensity at 486 nm against [EDTA] used to calculate the concentration of adventitious Zn^{2+} in 0.1 mol dm^{-3} NaPIPES adjusted to pH 6.6 in 50% aqueous ethanol. T = 298.2 K, slits = 5 nm, Ex λ = 358 nm. The equation of the line of best fit is shown top right.

There is a significant amount of scattering of the experimental points shown in Figure 2.7. This is due to the small variations in adventitious Zn^{2+} concentrations between solutions arising from non-buffer sources. Before establishing a washing protocol that included EDTA to remove Zn^{2+} adhered to surfaces, the scatter was more pronounced. The last point in the plot (at 1×10^{-6} mol dm^{-3} EDTA) has been omitted from the line of best fit as this fluorescence is low enough to be considered as zero within experimental error, and there was no significant change between this value and the one before it at 8×10^{-7} mol dm^{-3} EDTA.

2.2.3 : Zinquin-A Ultraviolet Titration

Problems in reliably reproducing EDTA titrations with little variation in the experimental points suggested the use of absorption spectra, rather than fluorescence spectra, due to the lower sensitivity of Zinquin-A absorption to small differences in adventitious Zn^{2+} concentration between solutions, due to the higher Zinquin-A concentrations used. Hence absorption spectra in the near ultraviolet region were determined for solutions with increasing Zinquin-A concentrations as described in Section 5.1.2.2. The 220 to 300 nm region was chosen for this titration as early absorption spectra showed absorbance due to adventitious Zn^{2+} in this region. Solutions containing EDTA in addition to Zinquin-A at the same concentrations were also measured so a comparison between spectra with and without adventitious Zn^{2+} could be made.

As described in detail below, the amount of adventitious Zn^{2+} common to all the solutions measured can be determined from the intercept of a plot of absorbance at the maximum wavelength for $[Zn(ZQA)_2]^{2-}$, 264 and 263 nm for 25% and 50% aqueous ethanol, respectively, versus Zinquin-A concentration. Comparing the line of best fit for the solutions with EDTA to the one for the solutions without EDTA gives an indication of the contribution of Zn^{2+} from the Zinquin-A solid alone.

At any wavelength, the total absorbance can be described as the sum of the absorbances of all the individual species. Thus the absorbance at any wavelength can be described as in Equation 2.5.

$$A = A(ZQA^{2-}) + A([ZQA.H]^{-}) + A(ZQA.H_2) + A([ZQA.H_3]^{+}) + A([Zn(ZQA)]) + A([Zn(ZQA)_2]^{2-})$$

$$= \varepsilon_{ZQA^{2-}}[ZQA^{2-}]l + \varepsilon_{[ZQA.H]^{-}}[ZQA.H^{-}]l + \varepsilon_{ZQA.H_2}[ZQA.H_2]l + \varepsilon_{[ZQA.H_3]^{+}}[ZQA.H_3^{+}]l + \varepsilon_{[Zn(ZQA)]}[Zn(ZQA)]l + \varepsilon_{[Zn(ZQA)_2]^{2-}}[Zn.(ZQA)_2^{2-}]l \quad (2.5)$$

where l is the cell path length (cm)

[X] is the concentration of species X (mol dm^{-3})

ε_X is the molar absorbance of species X (dm^3 mol^{-1} cm^{-1}), and

A is the absorbance.

l = 1 cm, so can be omitted from subsequent equations.

If all the adventitious Zn^{2+} present is found in only one complex, for example $[Zn(ZQA)_2]^{2-}$, the calculation is further simplified. Studies with MACSPECIES[23] showed that for solutions with greater than or equal to 7×10^{-5} or 1×10^{-5} mol dm^{-3} Zinquin-A in 25% and 50% aqueous ethanol, respectively, in excess of 90% of the adventitious Zn^{2+} was bound as $[Zn(ZQA)_2]^{2-}$ when the concentration of adventitious Zn^{2+} did not exceed 8×10^{-7} mol dm^{-3}. Hence under the experimental conditions used, it can be assumed that $[Zn(ZQA)_2{}^{2-}] \approx$ [Adv. Zn^{2+}] and that the concentration of $[Zn(ZQA)] \approx 0$. MACSPECIES also indicated that the majority of the remaining Zinquin-A would be monoprotonated as $[ZQA.H]^-$ under these conditions. This simplifies Equation 2.5 to Equation 2.6 below.

$$\begin{aligned} A &= \varepsilon_{[ZQA.H]^-}[ZQA.H^-] + \varepsilon_{[Zn(ZQA)_2]^{2-}}[Zn(ZQA)_2^{2-}] \\ &= \varepsilon_{[ZQA.H]^-}[ZQA.H^-] + \varepsilon_{[Zn(ZQA)_2]^{2-}}[\text{Adv. } Zn^{2+}] \end{aligned} \tag{2.6}$$

The concentration of adventitious Zn^{2+} can be described as a contribution from the Zinquin-A solid plus a contribution from the buffer, solvents, glassware and other sources which are independent of the concentration of Zinquin-A as shown in Equation 2.7 below.

$$[\text{Adv. } Zn^{2+}] = \mathbf{b} + \mathbf{a}[\text{Zinquin - A}]_{\text{Total}} \tag{2.7}$$

where **b** is the concentration of adventitious Zn^{2+} in the buffer (mol dm^{-3}), and
a is the percent of adventitious Zn^{2+} in the Zinquin-A solid.

Since each Zn^{2+} binds two ZQA^{2-} molecules, the concentration of free Zinquin-A can therefore be expressed as;

$$\begin{aligned} [ZQA.H^-] &= [\text{Zinquin - A}]_{\text{Total}} - 2[\text{Adv. } Zn^{2+}] \\ &= [\text{Zinquin - A}]_{\text{Total}} - 2(\mathbf{b} + \mathbf{a}[\text{Zinquin - A}]_{\text{Total}}) \end{aligned} \tag{2.8}$$

Substituting Equations 2.7 and 2.8 into Equation 2.6 gives;

$$\begin{aligned} A = {} & \varepsilon_{[ZQA.H]^-}([\text{Zinquin - A}]_{\text{Total}} - 2(\mathbf{b} + \mathbf{a}[\text{Zinquin - A}]_{\text{Total}})) \\ & + \varepsilon_{[Zn(ZQA)_2]^{2-}}(\mathbf{b} + \mathbf{a}[\text{Zinquin - A}]_{\text{Total}}) \end{aligned} \tag{2.9}$$

Expansion and collection of like terms;

$$A = \varepsilon_{[ZQA.H]^-}[\text{Zinquin - A}]_{\text{Total}} - 2\varepsilon_{[ZQA.H]^-}\mathbf{b} - 2\varepsilon_{[ZQA.H]^-}\mathbf{a}[\text{Zinquin - A}]_{\text{Total}} + \varepsilon_{[Zn(ZQA)_2]^{2-}}\mathbf{b} + \varepsilon_{[Zn(ZQA)_2]^{2-}}\mathbf{a}[\text{Zinquin - A}]_{\text{Total}} \quad (2.10)$$

$$= (\varepsilon_{[ZQA.H]^-} - 2\varepsilon_{[ZQA.H]^-}\mathbf{a} + \varepsilon_{[Zn(ZQA)_2]^{2-}}\mathbf{a})[\text{Zinquin - A}]_{\text{Total}} + \varepsilon_{[Zn(ZQA)_2]^{2-}}\mathbf{b} - 2\varepsilon_{[ZQA.H]^-}\mathbf{b}$$

Which is a straight line of the form y = mx + c, where m is the slope of the line, and c is the y-intercept. Hence the y-intercept obtained from extrapolating the plot of absorbance at a particular wavelength against Zinquin-A concentration gives the absorbance, $A_{(x\,=\,0)}$, at that wavelength due to Zinquin-A bound to adventitious Zn^{2+} from Zinquin-A independent sources, **b**. Wavelengths of 264 nm and 263 nm were used for 25% and 50% aqueous ethanol respectively as $[Zn(ZQA)_2]^{2-}$ has an absorption maximum at these wavelengths.

So at $[\text{Zinquin-A}]_{\text{Total}} = 0$ mol dm^{-3} (the y-intercept),

$$A_{(x=0)} = \varepsilon_{[Zn(ZQA)_2]^{2-}}\mathbf{b} - 2\varepsilon_{[ZQA.H]^-}\mathbf{b}$$
$$= \mathbf{b}(\varepsilon_{[Zn(ZQA)_2]^{2-}} - 2\varepsilon_{[ZQA.H]^-}) \quad (2.11)$$
$$\mathbf{b} = \frac{A_{(x=0)}}{\varepsilon_{[Zn(ZQA)_2]^{2-}} - 2\varepsilon_{[ZQA.H]^-}}$$

$\varepsilon_{[Zn(ZQA)_2]^{2-}}$ at 264 nm and 263 nm are known for 25% and 50% aqueous ethanol, respectively (see Sections 2.3.1 and 2.4.2) and $\varepsilon_{[ZQA.H]^-}$ can be obtained from the absorbances of the solutions with EDTA as described later in Equation 2.13. The values of $\varepsilon_{[ZQA.H]^-}$ obtained from this method are more accurate at this wavelength than those determined in Sections 2.3.1 and 2.4.2 as higher concentrations of Zinquin-A, and therefore higher absorbances, were used. Therefore, **b** can be calculated from the intercept, giving the concentration of adventitious Zn^{2+} arising from Zinquin-A independent sources.

Using this method, values for **b**, and therefore concentrations of adventitious Zn^{2+} from Zinquin-A independent sources, of 6.02×10^{-7} and 8.41×10^{-7} mol dm^{-3} were determined for 25% and 50% aqueous ethanol buffer, respectively. A value of 5.01×10^{3} for $\varepsilon_{[ZQA.H]^-}$, obtained from the slope of line b) in Figure 2.9, was used in the case of the 25% aqueous ethanol buffer and a similarly determined value of 5.20×10^{3} was used in the case of the 50% aqueous ethanol buffer. The plot of absorbance against Zinquin-A concentration obtained for 1.00×10^{-3} mol dm^{-3} NaPIPES, 0.1 mol dm^{-3} $NaClO_4$ adjusted to pH 6.6 in 25% aqueous ethanol is shown in Figure 2.9 (line a)) and a similar plot was obtained for 0.1 mol dm^{-3} NaPIPES adjusted to pH 6.6 in 50% aqueous ethanol.

The contribution to adventitious Zn^{2+} levels from the Zinquin-A solid, **a**, can be determined from the slope of the line described by Equation 2.10, which is plotted in Figure 2.9;

$$\begin{aligned} \text{Slope} &= \varepsilon_{[ZQA.H]^-} - 2\varepsilon_{[ZQA.H]^-}\mathbf{a} + \varepsilon_{[Zn(ZQA)_2]^{2-}}\mathbf{a} \\ &= \mathbf{a}(\varepsilon_{[Zn(ZQA)_2]^{2-}} - 2\varepsilon_{[ZQA.H]^-}) + \varepsilon_{[ZQA.H]^-} \\ \mathbf{a} &= \frac{\text{Slope} - \varepsilon_{[ZQA.H]^-}}{\varepsilon_{[Zn(ZQA)_2]^{2-}} - 2\varepsilon_{[ZQA.H]^-}} \end{aligned} \qquad (2.12)$$

If the line obtained from the solutions with no EDTA has a slope of $\varepsilon_{[ZQA.H]^-}$, it is evident from Equation 2.12 that the contribution to the adventitious Zn^{2+} concentration from the Zinquin-A solid, **a**, would be zero. Since adding EDTA removes Zn^{2+} from the Zinquin-A, and should therefore give a normal Beer's Law plot for $[ZQA.H]^-$ with a slope of $\varepsilon_{[ZQA.H]^-}$ (Equation 2.13), it is sufficient to compare the slopes of the experimental plots obtained with and without EDTA to estimate a value of **a** and therefore the contribution to adventitious Zn^{2+} from the Zinquin-A solid. If the lines appear parallel, then the slopes are approximately equal and therefore from Equation 2.12, $\mathbf{a} \approx 0$. This implies that the Zinquin-A solid used is free from Zn^{2+} contamination.

$$\begin{aligned} A &= \varepsilon_{[ZQA.H]^-}[ZQA.H^-] \\ &= \varepsilon_{[ZQA.H]^-}[\text{Zinquin - A}]_{\text{Total}} \end{aligned} \qquad (2.13)$$

If the experimental plots obtained are not parallel, and the solutions without EDTA form a line with a greater slope than those with, then from Equation 2.12, $\mathbf{a} > 0$ and there is an appreciable amount of Zn^{2+} contamination in the Zinquin-A solid. If this is the case, every time the concentration of Zinquin-A is increased, so too is the concentration of adventitious Zn^{2+} and therefore the absorbance due to $[Zn(ZQA)_2]^{2-}$. Figure 2.8 illustrates how the absorbance of free $[ZQA.H]^-$ can combine with absorbances due to Zn^{2+} in the buffer and the Zinquin-A solid to produce an experimental plot with a slope greater than predicted by Beer's Law for $[ZQA.H]^-$. Note that the absorbance due to Zn^{2+} from Zinquin-A independent sources is a constant amount whereas the other two sources are dependent upon the concentration of Zinquin-A and therefore increase with $[\text{Zinquin-A}]_{total}$.

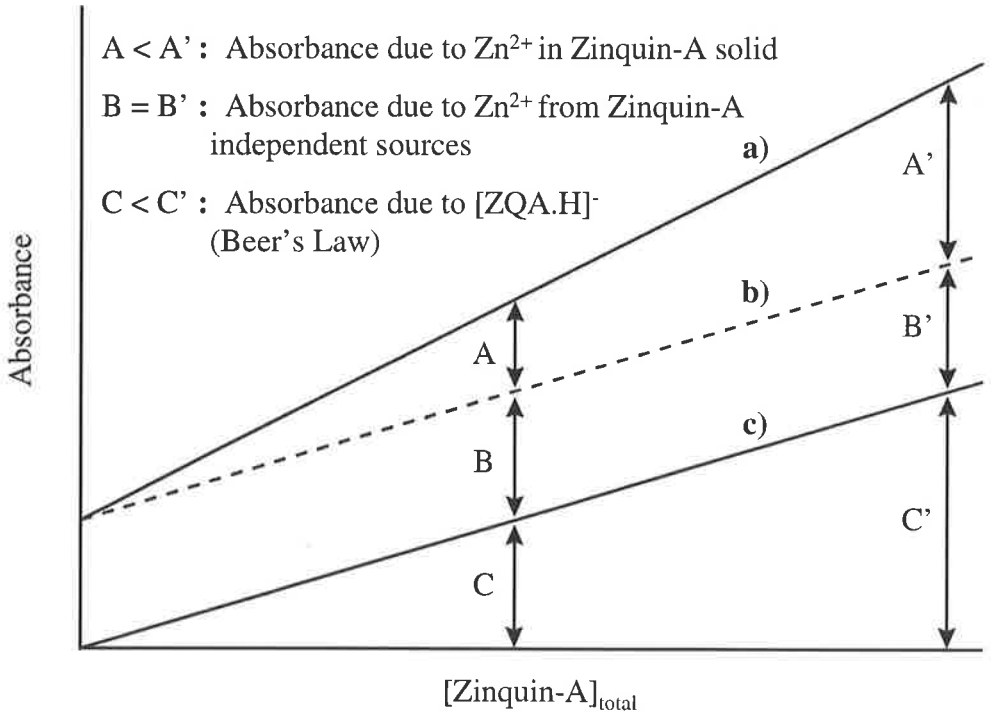

Figure 2.8 : Illustration of the various absorbances that can contribute to the observed experimental plot of absorbance against Zinquin-A concentration as discussed in the text. Line a) would be obtained when $\mathbf{a}, \mathbf{b} > 0$; b) when $\mathbf{a} = 0$, $\mathbf{b} > 0$; and c) when $\mathbf{a} = \mathbf{b} = 0$.

The absorbances obtained for each Zinquin-A concentration with EDTA have been included in Figure 2.9 below. Comparing the two plots, a) and b), it is evident that they are parallel within experimental error, indicating that for the 25% aqueous ethanol buffer, $\mathbf{a} \approx 0$ and hence there is negligible adventitious Zn^{2+} arising from the Zinquin-A solid. As could be expected, the corresponding plots for the 50% aqueous ethanol buffer were also parallel within experimental error, confirming that both batches of Zinquin-A were Zn^{2+} free.

As there is no adventitious Zn^{2+} in the Zinquin-A solid, the total adventitious Zn^{2+} concentration must be equivalent to the concentration from Zinquin-A independent sources, such as the buffer. Therefore the total adventitious Zn^{2+} is equal to **b**, that is, 6.02×10^{-7} and 8.41×10^{-7} mol dm^{-3} for 25% and 50% aqueous ethanol respectively. This is in relatively good agreement with the values obtained from the EDTA fluorescence titrations in Section 2.2.2.

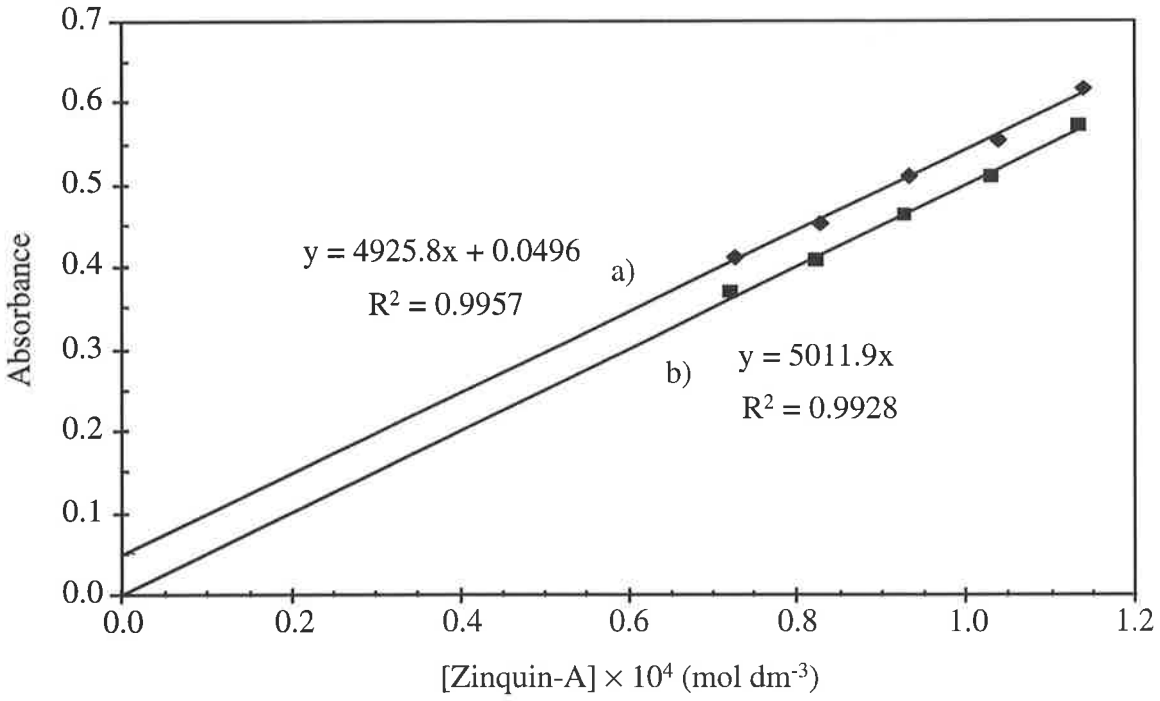

Figure 2.9 : Plots of absorbance at 364 nm against increasing Zinquin-A concentration used to calculate **a** and **b** and therefore the concentration of adventitious Zn^{2+} in 1.00×10^{-3} mol dm^{-3} NaPIPES, 0.1 mol dm^{-3} $NaClO_4$ adjusted to pH 6.6 in 25% aqueous ethanol. T = 298.2 K. a) line of best fit of the data with no EDTA (diamonds), b) line of best fit of the data with excess EDTA (squares).

2.2.4 : $[Zn(ZQA)_2]^{2-}$ Fluorescence Ratio Method

This method is an approximation, and is only valid for fluorescence spectra determined at high concentrations of Zinquin-A. Therefore the only set of data that it has been used for in this work is that for carbonic anhydrase (Section 4.6) and it is mentioned only briefly here. The $[Zn(ZQA)_2]^{2-}$ fluorescence ratio method assumes that at high Zinquin-A concentrations, all the adventitious Zn^{2+} is present as $[Zn(ZQA)_2]^{2-}$ in a similar way to the ultraviolet titration described in Section 2.2.3 above. If this is so, then because fluorescence is proportional to concentration, the approximate concentration of adventitious Zn^{2+} can be determined from a minimum of two fluorescence spectra by following the equations set out in Section 4.6. Using this method, a concentration of 9.11×10^{-7} mol dm^{-3} was obtained for the adventitious Zn^{2+} present in 0.1 mol dm^{-3} NaPIPES adjusted to pH 6.6 in 95% aqueous ethanol.

2.2.5 : A Comparison of Adventitious Zinc(II) Determination Methods

The four methods of determining adventitious Zn^{2+} concentrations used are listed below;

(a) Zinquin-A fluorescence titration fitting
(b) EDTA fluorescence titration
(c) Zinquin-A ultraviolet titration
(d) $[Zn(ZQA)_2]^{2-}$ fluorescence ratio

All produced reasonably consistent values for adventitious Zn^{2+} in the different buffer systems studied with the results obtained summarised in Table 2.2 below. Adventitious Zn^{2+} was not determined for the borate buffer used to study some of the ternary complexes at pH 10 (Sections 4.3 and 4.4) because the concentrations of added Zn^{2+} in these solutions were sufficiently high to ignore the very small change in concentration caused by adventitious Zn^{2+} and those with no added Zn^{2+} contained EDTA which preferentially complexes the adventitious Zn^{2+}, rendering it inaccessible by Zinquin-A.

	[Adventitious Zn^{2+}] in various Buffer Systems (mol dm^{-3})		
Method	1×10^{-3} mol dm^{-3} NaPIPES, 0.1 mol dm^{-3} $NaClO_4$, 25% aqueous ethanol, pH 6.6	0.1 mol dm^{-3} NaPIPES, 50% aqueous ethanol, pH 6.6	0.1 mol dm^{-3} NaPIPES, 95% aqueous ethanol, pH 6.6
(a)		1.03×10^{-6}	
(b)	4.95×10^{-7}	7.89×10^{-7}	
(c)	6.02×10^{-7}	8.41×10^{-7}	
(d)			9.11×10^{-7}

Table 2.2 : Values for the concentration of adventitious Zn^{2+} determined in various buffer systems by the methods; (a) Zinquin-A fluorescence titration fitting, (b) EDTA fluorescence titration, (c) Zinquin-A ultraviolet titration, (d) $[Zn(ZQA)_2]^{2-}$ fluorescence ratio.

As can be seen from the table above, the value of adventitious Zn^{2+} calculated varies with a change in buffer system and the method used. The lowest concentrations of adventitious Zn^{2+} were found in the 25% aqueous ethanol buffer system. This is most likely due to the lower concentration of NaPIPES buffer, which is now thought to be a significant contributor of adventitious Zn^{2+}. Another piece of evidence indicating this is the low fluorescence observed for Zinquin-A with no added Zn^{2+} in Figure 2.3 where a different buffer, HEPES in HBSS, was used. This fluorescence is only 1.2% of that observed for Zinquin-A with Zn^{2+} as compared with the spectrum with no added Zn^{2+} in Figure 2.4 which uses NaPIPES buffer and is 24% of the Zinquin-A spectrum with the maximum concentration of added Zn^{2+}.

The variation between methods is primarily due to the different approximations required by each method. The fluorescence titration method, (a), is perhaps one of the most accurate as it uses the most data, however, it also uses the assumption that ground state stability constants, such as those derived from potentiometric titrations, are equivalent to those that would be observed from fluorescence, as discussed in Section 2.2.1, and this may not be totally valid in this case. Another reason for the higher value observed in this case is the fact that buffer from a different batch number was used for this early experiment than the others. As the property of buffers often varies with batch number, it is quite possible that the solutions used had more adventitious Zn^{2+} in them than the later solutions.

The EDTA titration method, (b), has accuracy problems due to its high sensitivity to variations in adventitious Zn^{2+} between solutions which causes uncertainty in the x-intercept used to obtain the concentration of adventitious Zn^{2+}. This method can be improved by using more EDTA concentrations in the titration, however development of a method that is less sensitive to small changes in adventitious Zn^{2+} was chosen over this option.

The least accurate method used to determine adventitious Zn^{2+} concentration was the $[Zn(ZQA)_2]^{2-}$ fluorescence ratio method, (d). As mentioned in Sections 2.2.4 and 4.5, this is an approximate method only and assumes that all the Zn^{2+} present in both solutions used is complexed as $[Zn(ZQA)_2]^{2-}$. As stability constants are not known for this solvent system, the percentage of Zn^{2+} in this form can not be checked and therefore the validity of the method is unknown. This method could prove useful for systems where stability constants are known if the accuracy was increased by using more solutions and determining the concentration of adventitious Zn^{2+} graphically. However, it is likely that this method would experience problems due to the sensitivity of fluorescence to small changes in Zn^{2+} concentration in a similar way to the EDTA titrations. Bearing in mind the poor accuracy of this method, the result obtained in Table 2.2 is in relatively good agreement to the value obtained for the same concentration of buffer in 50% aqueous ethanol, as could be expected if NaPIPES is a major contributor of adventitious Zn^{2+}.

The most accurate method used for the determination of adventitious Zn^{2+} was the ultraviolet titration method, (c). There were several reasons for this. As the ultraviolet absorbance of Zinquin-A is less sensitive to a small change in adventitious Zn^{2+} concentration, less variation in the experimental points was observed than for the EDTA titrations, and an average value of adventitious Zn^{2+} could be determined with greater certainty. As stability constants are known in both solvent systems used, the assumption that all the Zn^{2+} present was bound as $[Zn(ZQA)_2]^{2-}$ could be validated using MACSPECIES[23], minimising errors due to invalid assumptions. This method also has the advantage over the fluorescence titration fitting method, (a), of requiring fewer experimental points to arrive at a satisfactory value for adventitious Zn^{2+}. The problem of the possible difference between stability constants observed in the ground and excited states is also not an issue in this method, as both potentiometric titrations and ultraviolet-visible spectra represent the ground state equilibrium. Another advantage of this method is its ability to identify Zn^{2+} contamination in the Zinquin-A solid,

which was not possible with methods (a) and (b). This method also showed reasonably good reproducibility, with similar values obtained for solutions made from different bulk buffer solutions with the same buffer batch number. Hence the concentrations of adventitious Zn^{2+} calculated by this method were chosen as the most accurate, and were used where appropriate.

It was observed in the EDTA titrations that individual solutions showed a small variation in adventitious Zn^{2+} concentration (Section 2.2.2). This was also highlighted when it was attempted to obtain a fluorescence titration, similar to that shown in Figure 2.4, with no contribution from adventitious Zn^{2+}. To achieve this, a concentration of EDTA equivalent to the calculated concentration of adventitious Zn^{2+} was added to all solutions in an attempt to selectively remove the adventitious Zn^{2+} alone and none of the added Zn^{2+}. Unfortunately, although an approximately correct shape for the titration was obtained, there was unacceptable scatter in the experimental points which can be attributed to the slight variation in adventitious Zn^{2+} concentration, from the calculated average, in each solution measured. For this reason, it was decided that the best method of dealing with the presence of adventitious Zn^{2+} was not to remove it, but to add its calculated concentration to that of the known added Zn^{2+} concentration for each solution and to add excess EDTA to all solutions in which no Zn^{2+} was to be present. It was also decided from these results that it was appropriate to quote, and use, the average concentration of adventitious Zn^{2+} calculated by the ultraviolet titration method to only one significant figure. Therefore the corrections to all added Zn^{2+} concentrations used in the 25% and 50% aqueous ethanol buffer systems were 6×10^{-7} and 8×10^{-7} mol dm^{-3}, respectively. With such a small concentration of adventitious Zn^{2+}, it is no surprise that the fluorescence spectra, which have the lowest added Zn^{2+} concentrations, were the only spectra significantly effected by its presence. Due to the large concentrations used in the potentiometric titrations and the spectra determined at pH 10, there was no need to include any correction for adventitious Zn^{2+} in these cases.

2.3 : Spectroscopy of Zinquin-A in 50% Aqueous Ethanol

The ultraviolet-visible and fluorescence spectra previously determined[24] for monoprotonated Zinquin-A and the Zn^{2+} complexes of Zinquin-A did not take the adventitious Zn^{2+} concentration present into account. In addition to this, the absorbance values obtained in the near ultraviolet region were much greater than the recommended maximum of 0.8 units. Hence these spectra have been reobtained, removing adventitious Zn^{2+} with EDTA where free Zinquin-A is of interest and adjusting the Zn^{2+} concentration by 8×10^{-7} mol dm^{-3} Zn^{2+} where Zn^{2+} is added. The concentrations used in the ultraviolet-visible region were diluted to give a reasonable absorbance in the 220 to 300 nm region and molar absorbances were calculated for each species using the MATLAB program AB12[25] which calculates the concentrations of all species present in two or more spectra and then calculates their molar absorbance. The same buffer system used in the previous study, 0.1 mol dm^{-3} NaPIPES adjusted to pH 6.6 in 50% aqueous ethanol, was used in this study. The ultraviolet-visible spectra for [Zn(ZQA)], $[Zn(ZQA)_2]^{2-}$ and $[ZQA.H]^-$ determined in this buffer system at 298.2 K, as described in Section 5.1.4, are shown in Figure 2.10 and the observed absorption maxima are included in Table 2.3.

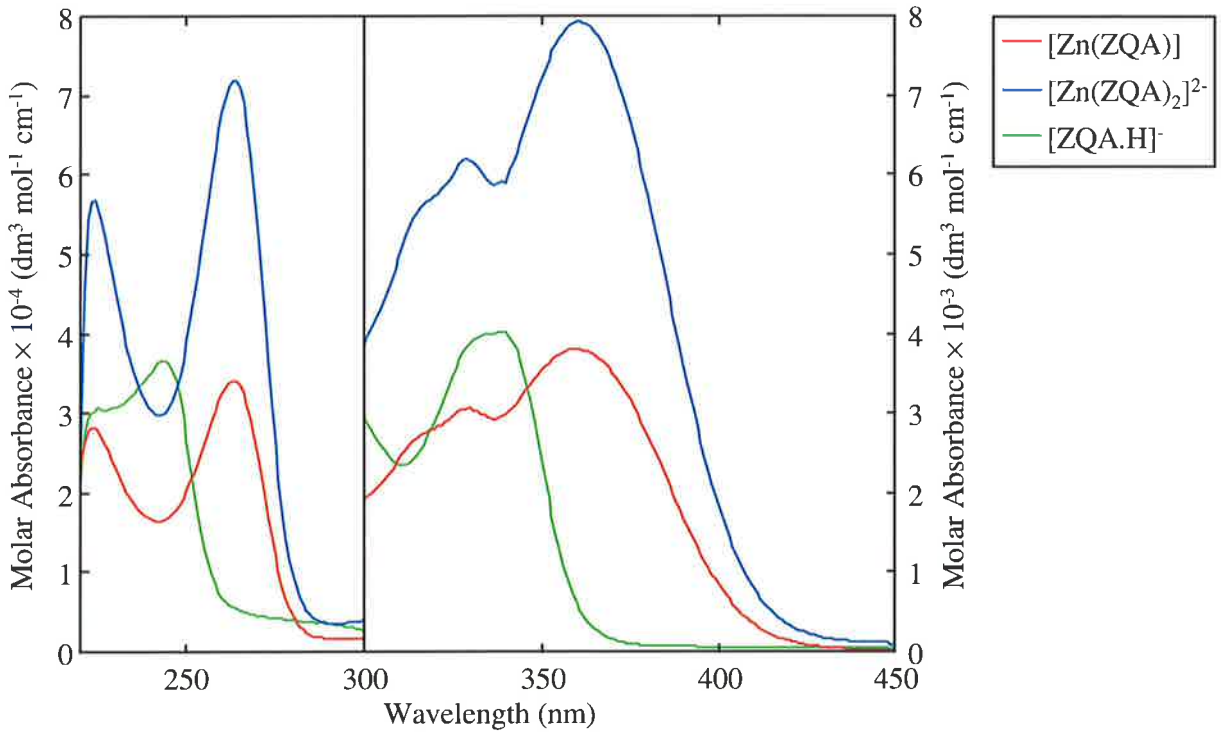

Figure 2.10 : The ultraviolet-visible spectra of [Zn(ZQA)], $[Zn(ZQA)_2]^{2-}$ and $[ZQA.H]^-$ measured in 50% aqueous ethanol, pH 6.6 and I = 0.1 (0.1 mol dm^{-3} NaPIPES), T = 298.2 K. Concentrations used are described in Section 5.1.4.

Species	Maximum Wavelength (nm) (Molar Absorbance ($dm^3\ mol^{-1}\ cm^{-1}$))				
$[ZQA.H]^-$	225 (3.06×10^4)	243 (3.66×10^4)	336 (3.99×10^3)		
[Zn(ZQA)]	224 (2.82×10^4)	263 (3.40×10^4)	[315] [2.68×10^3]	330 (3.07×10^3)	361 (3.81×10^3)
$[Zn(ZQA)_2]^{2-}$	224 (5.67×10^4)	263 (7.18×10^4)	[315] [5.52×10^3]	329 (6.19×10^3)	361 (7.92×10^3)

Table 2.3 : Maxima observed for the ultraviolet-visible spectra of some Zinquin-A species in 50% aqueous ethanol, pH 6.6 and I = 0.1 (0.1 mol dm^{-3} NaPIPES), shown in Figure 2.10. Values enclosed in square brackets describe the approximate position of shoulders rather than maxima.

These spectra compared fairly well to those obtained previously[24] with major differences in the wavelengths and molar absorbance values only observed at the lower wavelengths, where the previous spectra were less accurate. Ligand to metal charge transfer (LMCT) transitions are not possible in the Zn^{2+} complexes of Zinquin-A, as Zn^{2+} has filled *d* orbitals and therefore is unable to accept an electron from Zinquin-A. Similarly, no *d-d* transitions are observed for Zn^{2+} complexes. Therefore the ultraviolet-visible spectra obtained must result solely from Zinquin-A. Generally, ultraviolet-visible spectra arising from organic compounds are associated with transitions of electrons from a bonding (π) or lone pair (n) orbital to an unfilled antibonding (π^*) orbital. For conjugated molecules, the first type of transitions results in very intense ($\varepsilon \geq 1 \times 10^4$) spectral peaks in the near ultraviolet region whereas the second results in weaker (ε = 100 - 1×10^4) peaks at longer wavelengths in the ultraviolet-visible region. Hence it is likely that the peaks below 300 nm in Figure 2.10 are due to π to π^* transitions and those in the 300 to 450 nm region are due to the weaker n to π^* transitions.

The more conjugation present in organic molecules, the further the absorption peaks are shifted towards longer wavelengths. Hence it can be seen from Figure 2.10 and Table 2.3 that chelation of Zn^{2+} by Zinquin-A causes an increase in delocalisation of electrons in the molecule. This could be expected due to the increase in rigidity of the Zinquin-A anion that occurs upon chelation due to the restriction of both vibration in the quinoline ring and rotation about the sulphonamide nitrogen to quinoline bond. This would enhance the π orbital overlaps and therefore the delocalisation of electrons by keeping the conjugated portions of the molecule planar.

It can be seen from Figure 2.10 and Table 2.3 that the spectrum for $[Zn(ZQA)_2]^{2-}$ is almost exactly twice that observed for [Zn(ZQA)]. This is due to the presence of two chromophores in $[Zn(ZQA)_2]^{2-}$ which allows it to absorb twice as many photons than [Zn(ZQA)]. It can also be seen that although the spectrum for Zinquin-A changes significantly upon the complexation of Zn^{2+}, little change in the spectrum is observed upon adding a second Zinquin-A to this complex, indicating that the two bound Zinquin-A anions do not interact with each other in such a way as to modify their absorption spectra.

The spectra of Zinquin-A in various protonation states, ZQA^{2-}, $ZQA.H_2$ and $[ZQA.H_3]^+$, have been determined for completeness in case such species contributed to the ternary spectra studied in Chapter 4. NaPIPES buffer could not be used to obtain all of the pHs required for high percentage formation of these species, so the supporting electrolytes, and pHs, shown in Table 5.1 were used. The spectra obtained, as described in Section 5.1.4, are shown in Figure 2.11 below and the observed absorption maxima are included in Table 2.4. The spectrum and absorption maxima for $[ZQA.H]^-$ are included for comparison.

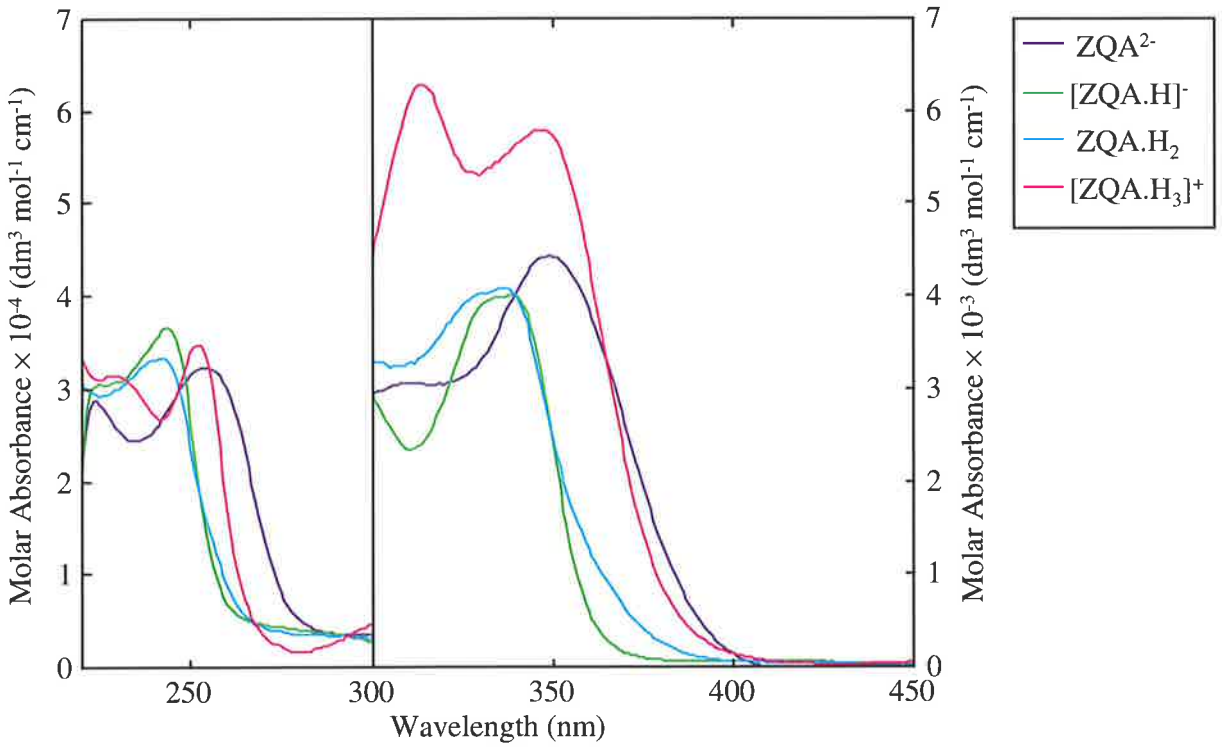

Figure 2.11 : The ultraviolet-visible spectra of ZQA^{2-}, $ZQA.H_2$ and $[ZQA.H_3]^+$ measured in 50% aqueous ethanol, with pHs and supporting electrolytes as listed in Table 5.1, T = 298.2 K. Concentrations used are described in Table 5.3. The spectrum for $[ZQA.H]^-$ previously presented (Figure 2.10) is also included for comparison.

Species	Maximum Wavelength (nm) (Molar Absorbance ($dm^3\ mol^{-1}\ cm^{-1}$))			
ZQA^{2-}	223 (2.88×10^4)	254 (3.22×10^4)	310 (3.06×10^3)	349 (4.43×10^3)
$[ZQA.H]^-$	225 (3.06×10^4)	243 (3.66×10^4)	336 (3.99×10^3)	
$ZQA.H_2$	242 (3.33×10^4)	[328] [3.98×10^3]	336 (4.12×10^3)	
$[ZQA.H_3]^+$	230 (3.15×10^4)	252 (3.48×10^4)	314 (6.28×10^3)	347 (5.80×10^3)

Table 2.4 : Maxima observed for the ultraviolet-visible spectra of the free Zinquin-A species in 50% aqueous ethanol, shown in Figure 2.11, with pHs and supporting electrolytes as listed in Table 5.1. Values enclosed in square brackets describe the approximate position of shoulders rather than maxima.

From Figure 2.11, it is evident that protonation of Zinquin-A has a different effect on the ultraviolet-visible absorption spectrum than complexation by Zn^{2+} as could be expected due to the greater changes induced in a molecule when it is chelated as opposed to protonated. The spectrum obtained for $ZQA.H_2$, which has both the sulphonamide and carboxylic acid protons present, is quite similar to that obtained for $[ZQA.H]^-$, which has only the sulphonamide proton present. As the main chromophore in Zinquin-A is the quinoline ring, the addition of a proton to the carboxylic acid moiety, which is somewhat removed from the ring, would have little effect on the spectrum observed. The shift to longer wavelengths upon deprotonation of $[ZQA.H]^-$ to ZQA^{2-} is due to the greater conjugation that occurs when the sulphonamide nitrogen is deprotonated due to the delocalisation of the resulting negative charge throughout the quinoline ring. As could be expected, the spectrum of ZQA^{2-} is the most similar to [Zn(ZQA)] of all the free Zinquin-A species, with the chelation of Zn^{2+} by ZQA^{2-} causing a further shift to longer wavelengths due to an increase in electron delocalisation through an increase in rigidity, as discussed previously. The spectrum of $[ZQA.H_3]^+$ is unlike any of the other spectra shown, possibly due to the fact that the quinoline nitrogen, which is an integral part of the main chromophore, is protonated and therefore positively charged. This would effect the electron density in the ring and therefore the electronic transitions observed. The unexpected shift of this spectrum to longer wavelengths is possibly due to the attraction of the ether oxygen and sulphonamide nitrogen lone pairs to the positively charged quinoline nitrogen, which may result in a slight increase in electron delocalisation within the molecule.

Understanding of these ultraviolet-visible spectra is essential when selecting an excitation wavelength to measure the fluorescence spectra of these species. Absorption is the essential precursor to fluorescence (refer to Appendix A for an overview) and therefore little fluorescence will be observed if excitation occurs at a wavelength where the species present have low molar absorbances. Two main options exist when selecting an excitation wavelength; either the wavelength at which the species of interest has a maximum molar absorbance, or a wavelength where all species present have the same molar absorbance (an isobestic point) can be used. The latter case was used in the previous study[24] and this has the advantage that any difference in fluorescence observed for the species that share the isobestic point is not due to different amounts of photons being absorbed.

For this study, however, an excitation wavelength of 358 nm, which is near to the absorption maximum at 361 nm, was chosen as it produced the maximum fluorescence intensity in an excitation spectrum (an excitation spectrum is obtained by varying the excitation wavelength while measuring the intensity of fluorescence obtained at a single wavelength). In this case it was not necessary to use the isobestic point of $[ZQA.H]^-$ and [Zn(ZQA)] at 346 nm as the excitation wavelength because $[ZQA.H]^-$ was found to be non-fluorescent at all excitation wavelengths between 200 and 450 nm, including its maximum at 336 nm. So the large difference in fluorescence observed between free and Zn^{2+} bound Zinquin-A (Figure 2.4) is not simply due to $[ZQA.H]^-$ absorbing less at the excitation wavelength than [Zn(ZQA)] and $[Zn(ZQA)_2]^{2-}$. The other free Zinquin-A species, ZQA^{2-}, $ZQA.H_2$ and $[ZQA.H_3]^+$, were similarly non-fluorescent when excited at 358 nm and 336 nm.

The large increase in fluorescence upon Zn^{2+} coordination is due to the extra rigidity induced in the Zinquin-A anion upon chelation of Zn^{2+}. This occurs in two different ways. The first is the cessation of rotation about the bond connecting the sulphonamide nitrogen to the quinoline ring. Once coordinated to Zn^{2+}, this bond is no longer able to rotate, allowing the lone pair of electrons, or the negative charge, on the nitrogen to delocalise into the ring more freely. This in turn increases the rigidity of that portion of the molecule. In a similar way, extra rigidity is induced in the quinoline moiety of Zinquin-A through the chelation of Zn^{2+} as the ring structure is held in a near planar arrangement, and vibration is limited. Structural rigidity has been found to be the cause of an increase in fluorescence in several other chelating molecules upon the complexation of a metal ion.[26] It is thought that the more rigid a molecule, the fewer radiationless decay processes, such as internal conversion and vibrational relaxation are available to it, leading to less quenching and therefore a more intense fluorescence spectrum.

The molar fluorescences of [Zn(ZQA)] and $[Zn(ZQA)_2]^{2-}$ were calculated from the fluorescence spectra shown in Figure 2.4 by using the MATLAB program, AB12[25] in conjunction with the Zn^{2+} stability constants shown in Table 2.1. As can be seen from Figure 2.12, the molar fluorescence spectra of [Zn(ZQA)] and $[Zn(ZQA)_2]^{2-}$ were found to have a maximum at 484 nm (9.86×10^7 dm^3 mol^{-1}) and 486 nm (6.67×10^7 dm^3 mol^{-1}), respectively, where the molar fluorescence values (per Zinquin-A anion) are given in brackets. The spectra in Figure 2.4 were also used to obtain Zn^{2+} stability constants for Zinquin-A. This was achieved by using the MATLAB program, SPECFIT[21], as described in Section 2.2.1, with all added Zn^{2+} concentrations adjusted for an adventitious Zn^{2+} value of 1.03×10^{-6} mol dm^{-3}. The stability constants obtained were log K_1 = 9.34 ± 0.01 and log K_2 = 9.95 ± 0.01, which compare well with those obtained by potentiometric titrations (Table 2.1). As the spectra of [Zn(ZQA)] and $[Zn(ZQA)_2]^{2-}$ are almost identical in shape, this method is less accurate than the potentiometric titration technique.[27]

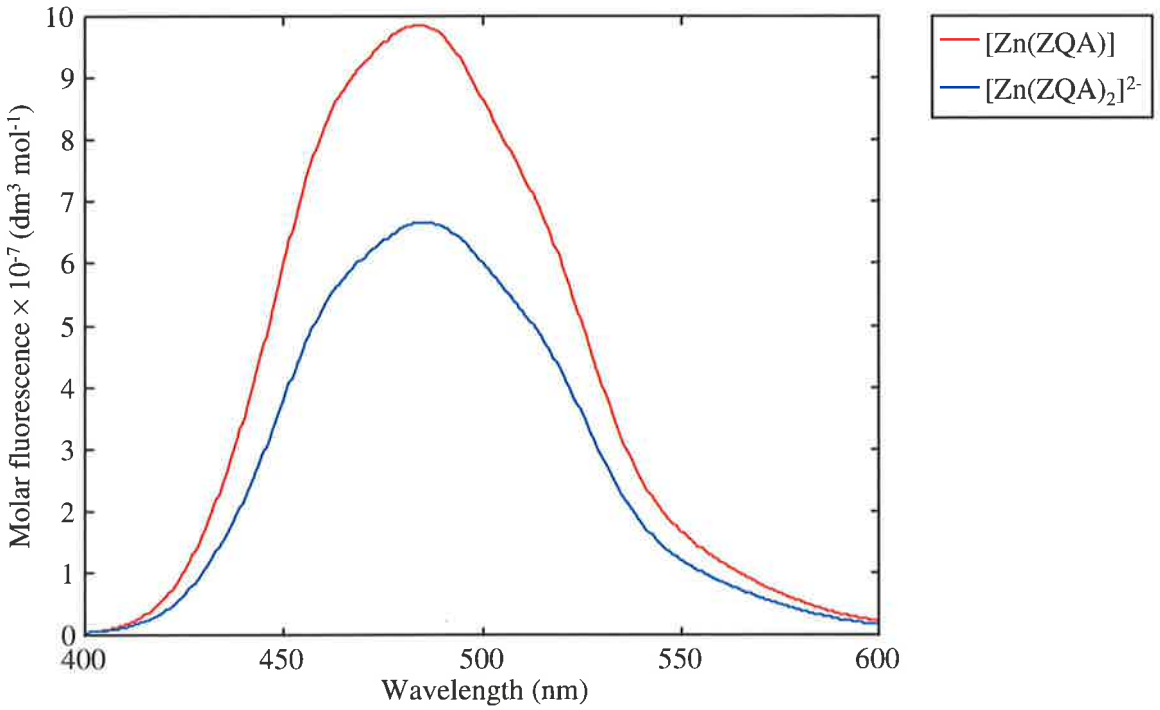

Figure 2.12 : Molar fluorescence spectra for [Zn(ZQA)] and $[Zn(ZQA)_2]^{2-}$ (per Zinquin-A anion) in 0.1 mol dm^{-3} NaPIPES, pH 6.6 and 50% aqueous ethanol, determined from log K_1 = 9.65, log K_2 = 9.46 and the spectra shown in Figure 2.4. The $[Zn(ZQA)_2]^{2-}$ spectrum is shown per Zinquin-A anion, to obtain the spectrum per complex, the spectrum shown must be multiplied by 2. T = 298.2 K, slits = 2.5 nm, Ex λ = 358 nm.

The molar fluorescence of [Zn(ZQA)] and $[Zn(ZQA)_2]^{2-}$ were redetermined using the same spectrophotometer used for all other fluorescence measurements in this work to allow direct comparisons (all fluorescence measurements are relative and depend upon the concentrations, slit widths and the instrument used, hence spectra determined on different instruments are not directly comparable). This was achieved, as described in Section 5.1.5, by measuring the relative fluorescence of six solutions with concentration ratios of $Zn(ClO_4)_2$ to Zinquin-A from 0.3:1 up to 40:1 (Figure 2.13). The concentrations used are listed in Table 5.6 and were chosen to give a good variation in the concentrations of [Zn(ZQA)] and $[Zn(ZQA)_2]^{2-}$ present in each solution. The MATLAB program, AB12[25] was used in conjunction with the Zn^{2+} stability constants in Table 2.1 to determine the molar fluorescence spectra shown in Figure 2.14 below. The molar fluorescence spectra of [Zn(ZQA)] and $[Zn(ZQA)_2]^{2-}$ have a maximum at 485 nm (5.16×10^7 dm^3 mol^{-1}) and 484 nm (3.36×10^7 dm^3 mol^{-1}), respectively, where the molar fluorescence values (per Zinquin-A anion) are given in brackets. It can be seen from Figures 2.12 and 2.14 that the ratio of the [Zn(ZQA)] spectrum to the $[Zn(ZQA)_2]^{2-}$ spectrum is essentially independent of the spectrophotometer used as expected, however, the intensities differ by a factor of approximately 2. This is most probably due to the combination of the larger slit widths used to determine the spectra in Figure 2.4 and the more sensitive photomultiplier on the spectrophotometer used to determine the spectra in Figure 2.13.

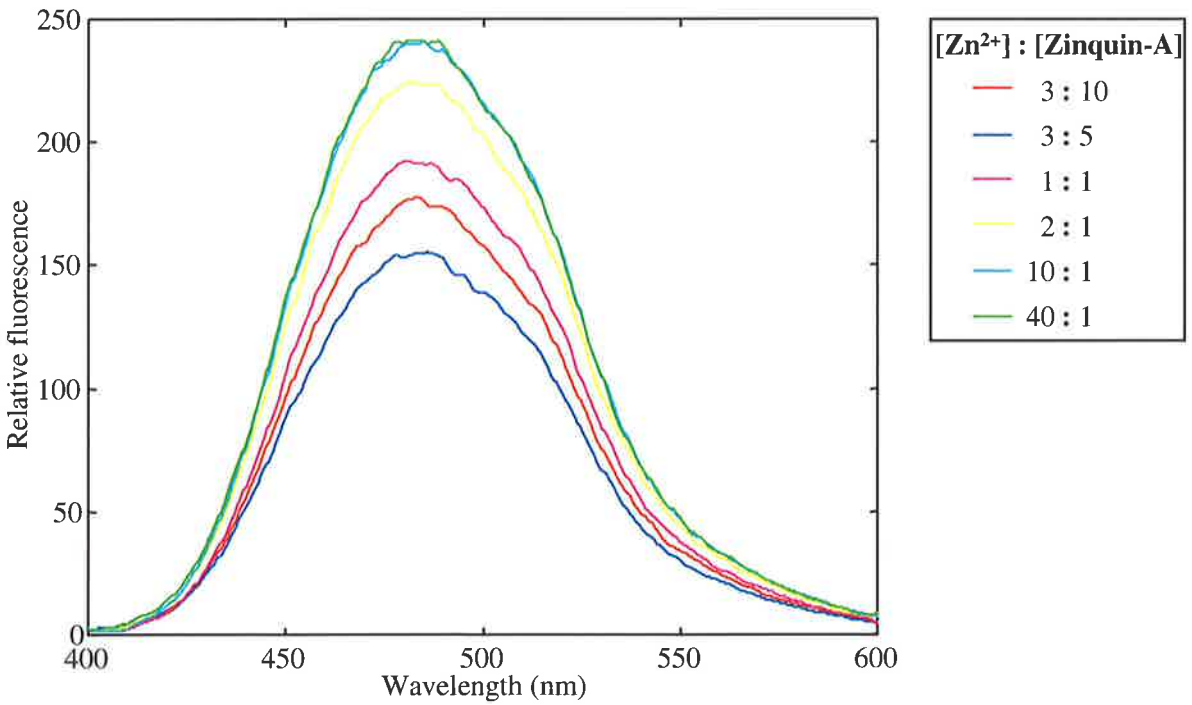

Figure 2.13 : Relative fluorescence determined for solutions with varying Zn^{2+} and Zinquin-A concentrations in 0.1 mol dm^{-3} NaPIPES, pH 6.6 and 50% aqueous ethanol, as described in Table 5.6. T = 298.2 K, slits = 2.5 nm, Ex λ = 358 nm.

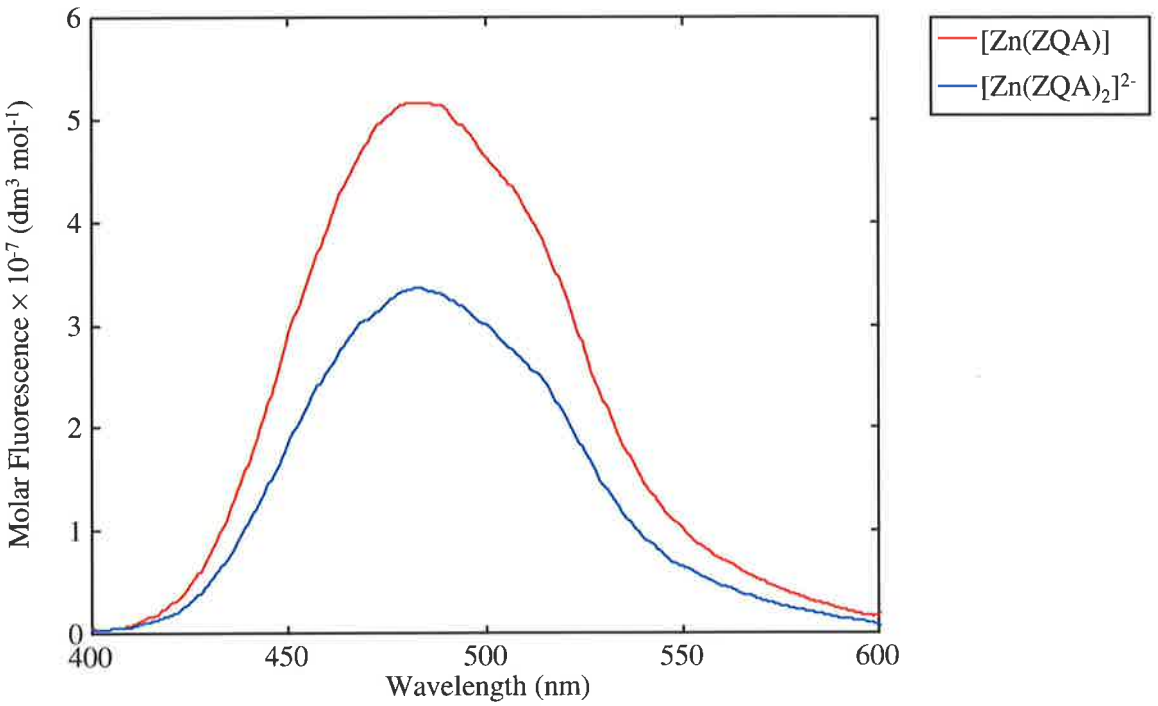

Figure 2.14 : The molar fluorescence spectra of [Zn(ZQA)] and $[Zn(ZQA)_2]^{2-}$ (per Zinquin-A anion) in 0.1 mol dm^{-3} NaPIPES, pH 6.6 and 50% aqueous ethanol, determined from log K_1 = 9.65, log K_2 = 9.46 and the spectra shown in Figure 2.13. The $[Zn(ZQA)_2]^{2-}$ spectrum is shown per Zinquin-A anion, to obtain the spectrum per complex, the spectrum shown must be multiplied by 2. T = 298.2 K, slits = 2.5 nm, Ex λ = 358 nm.

As can be seen in both Figures 2.12 and 2.14, $[Zn(ZQA)_2]^{2-}$ has a lower molar fluorescence intensity per Zinquin-A anion than that observed for [Zn(ZQA)]. This indicates that the addition of a second Zinquin-A anion to [Zn(ZQA)] causes greater quenching to occur for both the Zinquin-A anions in the resulting complex, $[Zn(ZQA)_2]^{2-}$. This could be expected due to the extra strain induced in $[Zn(ZQA)_2]^{2-}$ by the close proximity of the two Zinquin-A anions, which in turn induces greater vibration and therefore greater non-radiative relaxation or quenching. If the molar fluorescence per complex of [Zn(ZQA)] and $[Zn(ZQA)_2]^{2-}$ were compared, however, $[Zn(ZQA)_2]^{2-}$ would be more fluorescent than [Zn(ZQA)].

2.4 : The Effect of Structure on the Fluorescence of Sulphonamidoquinolines

Several ligands with similar moieties to Zinquin-A have been studied to examine the effect of structural differences on fluorescence and therefore gain a better understanding of the structural factors responsible for the formation of stable, highly fluorescent Zn^{2+} complexes. The structure of 8-(*p*-toluenesulphonamido)quinoline (*p*-TSQ.H) was chosen as the basic ligand structure for the potential fluorophores studied as this structure is equivalent to Zinquin-A with the quinoline substituents removed. Figure 2.15 shows the set of substituted quinolines used for comparison, which exhibit a number of variations on the basic ligand structure. Among other structural variations, this set includes ligands with an amide group in place of the sulphonamide group and a reversed sulphonamide group to ascertain any dependence of fluorescence on the presence or orientation of the sulphonamide group. The effect of changing the substituent bound to the sulphonamide sulphur and the effect of substitution of the quinoline ring should also be apparent from within this set of ligands. An abbreviation of 'L.H', where L^- is the deprotonated ligand, has been used here, as upon binding to Zn^{2+}, these ligands loose their sulphonamide proton and using this nomenclature allows the resulting complex to be represented by $[Zn(L)]^+$. The ligands were compared using potentiometric titrations, ultraviolet-visible spectroscopy and fluorescence spectroscopy as discussed below in Sections 2.4.1, 2.4.2 and 2.4.3, respectively.

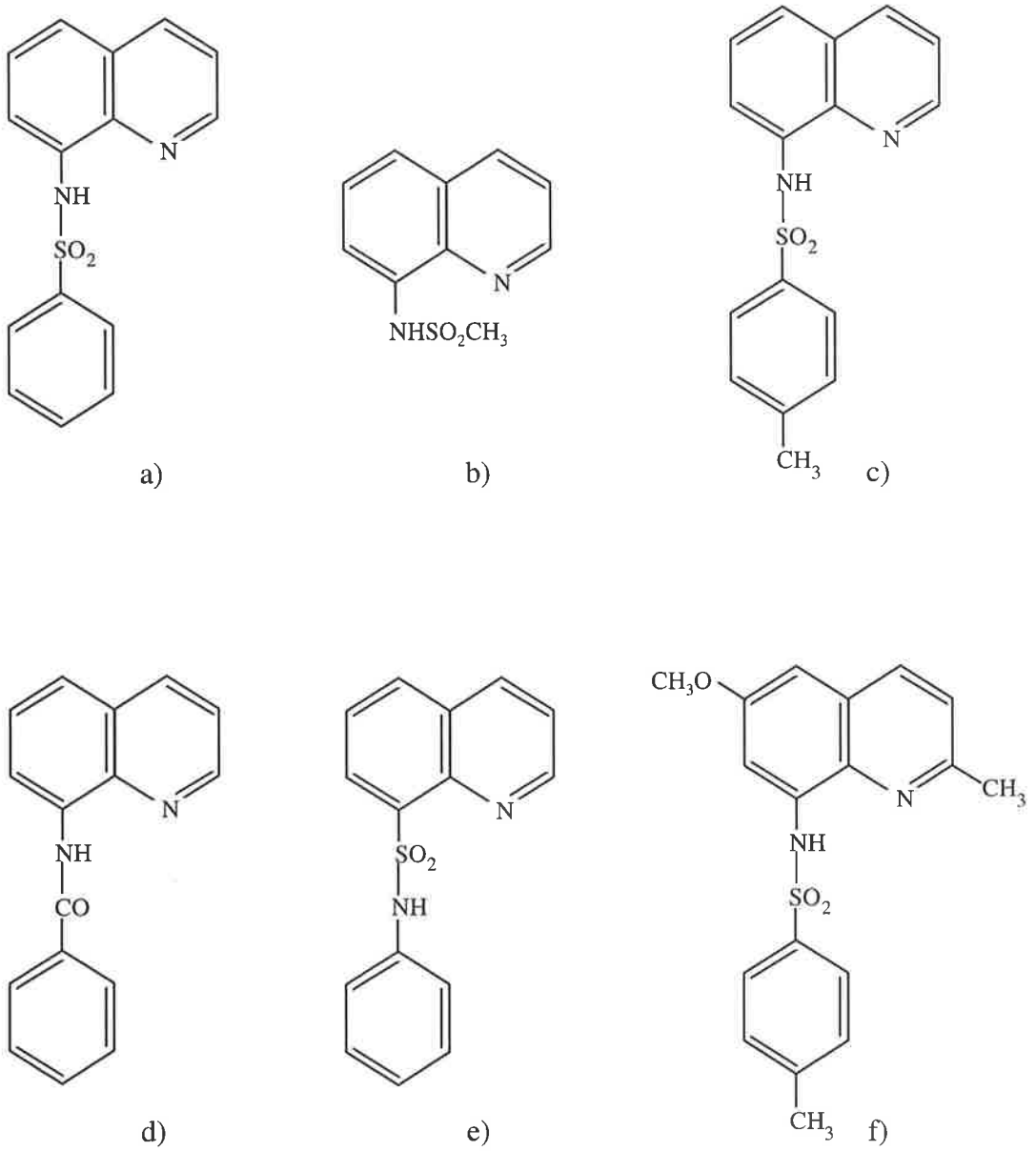

Figure 2.15 : The ligands studied to gain insight into the structure necessary for a strongly fluorescence Zn^{2+} fluorophore.

a) 8-(benzesulphonamido)quinoline (**BSQ.H**)

b) 8-(methanesulphonamido)quinoline (**MSQ.H**)

c) 8-(*p*-toluenesulphonamido)quinoline (***p*-TSQ.H**)

d) 8-(benzenecarbonamido)quinoline (**BCQ.H**)

e) 8-(quinolinesulphonamido)benzene (**QSB.H**)

f) 6-methoxy-2-methyl-8-(*p*-toluenesulphonamido)-quinoline (**MM-TSQ.H**)

2.4.1 : Potentiometric Titrations of Zinquin-A and Other Ligands in 25% Aqueous Ethanol

The pK_as and Zn^{2+} stability constants for the ligands in Figure 2.15 have been determined in 25% aqueous ethanol previously and are shown in Table 2.5.[28] This solvent system was chosen as it was the maximum percentage of water that allowed complete solubility of the ligands studied with the exception of *p*-TSQ for which 1% DMSO was added to the solvent system. To allow comparison of Zinquin-A with these ligands, its pK_as and Zn^{2+} stability constants were redetermined in 25% aqueous ethanol, I = 0.1 $dm^3\ mol^{-1}$ ($NaClO_4$) at 298.2 K, as described in Section 5.1.3. It was necessary to split the pK_a titrations into two fitting regions as Zinquin-A is associated with pK_as that differ greatly in value and a reasonable fit could not be obtained without removing the points in the middle of the curve. The omission of these data points is valid as in these areas the concentration ratios of the conjugate acid-base pairs, which are involved in the fitting of the pK_as, are very large or very small. This results in unacceptably large errors in these ratios. An example of a fitted Zinquin-A titration curve is shown in Figure 2.16. Where possible, the fitting regions were chosen to contain data points with pH values within the pK_a ± 1 pH unit, to ensure that between 10% and 90% of the ligand was present as the protonated species of interest, resulting in a balance between a sufficient number of data points and having the concentration ratios of the conjugate acid-base pairs in a reasonable range. For the same reason as discussed above, fitting regions where 10% to 90% of Zinquin-A was bound to Zn^{2+} were used for the determination of the stability constants.

The pK_as and stability constants determined in 25% aqueous ethanol were similar to those determined in 50% aqueous ethanol, with Zn^{2+} stability constants of log β_1 = 10.51 ± 0.08 and log β_2 = 19.31 ± 0.07 and the three acid dissociation constants observed, pK_{a1} = 10.13 ± 0.05, pK_{a2} =4.40 ± 0.02 and pK_{a3} = 3.08 ± 0.06, assigned to the sulphonamide, carboxylic acid and quinolinium protons, respectively. These constants can be described by Equations 2.1 to 2.4 used for the 50% aqueous ethanol solvent system in Section 2.1. The pK_as determined are all larger than those determined in 50% aqueous ethanol, indicating that Zinquin-A is less readily deprotonated when there is less water present in the solvent. This is to be expected as the greater the percentage of ethanol, the lower the ability of the solvent to solvate H^+.

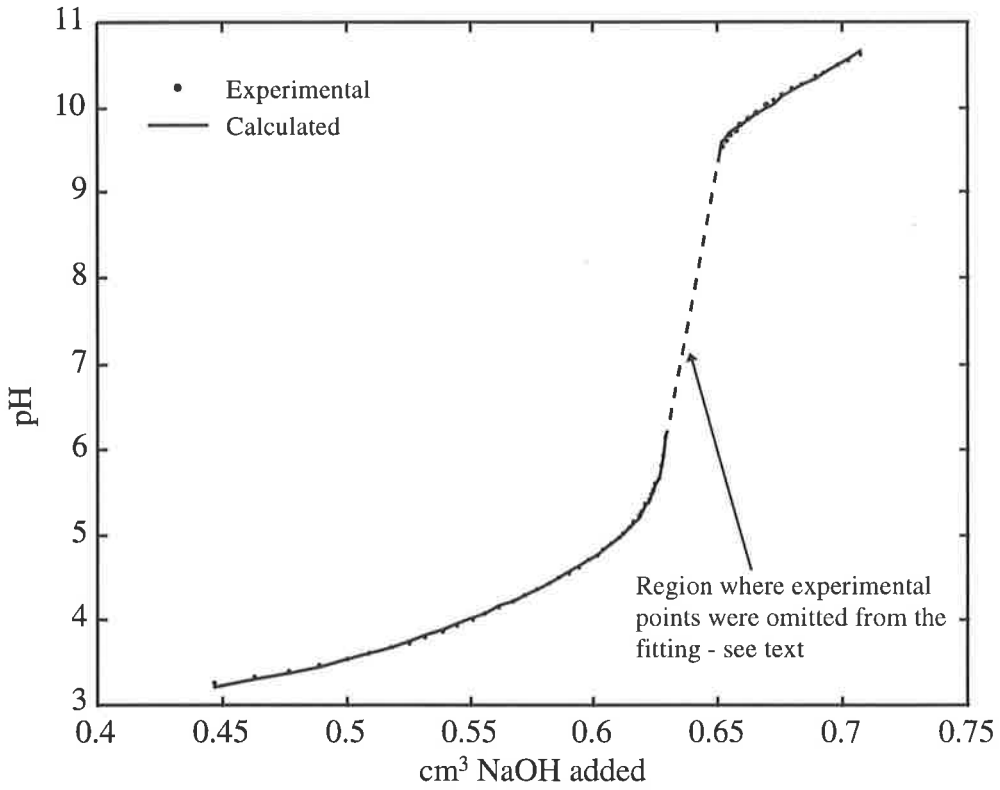

Figure 2.16 : A typical fitting of a titration curve obtained by the addition of 0.0974 mol dm^{-3} NaOH to 8.39×10^{-4} mol dm^{-3} Zinquin-A in 25% aqueous ethanol with 5.39×10^{-3} mol dm^{-3} $HClO_4$ and 0.10 mol dm^{-3} $NaClO_4$. This is one of three that were used for the calculation of the pK_as of Zinquin-A.

Ligand (L)	L.H	$[Zn(L)]^+$	$[Zn(L)_2]$
	pK_{a1}	$\log \beta_1$	$\log \beta_2$
BSQ^-	9.70 ± 0.08	8.5 ± 0.2	17.8 ± 0.1
$p\text{-}TSQ^-$	10.0 ± 0.3	8.8 ± 0.1	17.93 ± 0.07
MSQ^-	10.03 ± 0.07	9.2 ± 0.2	
BCQ^-	> 12	< 7.9	
QSB^-	10.5 ± 0.1	< 5.7	
$MM\text{-}TSQ^-$	10.19 ± 0.03	10.0 ± 0.3	20.3 ± 0.5
ZQA^{2-}	10.13 ± 0.05	10.51 ± 0.08	19.31 ± 0.07

Table 2.5 : Acid dissociation constants and Zn^{2+} stability constants determined in 25% aqueous ethanol for systems containing the ligands shown in Figure 2.15.[28] The corresponding values determined for Zinquin-A in this study are also included for comparison. T = 298.2 K and I = 0.10 ($NaClO_4$).

The ligands in Figure 2.15 have only two possible protonation sites, the sulphonamide (or amide in BCQ^-) nitrogen, and the quinoline nitrogen as, unlike Zinquin-A, they do not have a carboxylic acid moiety. The constant, pK_{a1} describes the loss of the sulphonamide (or amide in BCQ.H) proton, however no protonation of the quinoline nitrogen was observed, indicating that pK_{a2} is most likely below 2.[28] All the ligands studied showed similar pK_{a1}s, with the exception of the amide, BCQ.H, which appears to have a pK_{a1} outside the range easily determined by the potentiometric titration method.

It has been proposed that a change in geometry from octahedral to tetrahedral occurs when a second ligand is added to $[Zn(L)]^+$to form $[Zn(L)_2]$ as the stepwise stability constant for $[Zn(L)]^+$ ($\log K_1 = \log \beta_1$) is smaller than that observed for $[Zn(L)_2]$ ($\log K_2 = \log \beta_2 - \log \beta_1$) and this is in contrast to the decrease expected due to statistical effects.[28] It has been shown that steric hindrance of the sulphonamide group exerts a destabilising effect when $[Zn(L)_2]$ does not have tetrahedral geometry.[29] Other evidence for the tetrahedral geometry of $[Zn(L)_2]$ is the tetrahedral geometry of $[Cu(p\text{-}TSQ)_2]$ as determined by X-ray crystallography.[28] It is possible that this may also occur for Zinquin-A in both 25% and 50% aqueous ethanol.

Both BCQ^- and QSB^- formed small amounts of $[Zn(L)]^+$ (< 5%) and therefore $\log \beta_1$ could not be determined accurately, resulting in the upper limits quoted in Table 2.5. QSB^- has a larger bite distance (distance between the chelating nitrogens) than the other ligands, due to the reversal of its sulphonamide group, and was therefore expected to bind only weakly to Zn^{2+} and more strongly to larger cations. The low formation of $[Zn(BCQ)]^+$ is probably due to the greater delocalisation of the negative charge in BCQ^- onto the oxygen rather than the nitrogen of the amide than is observed for the sulphonamides which results in it being less available for binding to Zn^{2+}. All of the ligands shown in Figure 2.15 which contain the 8-sulphonamidoquinoline entity (BSQ^-, $p\text{-}TSQ^-$, MSQ^- and $MM\text{-}TSQ^-$) as well as Zinquin-A form strong $[Zn(L)]^+$ and $[Zn(L)_2]$ complexes with Zn^{2+} with the exception of MSQ^- for which no $[Zn(L)_2]$ is observed. As can be seen from comparing the $[Zn(L)]^+$ stability constants obtained for Zinquin-A and $MM\text{-}TSQ^-$ to the others, substitution of ether and methyl moieties on the quinoline ring increases the electron density in the ring, and hence the donating ability of the quinoline nitrogen with a subsequent increase in $[Zn(L)]^+$ stability constants. In contrast, variation in the group attached to the sulphonamide sulphur affected the observed stability constants to only a small extent, with the values obtained for the $[Zn(L)]^+$ complexes of BSQ^-, $p\text{-}TSQ^-$ and MSQ^- essentially the same within experimental error.

2.4.2 : Ultraviolet-Visible Spectroscopy of Zinquin-A and Other Ligands in 25% Aqueous Ethanol

A comparative study of the spectroscopic properties of the ligands in Figure 2.15 has been carried out,[28] however the fluorescence spectra observed for the ligands in the absence of Zn^{2+} showed significant intensity which indicated the likely presence of adventitious Zn^{2+} in the samples. Hence the ultraviolet-visible and fluorescence spectra of these ligands in both the free and Zn^{2+} coordinated states have been redetermined taking into account this adventitious Zn^{2+} by adjusting the concentrations of added Zn^{2+} and by adding EDTA to solutions where no added Zn^{2+} was required.

To aid in the selection of an excitation wavelength, the ultraviolet-visible spectra of the ligands in Figure 2.15 and Zinquin-A were determined in 1×10^{-3} mol dm^{-3} NaPIPES, 0.1 mol dm^{-3} $NaClO_4$ adjusted to pH 6.6 in 25% aqueous ethanol at 298.2 K, as described in Section 5.2.2 and Section 5.1.4, respectively. As for the spectra determined for Zinquin-A in 50% aqueous ethanol, both the spectra of the free and Zn^{2+} coordinated ligands showed absorption in the near ultraviolet and ultraviolet-visible regions, with higher intensities observed in the 200 to 300 nm region than the 300 to 450 nm region. In this case, however, the near ultraviolet region was of little interest as the 300 to 450 nm region was used to select an excitation wavelength, hence, spectra in the 200 to 300 nm region were only redetermined at lower concentrations for the Zinquin-A systems to allow comparison with the spectra obtained under similar conditions in 50% aqueous ethanol. The spectra obtained for $[ZQA.H]^{-}$, [Zn(ZQA)] and $[Zn(ZQA)_2]^{2-}$ are shown in Figure 2.17 and the spectra for the other ligand systems are shown in Figure 2.18. Table 2.6 shows the maxima observed for the Zinquin-A species in Figure 2.17 and Table 2.7 shows the maxima of all the spectra in Figure 2.18.

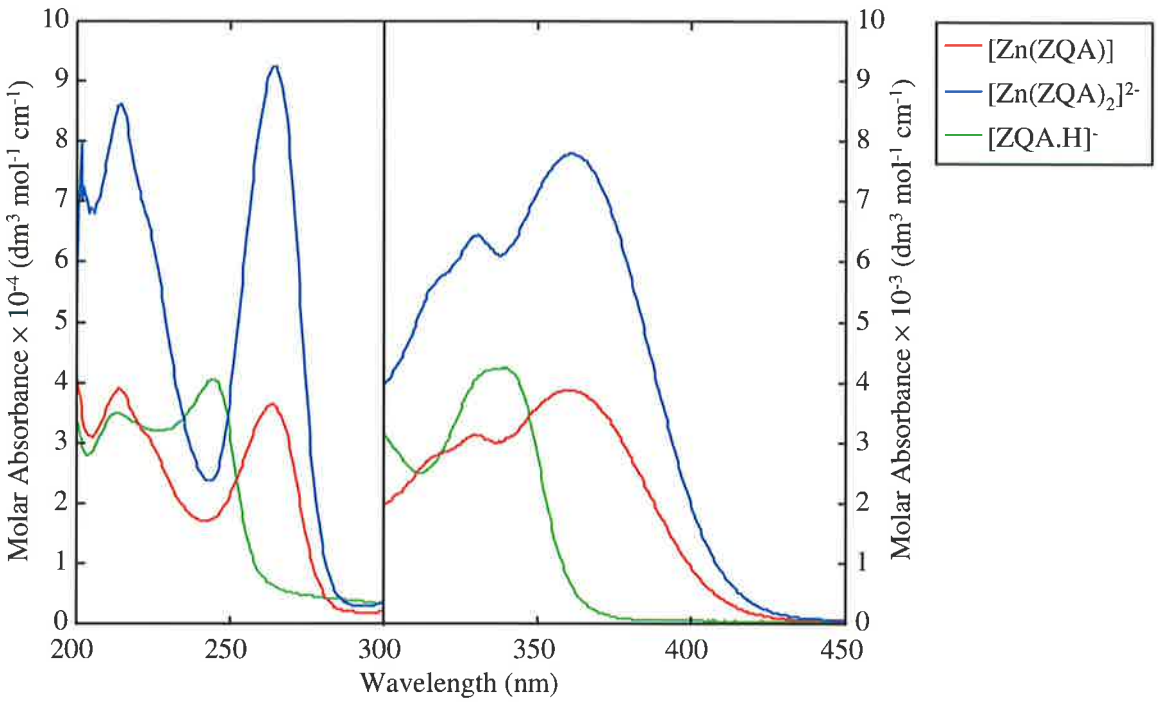

Figure 2.17 : The ultraviolet-visible spectra of [Zn(ZQA)], $[Zn(ZQA)_2]^{2-}$ and $[ZQA.H]^-$ measured in 1×10^{-3} mol dm^{-3} NaPIPES, 0.10 mol dm^{-3} $NaClO_4$, adjusted to pH 6.6 in 25% aqueous ethanol. T = 298.2 K. Concentrations used are described in Section 5.1.4.

Species	Maximum Wavelength (nm) (Molar Absorbance (dm^3 mol^{-1} cm^{-1}))					
$[ZQA.H]^-$	214 (3.49×10^4)	245 (4.06×10^4)	[289] [3.89×10^3]	336 (4.23×10^3)		
[Zn(ZQA)]	214 (3.91×10^4)	[224] [2.94×10^4]	264 (3.63×10^4)	[315] [2.74×10^3]	330 (3.12×10^3)	361 (3.88×10^3)
$[Zn(ZQA)_2]^{2-}$	215 (8.62×10^4)	[224] [6.26×10^4]	264 (9.25×10^4)	[315] [5.54×10^3]	331 (6.44×10^3)	361 (7.79×10^3)

Table 2.6 : Maxima observed for the ultraviolet-visible spectra of some Zinquin-A species in 1×10^{-3} mol dm^{-3} NaPIPES, 0.10 mol dm^{-3} $NaClO_4$, adjusted to pH 6.6 in 25% aqueous ethanol, shown in Figure 2.17. Values enclosed in square brackets describe the approximate position of shoulders rather than maxima.

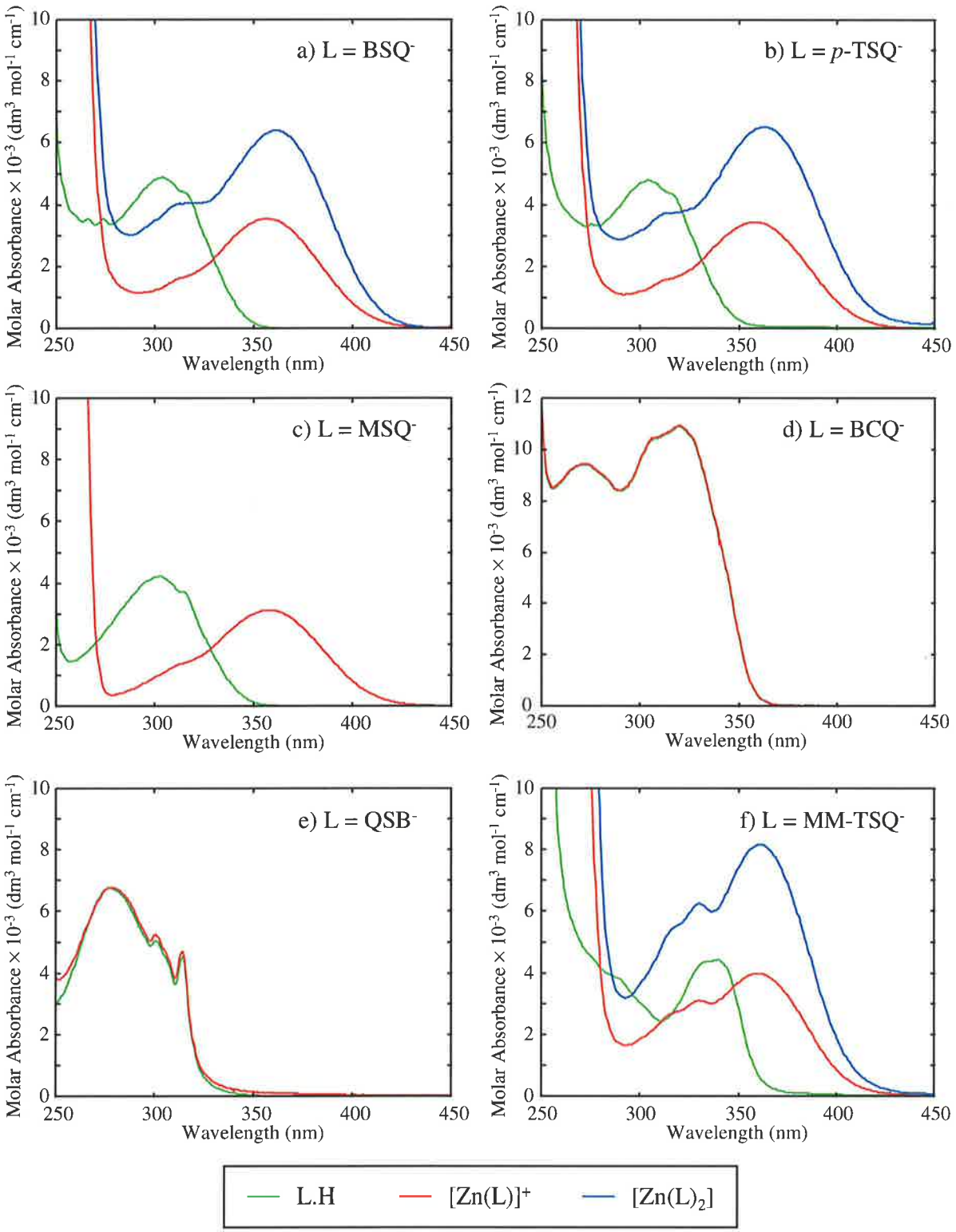

Figure 2.18 : Ultraviolet-visible spectra of L.H, $[Zn(L)]^+$ and $[Zn(L)_2]$ for the ligands shown in Figure 2.15. With the exception of d), all plots are shown with axes scaled to the same extent to allow easy comparison. All solutions were 1×10^{-3} mol dm^{-3} NaPIPES, 0.10 mol dm^{-3} $NaClO_4$, adjusted to pH 6.6 in 25% aqueous ethanol. Concentrations were as listed in Tables 5.8, 5.9 and 5.10. T = 298.2 K.

Species	Maximum Wavelength (nm) (Molar Absorbance ($dm^3\ mol^{-1}\ cm^{-1}$))			
BSQ.H	266 (3.54×10^3)	274 (3.55×10^3)	304 (4.89×10^3)	[317] [4.33×10^3]
$[Zn(BSQ)]^+$	[312] [1.60×10^3]	357 (3.55×10^3)		
$[Zn(BSQ)_2]$	[312] [4.03×10^3]	362 (6.40×10^3)		
p-TSQ.H	275 (3.37×10^3)	304 (4.80×10^3)	[317] [4.32×10^3]	
$[Zn(p\text{-}TSQ)]^+$	[312] [1.56×10^3]	357 (3.44×10^3)		
$[Zn(p\text{-}TSQ)_2]$	[312] [3.71×10^3]	363 (6.52×10^3)		
MSQ.H	303 (4.23×10^3)	[316] [3.57×10^3]		
$[Zn(MSQ)]^+$	[312] [1.34×10^3]	357 (3.12×10^3)		
BCQ.H	273 (9.41×10^3)	[281] [8.99×10^3]	306 (1.04×10^4)	320 (1.09×10^4)
$[Zn(BCQ)]^+$	273 (9.42×10^3)	[281] [9.02×10^3]	306 (1.04×10^4)	320 (1.09×10^4)
QSB.H	278 (6.76×10^3)	301 (5.06×10^3)	315 (4.53×10^3)	
$[Zn(QSB)]^+$	278 (6.78×10^3)	301 (5.24×10^3)	315 (4.69×10^3)	
MM-TSQ.H	[289] [3.82×10^3]	336 (4.38×10^3)		
$[Zn(MM\text{-}TSQ)]^+$	[315] [2.64×10^3]	330 (3.10×10^3)	361 (3.97×10^3)	
$[Zn(MM\text{-}TSQ)_2]$	[315] [5.34×10^3]	330 (6.24×10^3)	361 (8.16×10^3)	

Table 2.7 : Maxima observed for the ultraviolet-visible spectra of L.H, $[Zn(L)]^+$ and $[Zn(L)_2]$ for the ligands (L) shown in Figure 2.15 in 1×10^{-3} mol dm^{-3} NaPIPES, 0.10 mol dm^{-3} $NaClO_4$, adjusted to pH 6.6 in 25% aqueous ethanol. The spectra are shown in Figure 2.17. Values enclosed in square brackets describe the approximate position of shoulders rather than maxima.

Little change in the L.H spectrum was observed upon the complexation of Zn^{2+} by QSB^- and BCQ^-. As insufficient $[Zn(L)]^+$ was present in the titration solutions to obtain stability constants,[28] it seems most likely that this lack of change is due to the absence of $[Zn(L)]^+$ in the samples measured, indicating that the upper limits shown in Table 2.5 should perhaps be even lower. The spectra for QSB.H and BCQ.H are quite different from the spectra for the other L.H, indicating that the sulphonamide group influences the spectrum observed, possibly due to the delocalisation of the lone pair of electrons on its nitrogen into the quinoline ring to some extent.

A shift in the spectrum to longer wavelengths upon complexation with Zn^{2+} was observed for all the ligands in Figure 2.15, with the exception of QSB^- and BCQ^-. As was described for the Zinquin-A spectra in 50% aqueous ethanol (Section 2.3), this is due to a combination of the greater delocalisation of electrons arising from the delocalisation of the negative charge into the quinoline ring and an increase in rigidity, and therefore conjugation, arising from chelation.

By comparing the spectra and maxima for L.H, $[Zn(L)]^+$ and $[Zn(L)_2]$ for L = BSQ^-, *p*-TSQ^- and MSQ^- in Figure 2.18 and Table 2.7, it can be seen that changing the substituent attached to the sulphonamide sulphur affects the spectrum observed for each species very little, with the largest change occurring near 270 nm in the L.H spectra. The spectra for [MSQ.H] and $[Zn(MSQ)]^+$ are both of lower intensity than the corresponding species with BSQ^- and *p*-TSQ^-. Although no significant shift occurs in the maxima, this is most probably due to the absence of the benzene ring in MSQ^- which could be expected to contribute to the spectra for the other ligands due to its delocalised electrons. Hence, these spectra confirm that the main chromophore in these ligands is the quinoline ring.

Comparison of the spectra and maxima for L.H, $[Zn(L)]^+$ and $[Zn(L)_2]$ for L = ZQA^{2-} and MM-TSQ^- in Figures 2.17 and 2.18 and Tables 2.6 and 2.7, shows that the addition of the carboxylate group to MM-TSQ^- to form ZQA^{2-} also has very little effect on the spectra, as could be expected due to its separation from the main chromophore. In contrast, substitution of the quinoline ring does have a significant effect on the spectra of L.H, $[Zn(L)]^+$ and $[Zn(L)_2]$ as can be seen when the spectra for L = BSQ^-, *p*-TSQ^- and MSQ^- are compared to those with L = ZQA^{2-} and MM-TSQ^- (Figures 2.17 and 2.18). The spectrum for L.H is located at longer wavelengths for L = ZQA^{2-} and MM-TSQ^-, possibly due to an increase in electron

delocalisation due to the lone pair of electrons on the ether oxygen. The spectra for both $[Zn(L)]^+$ and $[Zn(L)_2]$ are effected less, with the greatest difference occurring between 310 and 335 nm where the number and location of maxima change. A slight increase in intensity for the $[Zn(L)]^+$ and $[Zn(L)_2]$ spectra is also observed. The fact that the spectra for $[Zn(L)]^+$ and $[Zn(L)_2]$ change less than those for L.H is possibly due to the negative charge on the bound ligand, which is delocalised to some extent in the quinoline ring, inhibiting the delocalisation of the lone pair of electrons on the ether oxygen.

The spectra for the unbound Zinquin-A species, ZQA^{2-}, $ZQA.H_2$ and $[ZQA.H_3]^+$ were also determined in 1×10^{-3} mol dm^{-3} NaPIPES, 0.1 mol dm^{-3} $NaClO_4$ adjusted to pH 6.6 in 25% aqueous ethanol at 298.2 K, as described in Section 5.1.4, to allow comparison to those obtained in 0.1 mol dm^{-3} NaPIPES, 50% aqueous ethanol (Section 2.3). These spectra are shown in Figure 2.19 below and the maxima observed are listed in Table 2.8. The spectra and maxima already presented for $[ZQA.H]^-$ have been included for comparison.

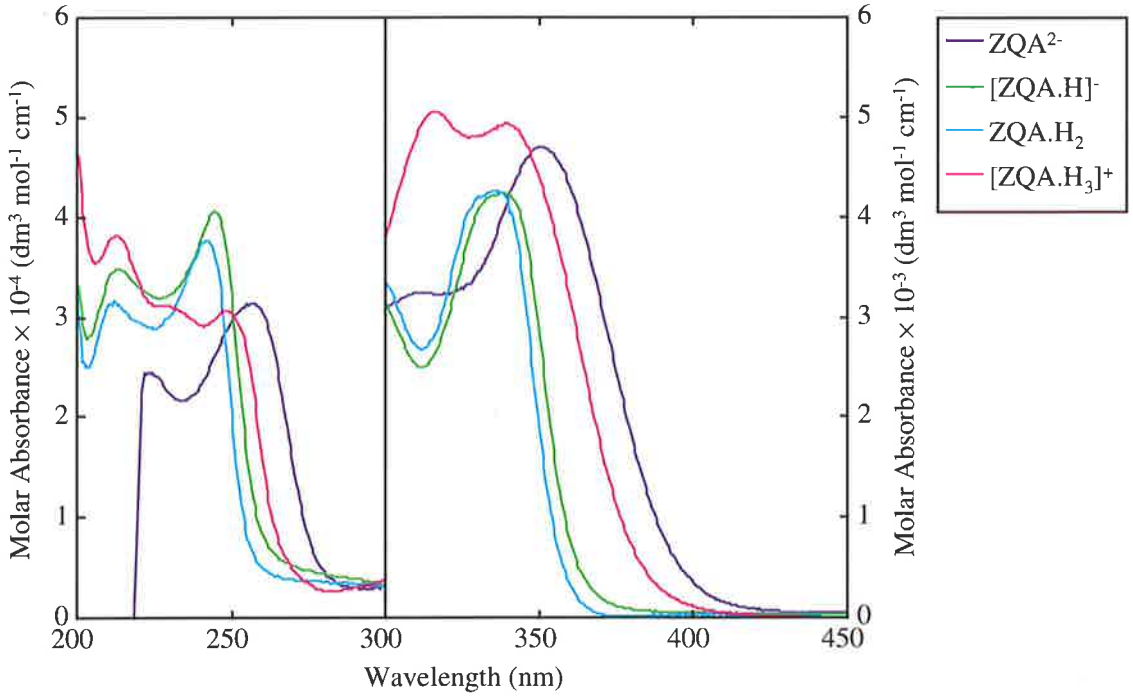

Figure 2.19 : The ultraviolet-visible spectra of ZQA^{2-}, $ZQA.H_2$ and $[ZQA.H_3]^+$ measured in 25% aqueous ethanol with pHs and supporting electrolytes as listed in Table 5.1, T = 298.2 K. Concentrations used are described in Table 5.2. The spectrum for $[ZQA.H]^-$ previously presented (Figure 2.17) is also included for comparison.

Species	Maximum Wavelength (nm) (Molar Absorbance (dm^3 mol^{-1} cm^{-1}))				
ZQA^{2-}	222 (2.44×10^4)	257 (3.14×10^4)	311 (3.24×10^3)	351 (4.70×10^3)	
$[ZQA.H]^-$	214 (3.49×10^4)	245 (4.06×10^4)	[289] [3.89×10^3]	336 (4.23×10^3)	
$ZQA.H_2$	212 (3.16×10^4)	242 (3.77×10^4)	335 (4.26×10^3)		
$[ZQA.H_3]^+$	213 (3.82×10^4)	[232] [3.09×10^4]	249 (3.07×10^4)	317 (5.06×10^3)	341 (4.97×10^3)

Table 2.8 : Maxima observed for the ultraviolet-visible spectra of the free Zinquin-A species in 25% aqueous ethanol, with pHs and supporting electrolytes as listed in Table 5.1, shown in Figure 2.19. Values enclosed in square brackets describe the approximate position of shoulders rather than maxima.

When comparing the spectra obtained for Zinquin-A species in the 25% aqueous ethanol solvent system (Figures 2.17 and 2.19) to those obtained in the 50% aqueous ethanol solvent system (Figures 2.10 and 2.11), the first thing that is noticed is the different wavelength ranges used. For the 50% aqueous ethanol systems, the buffer used for the solutions at pH 6.6 (0.1 mol dm^{-3} NaPIPES) absorbs very strongly below 220 nm and this causes negligible difference between the absorbance of the background and sample cells in the dual beam spectrophotometer, resulting in an inability to measure the sample's spectrum below 220 nm. Hence absorbances at wavelengths below 220 nm were not determined in this solvent system. For the 25% aqueous ethanol systems, however, the buffer used for the solutions at pH 6.6 (1×10^{-3} mol dm^{-3} NaPIPES) does not cause the same problem due to its lower concentration. Hence wavelengths as low as 200 nm were accessible in this solvent system. One exception to this was the spectrum for ZQA^{2-} determined in 0.1 mol dm^{-3} NaOH, 25% aqueous ethanol. The rapid drop off at 220 nm is due to the NaOH absorbing strongly, and absorbance at wavelengths after this drop off could not be determined.

Very little change is observed in the [Zn(ZQA)] spectrum upon changing the solvent system, except near 220 nm. In the 50% solvent system, there appears to be a maximum at 224 nm, however in the 25% solvent system, there is only a slight shoulder at this wavelength. This suggests that the maxima near 224 nm observed for the species in 50% aqueous ethanol may be an artefact of the buffer cut-off observed for this solvent system.

When looking in the 220 to 450 nm range, the largest change in the absorption maxima observed is for the $[ZQA.H_3]^+$ spectrum where a shift of 6 nm to a shorter wavelength and a 15% change in intensity is observed for the maximum at 347 nm when the solvent is changed from 50% to 25% aqueous ethanol. A 20% change in the intensity of the maximum near 317 nm is also observed. The spectrum of $[Zn(ZQA)_2]^{2-}$ also exhibits a significant change (20%) in intensity at 264 nm upon changing the solvent system. These changes arise from a change in solvating ability and other solvent effects upon increasing the percentage of ethanol in the solvent system. No other major changes are observed in the spectra upon changing the solvent system, with the maxima appearing at the same wavelengths ± 3 nm and with similar intensities in both solvent systems.

2.4.3 : Fluorescence Spectroscopy of Zinquin-A and Other Ligands in 25% Aqueous Ethanol

The fluorescence spectra for $[Zn(L)]^+$ and $[Zn(L)_2]$ (where applicable) were determined for all the ligands (L) shown in Figure 2.15 with the exception of L = BCQ^- or QSB^-, due to the negligible concentration of $[Zn(L)]^+$ present in the ultraviolet-visible spectra for these ligands. An excitation wavelength of 358 nm was used for all spectra as this wavelength was near the maxima for all the $[Zn(L)]^+$ and $[Zn(L)_2]$ complexes studied (see Table 2.7). All solutions contained 1×10^{-3} mol dm^{-3} NaPIPES, 0.1 mol dm^{-3} $NaClO_4$ adjusted to pH 6.6 in 25% aqueous ethanol and the concentrations of L.H and Zn^{2+} are shown in Tables 5.13 and 5.14. The fluorescence spectra for [Zn(ZQA)] and $[Zn(ZQA)_2]^{2-}$ were also redetermined in this solvent system, as described in Section 5.1.5, by measuring the relative fluorescence of six solutions with concentration ratios of Zn^{2+} to Zinquin-A from 0.25:1 up to 1000:1 (Figure 2.20). The concentrations used are listed in Table 5.5 and were chosen to give a good variation in the concentrations of [Zn(ZQA)] and $[Zn(ZQA)_2]^{2-}$ present in each solution. The MATLAB program, AB12[25] was used in conjunction with the Zn^{2+} stability constants in Table 2.5 to determine the molar fluorescence spectra (per Zinquin-A anion) shown in Figure 2.21 below. The molar fluorescence spectra of [Zn(ZQA)] and $[Zn(ZQA)_2]^{2-}$ have a maximum at 483 nm (5.56×10^7 dm^3 mol^{-1}) and 483 nm (6.17×10^7 dm^3 mol^{-1}), respectively, where the molar fluorescence values (per Zinquin-A anion) are given in brackets. These spectra are combined, in Figure 2.22, with the molar fluorescence spectra (per complex) determined for the Zn^{2+} complexes of the ligands, shown in Figure 2.15, which were determined in a similar way (see Section 5.2.3).

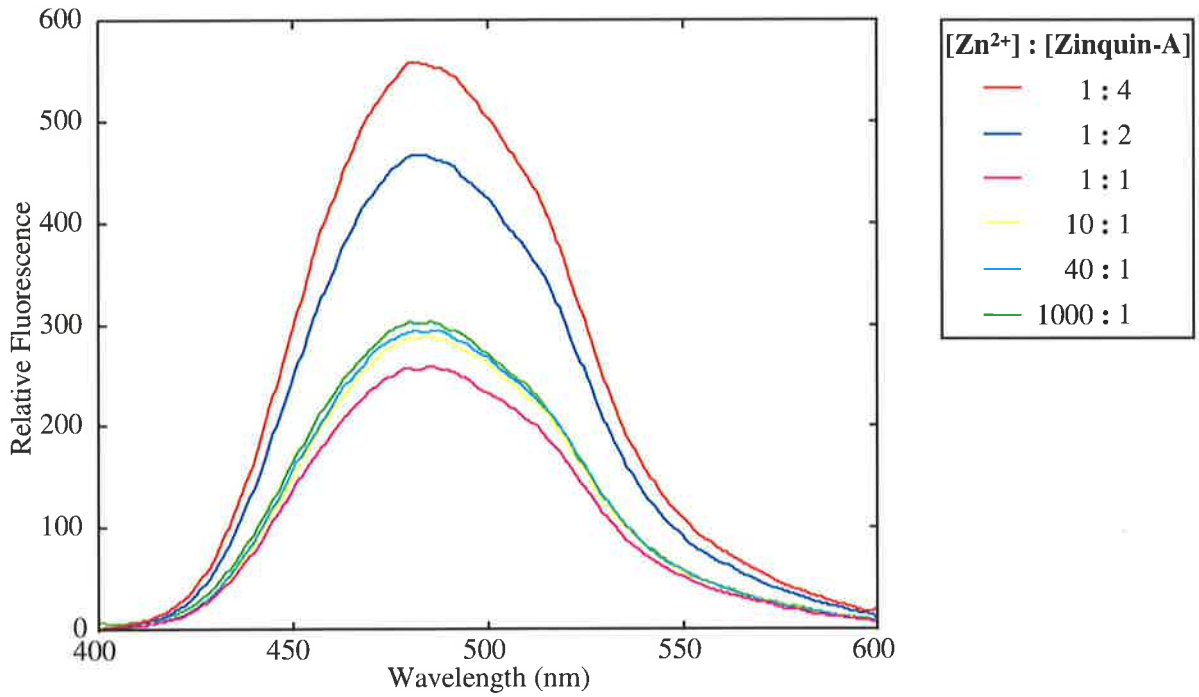

Figure 2.20 : Relative fluorescence determined for solutions with varying Zn^{2+} and Zinquin-A concentrations in 1×10^{-3} mol dm^{-3} NaPIPES, 0.1 mol dm^{-3} $NaClO_4$, pH 6.6 and 25% aqueous ethanol, as described in Table 5.5. T = 298.2 K, slits = 2.5 nm, Ex λ = 358 nm.

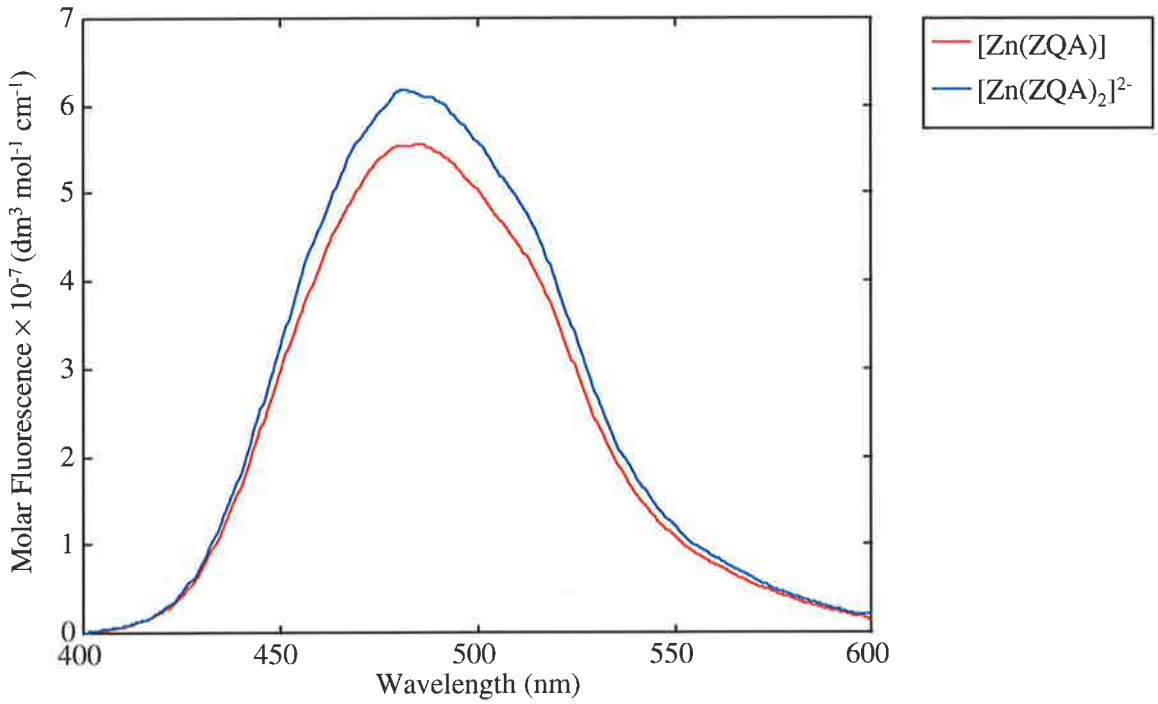

Figure 2.21 : Molar fluorescence spectra for [Zn(ZQA)] and $[Zn(ZQA)_2]^{2-}$ (per Zinquin-A anion) in 1×10^{-3} mol dm^{-3} NaPIPES, 0.1 mol dm^{-3} $NaClO_4$, pH 6.6 and 25% aqueous ethanol, determined from log K_1 = 10.51, log K_2 = 8.80 and the spectra shown in Figure 2.20 The $[Zn(ZQA)_2]^{2-}$ spectrum is shown per Zinquin-A anion, to obtain the spectrum per complex, the spectrum shown must be multiplied by 2. T = 298.2 K, slits = 2.5 nm, Ex λ = 358 nm.

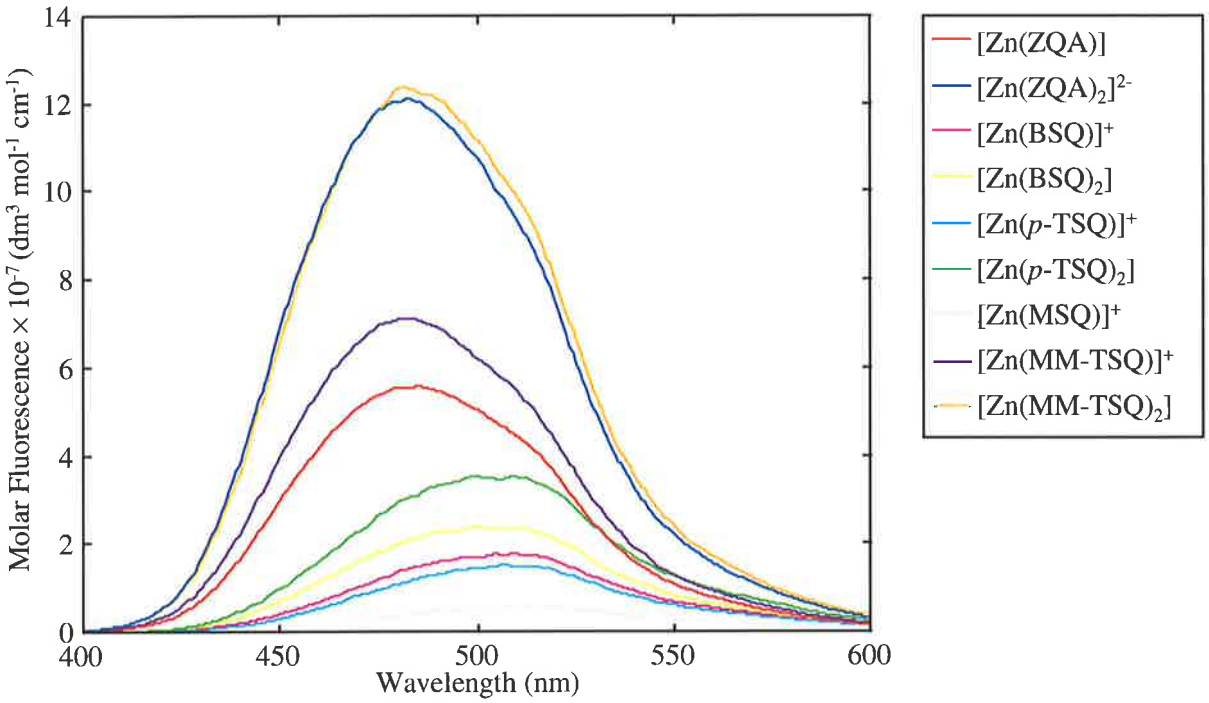

Figure 2.22 : Molar fluorescence determined for $[Zn(L)]^+$ and $[Zn(L)_2]$ (where applicable) for the ligands (L) in Figure 2.15 and for L = ZQA^{2-}. All solutions used have concentrations as described in Tables 5.13 and 5.14 and contain 1×10^{-3} mol dm^{-3} NaPIPES, 0.1 mol dm^{-3} $NaClO_4$, pH 6.6 in 25% aqueous ethanol. All spectra shown are per complex, to obtain the spectra per ligand, the $[Zn(L)_2]$ spectra must be divided by 2. T = 298.2 K, slits = 2.5 nm, Ex λ = 358 nm.

All of the free ligands (L.H) in Figure 2.15, ZQA^{2-}, $[ZQA.H]^-$, $ZQA.H_2$ and $[ZQA.H_3]^+$ were also studied as described in Sections 5.1.5 and 5.2.3, however, they were found to be non-fluorescent when excited at either 358 nm or near their absorption maxima (336 nm for $[ZQA.H]^-$ and $ZQA.H_2$, and as listed in Table 5.11 for the others). The large difference in the fluorescence of coordinated and free ligand can be attributed to the increase in rigidity accompanying chelation of Zn^{2+} as discussed for Zinquin-A in Section 2.3.

As can be seen from Figure 2.22, a wide range of fluorescence intensities was observed for the species studied. As each species absorbs a different amount at the excitation wavelength, the molar fluorescence intensities in Figure 2.22 were normalised for absorption by dividing by the molar absorbance of the species of interest at 358 nm (Table 2.9) to produce the adjusted molar fluorescence as shown in Figure 2.23. The intensity and location of the maxima observed are shown in Table 2.10.

Species	Molar Absorbance at 358 nm ($dm^3\ mol^{-1}\ cm^{-1}$)	Species	Molar Absorbance at 358 nm ($dm^3\ mol^{-1}\ cm^{-1}$)
$[Zn(BSQ)]^+$	3.54×10^3	$[Zn(MM\text{-}TSQ)]^+$	3.96×10^3
$[Zn(BSQ)_2]$	6.34×10^3	$[Zn(MM\text{-}TSQ)_2]$	8.11×10^3
$[Zn(p\text{-}TSQ)]^+$	3.43×10^3	[Zn(ZQA)]	3.86×10^3
$[Zn(p\text{-}TSQ)_2]$	6.42×10^3	$[Zn(ZQA)_2]^{2-}$	7.71×10^3
$[Zn(MSQ)]^+$	3.12×10^3		

Table 2.9 : Absorbances of the $[Zn(L)]^+$ and $[Zn(L)_2]$ studied at the excitation wavelength used to determine the fluorescence spectra, 358 nm.

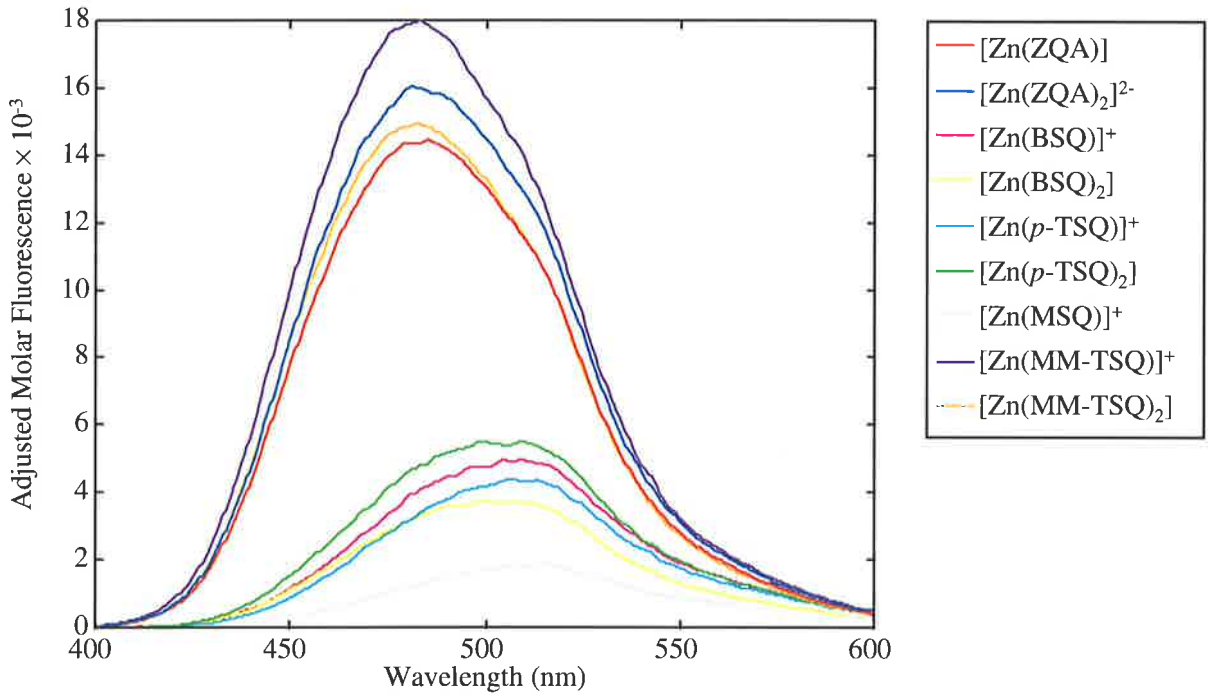

Figure 2.23 : Adjusted molar fluorescence observed for $[Zn(L)]^+$ and $[Zn(L)_2]$ (where applicable) for the ligands (L) in Figure 2.15 and for L = ZQA^{2-}. These spectra are derived from those in Figure 2.22 and contain 1×10^{-3} mol dm^{-3} NaPIPES, 0.1 mol dm^{-3} $NaClO_4$, pH 6.6 in 25% aqueous ethanol. T = 298.2 K, slits = 2.5 nm, Ex λ = 358 nm.

Species	Maximum Wavelength (nm)	Adjusted Molar Fluorescence
$[Zn(BSQ)]^+$	498	4.77×10^3
$[Zn(BSQ)_2]$	500	3.76×10^3
$[Zn(p\text{-}TSQ)]^+$	507	4.38×10^3
$[Zn(p\text{-}TSQ)_2]$	500	5.51×10^3
$[Zn(MSQ)]^+$	513	1.87×10^3
$[Zn(MM\text{-}TSQ)]^+$	483	1.80×10^4
$[Zn(MM\text{-}TSQ)_2]$	483	1.49×10^4
[Zn(ZQA)]	482	1.44×10^4
$[Zn(ZQA)_2]^{2-}$	482	1.60×10^4

Table 2.10 : Adjusted molar fluorescence maxima observed for $[Zn(L)]^+$ and $[Zn(L)_2]$ (where applicable) for the ligands (L) in Figure 2.15 and for L = ZQA^{2-}. The spectra are shown in Figure 2.23.

It is interesting to note from Figure 2.23 and Table 2.10 that the adjusted molar fluorescence for $[Zn(L)_2]$ is larger than that for $[Zn(L)]^+$ when L = ZQA^{2-} or p-TSQ^-. This is the opposite to what is observed when L = BSQ^- or MM-TSQ^- or for Zinquin-A in 50% aqueous ethanol (Figure 2.14). As mentioned in Section 2.3, the spectrum for $[Zn(L)_2]$ is expected to be lower once adjusted for the number of ligands present (or the amount absorbed at the excitation wavelength) as the presence of two ligands causes greater strain in the molecule and therefore greater quenching. There are two possible reasons for the exceptions to this observed for ZQA^{2-} and p-TSQ^-. The first is that the greater percentage of ethanol in the solvent affects $[Zn(L)_2]$ in a different way to $[Zn(L)]^+$ and causes greater quenching for [Zn(ZQA)] and $[Zn(p\text{-}TSQ)]^+$ than for $[Zn(ZQA)_2]^{2-}$ and $[Zn(p\text{-}TSQ)_2]$, respectively. The second, most likely, possibility is that the estimation of adventitious Zn^{2+} in these cases has not been accurate, due to the inherent differences in adventitious Zn^{2+} concentration between solutions. For this reason, it has been decided only to discuss the results obtained for $[Zn(L)]^+$ here as these are unaffected by adventitious Zn^{2+} due to the large concentration of added Zn^{2+} used.

The intensities of adjusted molar fluorescence observed at the maxima for $[Zn(L)]^+$ decrease in the order;

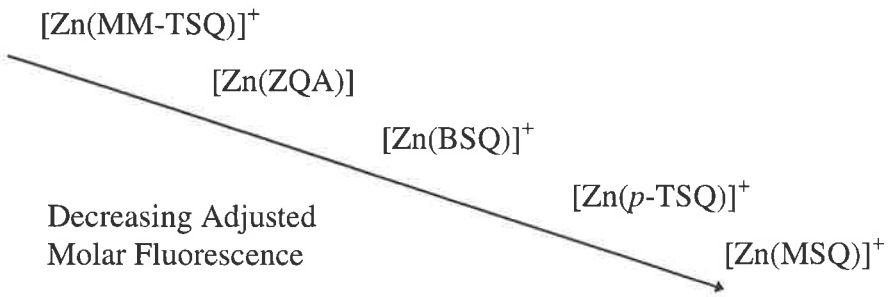

This indicates that substitution of the quinoline ring with electron donating groups is favourable for fluorescence as both $[Zn(MM\text{-}TSQ)]^+$ and [Zn(ZQA)] show a much higher fluorescence than the other $[Zn(L)]^+$. The presence of these groups also causes the maximum fluorescence to occur at a longer wavelength. The presence of the benzene ring attached to the sulphonamide nitrogen is also favourable for fluorescence, with $[Zn(MSQ)]^+$, which does not have this group, showing the lowest fluorescence for those ligands studied. Little difference is observed between the fluorescence spectrum of $[Zn(BSQ)]^+$ and $[Zn(p\text{-}TSQ)]^+$, indicating that the methylation of this benzene ring has little effect on the fluorescence spectrum observed. With the exception of the non-fluorescence of L.H found in this study, these results agree with those previously determined, which showed similar fluorescence intensities for $[Zn(L)]^+$.[28] The fluorescence of $[Zn(L)_2]$ was not determined in the previous study.[28] The value for maximum molar fluorescence of [Zn(ZQA)] in 25% aqueous ethanol (483 nm and an intensity of 5.56×10^7 dm^3 mol^{-1}) also agrees well with that obtained in 50% aqueous ethanol (485 nm with an intensity of 5.16×10^7 dm^3 mol^{-1}), showing little change upon changing the solvent system as could be expected due to the minimal change observed in the absorption spectra (Section 2.4.2).

2.5 : References

1. I. B. Mahadevan, M. C. Kimber, S. F. Lincoln, E. R. T. Tiekink, A. D. Ward, W. H. Betts, I. J. Forbes and P. D. Zalewski, *Aus. J. Chem.*, **49 (5)**, 561, 1996.

2. P. D. Zalewski, X. Jian, L. L. L. Soon, W. G. Breed, R. F. Seamark, S. F. Lincoln, A. D. Ward and F. Z. Sun, *Reprod. Fert. Dev.*, **8 (7)**, 1097, 1996.

3. P. D. Zalewski, S. H. Millard, I. J. Forbes, O. Kapaniris, A. Slavotinek, W. H. Betts, A. D. Ward, S. F. Lincoln and I. Mahadevan, *J. Histochem. and Cytochem.*, **42 (7)**, 877, 1994.

4. P. D. Zalewski, I. J. Forbes R. F. Seamark, R. Borlinghaus, W. H. Betts, S. F. Lincoln and A. D. Ward, *Chem. Biol.*, **1**, 153, 1994.

5. D. Berendji, V. Kolbbachofen, K. L. Meyer, O. Grapenthin, H. Weber, V. Wahn and K. D. Kroncke, *FEBS Lett.*, **405 (1)**, 37, 1997.

6. N. Wellinghausen, M. Martin and L. Rink, *Eur. J. Immunol.*, **27 (10)**, 2529, 1997.

7. M. Tsuda, K. Imaizumi, T. Katayama, K. Kitagawa, A. Wanaka, M. Tohyama, T. Takagi, *J. Neurosci.*, **17 (17)**, 6678, 1997.

8. R. D. Palmiter, T. B. Cole and S. D. Findley, *EMBO J.*, **15 (8)**, 1784, 1996.

9. I. A. Brand and J. Kleineke, *J. Biol. Chem.*, **271 (4)**, 1941, 1996.

10. P. Coyle, P. D. Zalewski, J. C. Philcox, I. J. Forbes, A. D. Ward, S. F. Lincoln, I. Mahadevan and A. M. Rofe, *Biochem. J.*, **303**, 781, 1994.

11. N. Wellinghausen, A. Fischer, H. Kirchner and L. Rink, *Cell. Immunol.*, **171 (2)**, 255, 1996.

12. P. D. Zalewski, I. J. Forbes and W. H. Betts, *Biochem. J.*, **296 (2)**, 403, 1993.

13. R. Y. Tsien, T. Possan and T. J. Rink, *J. Cell Biol.*, **94**, 325, 1982.

14. G. Grynkiewicz, M. Poenie and R. Y. Tsien, *J. Biol. Chem.*, **260**, 3440, 1985.

15. K. M. Hendrickson, T. Rodopoulos, P. A. Pittet, I. Mahadevan, S. F. Lincoln, A. D. Ward, T. Kurucsev, P. A. Duckworth, I. J. Forbes, P. D. Zalewski and W. H. Betts, *J. Chem. Soc., Dalton Trans.*, 3879, 1997.

16. "*Zinquin Information Sheet*", University of Adelaide, South Australia, Australia.

17. G. D. Christian and J. E. O'Reilly, "*Instrumental Analysis*", Allyn and Bacon, Inc., Boston, 2nd Edn., 1986.

18. J. J. R. Fausto da Silva and R. J. P. Williams, "*The Biological Chemistry of the Elements*", Oxford University Press, Oxford, 1992.

19. B. L. Vallee, *Physiol. Rev.*, **39**, 443, 1959.

20. A. S. Prasad, "*Biochemistry of Zinc*", Plenum Press, New York, 1993

21. A MATLAB program, T. Kurucsev, University of Adelaide, South Australia, Australia. Refer to Appendix E.

22. R. M. Smith and A. E. Martell, "*Critical Stability Constants*", Plenum Press, New York, **1**, 1975.

23. A Macintosh version (P. A. Duckworth) of the Fortran program SPE, A. E. Martell and R. J. Motekaitis, "*Determination and use of Stability constants*", Appendix III, VCH, 1990.

24. T. Rodopoulos, PhD Dissertation, The Chemistry Department, University of Adelaide, South Australia, Australia, 1993.

25. AB12 is a subroutine in the MATLAB program SPECFIT, T. Kurucsev, University of Adelaide, South Australia, Australia. Refer to Appendix E.

26. D. A. Skoog, "*Principles of Instrumental Analysis*", CBS Publishing, Philadelphia, 3rd Edn, 1985.

27. T. Kurucsev, University of Adelaide, South Australia, Australia, private communication.

28. C. Haskard, Honours Report, The Chemistry Department, University of Adelaide, South Australia, Australia, 1993.

29. H. Nakamura, T. Yoshida, M. Todoko, K. Ueno and M. Takagi, *Bull. Chem. Soc. Jpn.*, **57**, 2839, 1984.

CHAPTER 3

THE STUDY OF ZINC(II) IN CELLS AND NUCELI WITH ZINQUIN-A AND ZINQUIN-E

3.1 : Introduction

As previously discussed in Chapter 1, the study of intracellular Zn^{2+} is of great interest to medical researchers. The flux of Zn^{2+} in cells or tissues can be monitored as they progress through their life stages and the location of high Zn^{2+} concentrations within cells can be identified. Zinc(II) can also be loaded into cells to enable those with a low natural level of Zn^{2+} to be visualised using Zinquin-E. It is hoped that the tracing of Zn^{2+} in cells will shed light on the role that Zn^{2+} plays in life and the many diseases and conditions linked to altered Zn^{2+} levels (Section 1.1).

3.1.1 : Cell Structure

Figure 3.1 illustrates the various components that may be found in cells. It is important to note that cells of different types have differing organelles of differing sizes and the concentration of Zn^{2+} found in them also varies. Below is a brief description of some of the organelles illustrated in Figure 3.1.

The Nucleus

This is often the largest organelle found in a cell and contains the cell's chromosomes. Nuclei are roughly spherical in shape but vary in size and number, even growing and diminishing within the same cell. They are surrounded by a double membrane punctuated by pores of 30-100 nm diameter through which molecules can be transported. The nucleus contains enzymes and other proteins which have migrated through the nuclear membrane from the cytosol. Over 95% of all cellular DNA is located in the nucleus. In addition, each nucleus usually contains at least one nucleolus.

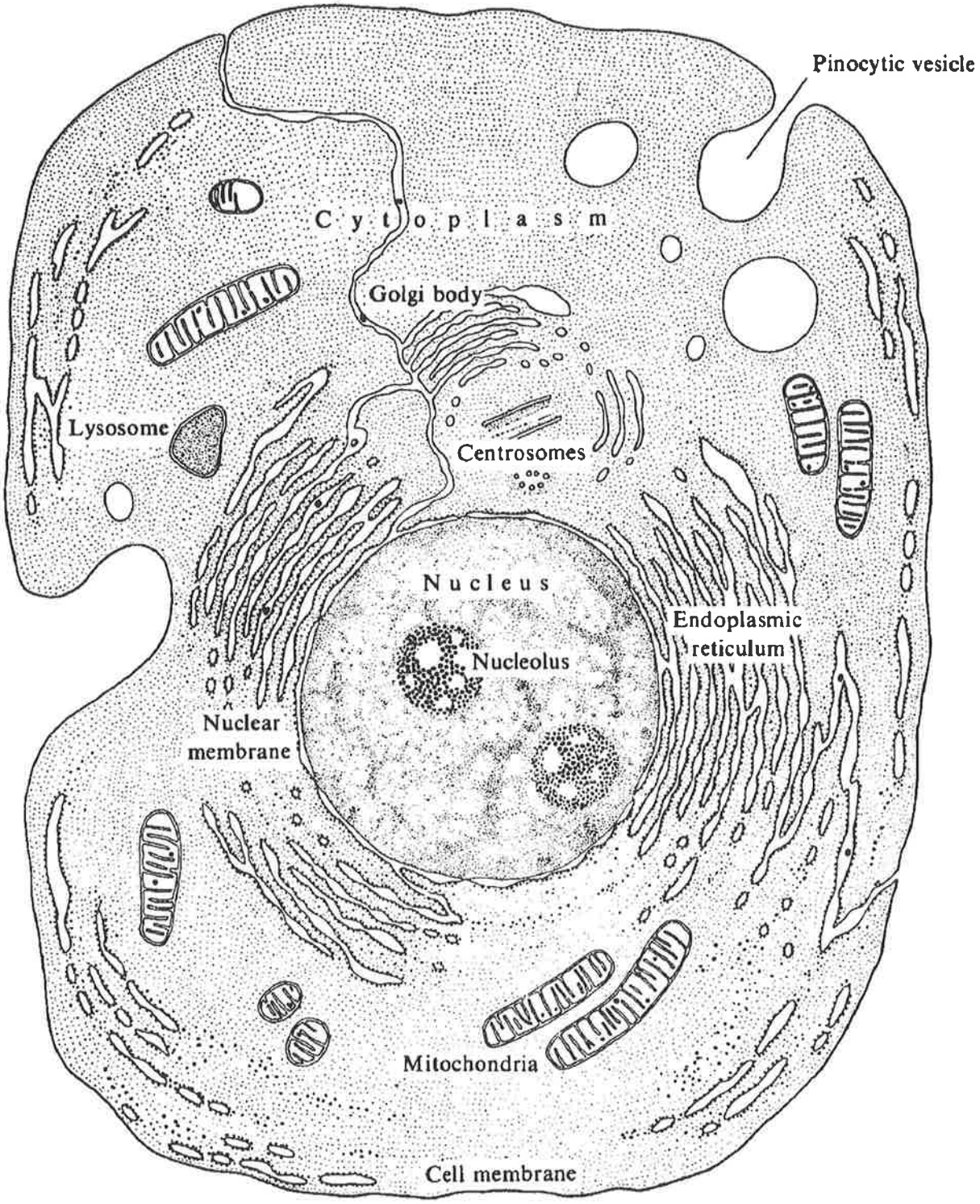

Figure 3.1 : The structure of a typical cell.[1] This modern diagram of a typical cell is based on what is seen in electron micrographs.

The Nucleolus

A spherical body taking up to 25% of the nuclear volume. It consists mainly of RNA and some proteins. Nucleoli can dwindle, disappear and reappear during the life of the cell.

The Endoplasmic Reticulum

The endoplasmic reticulum consists of a complex system of membranous sacks or cisternae which is often continuous with the outer nuclear membrane and can continue all the way to the cellular membrane. Two types exist, smooth-surfaced reticulum and rough-surfaced reticulum. The difference between them is the presence of small, electron dense, spherical particles attached to the surface of the rough version and not the smooth. The endoplasmic reticulum seems to be the sole site of membrane production in the cell and is also involved in protein synthesis and product transportation.

The Golgi Body

Also called the Golgi complex, Golgi apparatus or dictyosome, this is a system of roughly parallel interconnecting flattened cisternae situated close to the endoplasmic reticulum but physiologically distinct from it. A cell can have between one and a hundred of these apparatuses, with each Golgi body consisting of 6 to 30 cisternae. Golgi bodies are involved in the modification of glycoproteins and synthesis of vesicles and secretory granules. Secretory cells, such as exocrine cells of the pancreas, have prevalent and particularly well developed Golgi bodies.

The Mitochondria

Mitochondria, or large granules, are the second largest structure found in most cells. They can number from one to several thousand per cell and are either cylindrical or roughly spherical in shape. Their main distinctive feature is their membrane system which consists of a relatively smooth outer membrane, an intermembranous space, and a particularly highly structured inner membrane. The inner membrane forms numerous folds, called cristae, which penetrate the inner compartment, often at right angles to the long axis of the mitochondrion. It is thought that mitochondria are the sites of intracellular energy production and transduction. Several enzymes reside on the outer membrane while the inner membrane, with its small attached particles, is concerned with the generation of oxidative energy and its transduction into chemical energy and mechanical or osmotic work.

The Lysosomes

Lysosomes are diverse membrane bound organelles which are integral in the intracellular digestive system. They contain a large variety of hydrolytic enzymes and are produced by the Golgi body.

The Cytosol

This is the fluid or semi-fluid matrix of the cytoplasm in which the organelles are suspended.

The Cytoplasm

All intracellular contents excluding any nuclei but including membranes, organelles and cytosol.

The Vesicles

Fragments of membrane that have resealed to form hollow shells which can transport reagents about the cell

The Cellular Membrane

Also known as the plasma membrane, this is the exterior boundary of a cell. It appears to be a relatively rigid and organised structure consisting of a lipid bilayer coated on both sides by protein films. It controls the permeability of the cell and contains passages for the movement of specific molecules in and out of the cell. Due to the lipophilic nature of the membrane, uncharged molecules traverse into the cell with greater ease than charged molecules, which often require a transporter molecule or a specific channel. The membrane consists of phospholipids which have a polar 'head' and a hydrophobic double 'tail', as shown in Figure 3.2. This causes them to form bilayers where the hydrophobic portions are grouped together. Figure 3.3 shows a structure of a typical cell membrane. In this schematic view, a strip of the cellular membrane has been peeled off and magnified. This is an example of the fluid mosaic model of membrane structure as it contains proteins which are either partially or totally embedded in the phospholipid bilayer.[2] It has been shown that Zn^{2+} can coordinate to some of these proteins where it acts to protect the membrane by maintaining its structure and function.[3] Membranes are described as fluid because the phospholipids and proteins are constantly moving. Other organelles such as the nucleus have membranes of a similar construction.

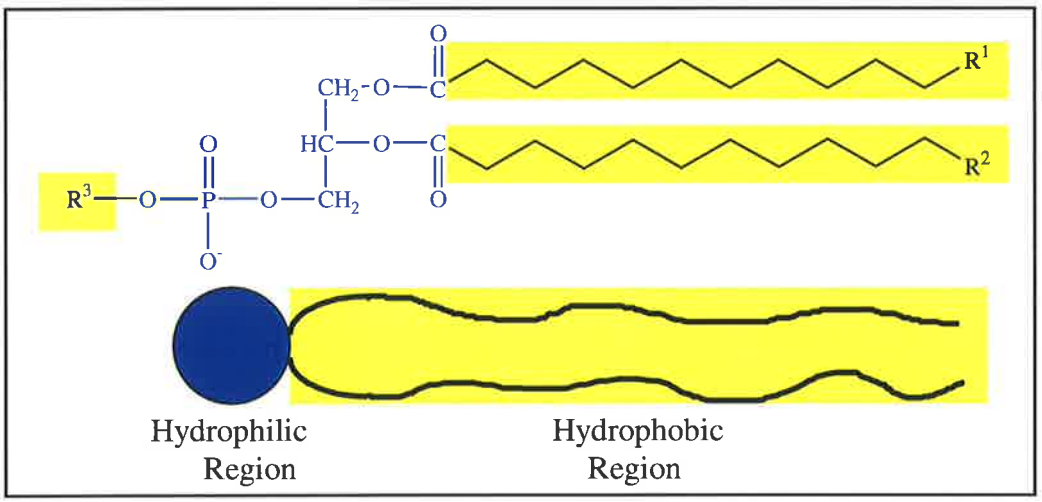

Figure 3.2 : An example of a phospholipid and its schematic representation.

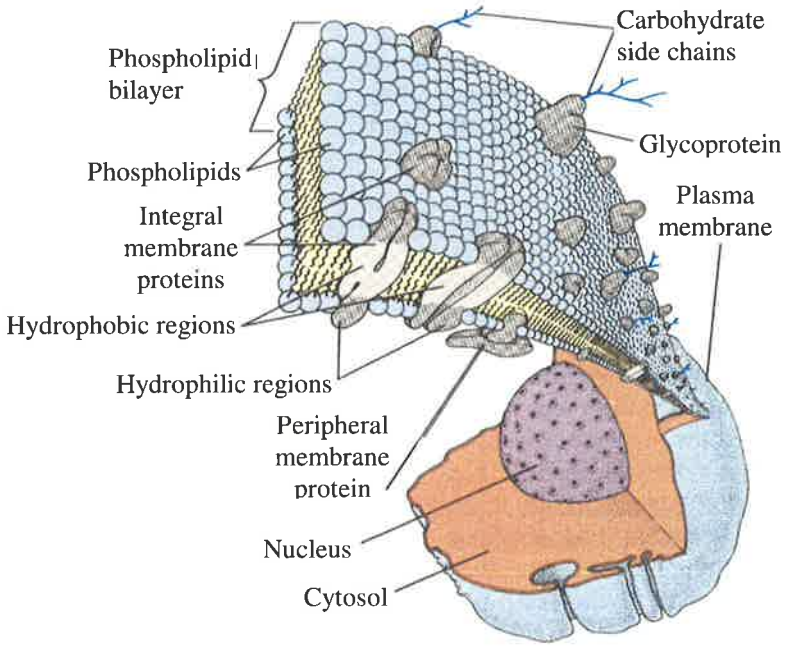

Figure 3.3 : A schematic diagram of the fluid mosaic model of membrane structure for a typical cell membrane.[4]

3.1.2 : Previous studies

A number of biological and biochemical studies have been carried out using Zinquin-E to visualise Zn^{2+} in cells and tissues including rat hepatocytes[5-7] and thymocytes,[8] T-lymphocytes (T-cells),[9,10] gerbil brain cells,[11] mouse and rat splenocytes,[8,12] mouse spermatozoa[13] and fibroblast cells,[12] BHK (baby hamster kidney) cells,[14] various pancreatic islet cells,[15] and human peripheral blood mononuclear[16] and chronic-lymphocytic-leukaemia[8] cells. Other studies have involved sheep eggs[17] and embryos as well as zebra fish.[18] Selected studies are mentioned in greater detail below, illustrating the diversity of cells and tissues studied.

Chronic-lymphocytic-leukaemia (CLL) cells

Some of the first cells to be studied with Zinquin-E were chronic-lymphocytic-leukaemia (CLL) cells.[8] These showed non-uniform fluorescence distribution within the cell, with what appeared to be nuclear shadows visible in some cells (indicated by arrows in Figure 3.4 below). Of more interest, however, are the smaller regions of high fluorescence intensity observed in these cells, as can be seen in Figure 3.4, which indicates localised high Zn^{2+} concentrations or high availability of Zn^{2+} for Zinquin-A complexation. This punctate distribution, often described as a 'starry sky', has also been observed for Jurkat T-cells[10] and is thought to be due to vesicular Zn^{2+}. The cells in Figure 3.4 were incubated in buffer containing 2.5×10^{-5} mol dm^{-3} $ZnSO_4$ and the Zn^{2+} ionophore pyrithione (1×10^{-6} mol dm^{-3}), which transports Zn^{2+} through the cellular membrane, before washing and subsequent incubation in a buffer containing 2.5×10^{-5} mol dm^{-3} Zinquin-E. Cells which were not incubated in both $ZnSO_4$ and pyrithione showed a much lower fluorescence intensity. Zinquin-E was effectively used to show that increasing the intracellular concentration of Zn^{2+} helped inhibit apoptosis.

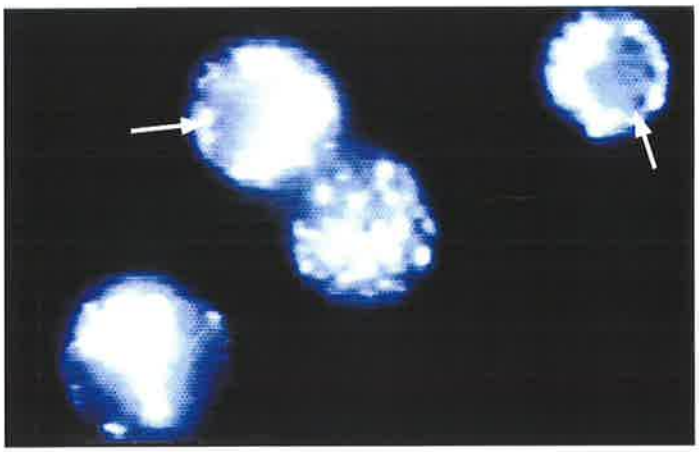

Figure 3.4 : Human chronic-lymphocytic-leukaemia (CLL) cells with increased intracellular Zn^{2+} concentration incubated in Zinquin-E.[8] Nuclear shadows are indicated with arrows.

Zebra Fish Embryos

One of the most complicated, and interesting, objects studied with Zinquin-E so far is the zebra fish.[18] These fish develop rapidly, progressing from a fertilised egg to a free swimming larvae within 48 hours. Another advantage with respect to using this fish for studies with Zinquin-E is that Zinquin-E does not kill them immediately and they can be observed over 48 hours giving an insight into the fluxes of Zn^{2+} involved in their maturation. Figure 3.5 shows a developing zebra fish embryo loaded with Zinquin-E at 24 hours maturation (top) and at 48 hours maturation (bottom). The images on the right of Figure 3.5 are microscopy images under normal light, while those on the left show the fluorescence observed from Zinquin-A bound to Zn^{2+} in the embryo. The concentration of Zn^{2+} available for Zinquin-A coordination increases in the fish as it matures, especially in the gut region (denoted by an arrow in Figure 3.5). However, the eyes remain low in available Zn^{2+} throughout its development.

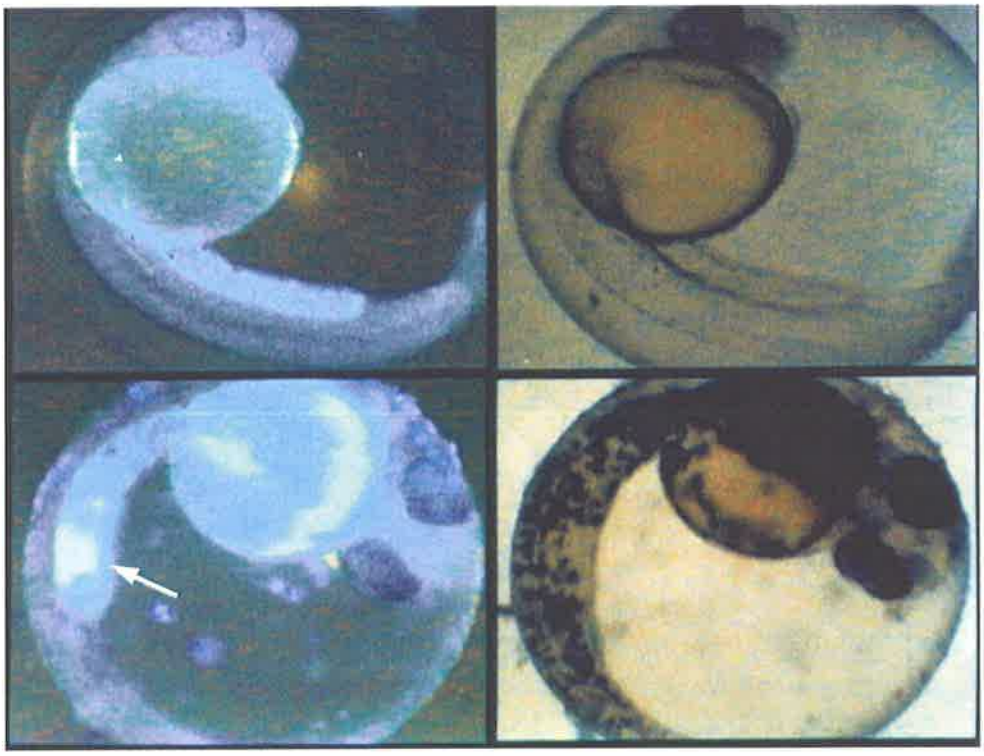

Figure 3.5 : A developing zebra fish shown at 24 hours development (top) and 48 hours development (bottom) with fluorescence due to Zinquin-E incubation shown on the left and a normal microscope image on the right. The high fluorescence observed in the gut region is highlighted with an arrow.

Hepatocytes

Rat hepatocytes (liver cells) have also been studied with Zinquin-E,[7] which was used to find a relationship between the natural Zn^{2+} chelating agent, metallothionein and intracellular Zn^{2+} concentrations. The hepatocytes showed intense extranuclear fluorescence, as can be seen in Figure 3.6, with greater intensity than that of rat splenocytes and thymocytes which were also studied.[7] The punctate or 'starry sky' fluorescence observed for lymphocytes[8] is not observed for these cells. Zinquin-A fluorescence was observed to be associated with high-molecular-mass protein fractions, metallothionein and some lower-molecular-mass entities including $[Zn(H_2O)_6]^{2+}$. Quenching was observed for fluorescence of Zinquin-A bound to Zn^{2+} which was already bound to metallothionein or other proteins. The results also suggest that Zinquin-A may remove Zn^{2+} from metallothionein, which then rapidly degrades. A positive logarithmic relationship was observed between Zinquin-A fluorescence and metallothionein concentration in these cells.[7]

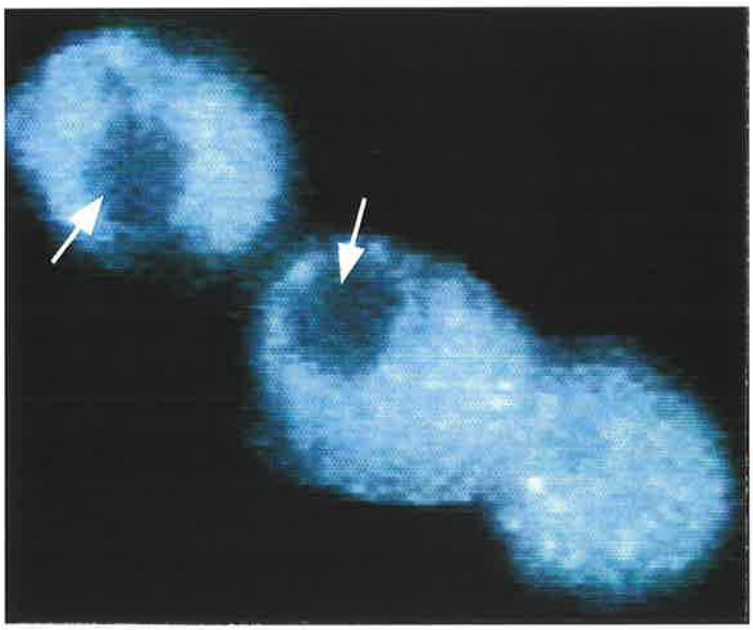

Figure 3.6 : Zinquin-A fluorescence in cultured rat hepatocytes incubated in 2.5×10^{-5} mol dm^{-3} Zinquin-E. Nuclear shadows are highlighted with arrows.

Reproductive Cells

Zinc(II) has been connected to fertility[19-22] and is known to be essential for growth and the gene expression.[23,24] It is therefore no surprise that both ova and spermatozoa are very rich in Zn^{2+} as has been shown by conventional studies[25-27] as well as with Zinquin-E.[13,17,28] Sheep ova retrieved from recently mated sheep have been studied at various stages of development, showing a marked increase in the concentration of Zn^{2+} available for Zinquin-A coordination as the egg grows.[17] Figure 3.7 shows three sheep ova of varying ages. The egg to the right is unfertilised, the egg to the left is approximately 1 day after fertilisation and the one in the middle is 8-16 days after fertilisation. These ages were determined using the morphology of the eggs as a guide. The zona pellucida is visible in all three eggs as a ring about the bulk of the egg. It is this structure which prevents additional spermatozoa from entering a fertilised egg by hardening after fertilisation. The increase in fluorescence of this region as the egg grows may indicate that Zn^{2+} is involved in this hardening. Although the fluorescence of the egg to the left appears to be diffuse and uniform, greater magnification shows a heterogeneous distribution with regions of varying fluorescence intensity.

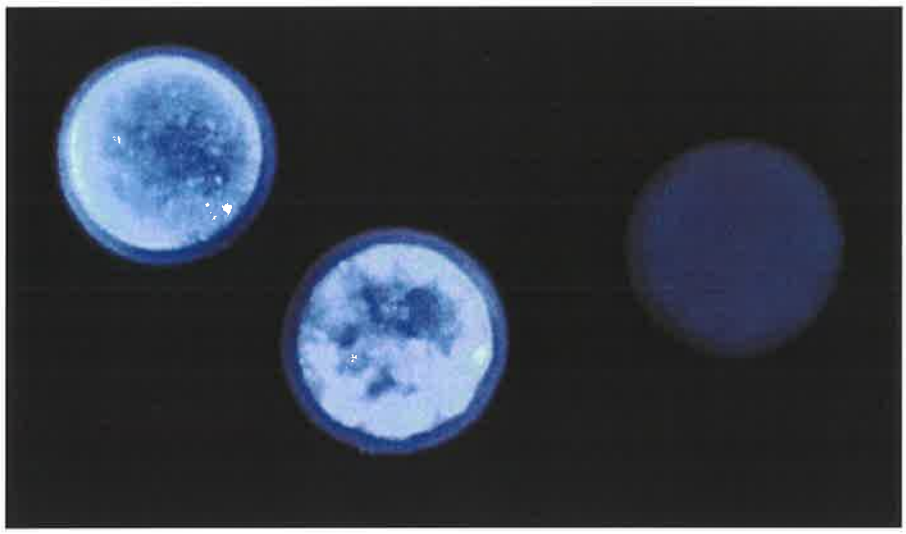

Figure 3.7 : Sheep ova stripped of surrounding cells with proteases and incubated in 2.5×10^{-5} mol dm^{-3} Zinquin-E. Left : 1 day after fertilisation, Middle : 8-16 days after fertilisation, Right : unfertilised.

As mentioned, spermatozoa are also very rich in Zn^{2+} and a low level of Zn^{2+} in human spermatozoa heads has been linked to infertility[25,29]. Both mouse[13] and human spermatozoa[28] have been studied with Zinquin-E and both show intense fluorescence within the spermatozoan head, with a lower fluorescence intensity associated with the tail (Figure 3.8). This high Zn^{2+} concentration in the head is thought to play a role in protecting the vital DNA information carried there from the surrounding environment. Despite the low fluorescence observed in the tail region, studies have shown that the actual concentration of Zn^{2+} is quite high,[26] this indicates that the Zn^{2+} in this region is tightly bound and protected from Zinquin-A and it is probably playing a structural role.

Figure 3.8 : Human spermatozoan incubated in 2.5×10^{-5} mol dm^{-3} Zinquin-E.

As can be seen from the work described, many different systems can be studied with the use Zinquin-E. Each of the examples shown above have different natural levels and distributions of Zn^{2+} and cell or tissue structure. Zinc(II) has been successfully studied in these systems, gaining insights into its role in apoptosis and fertilisation, its relationship with respect to metallothionein and its location and approximate concentration. Many questions about the mode of operation of Zinquin-E still exist. Various studies have suggested that Zinquin-E or Zinquin-A may not be able to gain entry into the nucleus,[7,8,10,15] that the fluorescence observed depends upon how Zn^{2+} is bound in the cell,[7,12] and that Zinquin-A can remove Zn^{2+} from some proteins[7] but not others.[8,10,12] This thesis, in part, discusses some of these issues and the likelihood of them occurring.

3.2 : Results and Discussion

As mentioned in Section 3.1, some cells, for example the hepatocytes[7] shown above, as well as pancreatic islet cells[15] and lymphoblastoid cells,[10] exhibit a definite shadow approximately where their nucleus is located. Other cells, such as Jurkat T-cells[10], CLL cells[8] and the colon cancer cells used in this study, show a less well defined, occasional nuclear shadow. There are several possible explanations for the observation of nuclear shadows.

(a) Zinquin-A penetrates the nucleus but there is no Zn^{2+} present for it to coordinate to.

(b) Zinquin-A penetrates the nucleus and there is Zn^{2+} present, but due to the nature of its binding, Zinquin-A is unable to coordinate to it.

(c) Zinquin-A penetrates the nucleus and coordinates to the Zn^{2+} present, but due to the surrounding environment, all fluorescence is quenched.

(d) Zinquin-A does not enter the nucleus.

Up until now it has been assumed that the hydrolysis of Zinquin-E to Zinquin-A depicted in Figure 2.2 occurs rapidly in the cell and that the fluorescence observed is due to complexes of Zinquin-A and Zn^{2+}, as discussed in Section 2.1. There is still some uncertainty surrounding this and hence it is possible that Zinquin-E remains unhydrolysed and the fluorescence observed is due to the complexes it forms with Zn^{2+}. If this was so, the above possibilities would exist for Zinquin-E, although the last possibility would be less likely bearing in mind the ability of Zinquin-E to readily traverse the cellular membrane. However, for the purpose of this discussion, it is assumed that the hydrolysis does occur and therefore it is the properties of Zinquin-A that are of interest in the cell.

Explanations (a) to (c) are hard to differentiate between experimentally and all are possible to some extent, except explanation (a), which is quite unlikely as it is contradicted by the observation that nuclei are very rich in Zn^{2+}, as shown by ^{65}Zn labelling studies,[24] the intranuclear presence of metallothionein[30] which is a strong Zn^{2+} coordinator,[31-33] the fact that Zn^{2+} can be incorporated into DNA binding proteins as a zinc finger[34,35] and that Zn^{2+} is also linked to the process of transcription[23,24] which occurs within the nucleus. In fact, nuclear Zn^{2+} has been estimated to constitute 25-40% of cellular Zn^{2+}.[36]

Option (b) is quite likely if the Zn^{2+} present in the nucleus is strongly coordinated by protein as Zinquin-A would then be unable to remove it to form fluorescent [Zn(ZQA)] or $[Zn(ZQA)_2]^{2-}$. For this to occur, the metalloenzyme or metalloprotein would need to have a higher affinity for Zn^{2+} than Zinquin-A, that is, have a stability constant, log $K_1 > 9.65$. In addition, if the Zn^{2+} coordination sphere is fully occupied or shielded by surrounding protein, it is unlikely that Zinquin-A can coordinate to the already bound Zn^{2+} to form a fluorescent ternary complex. It is possible that the Zn^{2+} in zinc fingers, which is very tightly coordinated, is sufficiently surrounded by the protein backbone and side chain structure to prevent Zinquin-A coordinating to it because to do so would cause a large distortion in the stable tertiary structure of the molecule.[12] It is also likely that Zn^{2+} which has other structural roles, such as in some enzymes, would also be strongly coordinated and protected from Zinquin-A in this manner.

Possibility (c) is suggested by results from this study (see Chapter 4) that indicate that the fluorescence of bound Zinquin-A varies with the surrounding coordination environment. It is possible that the coordination environment about Zn^{2+} in the nucleus causes non-radiative decay of the excited Zinquin-A species and therefore no fluorescence is observed. This theory is supported by work done with metallothionein in rat hepatocytes which showed that when Zinquin-A was bound to the Zn^{2+} in metallothionein, some quenching of fluorescence was observed.[7] The observation of an increase in Zinquin-A fluorescence in cells undergoing apoptosis (programmed cell death)[8, 10] can be used to support either the theory that not all Zn^{2+} is available for coordination (possibility (b)) or that the environment about some bound Zn^{2+} causes quenching (possibility (c)). This can be explained by the fact that any increase in fluorescence of a cell must come from Zn^{2+} already present in the cell changing its coordination environment if the medium about the cell is not rich in available Zn^{2+}.

The final suggestion, (d), arises from the fact that charged species are usually unable to pass through the lipophilic membranes found in cells, especially the cellular membrane, without an appropriate channel or transporter (see Section 3.1.1). It has been proposed that once inside the cell, the neutral Zinquin-E is hydrolysed to the acid, Zinquin-A, which is then prevented from re-traversing the cellular membrane by its negative charge (see Figure 2.2). Since the nucleus is enclosed in a double membrane, it is possible that Zinquin-A is unable to penetrate into the nucleus. This would result in the absence of fluorescence observed. However, it is still possible that Zinquin-A is able to migrate into the nucleus, as is suggested by the first three possibilities above. The nature of the nuclear membrane is different from that of the cellular membrane so it is possible that although Zinquin-A is unable to escape from the cellular membrane,[8] there exists a path for it to cross the nuclear membrane. This possibility is supported by the observation that other organelles surrounded by membranes, such as secretory granules of pancreatic islet cells, show Zinquin-A fluorescence.[15] However, this observation may also support the suggestion that Zinquin-E is not rapidly hydrolysed to Zinquin-A upon entering the cell.

It is likely that as the cell type is altered, so too are the contents of the nucleus and the properties of the nuclear membrane. This causes variations in nuclear shadow between cell types and is likely to be accompanied by a change in one or all of the possibilities offered above.

In order to determine whether or not Zinquin-A penetrates the nuclear membrane, it was decided to separate nuclei from their cells by the use of a detergent, NP40,[37] and study them separately. The detergent dismembers the cellular membrane, breaking it up and allowing the organelles and cytosol contained within to escape. The nuclei can then be removed from the resulting mixture by centrifugation. Using this method, the Zinquin-A and Zinquin-E fluorescence of LIM 1215 colon cancer cells and their nuclei were studied both with their natural level of Zn^{2+} and with an increased level obtained from incubation with $ZnSO_4$ and pyrithione, which allows the transport of Zn^{2+} through membranes. The technique of adding Zn^{2+} to cells was used to aid the visualisation of cells which have a naturally low concentration of Zn^{2+}. Fluorescence from both Zinquin-A and Zinquin-E incubated nuclei was studied to determine if either are able to penetrate the nuclear membrane. For completeness, the whole cells were also incubated in both the ester and the acid, although penetration of the acid through the cellular membrane was not expected due to its charged state. Several images were captured for each of the eight samples, ensuring that between 10 and 53 cells or nuclei were able to be measured for intensity. Samples of the cells and nuclei observed are shown in Figures 3.9 to 3.15 below. Using a computer to falsely colour an image is a method often used to give a better view of the change in intensity of fluorescence within a cell as the human eye is more sensitive to a change in colour than a change in brightness. Using this method, any heterogeneity within the cell can then be easily identified by the different colours observed. For this reason Figures 3.9 and 3.13 have been colour mapped, producing Figures 3.10 and 3.14, where black and dark blue represent a low fluorescence intensity and red represents a high fluorescence intensity. The parts of Figures 3.9 and 3.13 that show particularly low fluorescence (Section C of Figure 3.9 and Sections A and C of Figure 3.13) have also been modified using a colour map that is more sensitive to changes in low intensity to highlight the location of the cells and nuclei in these images (Figures 3.12 and 3.15). For the second colour map, blue represents low intensity fluorescence and green represents a more intense fluorescence.

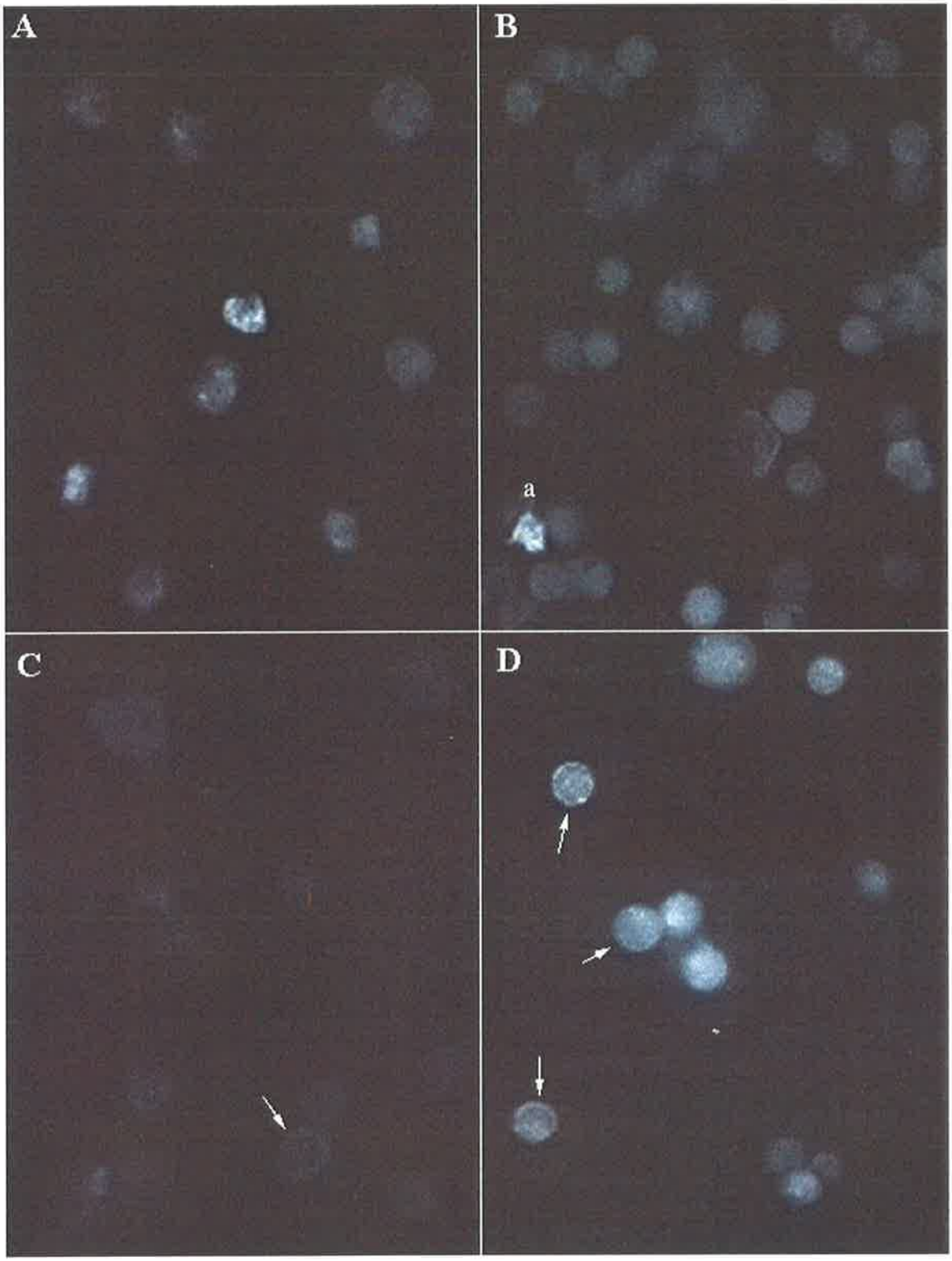

Figure 3.9 : Whole colon cancer cells incubated in Zinquin-A (A and B) and Zinquin-E (C and D). Sections B and D have increased intracellular Zn^{2+} levels due to $ZnSO_4$ and pyrithione incubation. The arrows indicate nuclear shadows and the bright cell denoted by 'a' is apoptotic. (magnification × 50)

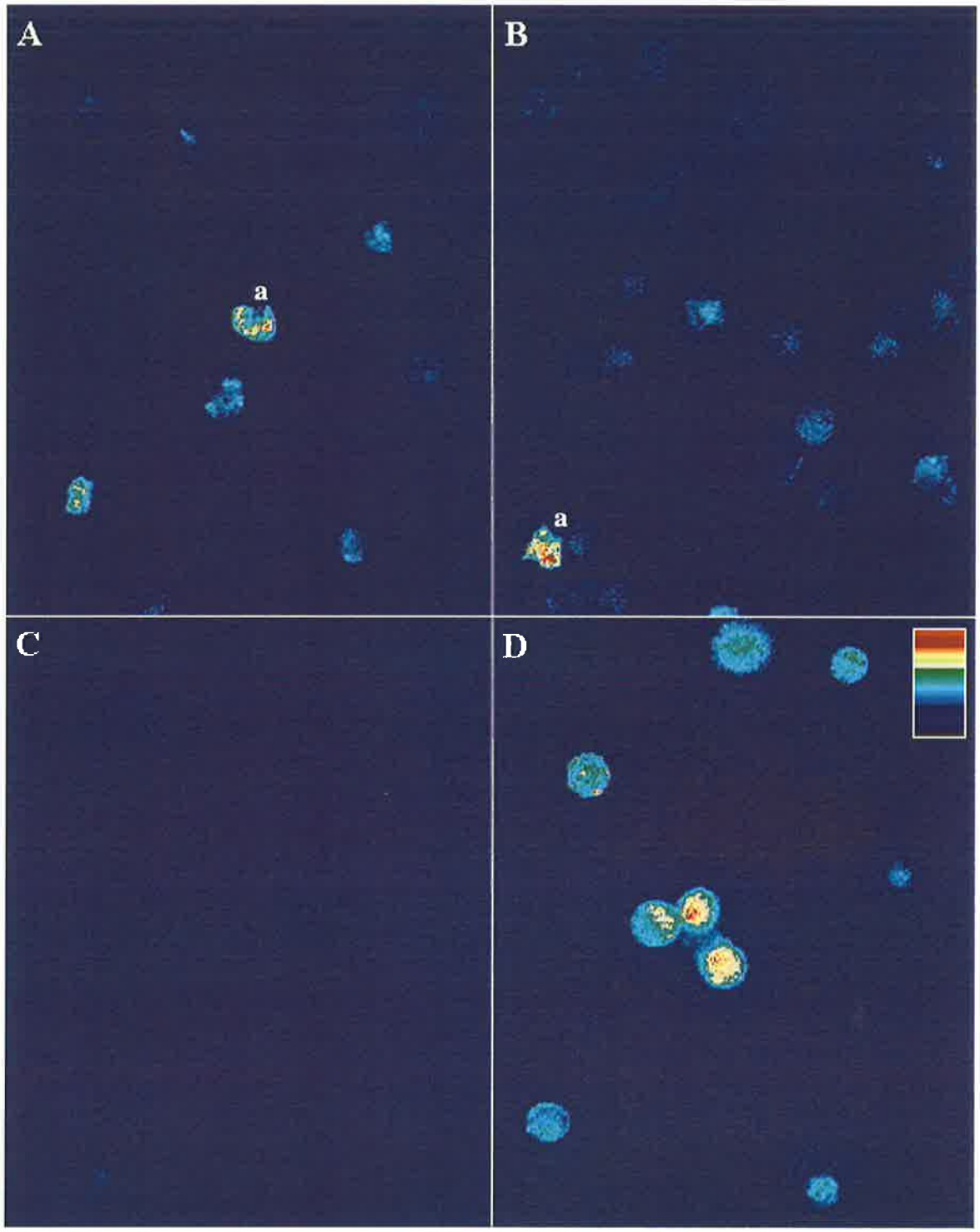

Figure 3.10 : Falsely coloured whole colon cancer cells incubated in Zinquin-A (A and B) and Zinquin-E (C and D). Sections B and D have increased intracellular Zn^{2+} levels due to $ZnSO_4$ and pyrithione incubation. These are the same cells as in Figure 3.9. Examples of apoptotic cells are marked with 'a' and the colour scale is shown in the top, right corner of Section D. (magnification × 50)

Cells release Zn^{2+} from strongly coordinated, well protected sites while undergoing apoptosis and hence an increase in fluorescence is observed within these cells as Zinquin-A coordinates to previously unavailable Zn^{2+}.[8, 10, 38] Cells with a fluorescence significantly higher than the average value are often in the process of apoptosis, however in this case, the incidence of unusually high fluorescence in cells appears to be greater than would normally be attributed to apoptosis alone, indicating some cells may have been damaged. A good example of an apoptotic cell is denoted by 'a' in Section B of Figure 3.9. This cell also shows the shrinkage and distortion associated with apoptosis. Figure 3.11 shows two dying cells which are blebbing (the appearance of nodules on the membrane exterior). This means the cellular membrane is breached and the cell contents begin to seep out. Note that despite the fact the left cell is incubated in Zinquin-A and the right in Zinquin-E, a high fluorescence intensity is observed for both. This is probably due to the fact that the cellular membrane no longer excludes the acid once blebbing occurs. This would also explain the occurrence of cells of high fluorescence in Sections A and B of Figures 3.9 and 3.10.

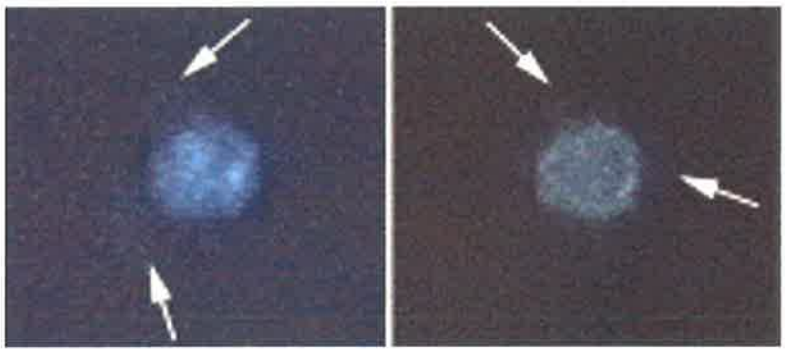

Figure 3.11 : Dying cells incubated in Zinquin-A (left) and Zinquin-E (right) showing blebbing (at arrows). Both have also been incubated in $ZnSO_4$ and pyrithione to increase intracellular Zn^{2+} concentrations. (magnification × 50, the left image was captured with the detector set to a more sensitive level than the right, hence the greater intensity of both cellular and background fluorescence.)

LIM 1215 Colon cancer cells have a low natural available Zn^{2+} concentration as can be seen by the very faint fluorescence observed for the Zinquin-E incubated cells in Section C of Figure 3.9. Locating the cells in this image is made easier by using a more sensitive colour map as in Figure 3.12. The lack of variation in the colours observed for the cells in the falsely coloured diagram indicates the uniformity of this very low fluorescence. Only one nuclear shadow is faintly visible (marked with an arrow in Section C of Figure 3.9).

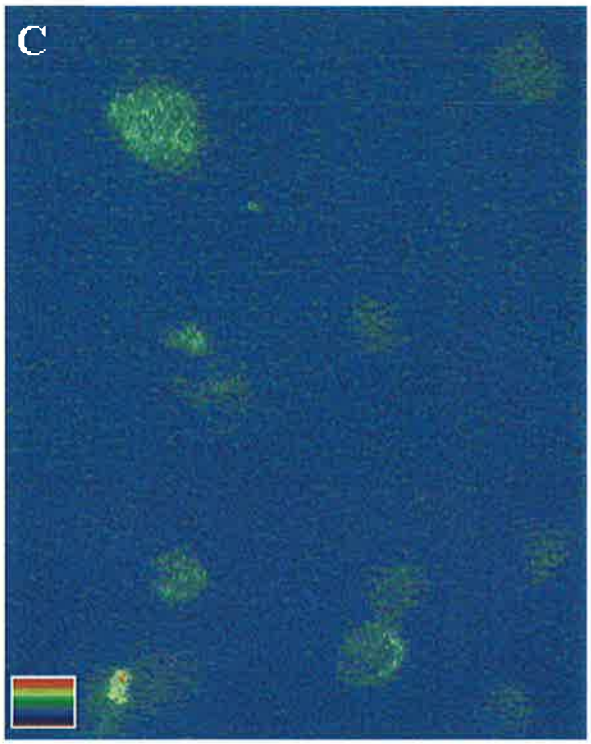

Figure 3.12 : Falsely coloured cells incubated in Zinquin-E with their natural concentration of Zn^{2+}. The cells are the same as in Section C of Figures 3.9 and 3.10, but with a more sensitive colour map. The colour scale is shown in the bottom, left corner. (magnification × 50)

As is evident from Section D of Figures 3.9 and 3.10, incubating the cells in $ZnSO_4$ and pyrithione before Zinquin-E incubation greatly increases the fluorescence observed as it increases the cytosolic Zn^{2+} concentration. The distribution of fluorescence is less uniform than those in Section C, as can be seen in both Figures 3.9 and 3.10, however it is still quite homogeneous compared to the fluorescence observed for some other types of cells. The clear definition between the nucleus and the remainder of the cell observed for hepatocytes,[15] pancreatic islet cells[7] and others,[10, 12] is not observed, with only occasional and slight nuclear shadows evident, as indicated by arrows in Section D of Figure 3.9. This could be due to the large size and flat shape of the nucleus in these cells which causes it to be easily hidden when the cell is orientated in certain ways, with overlapping fluorescing cytosol masking its position. Another explanation could be that some of the Zn^{2+} in the nucleus of these cancer cells may be in a different environment than in other nuclei and is therefore able to coordinate to, and fluoresce with, Zinquin-A.

Comparison of Sections A and B of Figures 3.9 and 3.10 shows little change in the fluorescence intensity of Zinquin-A incubated cells upon incubation in $ZnSO_4$ and pyrithione. The fluorescence observed for both is low and homogeneous, except for the two or three apoptotic cells which show a higher level of fluorescence as discussed previously. This would indicate that either no additional Zn^{2+} is reaching the cytosol or that Zinquin-A can not coordinate to the increased amount of Zn^{2+}. The former can be immediately ruled out as the cells are incubated in Zn^{2+} first, then Zinquin-A or Zinquin-E, so the same amount of Zn^{2+} should enter the Zinquin-A incubated cells as the Zinquin-E incubated cells. The latter would occur if Zinquin-A was unable to pass through the cellular membrane, as is expected due to its charge. It has been shown that cellular membranes often contain Zn^{2+}, usually bound to the membrane proteins,[3] as mentioned in Section 3.1.1. It is possible that Zinquin-A can bind to this Zn^{2+}, forming ternary complexes which produce the observed fluorescence. If this does not occur due to the nature of the membrane Zn^{2+} coordination, an alternative, but less likely, explanation exists; The observed fluorescence could be due to Zinquin-A that is bound to the cellular membrane, perhaps being partially embedded in the membrane matrix at the hydrophobic quinoline or toluene regions of the molecule. Being embedded in this manner may cause the increase in molecular rigidity required for the fluorescence of Zinquin-A, or may provide a convenient site for adventitious Zn^{2+} in the surrounding solution to coordinate.

As already mentioned, nuclei extracted from LIM 1215 colon cancer cells were also studied and examples of the fluorescence results obtained are shown in Figures 3.13 to 3.15 below.

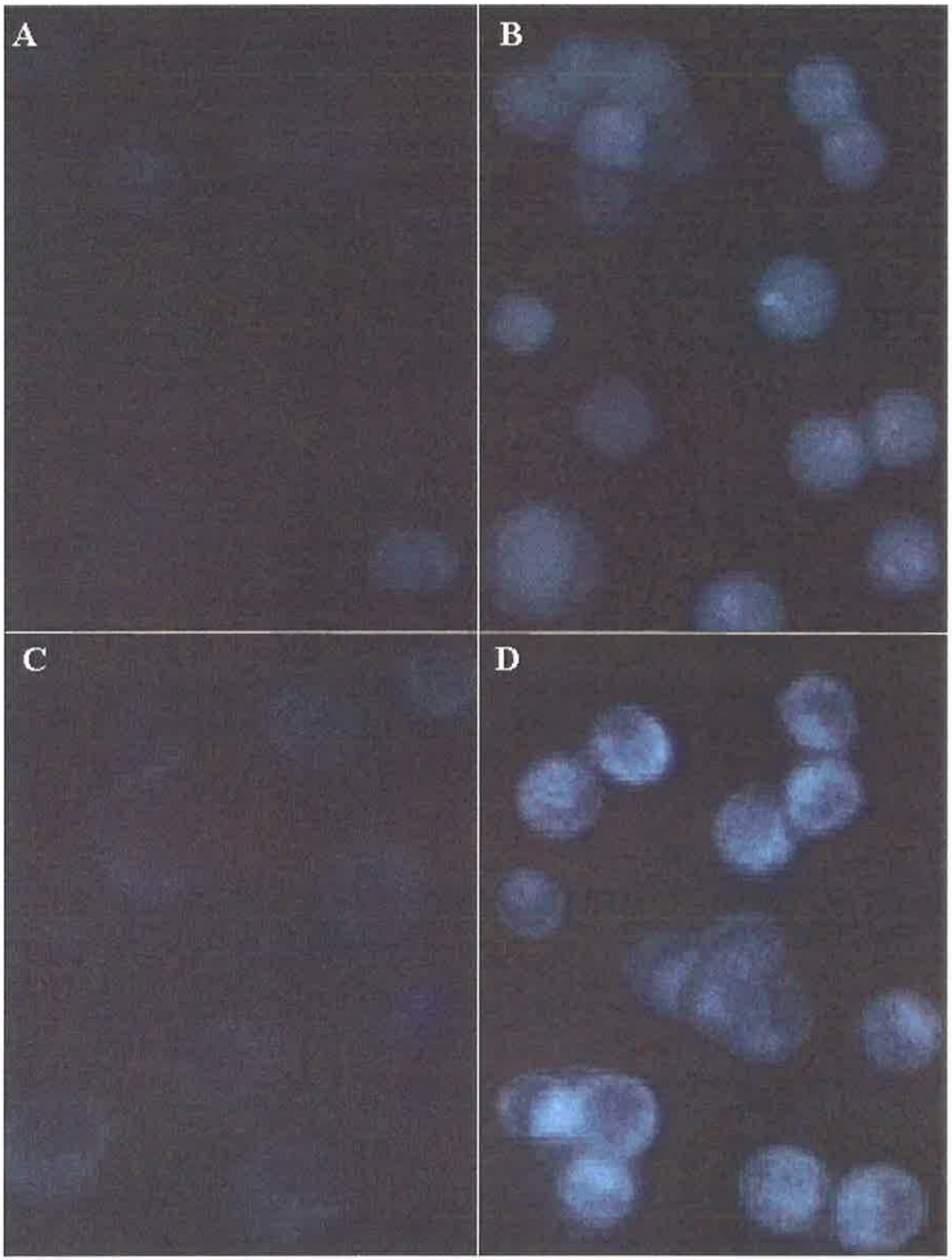

Figure 3.13 : Nuclei extracted from colon cancer cells incubated in Zinquin-A (A and B) and Zinquin-E (C and D). Sections B and D have increased intranuclear Zn^{2+} levels due to $ZnSO_4$ and pyrithione incubation of the cells before the extraction of the nuclei. (magnification × 50)

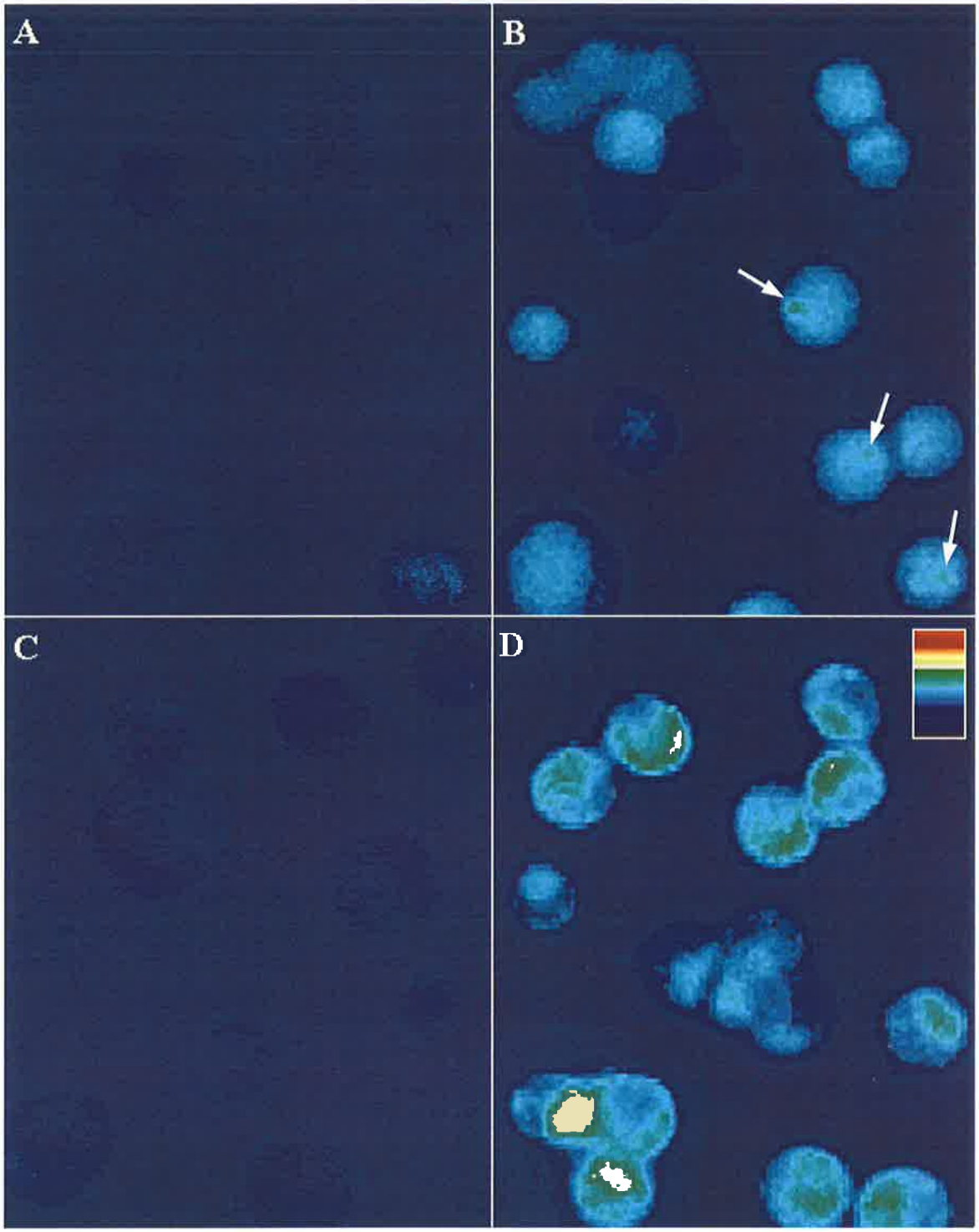

Figure 3.14 : Falsely coloured nuclei extracted from colon cancer cells incubated in Zinquin-A (A and B) and Zinquin-E (C and D). Sections B and D have increased intracellular Zn^{2+} levels due to $ZnSO_4$ and pyrithione incubation of the cells before the extraction of the nuclei. These are the same cells as in Figure 3.13. Nucleoli are indicated with arrows and the colour scale is in the top, right corner of Section D. (magnification × 50)

In looking at Figure 3.13, it is interesting to note the great increase in size of the nucleus once it has been extracted from the cell. Figures 3.9 and 3.13 are of the same magnification so it appears that the nucleus absorbs water and swells, growing to double the size of the cell. This swelling would also decrease the concentration of Zn^{2+} in the nucleus, although not the amount, causing a lower fluorescence than could be expected for unswollen nuclei.

Faint fluorescence was observed for both Zinquin-A and Zinquin-E in the nuclei with natural Zn^{2+} levels (Sections A and C in Figures 3.13 and 3.14), with Zinquin-A resulting in a slightly lower average intensity. Both of these sections have been falsely coloured with the more sensitive colour map in Figure 3.15 to locate the nuclei with greater ease. The increase in fluorescence upon pre-incubation of the cells that the nuclei were extracted from in $ZnSO_4$ and pyrithione (Sections B and D of Figures 3.13 and 3.14) suggests that both the ester and the acid are able to penetrate the nuclear membrane and the nuclear shadows observed in Figure 3.9 are due to a lower intensity of fluorescence and not an absence of it in the nucleus of these cells. It also proves that incubating cells in $ZnSO_4$ and pyrithione transports Zn^{2+} into the nucleus in addition to the cytosol despite the fact that nuclear shadows are often still visible.

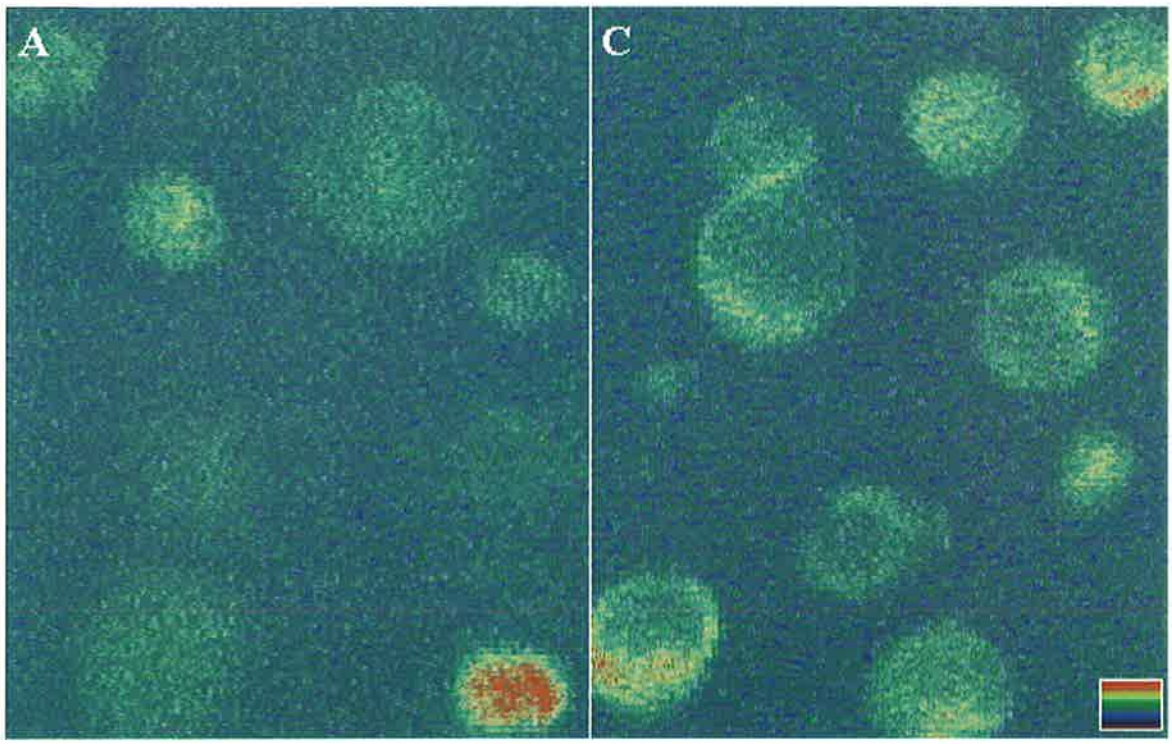

Figure 3.15 : Falsely coloured nuclei incubated in Zinquin-A (A) and Zinquin-E (C) with their natural concentration of Zn^{2+}. The cells are the same as in Sections A and C of Figures 3.13 and 3.14, but with a more sensitive colour map. The colour scale is shown in the bottom, right corner of Section C. (magnification × 50)

Evidence to support both these conclusions comes from a paper by Berendji *et al* (1997)[12] in which the effect of spontaneous NO· donors on Zn^{2+} availability was studied. It was found that the definite nuclear shadows observed in L929 fibroblast cells were removed upon treating the cells with NO· donors with a corresponding large increase in the cytosolic and nuclear fluorescence observed. This indicates that Zinquin-A does enter the nucleus of these cells, however the Zn^{2+} found there is either unavailable for coordination or in an environment that promotes Zinquin-A fluorescence quenching. The addition of NO· to the cell triggers the release of Zn^{2+} from the strongly coordinated, well protected sites, or changes the surrounding environment so that quenching no longer occurs, resulting in an increase in fluorescence. Berendji *et al* suggest that NO· destroys zinc finger or zinc finger related protein structures by the *S*-nitrosylation of cysteine residues which releases Zn^{2+} throughout the cell, particularly within the nucleus.

The fibroblast cells were also incubated in a Zn^{2+}-histidine complex which resulted in an increase in both cytosolic and nuclear fluorescence and the removal of nuclear shadows, indicating, as do the results with separated colon cancer nuclei, that incubation in a Zn^{2+} rich medium, with a Zn^{2+} transporter, increases both the cytosolic and nuclear Zn^{2+} concentration. However, variation between cells is observed. EL4 lymphocytes show no increase in fluorescence, in either the cytosol or nucleus, after incubation in Zn^{2+}-histidine complex[39] and the colon cancer cells used in this study, CLL cells[8] and T-cells[10] all show an increase in fluorescence, with the nuclear shadows still visible when incubated with $ZnSO_4$ and pyrithione. This illustrates that when Zn^{2+} is loaded into cells, it is partitioned in different environments in different cells and therefore the amount of fluorescence observed varies between cell types.

Further confirmation that Zinquin-A is able to penetrate the nuclear membrane in some cells comes from studies of spermatozoa as discussed in Section 3.1.2. It has been observed that the spermatozoan head is very rich in Zn^{2+} and shows a bright fluorescence (Figure 3.8). As can be seen in the rough diagram below, the nucleus of a spermatozoan fills the majority of the head area, indicating that this fluorescence must be emanating, at least in part, from the nucleus. Of course, if the assumption that Zinquin-E is hydrolysed to Zinquin-A in the cell is incorrect, these examples serve to prove Zinquin-E can enter the nucleus, as could be expected due to its neutral charge and hydrophobic regions.

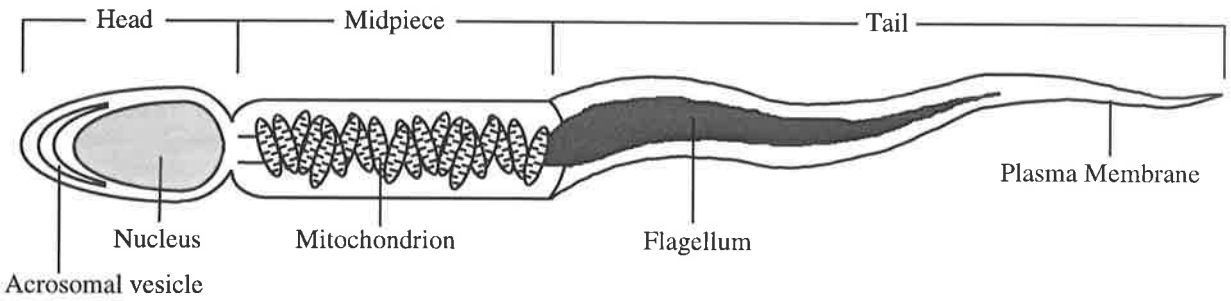

Figure 3.16 : A diagrammatic illustration of a spermatozoan.

Although Zinquin-A does not penetrate the cellular membrane, as discussed previously, it is still valid to propose that it can penetrate the nuclear membrane due to the properties of the nuclear membrane differing from those of the cellular membrane. An obvious example of these differing properties is the swelling of the extracted nuclei. The whole cells did not absorb water and swell to the same extent as the nuclei, indicating different permeabilities of their membranes. This would be expected as the cellular membrane protects the cell from extracellular influences and must therefore be stronger and more selective with respect to its permeability than the nuclear membrane. The nuclear membrane usually only has to contend with the contents of the cytoplasm, and therefore is not required to be as strong as the cellular membrane.

The distribution of fluorescence within the Zinquin-E incubated nuclei is quite different from that in the Zinquin-A incubated nuclei despite the average intensity being similar for both. The acid (Section A and B of Figures 3.13 and 3.14) produced a uniform fluorescence with occasional brighter dots which could be nucleoli[40] (these are better seen in the falsely coloured Figure 3.14 and are indicated by arrows in that figure) whereas the ester incubated nuclei (Sections C and D of Figures 3.13 and 3.14) show shadows similar to those seen in the cells. The non-uniform fluorescence distribution and the bright nucleoli help support the theory that the nucleus of these cells does contain some Zn^{2+}, and that the nuclear shadows observed in whole cells are not due to Zinquin-A having no Zn^{2+} to coordinate to in this case. It is unclear why this difference in fluorescence distribution is observed. Zinquin-E is unlikely to get hydrolysed under the conditions used to obtain the nuclei. Protease inhibitor was added to the lysis buffer used to extract and view the nuclei. This inhibits the enzymes that cleave amide linkages and prolongs the life of extracted nuclei but these enzymes also act as esterases and Zinquin-E will not be hydrolysed while they are inhibited. So, one possibility for the difference in fluorescence distribution is that Zinquin-E coordinates to Zn^{2+} intact, then due to slightly different quenching or coordination properties, a different fluorescence pattern is

observed. It is possible that the outer, high intensity fluorescence observed in the case of the ester is due to the collapsed cytoskeleton of the cell,[41] however, the fact that this is not observed in the case of Zinquin-A suggests that even if this is the case, the acid and ester are still interacting differently with any Zn^{2+} present.

The fluorescence in the images obtained of cells and nuclei under various conditions was quantified using Video Pro software which gave an average intensity within a designated area about the cell or nucleus. Randomly chosen background areas of approximately the same size as the cells or nuclei were also quantified. These results are graphed below in Figures 3.17 to 3.20.

As can be seen from Figures 3.17 and 3.19 and Tables 3.1 and 3.2, the background fluorescence is quite uniform for both the whole cells and the extracted nuclei, with averages between 25.6 and 27.2 and standard deviations of approximately 6% for the cells and averages between 36.2 and 37.4 and standard deviations of approximately 8% for the nuclei. This low background fluorescence is due to the Zinquin-A or -E still in the buffer that the cells or nuclei are suspended in and the scattering of the incident light from surrounding particles. The cells and nuclei were not washed after incubation with Zinquin-A or -E as they were already beginning to deteriorate by this time and washing would risk further damage, especially with respect to the delicate nuclei. Previous studies have shown that washing cells to remove Zinquin-E after incubation does not affect the fluorescence observed within the cell.[8] The greater background fluorescence for the nuclei can be attributed to either remnants of Zn^{2+} originating from the destroyed cellular tissue and decaying nuclei or the slight drift with time, over days, of the video detection intensity (the nuclei were studied on a different day from the cells). The latter is known to occur, however the former should not be fully ruled out, despite the removing of the majority of cell debris before incubation with Zinquin-A or -E, because the extracted nuclei decay relatively rapidly. To take into consideration the drift in detection intensity alone, the ratio of cell or nuclear intensity to background intensity can be used for comparison purposes.

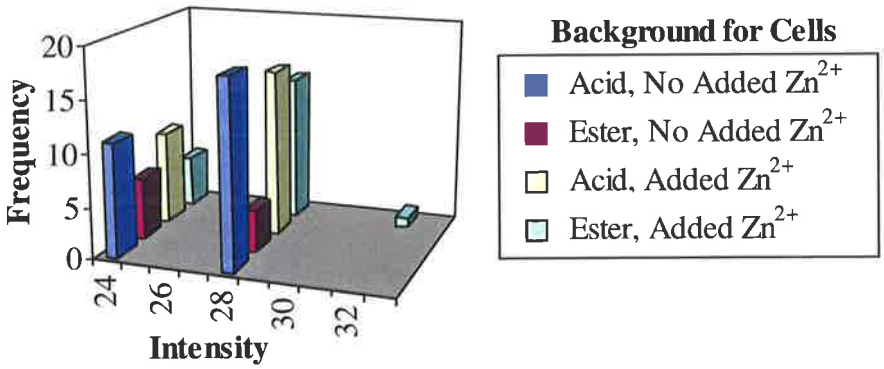

Figure 3.17 : Background fluorescence observed for colon cancer cells incubated in Zinquin-A or Zinquin-E with their natural level and an increased level of Zn^{2+}.

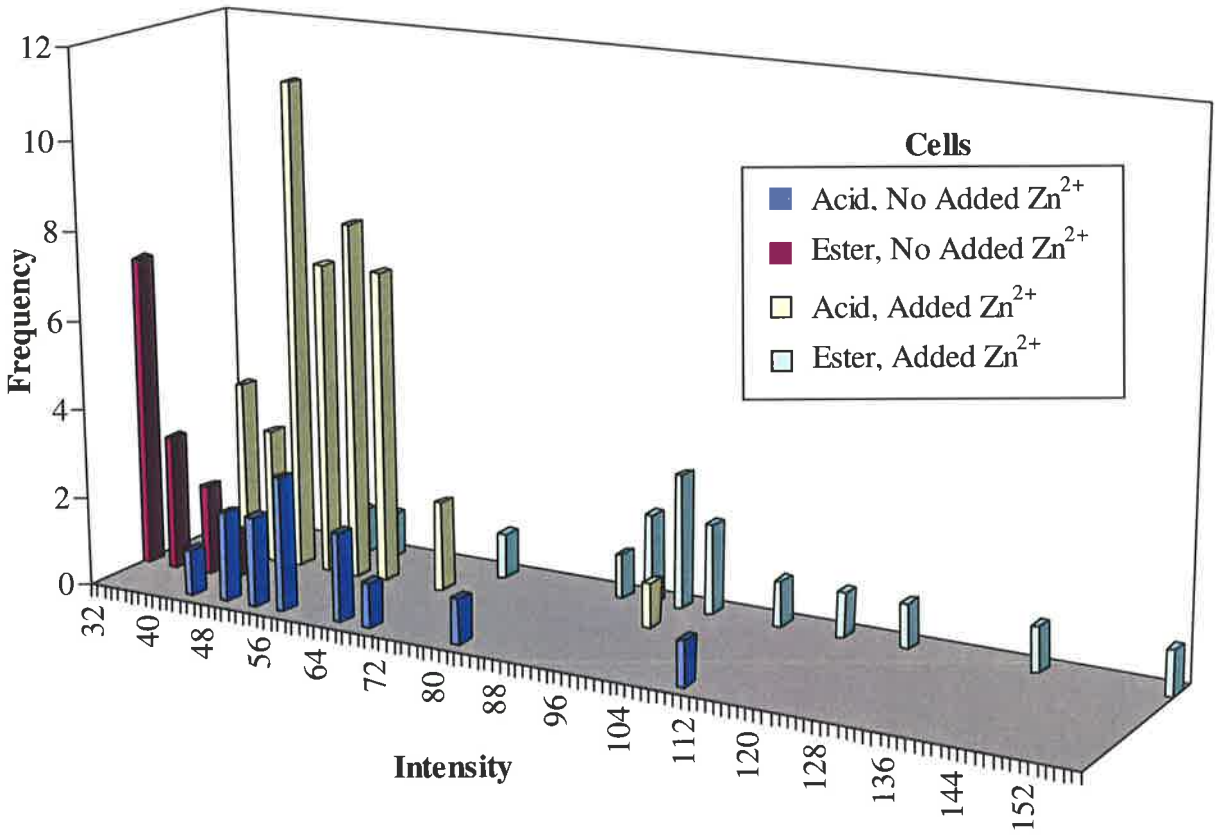

Figure 3.18 : Fluorescence of colon cancer cells incubated in Zinquin-A or Zinquin-E with their natural level and an increased level of Zn^{2+}.

Background	Average	Standard Deviation
Acid, no added Zn^{2+}	26.5	2.0
Ester, no added Zn^{2+}	25.6	2.1
Acid, added Zn^{2+}	26.6	2.0
Ester, added Zn^{2+}	27.2	2.1

Whole Cells	Average	Standard Deviation
Acid, no added Zn^{2+}	62.2	17.4
Ester, no added Zn^{2+}	35.3	4.4
Acid, added Zn^{2+}	54.1	9.7
Ester, added Zn^{2+}	100.4	27.4

Table 3.1 : Average intensity and its standard deviation for whole cells and their backgrounds under various conditions.

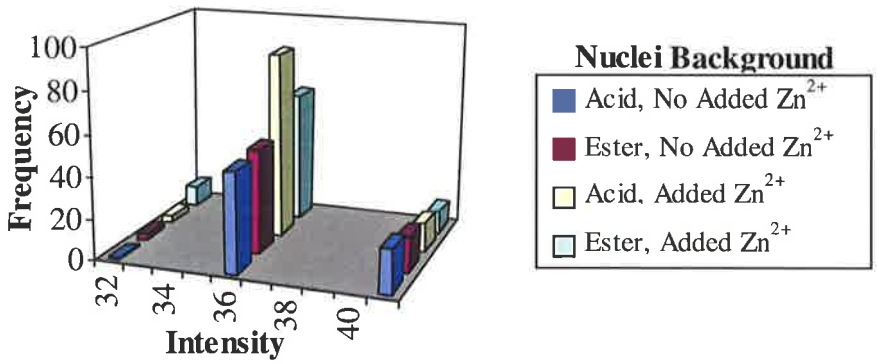

Figure 3.19 : Background fluorescence observed for nuclei extracted from colon cancer cells incubated in Zinquin-A or Zinquin-E with their natural level and an increased level of Zn^{2+}.

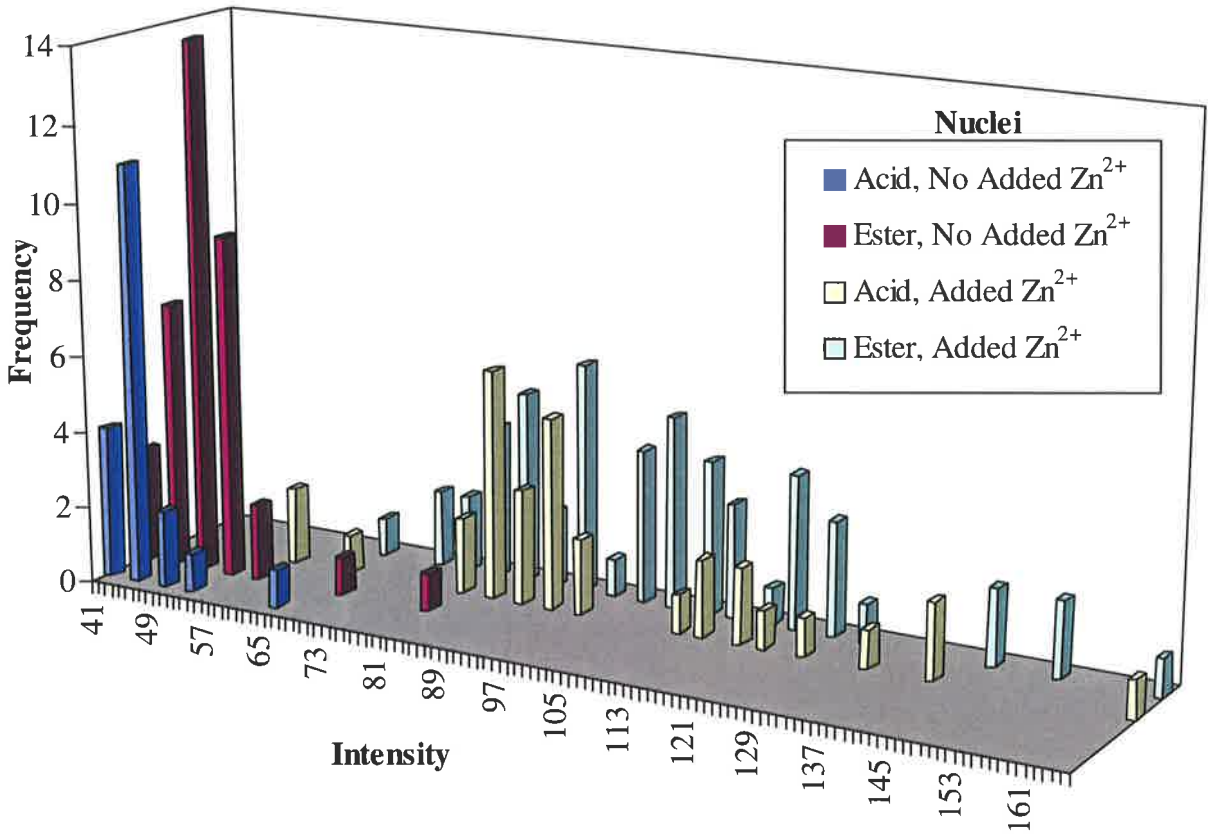

Figure 3.20 : Fluorescence of nuclei extracted from colon cancer cells incubated in Zinquin-A or Zinquin-E with their natural level and an increased level of Zn^{2+}.

Background	Average	Standard Deviation
Acid, no added Zn^{2+}	37.4	2.4
Ester, no added Zn^{2+}	37.0	2.4
Acid, added Zn^{2+}	36.6	1.9
Ester, added Zn^{2+}	36.2	2.3

Extracted Nuclei	Average	Standard Deviation
Acid, no added Zn^{2+}	46.1	5.5
Ester, no added Zn^{2+}	50.4	7.3
Acid, added Zn^{2+}	99.4	24.7
Ester, added Zn^{2+}	104.4	22.5

Table 3.2 : Average intensity and its standard deviation for extracted nuclei and their backgrounds under various conditions.

In contrast to the background intensities, the cell and nuclear intensities show a wide variation, up to a standard deviation of 28%. This is due to damaged cells which give higher readings, out of focus cells which give lower readings and cells at different stages of their life cycle which give varied readings. Further uncertainty is produced by clumps of cells which give higher readings near their centre than should be attributed to the cells found there and by cells which are overlapped, either in the same, or in different, focal planes. The same possibilities exist for nuclei and care was taken to avoid including cells and nuclei that were obviously overlapped or clumped. If enough cells and nuclei were sampled, it appears Maxwell-Boltzmann distributions of intensities would be observed.

Many of the points noted from the images alone are reiterated in these quantified values. The similarity in fluorescence of Zinquin-A incubated whole cells with and without added Zn^{2+} is quite evident from Figure 3.18 and the values in Table 3.1, with the average values agreeing within the standard deviation. The increase in fluorescence upon incubation in $ZnSO_4$ and pyrithione for the other cells and nuclei is also well illustrated. The similarity in average fluorescence, despite differences in the distribution of Zinquin-A and Zinquin-E fluorescence, for both sets of nuclei with enhanced Zn^{2+} levels (Figures 3.13 and 3.14) is also highlighted. Table 3.3 contains the ratios of fluorescence intensity and background intensity, allowing the cells and nuclei to be compared to some extent. Where Zinquin-E has been used, and it is therefore certain the fluorophore has entered the cells and nuclei, the nuclear fluorescence is equal to or lower than the corresponding cellular fluorescence, as may be expected due to the swelling of the nuclei and the fact they appear as shadows in the cellular images. The Zinquin-A incubated nuclei with a natural Zn^{2+} concentration also show a decrease in intensity compared to the corresponding whole cells, however, the nuclei with increased Zn^{2+} concentration show the opposite effect. This possibly supports the proposal that Zinquin-A coordinates to the outside of the cellular membrane and therefore the comparison of the cellular intensity to nuclear intensity is invalid in this case.

Whole Cells	Ratio
Acid, no added Zn^{2+}	2.3
Ester, no added Zn^{2+}	1.4
Acid, added Zn^{2+}	2.0
Ester, added Zn^{2+}	3.7

Extracted nuclei	Ratio
Acid, no added Zn^{2+}	1.2
Ester, no added Zn^{2+}	1.4
Acid, added Zn^{2+}	2.7
Ester, added Zn^{2+}	2.9

Table 3.3 : Ratio of cellular or nuclear fluorescence to background intensity for cells (left) and nuclei (right) under various conditions.

In conclusion, it is most likely that the nucleus of cells does contain Zn^{2+}, however in some cells, this Zn^{2+} is tightly bound with a coordination environment that either prevents the formation of ternary complexes by preventing Zinquin-A from coordinating to it or causes quenching of fluorescence of the ternary complex, if it forms. This results in a lower intensity fluorescence than observed in the cytosol, and the appearance of a nuclear shadow. It is evident that the occurrence of nuclear shadows is dependent upon cell type, and therefore it can not be confidently concluded that all separated nuclei will show the fluorescence observed in colon cancer cells. More studies are necessary to fully unravel the puzzles of nuclear shadows and the mechanisms of Zinquin-A or -E hydrolysis, coordination and fluorescence in cells. Some suggestions for future work on these topics are included in Section 6.1.

3.3 : References

1. J. Brachet, *Sci. Am.*, **205**, 3, 1961.

2. S. J. Singer, G. L. Nicholson, *Science*, **175**, 720, 1972.

3. W. J. Bettger and B. L. O'Dell, *Life Sci.*, **28**, 1425, 1981.

4. C. K. Mathews and K. E. van Holde, "*Biochemistry*", The Benjamin/Cummings Publishing Company, Inc, California, 1990.

5. J. W. Kleineke and I. A. Brand, *J. Pharmacol. Toxicol. Methods*, **38 (4)**, 181, 1997.

6. I. A. Brand and J. Kleineke, *J. Biol. Chem.*, **271 (4)**, 1941, 1996.

7. P. Coyle, P. D. Zalewski, J. C. Philcox, I. J. Forbes, A. D. Ward, S. F. Lincoln, I. Mahadevan and A. M. Rofe, *Biochem. J.*, **303**, 781, 1994.

8. P. D. Zalewski, I. J. Forbes and W. H. Betts, *Biochem. J.*, **296 (2)**, 403, 1993.

9. N. Wellinghausen, M. Martin and L. Rink, *Eur.J. Immunol.*, **27 (10)**, 2529, 1997.

10. P. D. Zalewski, I. J. Forbes R. F. Seamark, R. Borlinghaus, W. H. Betts, S. F. Lincoln and A. D. Ward, *Chem. Biol.*, **1**, 153, 1994.

11. M. Tsuda, K. Imaizumi, T. Katayama, K. Kitagawa, A. Wanaka, M. Tohyama, T. Takagi, *J. Neurosci.*, **17 (17)**, 6678, 1997.

12. D. Berendji, V. Kolbbachofen, K. L. Meyer, O. Grapenthin, H. Weber, V. Wahn and K. D. Kroncke, *FEBS Lett.*, **405 (1)**, 37, 1997.

13. P. D. Zalewski, X. Jian, L. L. L. Soon, W. G. Breed, R. F. Seamark, S. F. Lincoln, A. D. Ward and F. Z. Sun, *Reprod. Fertil. Dev.*, **8 (7)**, 1097, 1996.

14. R. D. Palmiter, T. B. Cole and S. D. Findley, *EMBO J.*, **15 (8)**, 1784, 1996.

15. P. D. Zalewski, S. H. Millard, I. J. Forbes, O. Kapaniris, A. Slavotinek, W. H. Betts, A. D. Ward, S. F. Lincoln and I. Mahadevan, *J. Histochem. Cytochem.*, **42 (7)**, 877, 1994.

16. N. Wellinghausen, A. Fischer, H. Kirchner and L. Rink, *Cell. Immunol.*, **171 (2)**, 255, 1996.

17. P. D. Zalewski, R. F. Seamark, P. Kotaras, F.-Z. Sun, unpublished.

18. P. D. Zalewski and R. F. Seamark, unpublished.

19. B. Wetterdal, *Acta. Radiol.*, **156** (suppl.), 3, 1958.

20. J. Parizek, J. C. Boursnell, M. P. Hay, A. Balbicky and D. M. Taylor, *J. Repod. Fertil.*, **12**, 501, 1966.

21. F. Timm and G. Schulz, *Histochemie*, **7**, 15, 1966.

22. B. L. Vallee and K. H. Falchuk, *Physiol. Rev.*, **73**, 79, 1993.

23. D. E. Epner and H. R. Herschman, *J. Cell. Physiol.*, **148**, 68, 1991.

24. R. J. Cousins and L. M. Lee-Ambrose, *J. Nutr.*, **122**, 56, 1992.

25. U. Kvist, L. Björndahk, G. M. Roomans and C. Lindholmer, *Acta Physiol. Scand.*,**125**, 297, 1985.

26. M. Morisawa and H. Mohri, *Exp. Cell Res.*, **70**, 311, 1972.

27. H. I. Calvin, F. H. F. Hwang and H. Wohlrab, *Biol. Reprod.*, **13**, 228, 1975.

28. P. D. Zalewski, unpublished.

29. S. Kjellberg, L. Björndahk and U. Kvist, *Int. J. Androl.*, **15**, 103, 1992.

30. C. Hogstrand, N. J. Gassman, B. Popova, C. M. Wood, P. J. Walsh, *J. Exp. Biol.*, **199 (11)**, 2543, 1996.

31. W. Raun, G. Wagner, E. Wörgötter, M. Vasak, J. H. R. Kägi and K. Wüthrich, *J. Mol. Biol.*, **187**, 125, 1986.

32. P. Schultze, E. Wörgötter, W. Braun, G. Wagner, M. Vašák, J. H. R. Kägi and K. Wüthrich, *J. Mol. Biol.*, **203**, 251, 1988.

33. J. H. R. Kägi and Y. Kojima, *Experientia Suppl.*, **52**, 25, 1987.

34. B. L. Vallee, J. E. Coleman and D. S. Auld, *Proc. Natl. Acad. Sci. USA*, **88**, 999, 1991.

35. H. Takatsuji, *Cellular & Molecular Life Sciences*, **54 (6),** 582, 1998.

36. R. J. Cousins, *Physiol. Rev.*, **65**, 238, 1986.

37. Z. Z. Chen, J. C. McGuire, K. L. Leach and J. C. Cambier, *J. Immunol.*, **138 (7)**, 2345, 1987.

38. P. D. Zalewski, I. J. Forbes and C. Giannakis, *Biochem. Inter.*, **24**, 1093, 1991.

39. K. -D. Kröncke, Biomedical Research Centre, Heinrich-Heine University, Düsseldorf, Germany, private communication.

40. P. D. Zalewski, Department of Medicine, University of Adelaide, Queen Elizabeth Hospital, South Australia, Australia, private communication.

41. M. Osborn and K. Weber, *Exp. Cell Res.*, **106**, 339, 1977.

CHAPTER 4

PROPERTIES OF ZINQUIN-A TERNARY COMPLEXES OF THE FORM [Zn(L)ZQA]

4.1 : Introduction

In Chapter 3 several examples of the use of Zinquin in cells and tissue were considered.[1-15] Although fluorescence is observed in many types of cells, and it has been shown that this fluorescence is due to the complexation of Zinquin-A to Zn^{2+} in those cells,[7, 12, 15] it is not known what kind of coordination environment the Zn^{2+} is in when it combines with Zinquin-A to produce the observed fluorescence. It is thought that all 'free', or readily available, Zn^{2+} dissolved in the cytosol will coordinate to Zinquin-A and produce fluorescent [Zn(ZQA)] and $[Zn(ZQA)_2]^{2-}$ due to the relatively large Zn^{2+} stability constant of Zinquin-A, however, the extent of Zinquin-A coordination to Zn^{2+} in other coordination environments is largely unknown. Since the concentration of 'free' Zn^{2+} is small in comparison with that of the tightly complexed Zn^{2+} in metalloenzymes[16] the effect of Zinquin-A in these other environments is of interest. Zinquin-A is incapable of removing strongly bound Zn^{2+}, that is, Zn^{2+} in complexes characterised by higher Zn^{2+} stability constants than those observed for Zinquin-A. In addition, it seems unlikely that Zinquin-A would be capable of simultaneously coordinating to strongly bound Zn^{2+} when it is totally surrounded, or protected by, protein or enzyme. Zinc(II) in the active sites of enzymes may fall into this category if the active site is inflexible and Zinquin-A is too large or the incorrect shape to enter it. It is also possible that the strongly bound Zn^{2+} in zinc fingers of DNA binding proteins is sufficiently surrounded by the protein backbone and side chain structure to prevent Zinquin-A coordinating to it, as discussed in Section 3.2.[6] Studies which have shown that the concentration of Zn^{2+} obtained from Zinquin-A fluorescence can be lower than that determined using atomic-absorption spectroscopy support the theory that not all Zn^{2+} in the cell is bound by Zinquin-A.[15] The greatest uncertainty is with respect to Zn^{2+} that exist in environments between these two extremes. Many proteins and enzymes are likely to have average Zn^{2+} affinities or Zn^{2+} coordination sites which are not well protected, allowing Zinquin-A access to the Zn^{2+}. In this case, there are two options. The distribution of Zn^{2+} between coordination environments is thermodynamically controlled, with the rate of achievement of thermodynamic equilibrium expected to vary with the nature of the

competing coordination sites. Thus, if given sufficient time, Zinquin-A can remove the Zn^{2+} from proteins or enzymes that have a lower affinity for Zn^{2+} than itself, forming fluorescent [Zn(ZQA)] or $[Zn(ZQA)_2]^{2-}$. Alternatively, the Zinquin-A may simultaneously coordinate to the Zn^{2+} without removing it, forming a ternary complex of the type [Zn(L)ZQA], where L is the protein or enzyme. As a complex of this type may have different modes of relaxation in the excited state than [Zn(ZQA)] or $[Zn(ZQA)_2]^{2-}$, it is possible that complexes of this type will exhibit different fluorescent properties from their binary equivalents.

As has been mentioned previously (Chapter 1), Zn^{2+} is often found as an integral part of enzymes where it is designed to generate nucleophiles, such as OH^-, RO^- and H^-, to attack electrophilic centres such as partially positive carbons of carbonyl functions. Many Zn^{2+} enzymes have been discovered, including carbonic anhydrase,[17-19] alcohol dehydrogenase,[20, 21] DNA and RNA polymerases,[22, 23] alkaline phosphatases[24, 25] and peptidases such as carboxypeptidase,[26-28] aminopeptidase,[29, 30] thermolysin[31-33] and β-lactamase.[34] The activity of these enzymes depends upon the presence of Zn^{2+} which is found in a stoichiometric amount. Many of these enzymes have been extensively studied and characterised, with their amino acid sequences and tertiary structures determined by X-ray crystallography. A brief description of some of these enzymes is provided in Section 1.1.1. Many non-enzymatic Zn^{2+} containing bioinorganic molecules have also been studied, such as DNA zinc fingers,[35, 36] metallothionien,[37-40] and insulin.[41]

Since many Zn^{2+} coordination sites in enzymes and proteins have nitrogen donor atoms (see Section 1.1.1), they can be approximated by using nitrogen containing macrocycles and ligands such as cyclen, cyclam, tacn, tacdo and tren (Figure 4.1). The two oxygen donor ligands in Figure 4.1, $NTA.H_3$ and TEA, have been included in this study to approximate enzymes and proteins which coordinate to Zn^{2+} with oxygen, and to allow a comparison between the effect of ligands with soft nitrogen and hard oxygen donors on Zinquin-A fluorescence. This set of ligands provides a convenient range to demonstrate the effect of variation in the number of donor atoms (the tetraamines, cyclen and cyclam, compared with the triamines, tacn and tacdo), variation in ring size (cyclen compared with cyclam and tacn compared with tacdo), variation in shape (macrocycles compared with acyclic ligands) and variation in donor atom, especially for the series tren, NTA^{3-} and TEA where the donor groups include amine, hydroxyl and carboxylate groups. Oxygen donor macrocycles were not used for this study as they have a high affinity for sodium ions and were therefore unsuitable for study under the conditions used.

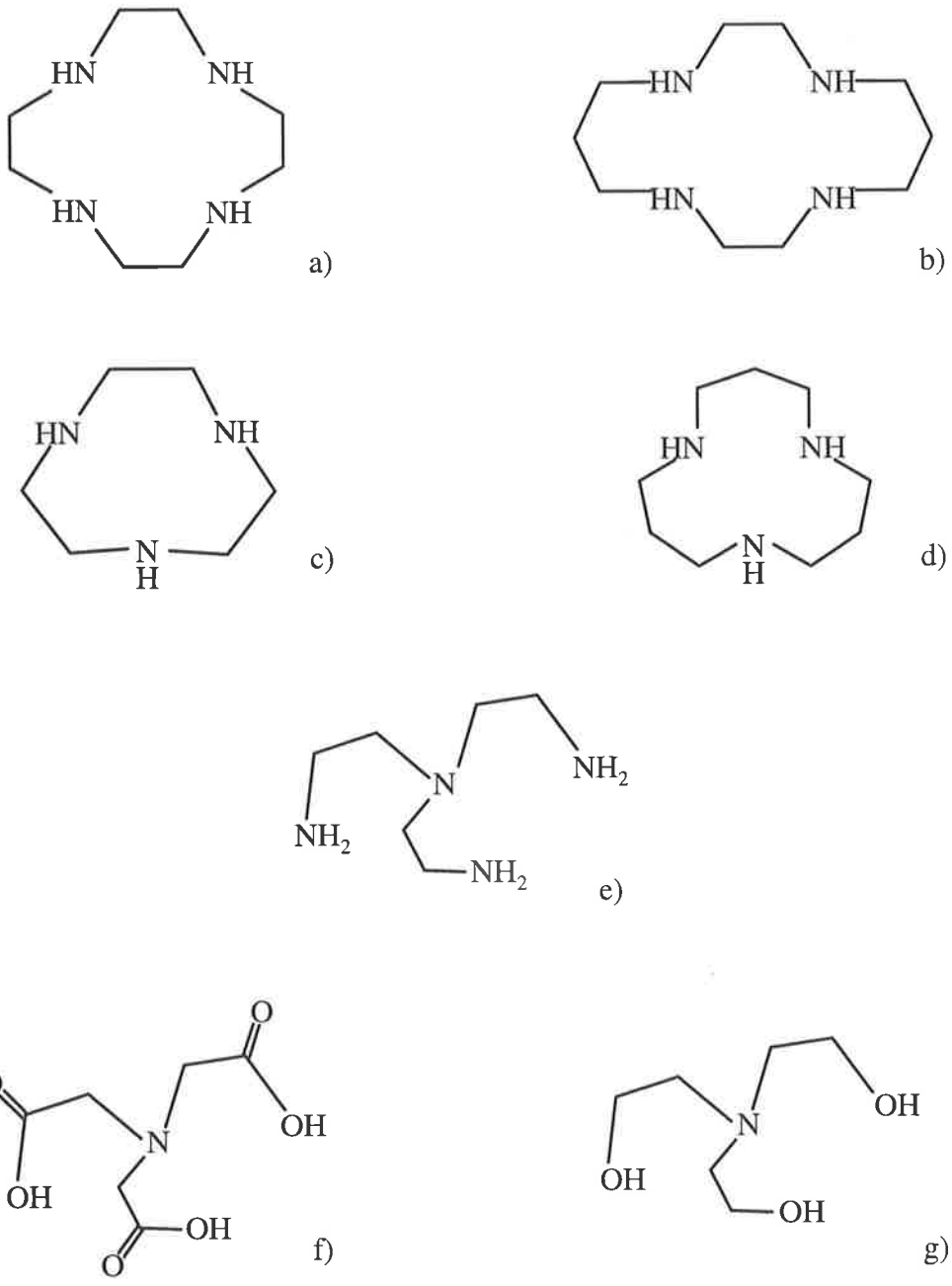

Figure 4.1 : Ligands used to study the effect of the environment surrounding Zn^{2+} on Zinquin-A fluorescence.

a) 1,4,7,10 - tetraazacyclododecane (**cyclen**)

b) 1,4,8,11 - tetraazacyclotetradecane (**cyclam**)

c) 1,4,7 - triazacyclononane (**tacn**)

d) 1,5,9 - triazacyclododecane (**tacdo**)

e) Tris(2-aminoethyl)amine (**tren**)

f) Nitrilotriacetic Acid (**NTA.H_3**)

g) Triethanolamine (**TEA**)

The use of ligands of the type shown in Figure 4.1 as models for enzymes and other biological entities is not without precedent. The macrocycles tacdo and cyclen, and various substituted macrocycles, bound to Zn^{2+} have been used to model the active sites of various Zn^{2+} containing enzymes such as carbonic anhydrase, alkaline phosphatase and β-lactamase.[42-50] Studies have shown that the crystal structure of $[Zn(tacdo)OH]^{+}$ has a similar geometry about the Zn^{2+} to that of the carbonic anhydrase active site,[51] and that $[Zn(tacdo)(H_2O)]^{2+}$ is similar to carbonic anhydrase in its increased anion affinity compared with $[Zn(H_2O)_6]^{2+}$.[43] It has been found that complexation with tacdo remarkably reduces the pK_a of water bound to Zn^{2+} from a value of about 9 for $[Zn(H_2O)_6]^{2+}$ to 7.3[42] which compares favourably with the pK_a ~7 attributed to the water attached to the Zn^{2+} in the active site of carbonic anhydrase.[19, 18] From these studies, and similar studies with cyclen, it has been proposed that the carbonic anhydrase mechanism involves the deprotonation of water attached to Zn^{2+} and the subsequent nucleophilic addition of the resulting OH^- to an electrophile. Cyclen has also been used to create artificial receptor molecules for nucleobases, nucleosides and nucleotides which mimic other biological roles of Zn^{2+} in the body.[52-55]

This study is concerned with the effect of the coordination environment of Zn^{2+} on the fluorescence of coordinated Zinquin-A in the cell. To this end, models were adopted which may partially simulate possible cellular environments as ternary complexes of the type [Zn(L)ZQA]. Initially, several questions are raised;

1. Do ternary complexes of the type [Zn(L)ZQA] form?
2. Do ternary complexes of the type [Zn(L)ZQA] fluoresce?
3. Is there any fluorescence dependence on the ligand used?

The formation of complexes can be easily studied using potentiometric titration methods. Due to the ternary nature of the complexes of interest, it was necessary to carry out three levels of titrations. Firstly, pK_as for the ligands to be used were characterised, then the stability constants of Zn^{2+} with these ligands were measured. Finally, all three components were combined to find the stability constants for the ternary [Zn(L)ZQA] complexes, using previously determined[3] Zinquin-A stability constants and pK_as.

The fluorescence of these ternary complexes can be studied once their stabilities have been determined so that the concentrations of all species in the fluorescing solution are known (Section 4.2). A fluorescence value for each ternary complex which is independent of the concentration of that complex was then determined as discussed later (Section 4.4). The ultraviolet-visible spectra of these ternary complexes were determined in a similar way (Section 4.3) and then used to take into account any difference in absorption at the excitation wavelength used for fluorescence determination (Section 4.4). These steps resulted in a set of fluorescence spectra which were compared to provide an insight into the effect of environment on Zinquin-A fluorescence.

4.2 : Potentiometric Titrations

4.2.1 : Acid Dissociation Constants of the Model Ligands

Acid dissociation constants, pK_as, were determined for the fully protonated forms of the ligands shown in Figure 4.1 in 50% aqueous ethanol at 298.2 K and I = 0.10 mol dm^{-3} ($NaClO_4$) as described in Section 5.4.2. A 50% aqueous ethanol solvent system was used because a balance between sufficient water to ensure that the pH electrode could function correctly and sufficient ethanol to readily dissolve Zinquin-A was required. For this reason, literature values for pK_as and stability constants in aqueous solution were redetermined in this solvent system. All of the ligands studied were found to have three detectable acid dissociation constants, K_{a1}, K_{a2}, and K_{a3} when fully protonated, as defined in Equations 4.1 to 4.6, except for TEA which has only one protonatable nitrogen. The fourth pK_as for protonated cyclam, cyclen, tren and NTA.H_3 were not observed as these are below the detection limit of the method used. The pK_as determined are shown in Table 4.1 below and can be compared with the literature values for these ligands in aqueous solution shown in Table 4.2.

$$[L.H]^+ \overset{K_{a1}}{\rightleftharpoons} L + H^+ \qquad (4.1)$$

$$[L.H_2]^{2+} \overset{K_{a2}}{\rightleftharpoons} [L.H]^+ + H^+ \qquad (4.2)$$

$$[L.H_3]^{3+} \overset{K_{a3}}{\rightleftharpoons} [L.H_2]^{2+} + H^+ \qquad (4.3)$$

$$K_{a1} = \frac{[L][H^+]}{[L.H^+]} \tag{4.4}$$

$$K_{a2} = \frac{[L.H^+][H^+]}{[L.H_2^{2+}]} \tag{4.5}$$

$$K_{a3} = \frac{[L.H_2^{2+}][H^+]}{[L.H_3^{3+}]} \tag{4.6}$$

Ligand (L)	$[L.H]^+$	$[L.H_2]^{2+}$	$[L.H_3]^{3+}$
	pK_{a1}	pK_{a2}	pK_{a3}
cyclen	10.52 ± 0.01	9.095 ± 0.004	1.74 ± 0.18
cyclam	11.15 ± 0.02	9.79 ± 0.01	1.56 ± 0.23
tacn	10.32 ± 0.04	6.40 ± 0.02	3.03 ± 0.04
tacdo	11.69 ± 0.05	6.80 ± 0.03	2.53 ± 0.03
tren	10.46 ± 0.03	9.44 ± 0.02	8.16 ± 0.03
NTA^{3-}	9.02 ± 0.04	3.11 ± 0.05	2.76 ± 0.06
TEA	7.43 ± 0.01		

Table 4.1 : pK_as for the ligands in Figure 4.1 at 298.2 K, I = 0.10 ($NaClO_4$), 50% aqueous ethanol solution.

The large errors associated with pK_{a3} for $[cyclen.H_3]^{3+}$ and $[cyclam.H_3]^{3+}$ are due to the low values of these constants. The potentiometric titration technique loses accuracy as the pK_as approach 2 as a lower limit and 11 as an upper limit. When the determined constants are outside these limits, larger errors are often observed. The titrations for the cyclen, cyclam, tacdo and $NTA.H_3$ systems were split into two fitting regions as these ligands are associated with pK_as that differ greatly in value and a reasonable fit could not be obtained without removing the points found in the middle of the curve. The omission of these data points is valid as in these areas as the concentration ratios of the conjugate acid-base pairs, which are involved in the fitting of the pK_as, are very large or very small. This results in unacceptably large errors in these ratios. An example of such a fitted titration curve is shown for cyclen in Figure 4.2. Where possible, the fitting regions were chosen to contain data points with pH values within the pK_a ± 1 pH unit, to ensure that between 10% and 90% of the ligand was present as the protonated species of interest, resulting in a balance between a sufficient number of data points and concentration ratios of the conjugate acid-base pairs in a reasonable range. It was not always possible to include this full range however, for example when a low pK_{a3} resulted in greater than 10% of the ligand as the protonated species of interest at the start of the titration.

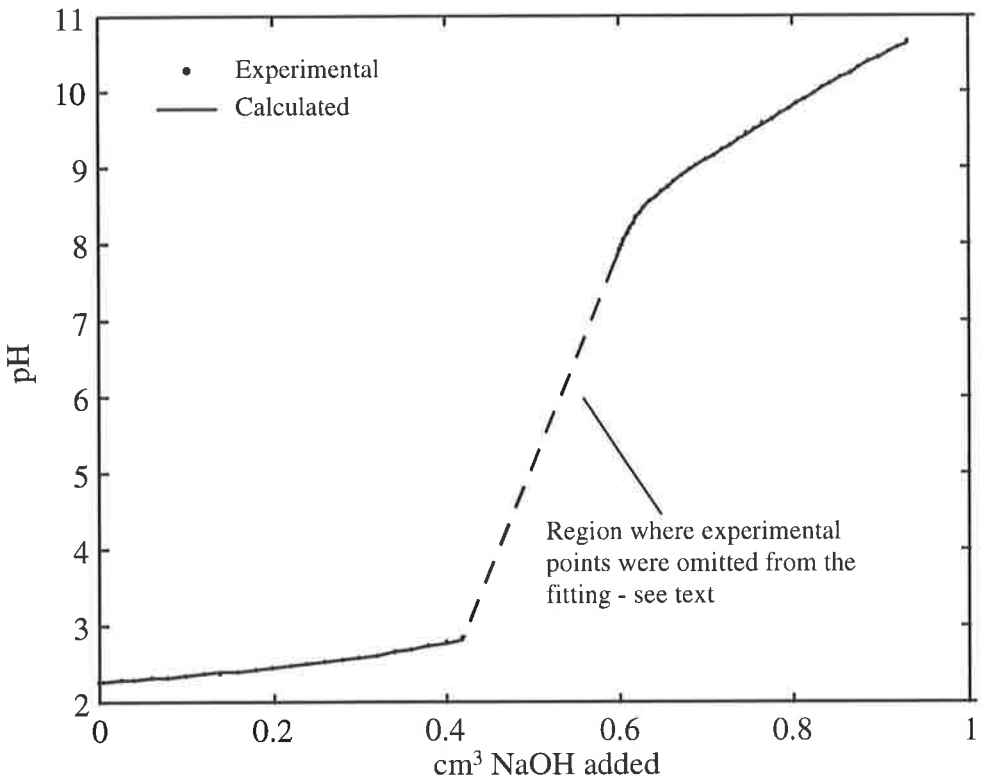

Figure 4.2 : A typical fitting of a titration curve obtained by the addition of 0.0997 mol dm^{-3} NaOH to 2.14×10^{-3} mol dm^{-3} cyclen in 50% aqueous ethanol with 1.00×10^{-2} mol dm^{-3} $HClO_4$ and 0.090 mol dm^{-3} $NaClO_4$. This is one of three that were used for the calculation of the pK_as of cyclen.

The pK_as obtained (Table 4.1) decrease from pK_{a1} to pK_{a3} for all of the ligands studied, except TEA which has only one pK_a. Two reasons exist for this. The first is a statistical effect, before any donors on the ligand have been protonated, there are three sites for a H^+ from solution to attach. Once there is one proton already attached to donor atoms of the ligand, there are only two sites available for a H^+ from solution to attach and therefore there exists a lower probability that this will occur with a subsequent decrease in pK_{a2} as compared with pK_{a1}. Similarly, if there are two protonated donors on the ligand, there remains only one site for H^+ binding and the probability of protonation, and therefore pK_{a3}, decreases further.

For the nitrogen donor ligands, the second, and more important, reason for decreasing pK_as is a result of the increasing charge. Protonating one nitrogen gives the ligand an overall single positive charge and a fairly large pK_{a1} is observed. Protonating a second nitrogen gives the ligand an overall 2+ charge and repulsion between the two H^+s results in a lower pK_{a2}. Protonating a third nitrogen, or fourth in the case of cyclam and cyclen, results in further repulsion between H^+s and therefore even lower pK_as.

The case for NTA.H_3 is slightly different as it is a tri-carboxylic acid. Removing a proton from NTA.H_3 forms $[NTA.H_2]^-$, a molecule with a singly negative charge which is delocalised within the carboxylic acid function and results in a low pK_{a3}. The removal of a second proton, resulting in an overall 2- charge, is harder as it requires more energy to remove a positive proton from a negative molecule than from a neutral one due to coulombic interactions. Hence pK_{a2} is larger than pK_{a3}. Finally, pK_{a1} is larger than pK_{a2}, and also considerably larger than would be observed for a mono-carboxylic acid, due to the even greater energy required to remove a positive proton from a molecule with a 2- charge. Despite this difficulty in removing positive entities from negative ones, NTA.H_3 has low pK_as due to its carboxylic acid functions that allow its deprotonated, negatively charged states to be resonance stabilised with the charge spread across more than one atom.

The lowest pK_{a1} determined was that for $[TEA.H]^+$. Fully protonated TEA has only one protonated site, the tertiary nitrogen, and this H^+ has a lower pK_a than the H^+s attached to the secondary nitrogens in the other ligands due to the steric and inductive effect of the additional R group attached to the ternary nitrogen. In principle, the oxygens of the hydroxyl groups are also protonatable, however, the pK_as for these equilibria are too low to measure.

The effect of adding successive protons to an acyclic ligand as compared with a macrocyclic ligand can be seen by comparing tren with the macrocycles, cyclen, cyclam, tacn and tacdo. As can be seen from Table 4.1, the pK_as of protonated tren decrease from pK_{a1} to pK_{a3} at a slower rate than those observed for the macrocycles. This is due to the fact that the nitrogens in tren are spatially separated on separate arms of the ligand, and not confined in near proximity to each other, as occurs in the macrocycles. Therefore, when protonated, there is less destabilising repulsion between the H^+s with a subsequent smaller decrease in pK_a for tren as compared with the macrocycles.

It is interesting to note the greater decrease from pK_{a1} to pK_{a2} observed for the protonated macrocycles with three nitrogens, tacn and tacdo, as compared with those with four, cyclen and cyclam. This difference arises from the fact that the nitrogens in tacn and tacdo are closer to each other and therefore when two of them are protonated, the two H^+s are closer and therefore experience greater repulsive forces than those in cyclam or cyclen. There is also a statistical contribution arising from the fact that there are only two nitrogens that can be protonated to form $[tacn.H_2]^{2+}$ and $[tacdo.H_2]^{2+}$ from the mono-protonated species as compared with the three available for $[cyclen.H]^+$ and $[cyclam.H]^+$.

The effect of macrocyclic ring size on pK_as is well illustrated by comparing the values obtained for protonated cyclen and tacn with the larger cyclam and tacdo respectively. It is found that pK_{a1} and pK_{a2} are lower for the two protonated macrocycles with a smaller ring size, cyclen and tacn. This can be attributed to the nearer proximity of the nitrogen bound H^+ to either nitrogen lone pairs or other H^+ in the smaller protonated macrocycles as compared with protonated macrocycles with larger ring sizes. This results in a greater electrostatic repulsion and a subsequent decrease in stability of the smaller protonated macrocycles. A decrease is not observed for pK_{a3} in this case, although it may be expected due to the same reasoning above, perhaps as a result of the greater experimental error associated with low pK_a values than indicated by the statistical errors quoted in Table 4.1. A decrease in all pK_as, however, is observed with decrease in ring size for the literature values determined in aqueous solution in Table 4.2.

Ligand (L)	$[L.H]^+$	$[L.H_2]^{2+}$	$[L.H_3]^{3+}$	$[L.H_4]^{4+}$
	pK_{a1}	pK_{a2}	pK_{a3}	pK_{a4}
cyclen [a]	10.7	9.7	1.73	0.94
cyclam [b]	11.59	10.62	2.42	1.61
tacn [c]	10.42 ± 0.02	6.82 ± 0.02	"strong acid"	
tacdo [d]	12.60	7.57	2.41	
tren [e]	10.14	9.43	8.41	
NTA^{3-} [e]	9.65	2.48	1.8	
TEA [f]	7.8			

a: Ref 70 , I = 0.2 ($NaClO_4$), **b:** Ref 71, I = 0.5 (KNO_3), **c:** Ref 72, I = 0.1 (KNO_3), **d:** Ref 58, I = 0.1 (KNO_3), **e:** Ref 56, I = 0.1, **f:** Ref 73, I = 0.1 (KCl)

Table 4.2 : Literature values of pK_as for the ligands in Figure 4.1 at 298.2 K and I as stated in aqueous solution.

As can be seen in Table 4.2 above, the values in 50% aqueous ethanol (Table 4.1) are similar to the literature values in 100% aqueous solution but are slightly lower in most cases. This decrease possibly indicates that the protonated ligand is less well solvated in a mixed solvent than in an aqueous solution and therefore, the equilibrium in Equation 4.1 lies further to the right in 50% aqueous ethanol than it would in water. This would result in an increase in K_{a1} and a subsequent decrease in pK_{a1} as observed. Similarly, a doubly protonated ligand is less well solvated than a singly protonated ligand and the equilibrium in Equation 4.2 also lies further to the right for a mixed solvent, than in water alone, resulting in a lower pK_{a2} than in water. The same reasoning can be used to explain the decrease observed for pK_{a3}. It is important to note, however, that the ionic strengths used to determine the pK_as quoted from the literature are not constant, and if they were determined at the same ionic strength as this paper, $I = 0.1$ ($NaClO_4$), slightly lower pK_as may have been obtained.[56]

4.2.2 : Stability Constants for the Model Ligands with Zinc(II)

Zinc(II) stability constants were determined for the ligands shown in Figure 4.1 in 50% aqueous ethanol at 298.2 K and $I = 0.10$ mol dm^{-3} ($NaClO_4$) as described in Section 5.4.2. All of the ligands were found to form complexes with Zn^{2+} as defined in Equations 4.7 - 4.16. The values of the stability constants determined are shown in Table 4.3 below and can be compared with the literature values for these ligands in aqueous solution shown in Table 4.4.

$$L + Zn^{2+} \overset{K_1}{\rightleftharpoons} [Zn(L)]^{2+} \quad (4.7)$$

$$L + [Zn(L)]^{2+} \overset{K_2}{\rightleftharpoons} [Zn(L)_2]^{2+} \quad (4.8)$$

$$[Zn(L)H]^{3+} \overset{K_{a1}'}{\rightleftharpoons} [Zn(L)]^{2+} + H^+ \quad (4.9)$$

$$[Zn(L)]^{2+} \overset{K_{aL}'}{\rightleftharpoons} [Zn(L)H_{-1}]^{+} + H^+ \quad (4.10)$$

$$[Zn(L)H_{-1}]^{+} \overset{K_{aL2}'}{\rightleftharpoons} [Zn(L)H_{-2}]^{2+} + H^+ \quad (4.11)$$

$$K_1 = \frac{[Zn(L)^{2+}]}{[L][Zn^{2+}]} \quad (4.12)$$

$$K_2 = \frac{[Zn(L)_2^{2+}]}{[L][Zn(L)^{2+}]} \quad (4.13)$$

$$K_{a1}' = \frac{[Zn(L)^{2+}][H^+]}{[Zn(L)H^{3+}]} \quad (4.14)$$

$$K_{aL}' = \frac{[Zn(L)H_{-1}^+][H^+]}{[Zn(L)^{2+}]} \quad (4.15)$$

$$K_{aL2}' = \frac{[Zn(L)H_{-2}][H^+]}{[Zn(L)H_{-1}^+]} \quad (4.16)$$

Ligand (L)	$[Zn(L)]^{2+}$	$[Zn(L)_2]^{2+}$	$[Zn(L)H_{-1}]^+$	$[Zn(L)H_{-2}]$	$[Zn(L)H]^{3+}$
	$\log K_1$	$\log K_2$	pK_{aL}'	pK_{aL2}'	pK_{a1}'
cyclen	15.34 ± 0.02		7.75 ± 0.05		3.60 ± 0.08
cyclam	14.43 ± 0.03		10.65 ± 0.13		
tacn	12.38 ± 0.07	9.18 ± 0.14			3.74 ± 0.05
tacdo	8.93 ± 0.03		7.60 ± 0.04		
tren	15.74 ± 0.04		11.13 ± 0.07		
NTA^{3-}	10.22 ± 0.03	3.03 ± 0.03	10.41 ± 0.04		
TEA			(-4.37 ± 0.07)*	7.45 ± 0.03	

*This is the -log of a cumulative constant, $K = \frac{[Zn(TEA)H_{-1}^+][H^+]}{[TEA][Zn^{2+}]}$, not K_{aL}'

Table 4.3 : Stability constants for the ligands in Figure 4.1 with Zn^{2+} at 298.2 K, I = 0.10 ($NaClO_4$), 50% aqueous ethanol solution.

Where possible, all titration data were fitted in regions where the complexes of interest were present at between 10% and 90% formation. Fits where species were present at less than 10% formation were not accepted. As was the case for the pK_a determinations in Section 4.2.1, the constants in Table 4.3 are dependent on the concentration ratios of the species in equilibrium. When these ratios become very large or very small, they are subject to large error. Accordingly, titration regions in which this occurred were not used in data fitting. This lead to split fitting regions for the tren, cyclam and $NTA.H_3$ systems where $[Zn(L)]^{2+}$ formed at a low pH and the hydroxy species formed at a high pH. The fit obtained for the cyclen system is shown in Figure 4.3 as an example of the fits obtained.

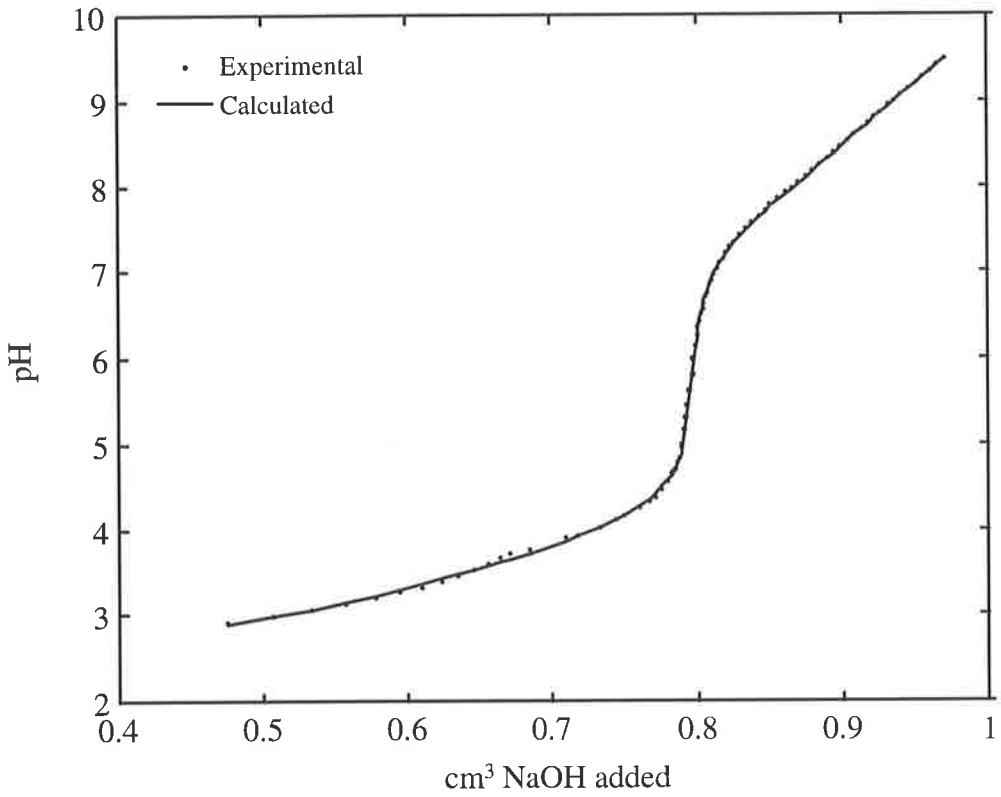

Figure 4.3 : A typical fitting of a titration curve obtained by the addition of 0.0997 mol dm^{-3} NaOH to 2.14×10^{-3} mol dm^{-3} cyclen in 50% aqueous ethanol with 1.00×10^{-2} mol dm^{-3} $HClO_4$ and 0.090 mol dm^{-3} $NaClO_4$, to which has been added 1.07×10^{-3} mol dm^{-3} $Zn(ClO_4)_2$. This is one of three that was used for the calculation of the stability constants of the Zn^{2+} complexes of cyclen.

All of the ligands, with the exception of TEA, were found to form reasonably stable $[Zn(L)]^{2+}$, with log K_1 between 8.93 and 15.74. $[Zn(TEA)]^{2+}$ is not observed due to the influence of Zn^{2+} on the donating OH or H_2O groups. Zinc(II) increases the acidity of the OH and H_2O groups so much that one of them readily loses a proton, forming either a hydroxy species (as discussed later) or the species shown as complex a) in Figure 4.4 in preference to $[Zn(L)]^{2+}$ which is observed for the other ligands. Although $[Zn(TEA)]^{2+}$ is probably in solution at some concentration, the fact that it can not be fitted for indicates that its concentration must be below 10% of the total ligand concentration. Since no stability constant can be determined for $[Zn(TEA)]^{2+}$, the stability constant for $[Zn(TEA)H_{-1}]^{+}$ can not be presented in the same form as the other $[Zn(L)H_{-1}]^{+}$ observed, and a cumulative stability constant must be used as mentioned in the footnote to Table 4.3. A second proton can also be removed, forming either a bi-hydroxy complex or complex b) or c) in Figure 4.4. From results discussed later (Page 118), it appears that it is protons from TEA that are dissociated, forming complexes a) and b) in Figure 4.4 rather than hydroxy species.

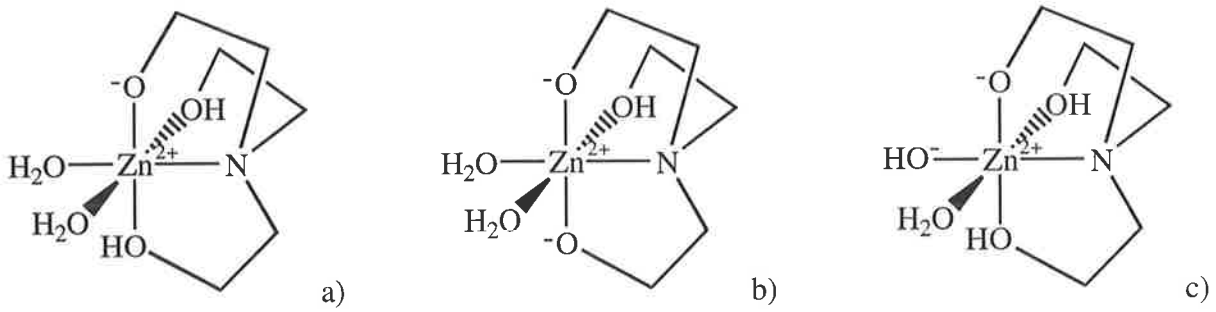

Figure 4.4 : Three Zn^{2+} complexes that TEA may form in 50% aqueous ethanol.

The macrocyclic tetraamines, cyclen and cyclam, have higher affinities for Zn^{2+} than the macrocyclic triamines, tacn and tacdo. This is most probably due to the greater number of donor atoms in cyclen and cyclam, which allows them to coordinate more tightly to Zn^{2+}. Tacdo has the smallest Zn^{2+} stability constant observed, with log K_1 = 8.93. This value is lower than those for both cyclen and cyclam as just discussed, and lower than that for tacn possibly because it forms 6 membered chelate rings about the Zn^{2+}, which are less favourable for coordination than the 5 membered chelate rings formed in tacn and many other strong Zn^{2+} coordinators, as exemplified by EDTA.[57] The effect of 6 membered chelate rings, and a general increase in macrocycle ring size, can also be used to explain the lower stability constant obtained for $[Zn(cyclam)]^{2+}$ as compared with $[Zn(cyclen)]^{2+}$.

The most stable complex formed is $[Zn(tren)]^{2+}$, with log K_1 = 15.74. This is possibly due to a combination of its nitrogen donors, which are softer than the oxygen donors of NTA^{3-} and TEA and which therefore coordinate better to the borderline soft Zn^{2+}, and the fact that tren is a more flexible molecule than the rigid macrocycles, and can therefore maintain a more octahedral geometry about the Zn^{2+}. However, the stability of $[Zn(tren)]^{2+}$ and $[Zn(cyclen)]^{2+}$ are quite similar, as could be expected from the similarity in their structures. As can be seen in Figure 4.1, both have four nitrogen donors and form 5 membered chelate rings with Zn^{2+}.

Complexes of the form, $[Zn(L)_2]^{2+}$, were observed for tacn and NTA^{3-} only. Tacn is the smallest of the macrocycles studied and it appears that the other macrocycles are too large to allow $[Zn(L)_2]^{2+}$ to form due to unfavourable steric interactions when two of the ligands are crowded about one Zn^{2+}. Tren is also unlikely to form $[Zn(tren)_2]^{2+}$ because it coordinates by four nitrogens and one of these would have to detach from the Zn^{2+} to allow another tren to coordinate by 3 of its nitrogens, this is unlikely to occur due the high stability of $[Zn(tren)]^{2+}$. This reasoning can also be applied to cyclen and cyclam not forming $[Zn(L)_2]^{2+}$, in addition to the steric reason mentioned above. The large error quoted for the stability constant of $[Zn(tacn)_2]^{2+}$ in Table 4.3 arises from the slow complexation rate observed for this species. This resulted in the use of a longer than usual delay in recording the potential to allow equilibrium to be reached.

Unlike tren, NTA^{3-} does form $[Zn(L)_2]^{2+}$ with Zn^{2+}, despite probably coordinating to it at four sites in $[Zn(L)]^{2+}$. The reason for this is most likely the lower affinity for Zn^{2+} of oxygen than nitrogen, due to the hard character of oxygen as compared with the softer character of nitrogen and Zn^{2+}. This leads to the possibility that one of the carboxylate arms of NTA^{3-} leaves the Zn^{2+}, allowing a second NTA^{3-} molecule to coordinate with its tertiary nitrogen and two of its carboxylate arms, forming $[Zn(NTA)_2]^{4-}$ as observed. As expected, due to the large negative charge that exists on this complex, it is not very stable as indicated by the low value for its stability constant in Table 4.3.

Zinc(II) complexes readily lose a proton from an attached water molecule to form hydroxy species in water such as that shown for cyclam in Figure 4.5.[42] All of the ligands studied (with the possible exception of TEA) were found to form these species, however, the hydroxy species for tacn precipitated from solution at about pH 8.5, preventing its pK_{aL}' from being determined. Similar results were obtained by Kimura *et al* (1990)[51] and Zompa (1978).[58] An example of a tacn titration showing the formation of a precipitate, and the evidence of slow $[Zn(tacn)_2]^{2+}$ formation, is shown in Figure 4.6. This titration was run with a maximum delay of 3000 seconds to allow the slow forming complex to equilibrate. A brief discussion on using SUPERQUAD[59] to fit hydroxy species is presented in Section 5.4.2.1.

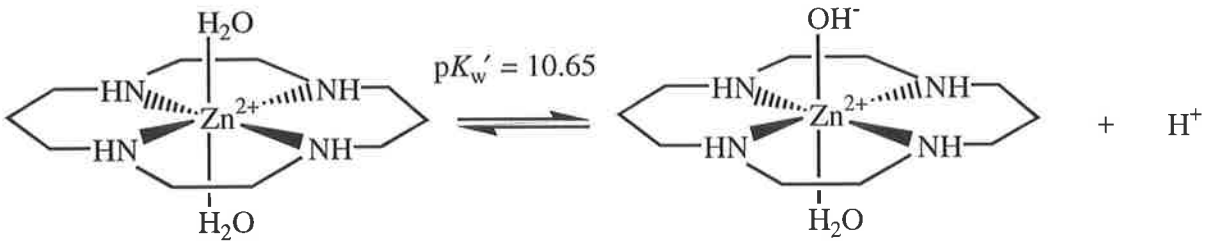

Figure 4.5 : The equilibrium describing the formation of a hydroxy species from $[Zn(cyclam)(H_2O)_2]^{2+}$.

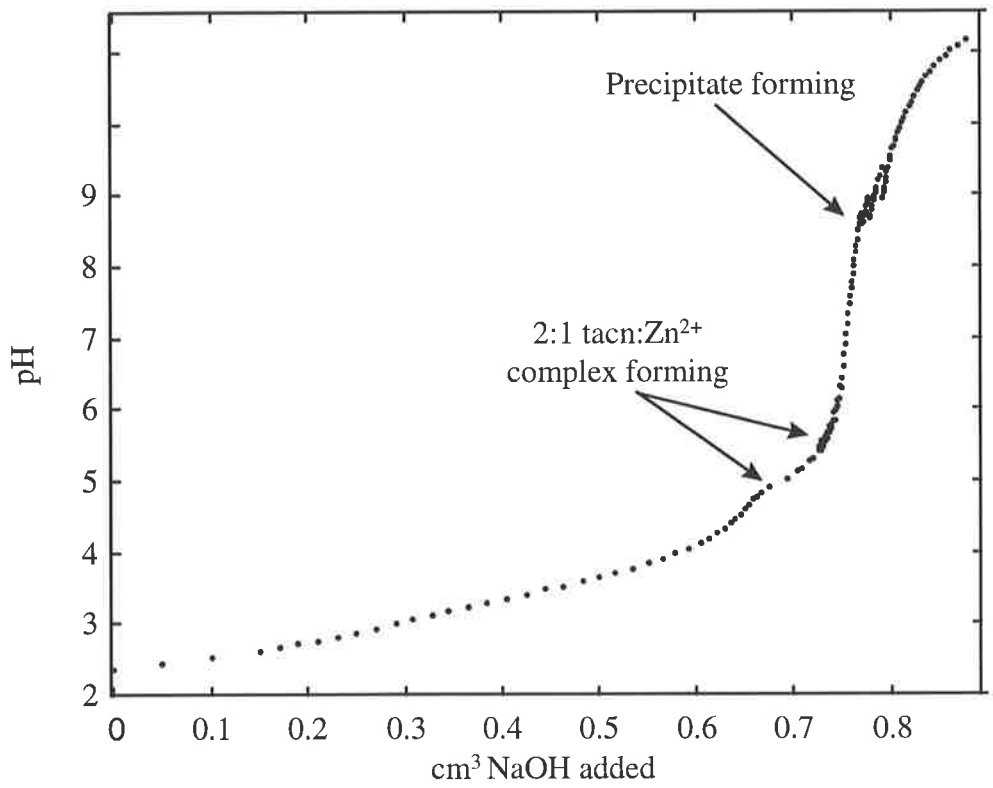

Figure 4.6 : Titration curve observed when 0.100 mol dm^{-3} NaOH was added to a solution containing 1.99×10^{-3} mol dm^{-3} tacn, 9.950×10^{-4} mol dm^{-3} $Zn(ClO_4)_2$ and 2.00×10^{-3} mol dm^{-3} $HClO_4$ in 50% aqueous ethanol. T = 298.2 K, I = 0.1 ($NaClO_4$).

From Table 4.3, it appears that the macrocyclic tetraamine complexes are less acidic than the triamine (tacdo) complex. This is consistent with the findings of Kimura *et al* (1990)[51] who studied the pK_{aL}' of various tetraamine and triamine macrocycles. It appears that when there are fewer donor atom in the ligand, the water is held more tightly by the Zn^{2+} and the O-H bonds are therefore weakened, facilitating the loss of a proton to form the hydroxy species observed. Therefore the triamine complex, $[Zn(tacdo)(H_2O)_n]^{2+}$, has a low pK_{aL}' compared with that of its tetraamine analogues and $[Zn(H_2O)_6]^{2+}$ which has $pK_{aL}' = 9.0$.[60] If the pK_{aL}' of $[Zn(tacn)]^{2+}$ could be measured, it is likely that it too would be lower than the tetraamines.

$[Zn(cyclen)(H_2O)_2]^{2+}$ is much more acidic than $[Zn(cyclam)(H_2O)_2]^{2+}$. This is probably due to the different structures of these Zn^{2+} complexes in solution. Cyclen forms a folded *cis* conformation about the Zn^{2+} (Figure 4.7)[61] whereas the cyclam occupies a square planar arrangement about the equatorial coordination sites of Zn^{2+} as shown schematically in Figure 4.5.[62] This was confirmed during force field molecular modelling studies using the INSIGHT II package (see Section 4.5). It was found that the most stable (lowest energy) conformation for cyclen in $[Zn(cyclen)(H_2O)_2]^{2+}$ was the *cis* conformation with all but one N-H bond facing towards the Zn^{2+}. In contrast, the most stable conformation for cyclam in $[Zn(cyclam)(H_2O)_2]^{2+}$ was the *trans* conformation with two adjacent N-H bonds facing towards the Zn^{2+} and the other two facing away. Hence, the waters which occupy the remaining coordination sites of Zn^{2+} in $[Zn(cyclen)(H_2O)_2]^{2+}$ are *cis* whereas those in $[Zn(cyclam)(H_2O)_2]^{2+}$ are *trans*. This allows hydrogen bonding between the waters bound to the Zn^{2+} in the cyclen complex, weakening the O-H bonds and causing a lower pK_{aL}' than found for $[Zn(cyclam)(H_2O)_2]^{2+}$ where no hydrogen bonding is possible.

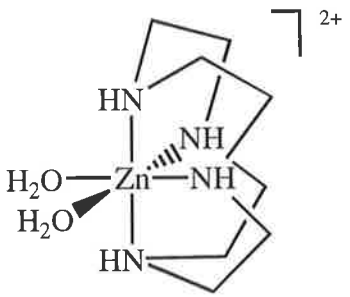

Figure 4.7 : A schematic diagram of the *cis* conformation adopted by cyclen when bound to Zn^{2+}.

Neither of the two acyclic ligand complexes that show a water dissociation constant, $[Zn(tren)(H_2O)_n]^{2+}$ and $[Zn(NTA)(H_2O)_n]^-$, are particularly acidic, perhaps indicating that only certain macrocycles are capable of creating the correct environment about the Zn^{2+} to appreciably lower the pK_{aL}' of the bound water. $[Zn(NTA)(H_2O)_n]^-$ has a slightly lower pK_{aL}' than that observed for $[Zn(tren)(H_2O)_n]^{2+}$. This could be due to hydrogen bonding between the bound water and the O^- of the carboxylic acid group which would weaken the O-H bonds of water to some extent. This hydrogen bonding was observed in the force field molecular modelling studies (Section 4.5), with distances between the three O^- groups of NTA^{3-} and the Hs of bound water in $[Zn(NTA)(H_2O)_2]^-$ of 1.9256, 1.9788 and 1.8839 Å. No similar hydrogen bonding was observed in $[Zn(tren)(H_2O)_2]^{2+}$.

Protonated complexes of the form, $[Zn(L)H]^{3+}$, were observed only for the smaller macrocycles, cyclen and tacn at low pHs. The pK_{a1}s obtained are almost the same within experimental error and represent the complex formed by Zn^{2+} and tacn or cyclen with one nitrogen of the macrocycle protonated. These species were not found in great concentrations, but sufficient was present to obtain satisfactory fits to the experimental curves.

Literature values in aqueous solution have been reported for all of the species found with the exception of the $[Zn(L)H]^{3+}$ and all of the TEA complexes studied. These values are shown in Table 4.4.

Ligand (L)	$[Zn(L)]^{2+}$	$[Zn(L)_2]^{2+}$	$[Zn(L)H_{-1}]^{+}$
	log K_1	log K_2	pK_{aL}'
cyclen	16.2 [a]		8.02 ± 0.03 [b]
cyclam	15.5 [a]		9.77 ± 0.05 [b]
tacn [c]	11.7	10.0	
tacdo [b]	8.41 ± 0.02		7.30 ± 0.02
tren	14.5 [d]		10.26 ± 0.02 [e]
NTA^{3-} [d]	10.66	3.58	3.55*

a: Ref 74 , I = 0.2 ($NaClO_4$), **b:** Ref 51, I = 0.1 ($NaClO_4$), **c:** Ref 75, I = 0.1 (KNO_3), **d:** Ref 56, I = 0.1, **e:** Ref 76, I = 1.0, ($NaClO_4$)

*This is the log of a different constant, $K = \frac{[Zn(NTA)OH^{2-}]}{[Zn(NTA)^{-}][OH^{-}]}$, not K_{aL}'.

pK_{aL}' in Table 4.3 can be converted to the same form by the equation; log $K = pK_w - pK_{aL}'$ which gives log K = 4.00 in 50% aqueous ethanol with pK_w = 14.41.

Table 4.4 : Literature values of stability constants for the ligands in Figure 4.1 with Zn^{2+} at 298.2 K and I as stated in aqueous solution.

The values determined in this work (Table 4.3) follow approximately the same trends as the literature values in water (Table 4.4), with the exception of the $[Zn(cyclen)]^{2+}$ and $[Zn(cyclam)]^{2+}$ in Table 4.4 which appear to have larger stability constants than expected. This can be explained by the greater ionic strength used to determine these literature values. If they were determined at I = 0.1 ($NaClO_4$), lower values could be expected.[56] Most of the values determined in 50% aqueous ethanol are higher than those determined in 100% aqueous solution. This perhaps indicates that for $[Zn(L)]^{2+}$ and $[Zn(L)_2]^{2+}$, the Zn^{2+} is less well solvated in a mixed solvent such as 50% aqueous ethanol as compared with water and therefore a ligand can more readily displace the coordinating solvent molecules and form a complex. This would result in the increase in stability constants observed.

4.2.3 : Stability Constants for the Ternary Complexes, [Zn(L)ZQA]

Stability constants which describe ternary complexes formed between Zinquin-A, Zn^{2+} and the ligands shown in Figure 4.1 were determined in 50% aqueous ethanol at 298.2 K and $I = 0.10$ mol dm^{-3} ($NaClO_4$) as described in Section 5.4.2. All of the ligands were found to form ternary complexes with Zinquin-A and Zn^{2+} as defined in Equations 4.17 to 4.28. The stepwise stability constants determined are shown in Table 4.5 below.

$$[Zn(L)]^{2+} + ZQA^{2-} \overset{K_3}{\rightleftharpoons} [Zn(L)ZQA] \quad (4.17)$$

$$[Zn(L)H_{-1}]^{+} + ZQA^{2-} \overset{K_4}{\rightleftharpoons} [Zn(L)ZQA.H_{-1}]^{-} \quad (4.18)$$

$$[Zn(L)H_{-2}] + ZQA^{2-} \overset{K_5}{\rightleftharpoons} [Zn(L)ZQA.H_{-2}]^{-2} \quad (4.19)$$

$$[Zn(L)ZQA.H]^{+} \overset{K_{a1}''}{\rightleftharpoons} [Zn(L)ZQA] + H^{+} \quad (4.20)$$

$$[Zn(L)ZQA.H_2]^{2+} \overset{K_{a2}''}{\rightleftharpoons} [Zn(L)ZQA.H]^{+} + H^{+} \quad (4.21)$$

$$[Zn(L)ZQA.H_{-1}]^{-} \overset{K_{aL2}''}{\rightleftharpoons} [Zn(L)ZQA.H_{-2}]^{-2} + H^{+} \quad (4.22)$$

$$K_3 = \frac{[Zn(L)ZQA]}{[ZQA^{2-}][Zn(L)^{2+}]} \quad (4.23)$$

$$K_4 = \frac{[Zn(L)ZQA.H_{-1}^{-}]}{[ZQA^{2-}][Zn(L)H_{-1}^{+}]} \quad (4.24)$$

$$K_5 = \frac{[Zn(L)ZQA.H_{-2}^{2-}]}{[ZQA^{2-}][Zn(L)H_{-2}]} \quad (4.25)$$

$$K_{a1}'' = \frac{[Zn(L)ZQA][H^{+}]}{[Zn(L)ZQA.H^{+}]} \quad (4.26)$$

$$K_{a2}'' = \frac{[Zn(L)ZQA.H^+][H^+]}{[Zn(L)ZQA.H_2^{2+}]} \quad (4.27)$$

$$K_{aL2}'' = \frac{[Zn(L)ZQA.H_{-2}^{2-}][H^+]}{[Zn(L)ZQA.H^-_1]} \quad (4.28)$$

Ligand (L)	[Zn(L)ZQA]	[Zn(L)ZQA.H]$^+$	[Zn(L)ZQA.H$_2$]$^{2+}$	[Zn(L)ZQA.H$_{-1}$]$^-$	[Zn(L)ZQA.H$_{-2}$]$^{2-}$	
	log K_3	pK_{a1}''	pK_{a2}''	log K_4	pK_{aL2}''	log K_5
cyclen	8.23 ± 0.05					
cyclam	4.36 ± 0.18					
tacn	8.45 ± 0.10					
tacdo	10.00 ± 0.06	6.30 ± 0.04	5.67 ± 0.08			
tren	11.53 ± 0.06	4.54 ± 0.05				
NTA^{3-}	5.92 ± 0.15	7.66 ± 0.15	3.94 ± 0.02			
TEA				9.87 ± 0.08	8.92 ± 0.08	8.41 ± 0.09

Table 4.5 : Ternary stability constants for the ligands in Figure 4.1 with Zinquin-A and Zn^{2+} at 298.2 K, I = 0.10 ($NaClO_4$), 50% aqueous ethanol solution.

Where possible, all titrations were fitted in regions where the complexes of interest were present at between 10% and 90% formation. Fits where species were present at less than 10% formation were not accepted. As was the case for the protonation and Zn^{2+} stability constant determinations in Section 4.2.1 and 4.2.2, it was necessary to omit experimental points where the concentration ratios of the species in equilibrium were very large or very small. The fit obtained for the tacdo system is shown in Figure 4.8 as an example of the fits obtained.

As can be seen in Table 4.5, all of the ligands shown in Figure 4.1 form [Zn(L)ZQA] except TEA which is consistent with $[Zn(TEA)]^{2+}$ also not being observed. However, $[Zn(TEA)ZQA.H_{-1}]^-$ and $[Zn(TEA)ZQA.H_{-2}]^{2-}$ were formed, consistent with $[Zn(TEA)H_{-1}]^+$ and $[Zn(TEA)H_{-2}]$ forming ternary complexes in a similar way to the other $[Zn(L)]^{2+}$ complexes. As TEA and Zinquin-A bind at four and two Zn^{2+} coordination sites, respectively, the proton lost from $[Zn(TEA)ZQA.H_{-1}]^-$ and $[Zn(TEA)ZQA.H_{-2}]^{2-}$ is unlikely to be derived from a water bound at a seventh Zn^{2+} coordination site. This lends support to the earlier proposal that the protons lost from $[Zn(TEA)]^{2+}$ are lost from TEA itself as discussed on Page 111. No other deprotonated ternary species are observed as adding ZQA^{2-} to $[Zn(L)]^{2+}$ takes up two coordination sites which leaves only one or no sites available for coordination of

H_2O. For the ternary complexes of tacdo and tacn, which bind at three Zn^{2+} coordination sites, although a water molecule is likely to be bound to Zn^{2+} at the sixth site, a hydroxy species is not formed because the favourable positive charge on the molecule, that helped drive the dissociation of water in the $[Zn(L)(H_2O)]^{2+}$ complex, no longer exists.

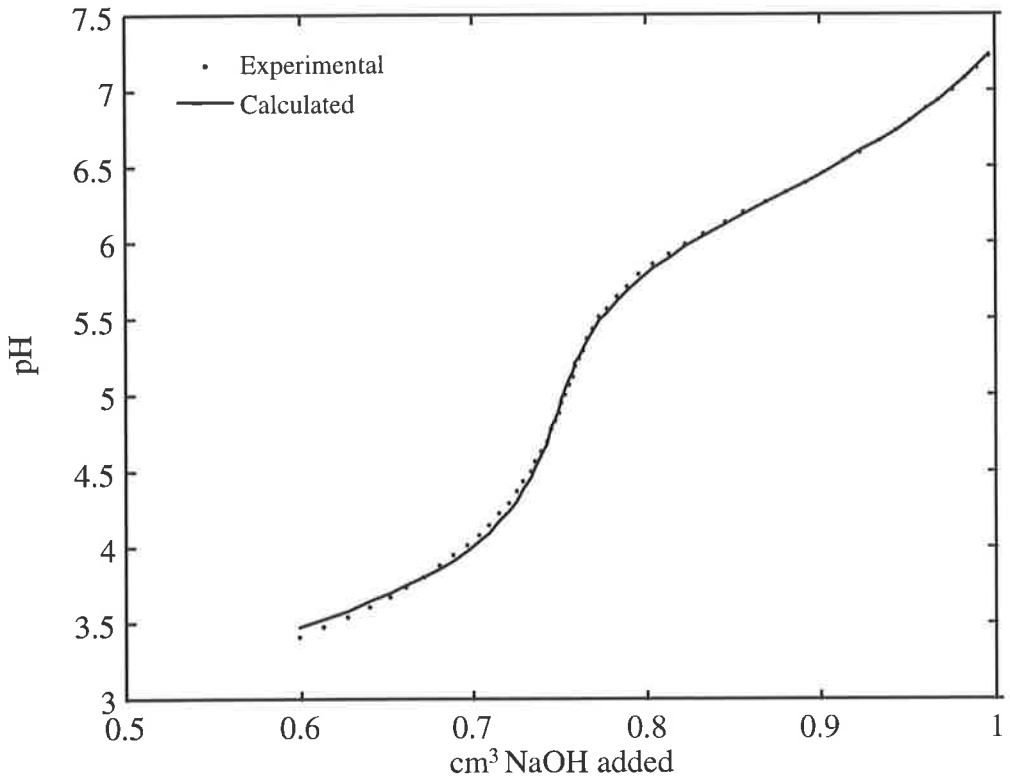

Figure 4.8 : A typical fitting of a titration curve obtained by the addition of 0.0997 mol dm^{-3} NaOH to 2.02×10^{-3} mol dm^{-3} tacdo in 50% aqueous ethanol with 4.04×10^{-3} mol dm^{-3} $HClO_4$ and 0.096 mol dm^{-3} $NaClO_4$, to which has been added 1.00×10^{-3} mol dm^{-3} $Zn(ClO_4)_2$ and 1.00×10^{-3} mol dm^{-3} Zinquin-A. This is one of three that was used for the calculation of the stability constants of [Zn(tacdo)ZQA] and its protonated forms.

As could be expected, the addition of the negatively charged ZQA^{2-} to $[Zn(TEA)H_{-1}]^{+}$, to form a ternary complex, inhibits the dissociation of a second proton from coordinated TEA. The pK_{aL2}'' = 8.92 observed for $[Zn(TEA)ZQA.H_{-1}]^{-}$ is therefore higher than pK_{aL}' = 7.45 observed for the binary $[Zn(TEA)H_{-1}]^{+}$.

A wide range of stabilities are observed for [Zn(L)ZQA], with the determined stepwise stability constants ranging from log K_3 = 4.36 for [Zn(cyclam)ZQA] to log K_3 = 11.53 for [Zn(tren)ZQA]. Tren gives the highest stability once again due to its nitrogen donors, which coordinate strongly to Zn^{2+}, and its greater flexibility compared with the polyamine macrocycles, which allows Zinquin-A to also coordinate to Zn^{2+}. The structure of $[Zn(cyclam)]^{2+}$, however, inhibits Zinquin-A coordination. Due to its size, cyclam prefers to occupy equatorial coordination sites on Zn^{2+} as discussed previously, so it must change conformation to a less energetically favourable *cis* form before two adjacent coordination sites are available for Zinquin-A coordination. The extra energy required to affect this, and the low probability of it occurring when the molecules collide in solution, leads to a low stability constant. The other alternative is that Zinquin-A coordinates by only one nitrogen to the Zn^{2+} at one of its spare axial coordination sites. This alternative would also result in a low stability constant as no favourable chelate effect would occur for Zinquin-A and it would easily detach from the Zn^{2+} again.

The complexes, [Zn(tacn)ZQA] and [Zn(tacdo)ZQA], which contain triamine macrocycles, have higher stability constants than [Zn(cyclen)ZQA] and [Zn(cyclam)ZQA], which contain tetraamine macrocycles, as could be expected for two reasons. Firstly, they leave a greater number of Zn^{2+} coordination sites free and therefore there is a greater probability that a Zinquin-A molecule can coordinate, and secondly, as a larger space remains free about the Zn^{2+}, fewer steric interactions would exist between the triamines and Zinquin-A than if four coordination sites were occupied by a tetraamine.

The complex, $[Zn(NTA)ZQA]^{3-}$ has a relatively low ternary stability constant (log K_3 = 5.92) which is probably due to the negatively charged $[Zn(NTA)]^-$ repelling the negatively charged ZQA^{2-}, inhibiting the formation of a complex between them. It is because of this unfavourable coulombic interaction that $[Zn(NTA)ZQA]^{3-}$ has a pK_{a1}'' at a high pH of 8.33, resulting in it being protonated at neutral pHs. There is also a pK_{a2}'' that indicates that the ternary complex is doubly protonated at low pH to form a singly negatively charged complex, $[Zn(NTA)ZQA.H_2]^-$. Protonated species of this type are also observed for tacdo and tren.

These [Zn(L)ZQA] stability constants, in conjunction with the binary Zn^{2+} stability constants and Zinquin-A and ligand pK_as, can be used to calculate the concentration in solution of all species at any pH. This concentration is usually expressed as a percentage of the total Zinquin-A concentration as in Figure 4.9, which shows an example of a ternary complex which forms readily, [Zn(tren)ZQA]. Figure 4.10 shows [Zn(tacn)ZQA], which is formed in a smaller amount than the others, not exceeding 50% formation. This is due to the high stability of the $[Zn(tacn)_2]^{2+}$ species which, although not shown here, begins to form at approximately the same pH as the ternary species, [Zn(tacn)ZQA], and incorporates both Zn^{2+} and tacn, making them unavailable to form [Zn(tacn)ZQA]. This suggests that Zinquin-A would also be unable to coordinate to strongly coordinated Zn^{2+} that is well protected, or surrounded by protein in the cell. Figure 4.11 shows a ternary complex that does not form until high pH, [Zn(cyclam)ZQA]. The concentrations chosen for each of these figures are those that were used for the determination of the ternary complex fluorescence at pH 6.6 for the tren and tacn systems, and at pH 10 for the cyclam system (see Sections 4.4 and 5.4.4). [Zn(L)ZQA] are shown in purple and all species not containing Zinquin-A are omitted for simplification. Speciation plots for the other ternary complexes can be found in Appendix C.

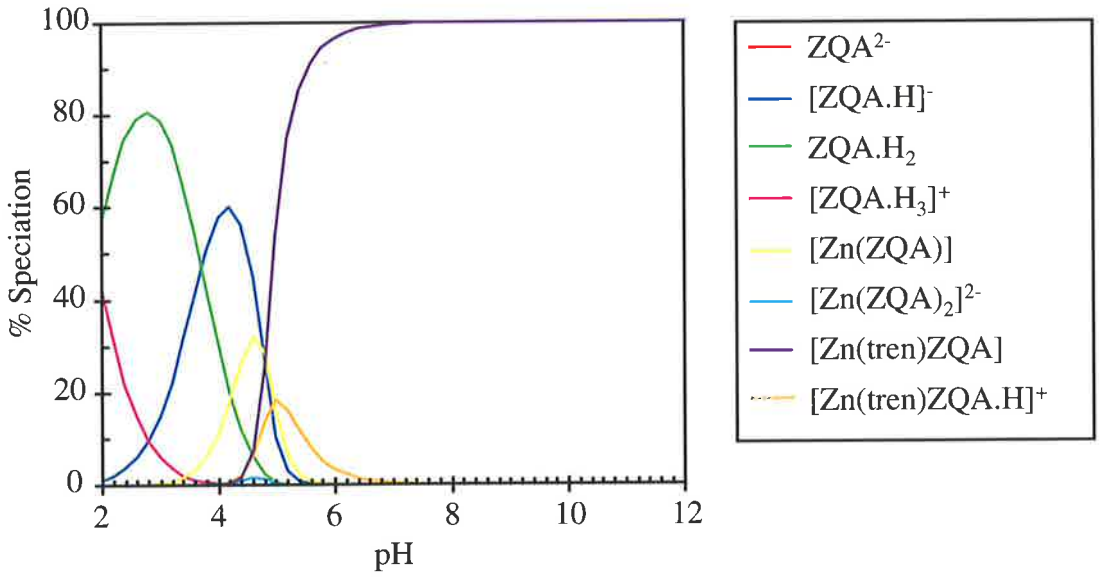

Figure 4.9 : Speciation plot for a solution containing 1.00×10^{-4} mol dm^{-3} tren, 4.58×10^{-5} mol dm^{-3} $Zn(ClO_4)_2$ and 9.84×10^{-6} mol dm^{-3} Zinquin-A, showing the species present in 50% aqueous ethanol at various pH. % Speciation is shown relative to the total concentration of Zinquin-A, $I = 0.1$ ($NaClO_4$) and $T = 298.2$ K.

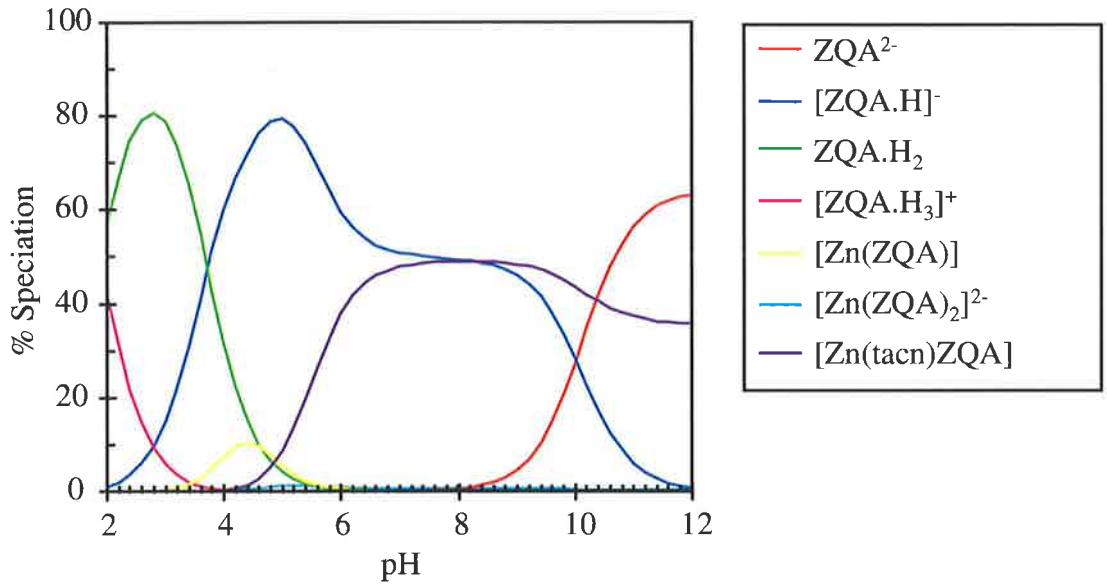

Figure 4.10 : Speciation plot for a solution containing 1.01×10^{-4} mol dm^{-3} tacn, 4.58×10^{-5} mol dm^{-3} $Zn(ClO_4)_2$ and 9.84×10^{-6} mol dm^{-3} Zinquin-A, showing the species present in 50% aqueous ethanol at various pH. % Speciation is shown relative to the total concentration of Zinquin-A, $I = 0.1$ ($NaClO_4$) and $T = 298.2$ K.

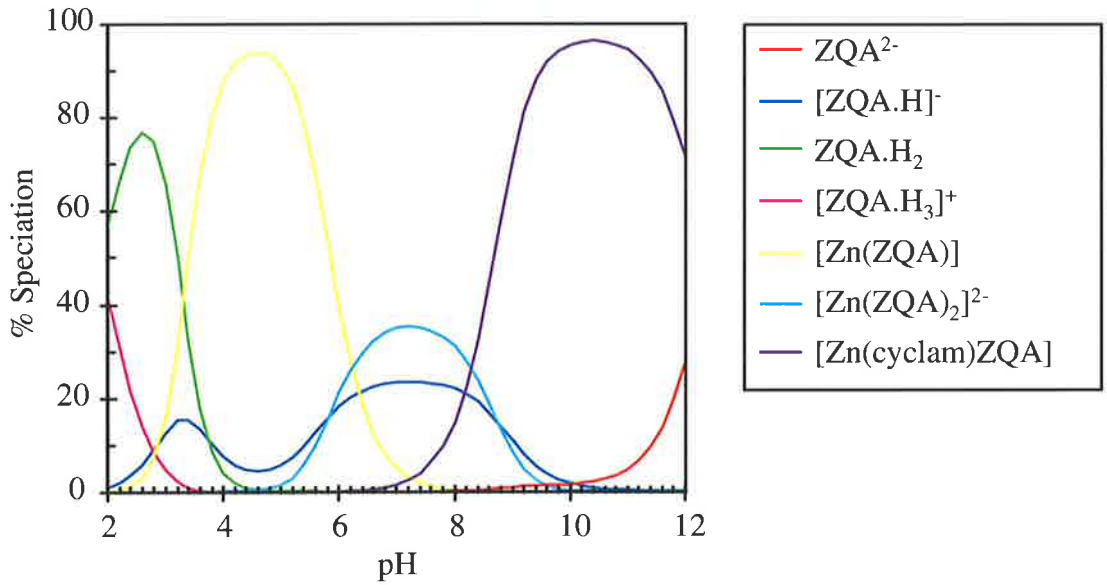

Figure 4.11 : Speciation plot for a solution containing 4.99×10^{-3} mol dm^{-3} cyclam, 3.01×10^{-3} mol dm^{-3} $Zn(ClO_4)_2$ and 1.04×10^{-5} mol dm^{-3} Zinquin-A, showing the species present in 50% aqueous ethanol at various pH. % Speciation is shown relative to the total concentration of Zinquin-A, $I = 0.1$ ($NaClO_4$) and $T = 298.2$ K.

The case of the cyclam ternary complex is perhaps the most interesting as it forms to a lesser extent at physiological pH (near pH 7) than all of the other ternary complexes studied, illustrating that Zinquin-A may not be able to form ternary complexes with all types of Zn^{2+} in a cell. In this case, the Zinquin-A is able to remove the Zn^{2+} from cyclam, despite the high stability of $[Zn(cyclam)]^{2+}$ (log K_1 = 14.43), forming $[Zn(ZQA)_2]^{2-}$. Figure 4.12 shows the species present in a solution containing just Zn^{2+} and cyclam, at the same concentrations as in Figure 4.11, with no Zinquin-A added. As can be seen, at pH 7, 100% of the Zn^{2+} present is complexed by cyclam, forming $[Zn(cyclam)]^{2+}$. Therefore, when Zinquin-A is added, it must remove some of the Zn^{2+} from cyclam to form $[Zn(ZQA)_2]^{2-}$ seen in Figure 4.11. However, Zinquin-A is not strong enough to remove enough Zn^{2+} from cyclam to have all of the Zinquin-A bound, as can be seen by the significant amount of $[ZQA.H]^{-}$ in Figure 4.11 at pH 7.

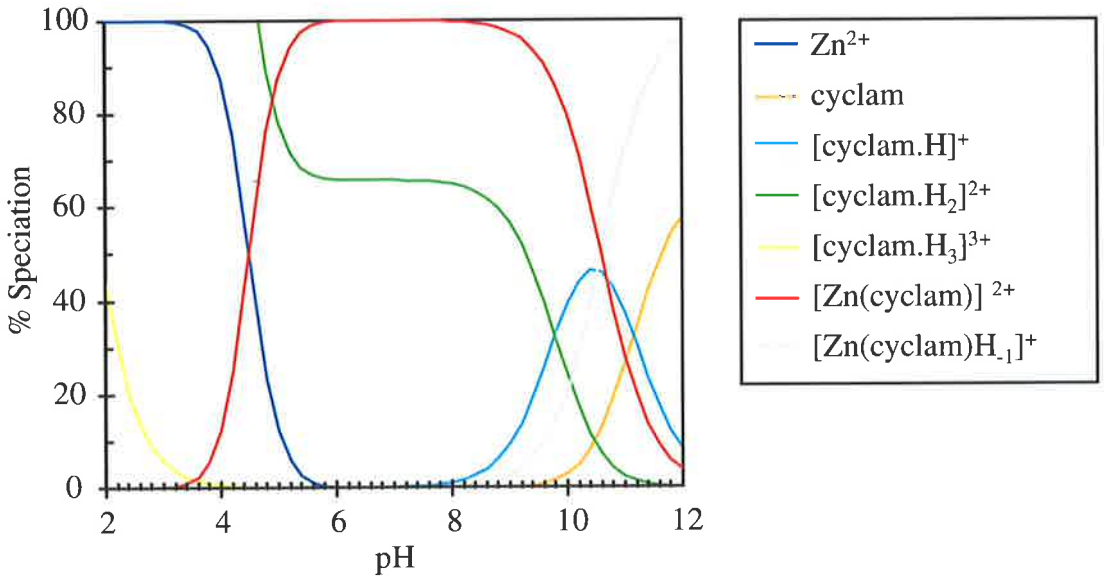

Figure 4.12 : Speciation plot for a solution containing 4.99×10^{-3} mol dm^{-3} cyclam and 3.01×10^{-3} mol dm^{-3} $Zn(ClO_4)_2$, showing the species present in 50% aqueous ethanol at various pH. % Speciation is shown relative to the total concentration of Zn^{2+}, I = 0.1 ($NaClO_4$) and T = 298.2 K.

From these results it is plain that the environment about Zn^{2+} does effect the ability of a Zinquin-A molecule to coordinate to it, and it is reasonable that in the cell, Zinquin-A does not coordinate to all Zn^{2+} with equal affinity, and may remove the Zn^{2+} from cellular coordination sites in some cases, or not coordinate to it at all in others.

4.3 : Ultraviolet-Visible Spectroscopy of the Ternary Complexes, [Zn(L)ZQA]

The ultraviolet-visible spectra of the [Zn(L)ZQA] ternary complexes studied by potentiometric titrations were determined at 298.2 K in 50% aqueous ethanol, at pH 6.6 (0.1 mol dm^{-3} NaPIPES) or pH 10 (0.1 mol dm^{-3} H_3BO_3), as described in Section 5.4.3. A pH of 6.6 was used for the majority of the ternary complexes as this showed a high percentage of formation for them and was reasonably close to physiological pH. However, some ternary complexes were present as the protonated form to some extent at this pH. This is exemplified by the tacdo system which contained [Zn(tacdo)ZQA] in addition to $[Zn(tacdo)ZQA.H]^+$, and the $NTA.H_3$ system which contained almost solely $[Zn(NTA)ZQA.H]^{2-}$ at this pH. The spectra for both [Zn(L)ZQA] and $[Zn(L)ZQA.H]^+$ of tacdo and NTA^{3-} could be derived from the spectra obtained at both pH 6.6 and 10. As can be seen from Figure 4.11, [Zn(cyclam)ZQA] does not form until high pH, hence, its spectrum was determined at pH 10 alone. Only the spectra of [Zn(L)ZQA] were determined for the other ligand systems in Figure 4.1 at pH 6.6, with the exception of TEA for which the spectrum of $[Zn(TEA)ZQA.H_{-1}]^-$ was determined.

Due to a large difference in molar absorptivity between the near ultraviolet and ultraviolet-visible regions, spectra for the two regions were determined separately. The concentrations used to determine the spectra were chosen so as to give the maximum percentage of formation of the species of interest at the desired pH. These concentrations were found by varying the individual concentrations of ligand, $Zn(ClO_4)_2$ and Zinquin-A (within basic guidelines as discussed below) in the program MACSPECIES[63] which uses the stability constants derived from the potentiometric titrations to calculate the concentration of all species in solution at any pH. For the ultraviolet-visible spectra, the general guidelines used for the optimal concentration determination were;

(a) the Zinquin-A concentration was to be approximately 1×10^{-4} mol dm^{-3} in the visible region and 2×10^{-5} mol dm^{-3} in the ultraviolet region to ensure the absorbance was between 0.2 and 0.7.

(b) the ligand concentration was not to exceed approximately 5×10^{-3} mol dm^{-3} to ensure the buffer (0.1 mol dm^{-3}) could still work effectively.

(c) the ligand concentration was to be greater than the $Zn(ClO_4)_2$ concentration to ensure no $[Zn(H_2O)_6]^{2+}$, which could precipitate as $Zn(OH)_2$, was present.

(d) the formation of other absorbing species, ZQA^{2-}, $[ZQA.H]^-$, $ZQA.H_2$, $[ZQA.H_3]^+$, [Zn(ZQA)] and $[Zn(ZQA)_2]^{2-}$, was to be minimised.

(e) the formation of the ternary complex of interest, usually [Zn(L)ZQA], was to be maximised.

Using these guidelines, the concentrations presented in Tables 5.17 and 5.18 were determined as the most appropriate to use. Unfortunately, only [Zn(tren)ZQA] and [Zn(tacdo)ZQA] were found to form to greater than 99%, leaving species such as $[ZQA.H]^-$, [Zn(ZQA)] and $[Zn(ZQA)_2]^{2-}$, which absorb in the region of interest, present in the spectra for all other systems. The concentrations of all Zinquin-A containing species present at greater than 2% formation in each solution used, for both wavelength regions, are included in Appendix D. The large concentrations of ligand in various states of protonation in these solutions could be ignored as each spectrum was run against a blank containing the ligand (L), $Zn(ClO_4)_2$ and the buffer which would remove the small contribution of these species to the absorbance (the percentage of ligand (L) complexed in [Zn(L)ZQA] did not exceed 10%). The contributions due to Zinquin-A species, however, must be dealt with using a different method. Since the molar absorbance spectra of these Zinquin-A species (listed in (d) above) have been determined under similar conditions (see Section 2.3), it is possible to calculate the contribution that they make to the spectrum from their concentration. The contribution can then be subtracted from the spectrum of the mixture, giving the absorbance due to the ternary species of interest only. This method relies on the assumption that the absorbance of a solution is equal to the sum of the individual absorbances arising from all components of that solution. Once the absorbances were obtained for each ternary species on its own, they were divided by the concentration of that species in the solution measured to normalise the absorbance for concentration. The final spectra obtained are shown in Figures 4.13 and 4.14. The spectra already presented for $[ZQA.H]^-$, [Zn(ZQA)] and $[Zn(ZQA)_2]^{2-}$ (see Section 2.3) are also included in these figures for comparison. The spectra for the complexes of the oxygen donor ligands are shown separately from those of the nitrogen donor ligands for simplicity. The maxima are listed for all of the species studied in Table 4.6.

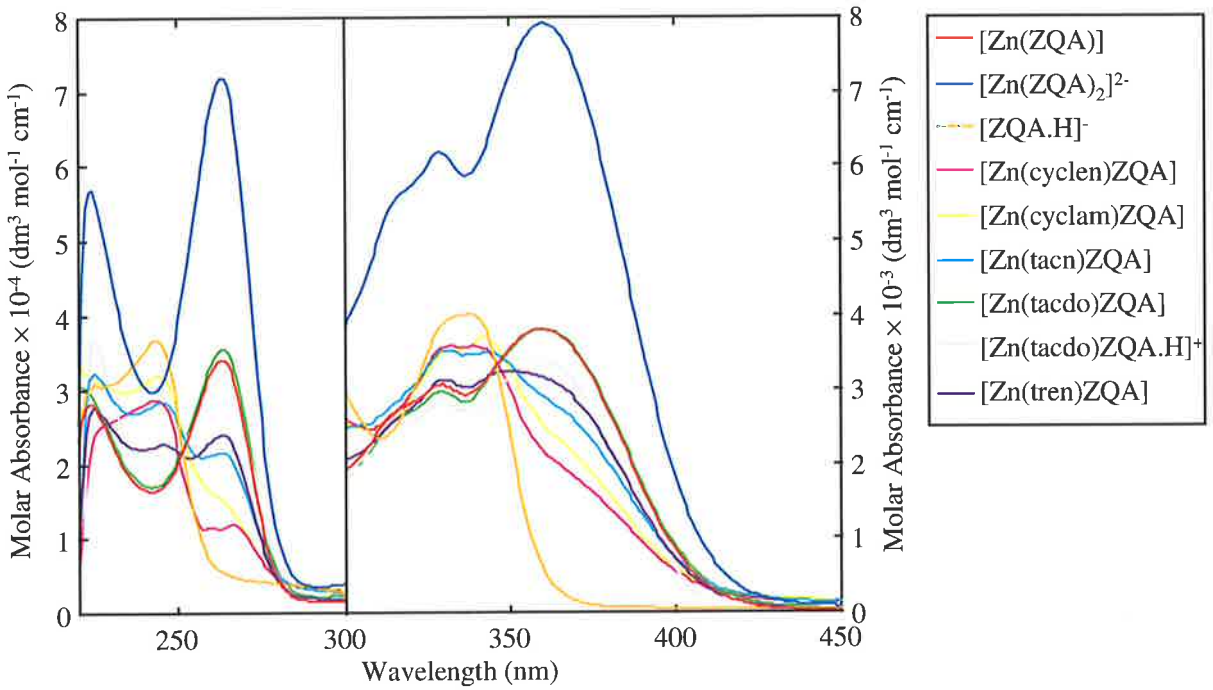

Figure 4.13 : Ultraviolet-visible spectra determined for the ternary complexes of the ligands in Figure 4.1 with nitrogen donors are compared with those determined for Zinquin-A species in Chapter 2. Spectra determined at pH 6.6 (0.1 mol dm^{-3} NaPIPES) are combined with those at pH 10 (0.1 mol dm^{-3} H_3BO_3), T = 298.2 K, concentrations for Zinquin-A species as described in Section 5.1.4 and for the others as listed in Table 5.13 (RHS) and Table 5.14 (LHS).

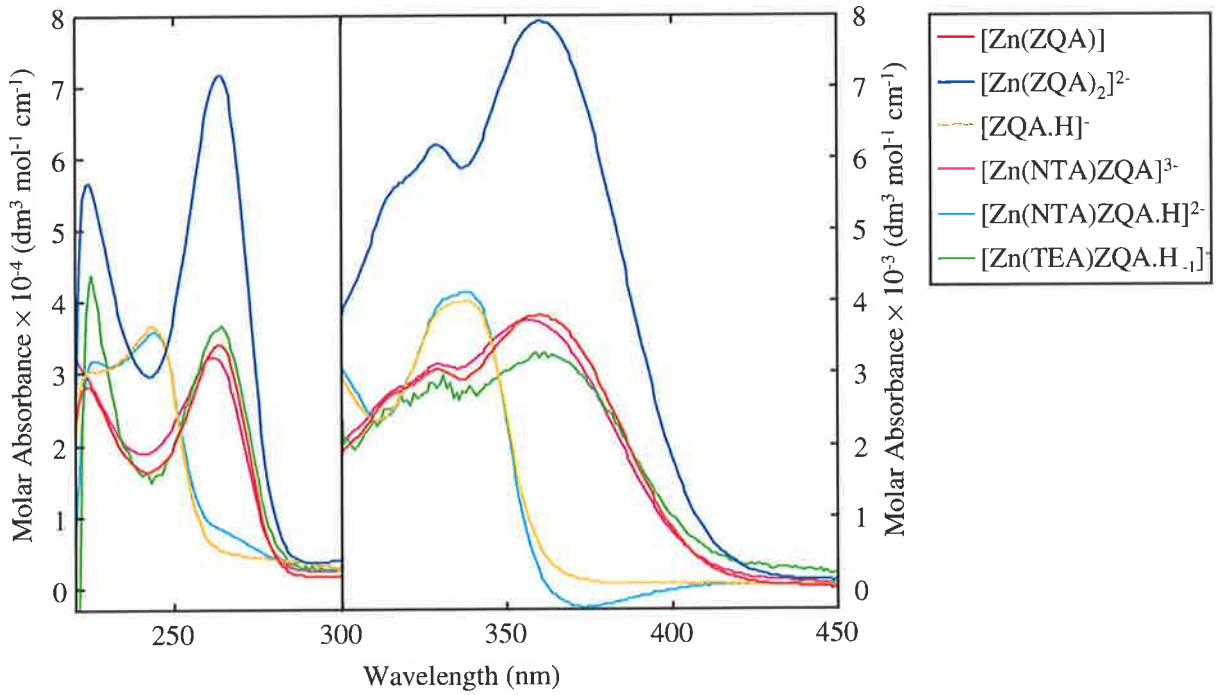

Figure 4.14 : Ultraviolet-visible spectra determined for the ternary complexes of the ligands in Figure 4.1 with oxygen donors are compared with those determined for Zinquin-A species in Chapter 2. Spectra determined at pH 6.6 (0.1 mol dm^{-3} NaPIPES) are combined with those at pH 10 (0.1 mol dm^{-3} H_3BO_3), T = 298.2 K, concentrations for Zinquin-A species as described in Section 5.1.4 and for the others as listed in Table 5.13 (RHS) and Table 5.14 (LHS).

Complex	Maximum Wavelength (nm) (Molar Absorbance ($dm^3\ mol^{-1}\ cm^{-1}$))						
[Zn(cyclen)ZQA]	[225] $[2.39\times10^4]$	243 (2.87×10^4)	260 (1.16×10^4)	267 (1.20×10^4)	333 (3.58×10^3)	339 (3.58×10^3)	[368] $[1.88\times10^3]$
[Zn(cyclam)ZQA]	244 (3.20×10^4)	[263] $[1.54\times10^4]$	331 (3.53×10^3)	341 (3.71×10^3)	[368] $[2.65\times10^3]$		
[Zn(tacn)ZQA]	225 (3.25×10^4)	245 (2.83×10^4)	263 (2.17×10^4)	[315] $[2.82\times10^3]$	330 (3.52×10^3)	345 (3.51×10^3)	[368] $[2.65\times10^3]$
[Zn(tacdo)ZQA]	223 (2.97×10^4)	264 (3.54×10^4)	[315] $[2.59\times10^3]$	329 (2.98×10^3)	361 (3.81×10^3)		
$[Zn(tacdo)ZQA.H]^+$	224 (3.69×10^4)	263 (3.15×10^4)	[315] $[2.48\times10^3]$	330 (2.86×10^3)	361 (3.39×10^3)		
[Zn(tren)ZQA]	225 (2.76×10^4)	245 (2.27×10^4)	263 (2.40×10^4)	[315] $[2.58\times10^3]$	330 (3.12×10^3)	351 (3.24×10^3)	
$[Zn(NTA)ZQA]^{3-}$	261 (3.22×10^4)	[315] $[2.73\times10^3]$	330 (3.12×10^3)	356 (3.73×10^3)			
$[Zn(NTA)ZQA.H]^{2-}$	225 (3.18×10^4)	244 (3.59×10^4)	[267] $[7.44\times10^3]$	336 (4.11×10^3)			
$[Zn(TEA)ZQA.H_{-1}]^-$	225 (4.36×10^4)	264 (3.67×10^4)	330 (2.95×10^3)	361 (3.27×10^3)			
$[ZQA.H]^-$	225 (3.06×10^4)	243 (3.66×10^4)	336 (3.99×10^3)				
[Zn(ZQA)]	224 (2.82×10^4)	263 (3.40×10^4)	[315] $[2.68\times10^3]$	330 (3.07×10^3)	361 (3.81×10^3)		
$[Zn(ZQA)_2]^{2-}$	224 (5.67×10^4)	263 (7.18×10^4)	[315] $[5.52\times10^3]$	329 (6.19×10^3)	361 (7.92×10^3)		

Table 4.6 : Maxima observed for the ultraviolet-visible spectra of the ternary complexes of the ligands in Figure 4.1. The maxima presented in Chapter 2 for some Zinquin-A species are included for comparison. The spectra are shown in Figures 4.13 and 4.14. Values enclosed in square brackets describe the approximate position of shoulders rather than maxima.

Unfortunately, one of the first things that is noted from Figures 4.13 and 4.14 is the poor quality of some of the spectra, in particular that obtained for TEA. This is an artefact of the method used to obtain the ternary spectrum alone and arises from the subtraction of significant absorbances due to other species from the raw spectrum. Dividing the resulting absorbance by a small concentration to obtain molar absorbance then considerably magnifies any imperfections in the spectrum. For the case of TEA, the ternary complex could only be formed to a maximum of 15% at pH 6.6 while following the aforementioned guidelines for optimal concentration determination. This meant that the remainder of the Zinquin-A was present as [Zn(ZQA)] which produced the majority of the raw absorption spectrum observed. Once this

contribution was subtracted, a low intensity spectrum remained which could be assumed to be due to $[Zn(TEA)ZQA.H_{-1}]^-$, as illustrated in Figure 4.15. Dividing this spectrum by the low concentration of $[Zn(TEA)ZQA.H_{-1}]^-$ present, 2.93×10^{-6} mol dm^{-3} or 1.26×10^{-5} mol dm^{-3} for ultraviolet and visible regions, respectively, produced the spectrum shown in Figure 4.14 which is considerably less smooth than the original raw spectrum obtained.

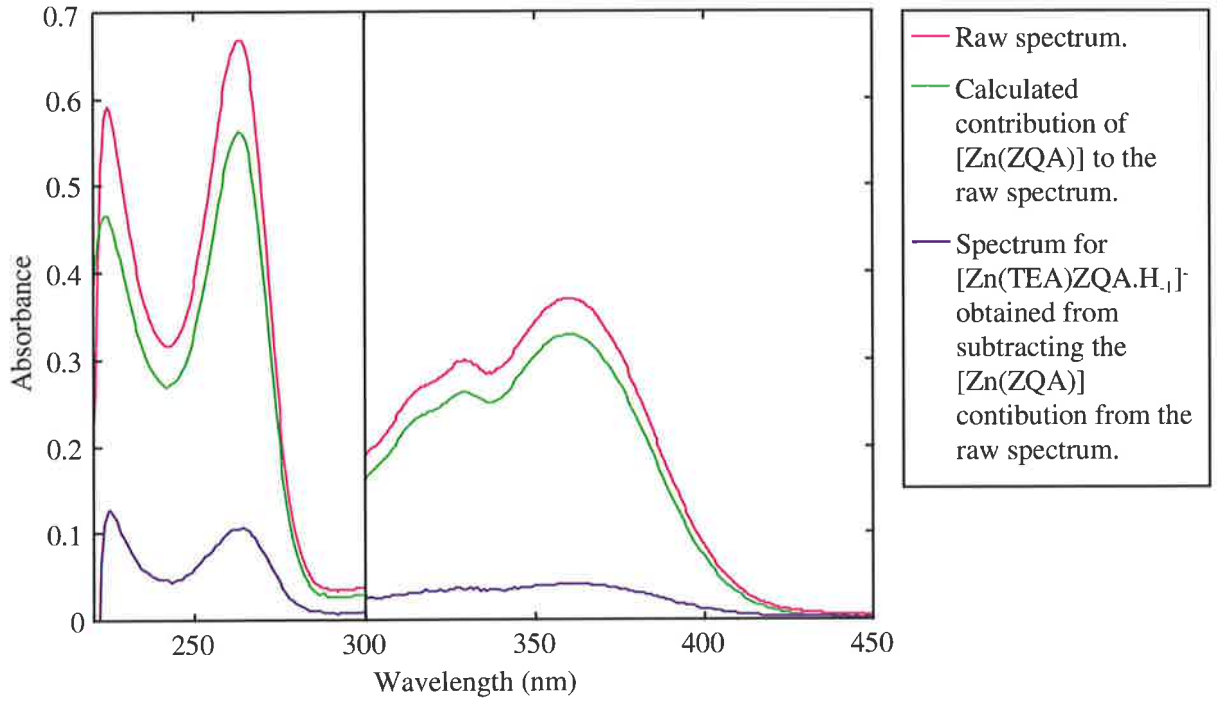

Figure 4.15 : An example of converting a raw spectrum to that for a ternary species alone by subtracting absorbance due to other species. The case for the TEA system is shown. The raw spectra contain 5.20×10^{-3} mol dm^{-3} TEA, 3.01×10^{-3} or 4.51×10^{-4} mol dm^{-3} $Zn(ClO_4)_2$ and 1.97×10^{-5} or 9.85×10^{-5} mol dm^{-3} Zinquin-A on the left and the right side respectively.

The complex, $[Zn(ZQA)_2]^{2-}$ has a greater absorbance than the other complexes shown because it contains two Zinquin-A anions and can therefore absorb twice as strongly as a complex containing only one. When this spectrum is halved in intensity, it is very similar to the [Zn(ZQA)] spectrum shown. The other spectra in Figures 4.13 and 4.14 appear to be similar to either the $[ZQA.H]^-$ spectrum, the [Zn(ZQA)] spectrum or a combination of the two. There appears to be a gradual change in the position of the maximum from near 340 nm ('$[ZQA.H]^-$ like'), to near 360 nm ('[Zn(ZQA)] like') with a change in ternary complex, which is most readily observed at wavelengths around 360 nm where $[ZQA.H]^-$ absorbs very little and [Zn(ZQA)] absorbs strongly. The absorbance at this wavelength decreases in the order;

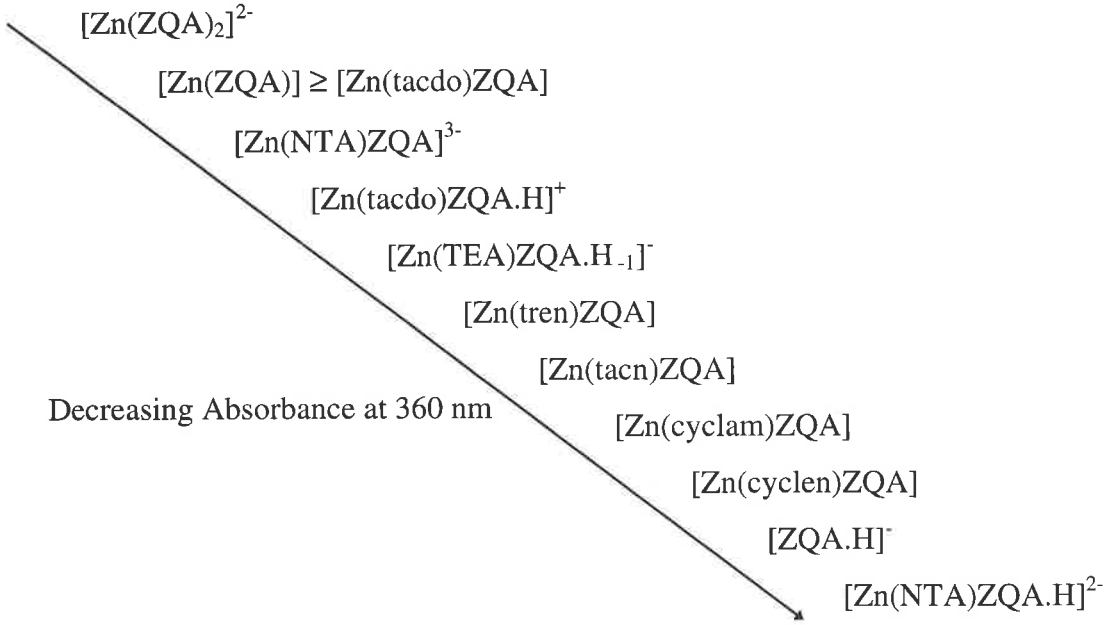

A similar order was observed at wavelengths near 263 nm where $[ZQA.H]^-$ again absorbs very little and [Zn(ZQA)] absorbs strongly. The difference in order observed at this wavelength is possibly due to the decreased accuracy in the 220 to 300 nm region which arises from a greater absorbance due to the buffer and ligand in the sample measured. Although this background absorbance is removed from the spectrum by the use of a blank as describe previously, the uncertainty in the values obtained increases. At wavelengths where both $[ZQA.H]^-$ and [Zn(ZQA)] absorb significantly, the order was not as well defined, however, the absorbances at 336 nm, where $[ZQA.H]^-$ has a maximum, appear to decrease in roughly the reverse order to above, if $[Zn(ZQA)_2]^{2-}$ is ignored.

It is interesting to note that the spectrum of [Zn(tacdo)ZQA] is almost identical to that of [Zn(ZQA)] in both wavelength regions and that the spectrum of $[Zn(tacdo)ZQA.H]^+$ is much the same but with a slightly lower molar absorbance. The spectrum of $[Zn(NTA)ZQA]^{3-}$ is also quite similar to that of [Zn(ZQA)], but its maximum at 356 nm is shifted slightly towards a lower wavelength compared with that observed for [Zn(ZQA)] at 360 nm. This indicates that in these complexes the presence of either tacdo or NTA^{3-} has little effect on the absorption of the Zinquin-A anion. It is therefore possible that tacdo and NTA^{3-} do not impose significant strain in the Zn^{2+} complex, which in turn does not force a large change in the geometry or conformation of Zinquin-A. It is likely that due to its flexibility resulting from its large ring size, and fewer donor atoms, tacdo exerts little geometric constraint upon the Zinquin-A anion which shares the Zn^{2+} that it is bound to, causing little change in the

spectrum. The shift to a lower wavelength observed for the spectrum of $[Zn(NTA)ZQA]^{3-}$, possibly could be due to the high negative charge on this ligand which effects the electron density of Zn^{2+} and therefore effects the energy levels of the coordinated Zinquin-A.

Another observation that stands out is that the $[Zn(NTA)ZQA.H]^{2-}$ spectrum is very similar to the $[ZQA.H]^{-}$ spectrum. The fact that this spectrum has an absorbance below zero near 380 nm is most definitely due to the aggregation of errors throughout the method used to obtain this spectrum. It appears that the small contribution of $[Zn(ZQA)_2]^{2-}$ to the raw spectrum (3.5%) has been over estimated. This could be due to the relatively small errors associated with the potentiometric titrations of Zinquin-A, NTA^{3-} and the ternary species, and the absorption spectra of both [Zn(ZQA)] and the ternary system, combining in an unfavourable way, producing a significantly larger error. Before converting to molar absorbance, however, the absorbance was only a maximum of 0.001 units below zero near 380 nm as compared with the maximum absorbance of 0.21 at 336 nm for the spectrum adjusted for [Zn(ZQA)] absorbance. Nevertheless, the similarity between the $[Zn(NTA)ZQA.H]^{2-}$ and $[ZQA.H]^{-}$ spectra indicates that the Zinquin-A anion is in a similar state in both species which seems to suggest that it is the Zinquin-A that is protonated in $[Zn(NTA)ZQA.H]^{2-}$ rather than a carboxylate of NTA^{3-}. This is quite possible when the pK_as of $[ZQA.H]^{-}$ and $NTA.H^{2-}$ are compared. $[ZQA.H]^{-}$ has the higher pK_a, 10.01 ± 0.02, as compared with 9.02 ± 0.04 for $NTA.H^{2-}$, and therefore ZQA^{2-} is more basic than NTA^{3-} and would tend to be protonated first. This explains the large change in the spectra between $[Zn(NTA)ZQA.H]^{2-}$ and $[Zn(NTA)ZQA]^{3-}$ in Figure 4.14.

In contrast, the spectrum of [Zn(tacdo)ZQA] does not change as significantly upon protonation. The only change observed is a slight decrease in molar absorbance at all wavelengths, except those below 250 nm where the uncertainty in the spectrum is greater. This indicates that it is most likely that the tacdo becomes protonated rather than the Zinquin-A anion as could be expected upon comparison of their pK_as. In this case, the pK_a of tacdo is larger than that of Zinquin-A, 11.69 ± 0.05 compared with 10.01 ± 0.02, and therefore tacdo should be protonated first.

After $[Zn(NTA)ZQA.H]^{2-}$, the two tetraamine macrocycles, cyclen and cyclam, are the most '$[ZQA.H]^-$ like' of the ligands studied. This may be due to the fact that they occupy four Zn^{2+} coordination sites and are reasonably rigid and, apart from the effect of this on the level of strain in the complex, would therefore interact more closely with the Zinquin-A anion than either a triamine or a more flexible acyclic tetraamine. This interaction appears to effect the Zinquin-A anion in a similar, but not identical, way to protonation.

For both the triamine and tetraamine macrocycles, [Zn(L)ZQA] formed by the larger macrocycles, tacdo and cyclam, are more '[Zn(ZQA)] like' than the complexes formed by the smaller macrocycles, tacn and cyclen, respectively. This indicates that the smaller macrocycles interact more with the bound Zinquin-A anion than the larger ones. When looking at the acyclic ligands, the order observed for the molar absorbance at 360 nm of [Zn(L)ZQA] is $[Zn(NTA)ZQA]^{3-}$ > $[Zn(TEA)ZQA.H]^{2-}$ > [Zn(tren)ZQA]. This indicates that the harder oxygens in NTA^{3-} and TEA effect the Zinquin-A anion less than the softer amine nitrogens of tren. This trend could also be an effect of charge, with a more negative charge on the ligand causing less change in the spectrum, perhaps because electrostatic repulsion between ZQA^{2-} and either NTA^{3-} or $[TEA.H_{-1}]^-$ causes the ligand to be further away from the Zinquin-A anion, with a concomitant lowering of the corresponding steric interaction between them.

4.4 : Fluorescence Spectroscopy of the Ternary Complexes, [Zn(L)ZQA]

The fluorescence spectra of the [Zn(L)ZQA] ternary complexes studied by potentiometric titrations were determined at 298.2 K in 50% aqueous ethanol, at pH 6.6 (0.1 mol dm^{-3} NaPIPES) or pH 10 (0.1 mol dm^{-3} H_3BO_3), as described in Section 5.4.4. An excitation wavelength of 358 nm was used as this produced the maximum fluorescence for the Zn^{2+} complexes of Zinquin-A as discussed in Section 2.3. Slit widths of 2.5 nm were used and averages of four spectra were obtained. The pHs of 6.6 and 10 were chosen for the same reasons they were chosen for the ultraviolet-visible spectra, as discussed in Section 4.3. Again both the tacdo and NTA.H_3 systems contained a significant amount of the protonated ternary complex at pH 6.6 and the spectra presented here are derived from both the pH 6.6 and pH 10 spectra. The spectrum for [Zn(cyclen)ZQA] was again determined solely at pH 10 due to its low stability at pH 6.6 and the spectrum of $[Zn(TEA)ZQA.H_{-1}]^-$ was determined for the TEA system. The concentrations used for the spectra were chosen using the same method as for the ultraviolet-visible spectra with the following guidelines;

(a) the Zinquin-A concentration was to be approximately 1×10^{-5} mol dm^{-3} to ensure that the fluorescence was between 20 and 900 units.

(b) the ligand concentration was not to exceed approximately 5×10^{-3} mol dm^{-3} to ensure the buffer (0.1 mol dm^{-3}) could still work effectively.

(c) the ligand concentration was to be greater than the $Zn(ClO_4)_2$ concentration to ensure no $[Zn(H_2O)_6]^{2+}$ was present in solution, preventing precipitation of $Zn(OH)_2$.

(d) the formation of other fluorescing species, [Zn(ZQA)] and $[Zn(ZQA)_2]^{2-}$, was to be minimised (the other Zinquin-A species do not fluoresce).

(e) the formation of the ternary complex of interest, usually [Zn(L)ZQA], was to be maximised.

Using these guidelines, the concentrations presented in Table 5.19 were determined as the most appropriate to use. Speciation plots for each ligand system showing the formation of each Zinquin-A containing species present with respect to pH for these concentrations are shown in Appendix C. Once again only [Zn(tacdo)ZQA] and [Zn(tren)ZQA] were found to form to greater than 99%, leaving small concentrations of species such as [Zn(ZQA)] and

$[Zn(ZQA)_2]^{2-}$, which fluoresce, present in the spectra for all other systems. The concentrations of all Zinquin-A containing species present at greater than 2% formation in each solution used are included in Appendix D. The presence of $[ZQA.H]^-$ and the ligand (L) in various protonation states was of no concern as these species do not fluoresce. The small amount of fluorescence due to the buffer and ligand, was removed by the use of a blank which contained the ligand, $Zn(ClO_4)_2$ and buffer. Since the molar fluorescences of [Zn(ZQA)] and $[Zn(ZQA)_2]^{2-}$ have been determined under similar conditions (see Section 2.3), it is possible to remove any contribution they make to the observed spectrum by the same method used for the ultraviolet-visible spectra (Section 4.3). Once the fluorescence of each ternary species of interest was determined, it was divided by the concentration of that species in the solution measured to normalise the fluorescence for concentration, giving molar fluorescence, as shown in Figure 4.16. The molar fluorescences previously presented for [Zn(ZQA)] and $[Zn(ZQA)_2]^{2-}$ (see Section 2.3) have been included for comparison. The location and intensity of the maxima observed are included in Table 4.7.

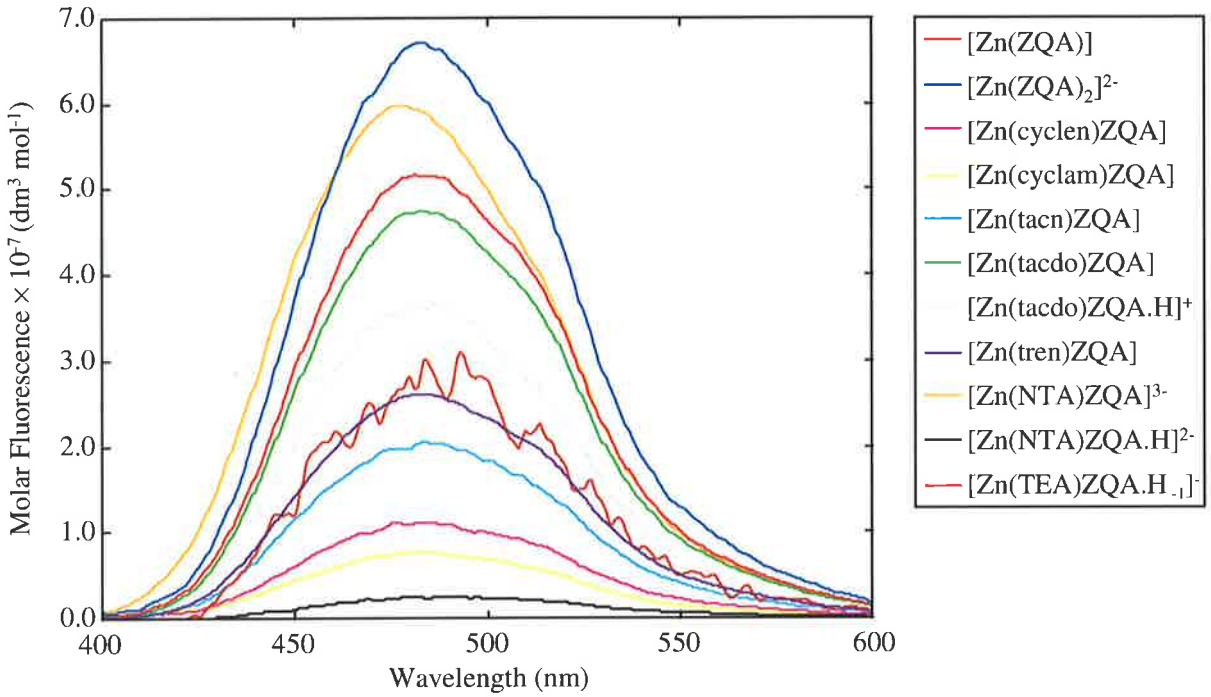

Figure 4.16 : Molar fluorescence* spectra determined for the ligands in Figure 4.1 are compared with those determined for Zinquin-A species in Chapter 2. Spectra determined at pH 6.6 (0.1 mol dm^{-3} NaPIPES) are combined with those at pH 10 (0.1 mol dm^{-3} H_3BO_3), concentrations for Zinquin-A species as described in Section 5.1.5 and for the others as listed in Table 5.19. The $[Zn(ZQA)_2]^{2-}$ spectrum is shown per complex, to obtain the spectrum per Zinquin-A anion, the spectrum shown must be divided by 2. T = 298.2 K, slits = 2.5 nm, Ex λ = 358 nm. (* All fluorescence measurements are relative and fluorescence is often referred to as 'relative' fluorescence)

Species	Maximum Wavelength (nm)	Molar Fluorescence
[Zn(cyclen)ZQA]	484	1.11×10^7
[Zn(cyclam)ZQA]	484	7.62×10^6
[Zn(tacn)ZQA]	484	2.05×10^7
[Zn(tacdo)ZQA]	484	4.74×10^7
$[Zn(tacdo)ZQA.H]^+$	484	3.68×10^7
[Zn(tren)ZQA]	484	2.61×10^7
$[Zn(NTA)ZQA]^{3-}$	478	5.98×10^7
$[Zn(NTA)ZQA.H]^{2-}$	488	2.52×10^6
$[Zn(TEA)ZQA.H_{-1}]^-$	~ 492	~ 2.78×10^7
[Zn(ZQA)]	485	5.16×10^7
$[Zn(ZQA)_2]^{2-}$	484	6.72×10^7

Table 4.7 : Molar fluorescence maxima observed for the ternary complexes of the ligands in Figure 4.1 and the Zn^{2+} complexes of Zinquin-A. The spectra are shown in Figure 4.16.

It can be seen that changing the ligand in the ternary complex significantly effects the fluorescence spectrum observed, with molar fluorescence values evenly distributed between 6.72×10^7 and 2.52×10^6 dm^3 mol^{-1} cm^{-1}. The order of decreasing molar fluorescence at the maxima is;

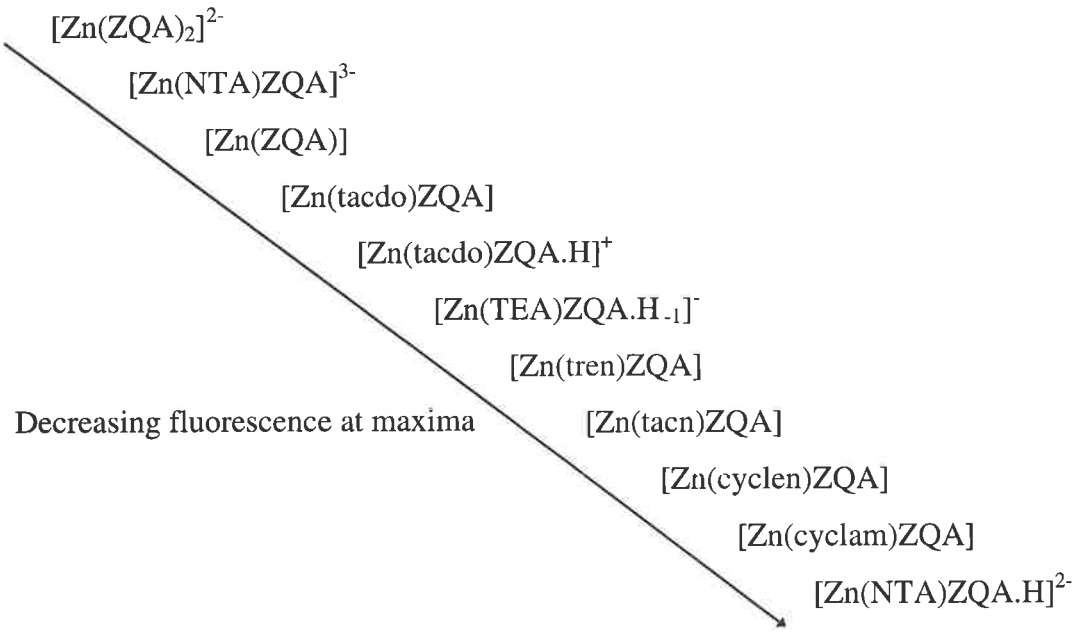

This order is very similar to the order of molar absorbance at 360 nm presented in Section 4.3 and tends to suggest that the amount absorbed at the excitation wavelength, 358 nm, may be the major contributor to this trend. This is reasonable as the intensity of fluorescence observed is dependent upon the amount of light absorbed. The more light, and therefore energy, that is absorbed by a complex, the greater the population of the excited state and therefore the greater the probability that this excess energy is emitted as fluorescence. To take this fact into account, each molar fluorescence spectra was then divided by the molar absorbance of that species at 358 nm, shown in Table 4.8. This produced the adjusted molar fluorescence shown in Figures 4.17 and 4.18 which is independent of both concentration and ability to absorb at 358 nm. The spectra already presented for [Zn(ZQA)] and $[Zn(ZQA)_2]^{2-}$ (see Section 2.3 and Figure 4.16 above) have also been adjusted for the amount absorbed at the excitation wavelength and are included in these figures for comparison. The spectra for the oxygen donor ligands are shown separately from the nitrogen donor ligands for simplicity. The maxima are listed for all of the species studied in Table 4.9.

Species	Molar Absorbance at 358 nm ($dm^3\ mol^{-1}\ cm^{-1}$)	Species	Molar Absorbance at 358 nm ($dm^3\ mol^{-1}\ cm^{-1}$)
[Zn(cyclen)ZQA]	2.29×10^3	$[Zn(NTA)ZQA]^{3-}$	3.73×10^3
[Zn(cyclam)ZQA]	2.64×10^3	$[Zn(NTA)ZQA.H]^{2-}$	4.86×10^2
[Zn(tacn)ZQA]	2.97×10^3	$[Zn(TEA)ZQA.H_{-1}]^{-}$	3.25×10^3
[Zn(tacdo)ZQA]	3.79×10^3	[Zn(ZQA)]	3.79×10^3
$[Zn(tacdo)ZQA.H]^{+}$	3.38×10^3	$[Zn(ZQA)_2]^{2-}$	7.88×10^3
[Zn(tren)ZQA]	3.19×10^3		

Table 4.8 : Absorbances of the ternary and Zn^{2+} complexes of Zinquin-A studied, at the excitation wavelength used to determine the fluorescence spectra, 358 nm.

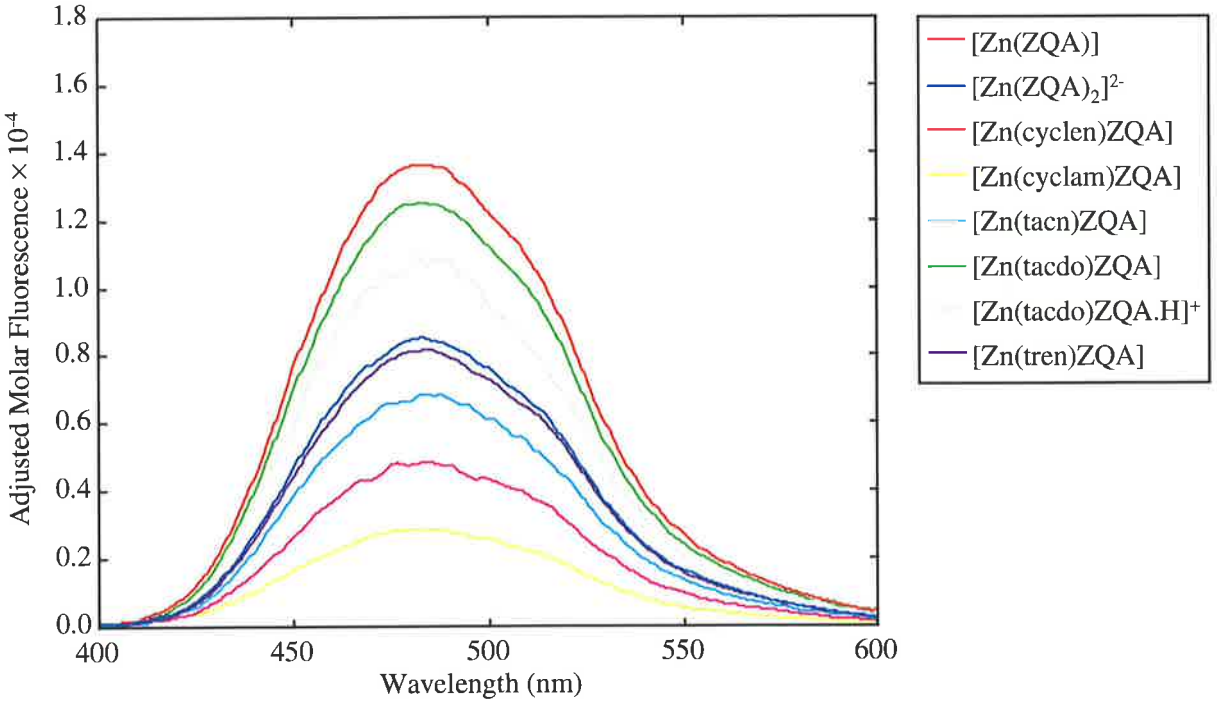

Figure 4.17 : Adjusted molar fluorescence spectra determined for the ligands in Figure 4.1 with nitrogen donors are compared with those determined for Zinquin-A species in Chapter 2. Spectra determined at pH 6.6 (0.1 mol dm^{-3} NaPIPES) are combined with those at pH 10 (0.1 mol dm^{-3} H_3BO_3), concentrations for Zinquin-A species as described in Section 5.1.5 and for the others as listed in Table 5.19. T = 298.2 K, slits = 2.5 nm, Ex λ = 358 nm.

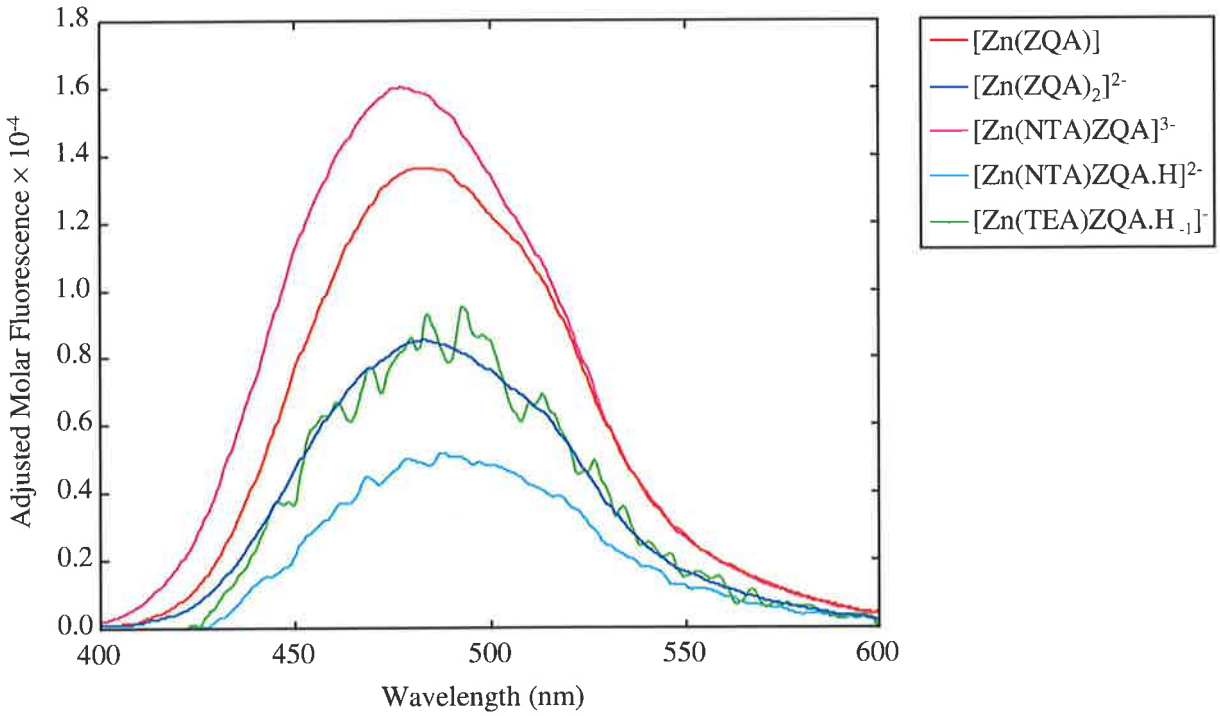

Figure 4.18 : Adjusted molar fluorescence spectra determined for the ligands in Figure 4.1 with oxygen donors are compared with those determined for Zinquin-A species in Chapter 2. Spectra determined at pH 6.6 (0.1 mol dm^{-3} NaPIPES) are combined with those at pH 10 (0.1 mol dm^{-3} H_3BO_3), concentrations for Zinquin-A species as described in Section 5.1.5 and for the others as listed in Table 5.19. T = 298.2 K, slits = 2.5 nm, Ex λ = 358 nm.

Species	Maximum Wavelength (nm)	Adjusted Molar Fluorescence
[Zn(cyclen)ZQA]	484	4.85×10^3
[Zn(cyclam)ZQA]	484	2.88×10^3
[Zn(tacn)ZQA]	484	6.89×10^3
[Zn(tacdo)ZQA]	484	1.25×10^4
$[Zn(tacdo)ZQA.H]^+$	484	1.07×10^4
[Zn(tren)ZQA]	484	8.18×10^3
$[Zn(NTA)ZQA]^{3-}$	478	1.60×10^4
$[Zn(NTA)ZQA.H]^{2-}$	488	5.19×10^3
$[Zn(TEA)ZQA.H_{-1}]^-$	~ 492	~ 8.92×10^3
[Zn(ZQA)]	485	1.36×10^4
$[Zn(ZQA)_2]^{2-}$	484	8.53×10^3

Table 4.9 : Adjusted molar fluorescence maxima observed for the ternary complexes of the ligands in Figure 4.1 and the Zn^{2+} complexes of Zinquin-A. The spectra are shown in Figures 4.17 and 4.18.

Once again, a very noisy spectrum was obtained for $[Zn(TEA)ZQA.H_{-1}]^-$ due to the subtraction of large amounts of fluorescence due to $[Zn(ZQA)_2]^{2-}$, which formed to 84%, from the raw spectrum and the subsequent division by the small concentration of $[Zn(TEA)ZQA.H_{-1}]^-$ which only formed to 15%. The spectra for $[Zn(NTA)ZQA.H]^{2-}$ and $[Zn(tacdo)ZQA.H]^+$ are also noisier than could be expected. This is again due to the calculations performed to arrive at the spectrum shown.

Unlike the molar spectra in Figure 4.16, the adjusted molar fluorescence spectrum for $[Zn(ZQA)_2]^{2-}$ is not greater in intensity than the spectrum of [Zn(ZQA)] as may be expected due to the presence of two Zinquin-A anions. This is because adjusted molar fluorescence is obtained from the molar fluorescence which is divided by the amount the species of interest absorbs at the excitation wavelength (358 nm). Hence, the factor of two arising from the presence of two Zinquin-A anions in $[Zn(ZQA)_2]^{2-}$ cancels out as it is present in both the molar absorption spectrum and the molar fluorescence spectrum.

All of the spectra observed have approximately the same shape and maximum wavelength but differing intensities, except $[Zn(NTA)ZQA]^{3-}$ which is shifted to slightly lower wavelengths. This shift correlates well with the shift towards lower wavelengths observed for the peak at 356 nm in the ultraviolet-visible spectrum of this complex as compared with [Zn(ZQA)] which has a maximum at 360 nm (see Table 4.6). The adjusted molar fluorescence at 484 nm, which is the maximum for the majority of complexes, decreases in the order;

$[Zn(NTA)ZQA]^{3-}$
[Zn(ZQA)]
[Zn(tacdo)ZQA]
$[Zn(tacdo)ZQA.H]^{+}$
$[Zn(TEA)ZQA.H_{-1}]^{-}$
$[Zn(ZQA)_2]^{2-}$
[Zn(tren)ZQA]
Decreasing fluorescence at 484 nm
[Zn(tacn)ZQA]
$[Zn(NTA)ZQA.H]^{2-}$
[Zn(cyclen)ZQA]
[Zn(cyclam)ZQA]

Interestingly, this order is still quite similar to the order observed for the molar absorbance at 360 nm, despite dividing by the amount absorbed. This suggests that the ability of the complexes to absorb at the excitation wavelength is not the only contributing factor to the amount of fluorescence observed. It appears that different ligands cause different amounts of non-radiative relaxation, or quenching, in the ternary complexes. The trend observed for molar absorbance was explained in terms of the interaction of the ligand with the Zinquin-A anion in the ternary complex (Section 4.3). The greater the interaction with Zinquin-A, the greater the change in the absorption spectrum compared with the [Zn(ZQA)] absorption spectrum as the energy levels in Zinquin-A are changed to a greater extent. A similar reasoning can be used to explain the trend above. The more a ligand induces strain in the structure of the complex, the more it is likely to induce quenching of the Zinquin-A anion. This explains the similarity between the two trends. Combined with this effect is the influence of the flexibility of the complex as a whole. Flexible moieties in a complex may induce vibrational relaxation in the Zinquin-A anion and therefore complexes with such moieties may exhibit lower fluorescence intensities due to quenching. However, it appears that the latter

effect is only influential in the case of [Zn(cyclen)ZQA] and [Zn(cyclam)ZQA] where the fluorescence trend deviates from the absorbance trend and the larger cyclam causes more quenching despite inducing less strain in the complex and interacting less with the Zinquin-A anion than the smaller cyclen. The results also indicate that a second Zinquin-A anion in $[Zn(ZQA)_2]^{2-}$ causes additional quenching despite it having very little effect on the absorption spectrum adjusted for the number of Zinquin-A anions present.

The spectrum of $[Zn(NTA)ZQA.H]^{2-}$ results in another obvious change in the trend compared with what was observed for the absorbance. It has the lowest molar absorbance at 360 nm of all spectra studied and is very '$[ZQA.H]^-$ like'. Hence, it could be expected that it would have a very low fluorescence as $[ZQA.H]^-$ does not fluoresce at all. Yet it has a higher adjusted molar fluorescence than [Zn(cyclen)ZQA] and [Zn(cyclam)ZQA] which have larger molar absorbances at 360 nm and are therefore less '$[ZQA.H]^-$ like' than $[Zn(NTA)ZQA.H]^{2-}$. It is possible that this anomaly in the observed trend occurs due to the experimental error inherent in the molar absorbance data for $[Zn(NTA)ZQA.H]^{2-}$ as discussed in Section 4.3. This experimental error causes the molar absorbance of $[Zn(NTA)ZQA.H]^{2-}$ to drop below zero between approximately 363 nm and 400 nm and therefore it is conceivable for the molar absorbance obtained at 358 nm to also be lower than should be expected. This would result in the higher adjusted molar fluorescence observed, since the molar fluorescence would be divided by a smaller molar absorbance than expected, producing larger values of adjusted molar fluorescence than expected. The fact that fluorescence is still observed despite the similarity of the absorption spectrum to that of $[ZQA.H]^-$ indicates that although the complex is most likely protonated on one of the Zinquin-A sites (see Section 4.3), the Zinquin-A anion is still able to coordinate to the Zn^{2+} which induces the rigidity necessary for fluorescence emission (see Section 2.3).

It should be noted that the fluorescence observed in cells incubated with Zinquin-E is dependent upon both the ability of the bound Zinquin-A anion to absorb light at a wavelength appropriate to produce fluorescence and quenching effects. The use of adjusted molar fluorescence here is a convenient way to study the effect of the surrounding environment on the relaxation and quenching of bound Zinquin-A anions alone.

The MATLAB program BANDANAL[64] was used to fit Gaussian curves to the adjusted molar fluorescence spectra obtained for each ternary complex studied. This program utilises a resolution enhancement algorithm[65] which indicates the likely position of substructural curves which may be components of the spectrum. These positions can then be used as initial parameters for fitting Gaussian curves to the spectrum. It is quite likely that when Gaussian curves are fitted correctly to a fluorescence spectrum, they represent the vibrational fine structure of the electronic transition producing the fluorescence. (see Appendix A for an overview of spectroscopy theory). Hence, the wavelengths describing the maxima of the fitted Gaussian curves describe the energy differences between the ground vibrational level of the excited electronic state and the various accessible vibrational levels in the ground electronic state. The intensities of the Gaussian curves give an indication of the population, after relaxation, of each vibrational level of the ground electronic state represented, and therefore the probability of that transition occurring. If the ground and excited electronic state potential energy curves change their relative positions, a change in the intensity profile will be observed (see Figure A.3). Hence, fitting Gaussian curves to the ternary complex spectra can provide a simple deconvolution of the spectra and therefore give;

(a) an illustration of the similarity of all the spectra by studying their substructure

(b) a crude estimate of the separation of the vibrational energy levels in the ground electronic state for each ternary complex and

(c) an estimate of the relative shift between the potential energy curves of the ground and excited electronic states with a change in ternary complex.

An example of a fitted spectrum is shown for [Zn(tren)ZQA] in Figure 4.19. Fits of Gaussian curves to all of the adjusted molar fluorescence spectra shown in Figures 4.17 and 4.18 are presented in Appendix B. The intensity values obtained for each Gaussian curve were converted to relative intensities for each spectrum by dividing each intensity by the intensity of the third maximum which was the one closest to 484 nm and the most intense maximum. The results are shown, to the nearest whole nm, in Table 4.10. The low intensity Gaussian curve with a maximum near 428 nm, labelled as 'Curve 1' in Figure 4.19 and Table 4.10, could not be fitted to all spectra, however, in such cases the values obtained for the other Gaussian curves were not significantly effected.

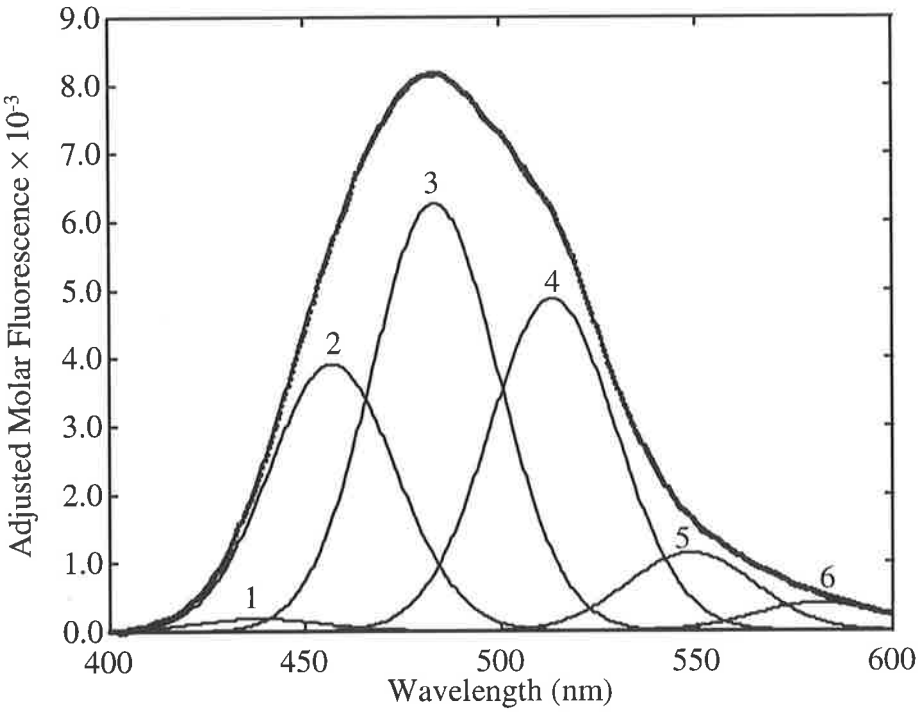

Figure 4.19 : An example of Gaussian curves that have been fitted to the [Zn(tren)ZQA] fluorescence spectrum. The experimental data is represented as points, the spectrum fitted to these points is a line passing near to them and the remaining curves represent Gaussian curves which add up to give the fitted spectrum. The numbers indicate the labelling of the curves used in Tables 4.10 and 4.11. Appendix B contains similar figures for all of the complexes studied.

BANDANAL[64] produced good fits of Gaussian curves to the adjusted molar fluorescence spectra of the various species studied. This indicates that there is a high probability that the values obtained from these fittings represent the vibrational fine structure of the spectra. However, the lowest wavelength Gaussian curve, labelled as 'Curve 1' in Figure 4.19 and Table 4.10, has a large error associated with it in most cases (see Appendix B) arising from its low intensity and subsequent susceptibility for baseline errors. Despite its uncertainty, this curve was included in the fits where possible, as a fit for some spectra could not be obtained without it. Due to its low intensity and large errors, Curve 1 has been omitted from any comparisons of the wavelengths and relative intensities of the fitted Gaussian curves. This omission is validated by the small contribution this curve makes to the fitted spectrum.

Complex	Maximum Wavelength of Gaussian Curve (nm) (Relative Intensity)					
	Curve 1	Curve 2	Curve 3	Curve 4	Curve 5	Curve 6
[Zn(cyclen)ZQA]	428 (0.045)	456 (0.65)	482 (1.00)	512 (0.82)	544 (0.21)	577 (0.084)
[Zn(cyclam)ZQA]	421 (0.074)	455 (0.63)	482 (1.00)	513 (0.77)	547 (0.19)	580 (0.068)
[Zn(tacn)ZQA]	418 (0.015)	457 (0.69)	485 (1.00)	514 (0.75)	548 (0.19)	582 (0.064)
[Zn(tacdo)ZQA]	438 (0.030)	457 (0.67)	484 (1.00)	513 (0.79)	547 (0.19)	580 (0.067)
$[Zn(tacdo)ZQA.H]^{+}$		458 (0.73)	486 (1.00)	516 (0.68)	551 (0.16)	583 (0.057)
[Zn(tren)ZQA]	438 (0.029)	457 (0.63)	483 (1.00)	514 (0.78)	549 (0.18)	581 (0.064)
$[Zn(NTA)ZQA]^{3-}$	433 (0.100)	455 (0.76)	483 (1.00)	513 (0.70)	548 (0.16)	581 (0.053)
$[Zn(NTA)ZQA.H]^{2-}$		461 (0.70)	488 (1.00)	516 (0.82)	550 (0.26)	586 (0.085)
$[Zn(TEA)ZQA.H_{-1}]^{-}$		459 (0.69)	489 (1.00)	518 (0.59)	550 (0.16)	581 (0.056)
[Zn(ZQA)]	424 (0.013)	457 (0.65)	483 (1.00)	513 (0.80)	548 (0.19)	582 (0.064)
$[Zn(ZQA)_2]^{2-}$	429 (0.032)	458 (0.68)	484 (1.00)	514 (0.77)	549 (0.19)	582 (0.061)

Table 4.10 : Data describing the Gaussian curves that can be fitted to the ternary complex fluorescence spectra. The wavelengths are rounded to the nearest whole number and the relative intensities were calculated as defined in the text. Appendix B contains the complete data and figures for these fits.

It can been seen from Table 4.10 and the figures in Appendix B that, excluding the values for Curve 1, both the wavelengths and relative intensities obtained are fairly independent of the ligand in the ternary complex. To help illustrate this, the averages of both the wavelengths and relative intensities obtained are shown in Table 4.11, along with their standard deviations. It can be seen that the standard deviations associated with the average wavelength values are small, being less than 0.5% of the associated wavelengths. The variance in the relative intensities shown in Table 4.10 is also reasonable, with standard deviations between 6.0% and 15.8% of the associated average value.

Gaussian Curve	Average Wavelength (nm)	Standard Deviation	Average Relative Intensity	Standard Deviation
1	428.6	7.44	0.042	0.030
2	457.4	1.69	0.680	0.040
3	484.5	2.25	1.000	0.000
4	514.2	1.78	0.752	0.070
5	548.3	1.90	0.189	0.028
6	581.4	2.20	0.066	0.010

Table 4.11 : The average wavelengths and relative intensities, and their standard deviations, are shown for each Gaussian curve in Table 4.10.

The similarity in the shape of all the adjusted molar fluorescence spectra is quite evident in Table 4.10 as the wavelengths and relative intensities of the fitted Gaussian curves are very similar. The apparent shift of the $[Zn(NTA)ZQA]^{3-}$ spectrum to lower wavelengths appears to arise from a combination of a change in the relative intensities of the second and third component Gaussian curves, and a very small shift of all the curves to lower wavelengths relative to some of the other complexes.

The fact that the wavelengths of the component Gaussian curves remain relatively constant upon changing the ligand in the ternary complex, tends to suggest that upon coordinating to Zn^{2+} that is already bound by a ligand, the energies of the observed transitions remain relatively unchanged. That is, the energy separations between the lowest vibrational level of the Zinquin-A anion excited electronic state and the accessible vibrational levels of the ground electronic state remain relatively unchanged. Therefore the energy separations of the ground electronic state vibrational levels remain constant as does the energy separation of the lowest vibrational level of the ground and excited electronic states. Thus, the energies marked as a) to e) in Figure 4.20 remain essentially the same for all ternary complexes is studied.

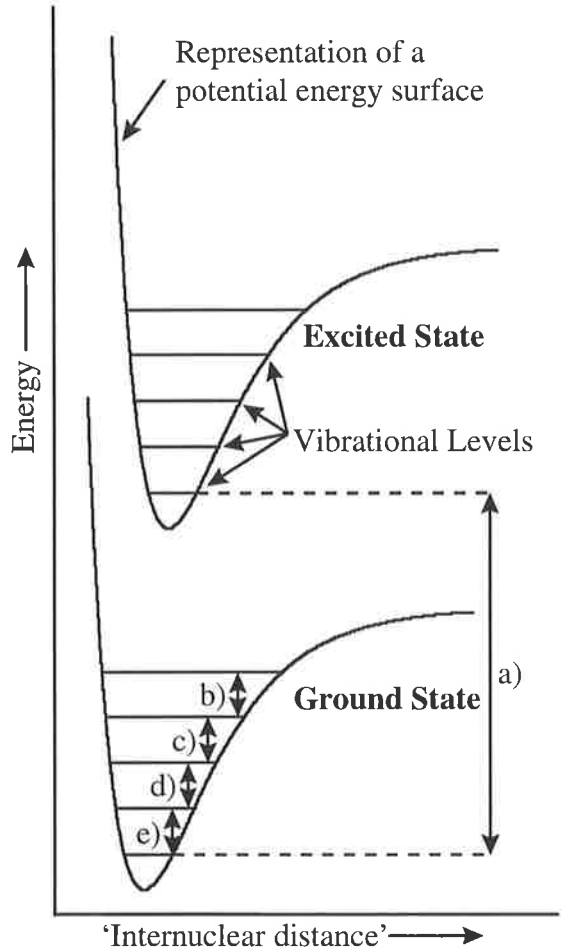

Figure 4.20 : A simplistic representation of the ground and excited electronic state potential energy surfaces and their vibrational energy levels. a) indicates the energy difference between the two electronic states and b) to e) indicate the energy separations of the vibrational levels of the ground electronic state, as discussed in the text.

The small variation in the relative intensities of the component Gaussian curves with a change in ligand, indicates that the populations, after relaxation, of the vibrational levels of the ground electronic state remain approximately constant irrespective of the ligand used. This would arise if there was no change in the relative positions of the potential energy surfaces involved, and therefore no change in the transition dipole moment for the individual transitions observed. This can be explained in simplified terms by the Franck-Condon principle where a transition is only observed when there is a sufficient overlap of a probability function in the excited electronic state (usually the lowest vibrational level) with a probability function in the ground electronic state. The intensity of the resulting transition is proportional to the amount of overlap of the probability functions. It is common for several ground state probability functions to overlap with the excited state probability function by varying degrees, producing a spectrum consisting of several transitions of differing intensities. If there is no

change in the overlap of these probability functions with a change in ligand, there would therefore be no significant change in the relative intensities of the component Gaussian curves observed. As can be seen in Figure A.3, this would occur if changing the ligand had little or no effect on the relative positions of the excited and the ground electronic state potential energy surfaces (see Appendix A for more detail). Hence, the variation in the adjusted molar fluorescence intensity with a change in ternary complex must be due to differences in quenching, reflecting subtle changes in the environment of the Zinquin-A anion.

To obtain information about the excited state vibrational levels, and for completeness, Gaussian curves were also fitted to the molar absorbance spectra obtained for each ternary complex studied (Section 4.3), in the region of 300 to 450 nm, using the same MATLAB program, BANDANAL,[64] used for the fluorescence spectra. As for the fitting of Gaussian curves to the fluorescence spectra, it is quite likely that when Gaussian curves are fitted correctly to an absorption spectrum, they also represent the vibrational fine structure of the electronic transition producing the absorption. The difference between the two is that the electronic transition for absorption is an excitation, compared with a relaxation for fluorescence (see Appendix A for an overview of spectroscopy theory). Hence, the wavelengths describing the maxima of the fitted Gaussian curves in this case describe the energy differences between the ground vibrational level of the ground electronic state and the various accessible vibrational levels in the excited electronic state. The intensities of the Gaussian curves give an indication of the population, after excitation, of each vibrational level of the excited electronic state represented, and therefore the probability of that transition occurring.

Examples of fitted spectra are shown for $[Zn(NTA)ZQA]^{3-}$, which is '[Zn(ZQA)] like', and [Zn(cyclen)ZQA], which is '$[ZQA.H]^-$ like', in Figures 4.21 and 4.22, respectively. Fits for all of the ternary complexes studied are combined with fits obtained for the spectra of $[ZQA.H]^-$, [Zn(ZQA)], and $[Zn(ZQA)_2]^{2-}$ in Appendix B. The intensity values obtained for each Gaussian curve were converted to relative intensities for each spectrum by dividing each intensity by the intensity of the third maximum which was the one closest to 350 nm (except $[Zn(TEA)ZQA.H_{-1}]^-$, for which the second maximum was used), as this was the most intense maximum in most cases. The results are shown, to the nearest whole nm, in Table 4.12.

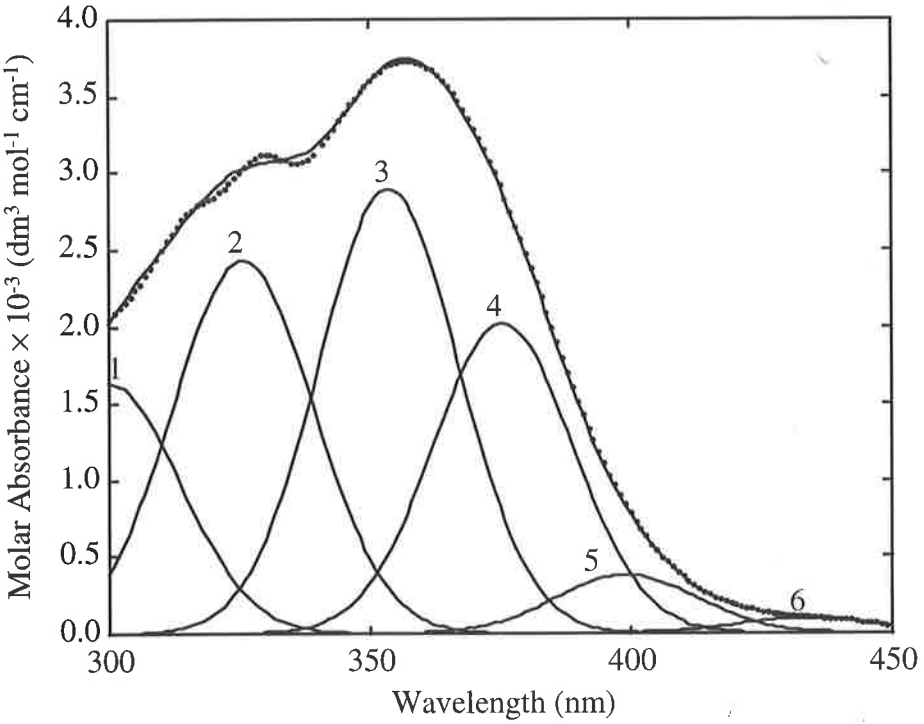

Figure 4.21 : An example of Gaussian curves that have been fitted to the $[Zn(NTA)ZQA]^{3-}$ absorption spectrum. The experimental data ~~is~~ are represented as points, the spectrum fitted to these points is a line passing near to them and the remaining curves represent Gaussian curves which add up to give the fitted spectrum. The numbers indicate the labelling of the curves used in Tables 4.12 and 4.13.

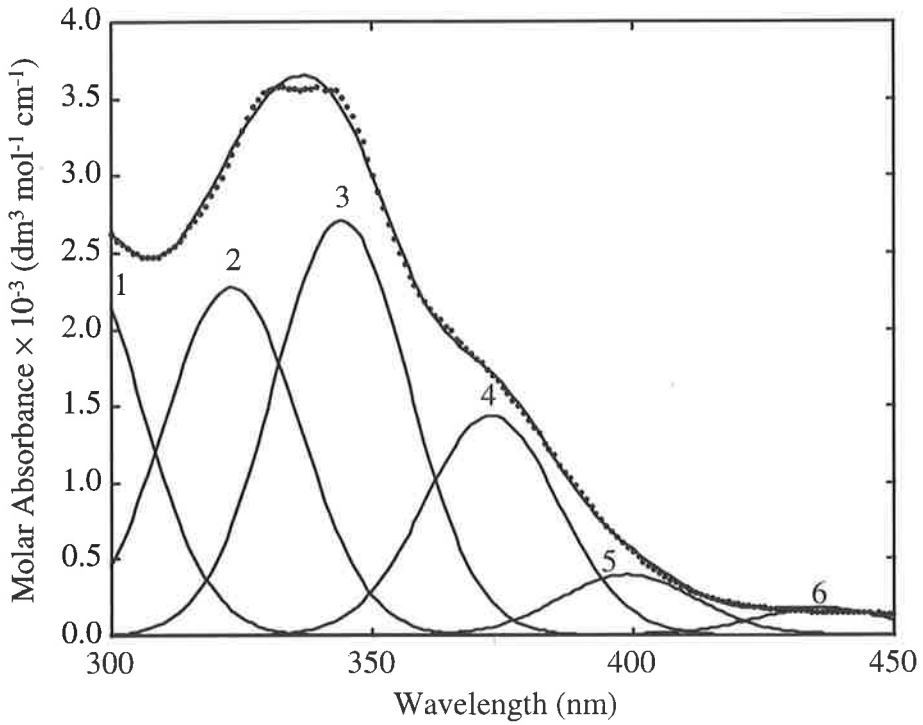

Figure 4.22 : An example of Gaussian curves that have been fitted to the [Zn(cyclen)ZQA] absorption spectrum. The experimental data ~~is~~ are represented as points, the spectrum fitted to these points is a line passing near to them and the remaining curves represent Gaussian curves which add up to give the fitted spectrum. The numbers indicate the labelling of the curves used in Tables 4.12 and 4.13.

	Maximum Wavelength of Gaussian Curve (nm) (Relative Intensity)					
Complex	Curve 1	Curve 2	Curve 3	Curve 4	Curve 5	Curve 6
[Zn(cyclen)ZQA]	293 (0.93)	323 (0.84)	344 (1.00)	373 (0.53)	399 (0.15)	436 (0.063)
[Zn(cyclam)ZQA]	293 (0.82)	323 (0.78)	345 (1.00)	373 (0.56)	399 (0.14)	435 (0.068)
[Zn(tacn)ZQA]	294 (0.89)	325 (1.03)	348 (1.00)	374 (0.76)	401 (0.16)	438 (0.068)
[Zn(tacdo)ZQA]	302 (0.50)	326 (0.82)	354 (1.00)	376 (0.79)	397 (0.18)	431 (0.031)
$[Zn(tacdo)ZQA.H]^{+}$	302 (0.55)	328 (0.82)	357 (1.00)	380 (0.59)		
[Zn(tren)ZQA]	298 (0.70)	326 (1.01)	352 (1.00)	374 (0.82)	396 (0.19)	433 (0.024)
$[Zn(NTA)ZQA]^{3-}$	300 (0.56)	326 (0.84)	354 (1.00)	376 (0.70)	399 (0.13)	434 (0.034)
$[Zn(NTA)ZQA.H]^{2-}$	301 (0.78)	324 (0.78)	341 (1.00)			
$[Zn(TEA)ZQA.H_{-1}]^{-}$	316 (0.78)	366 (1.00)	438 (0.084)			
$[ZQA.H]^{-}$	299 (0.82)	324 (0.79)	342 (1.00)	374 (0.034)		
[Zn(ZQA)]	303 (0.56)	327 (0.85)	354 (1.00)	375 (0.78)	394 (0.20)	424 (0.018)
$[Zn(ZQA)_2]^{2-}$	303 (0.53)	327 (0.81)	355 (1.00)	376 (0.75)	398 (0.16)	433 (0.023)

Table 4.12 : Data describing the Gaussian curves that can be fitted to the ternary complex absorption spectra. The wavelengths are rounded to the nearest whole number and the relative intensities were calculated as defined in the text. Appendix B contains the complete data and figures for these fits.

Unlike the case for the adjusted molar fluorescence, BANDANAL[64] was not fully effective in fitting Gaussian curves to the ternary complex absorption spectra. The reason for this lies in the method used by BANDANAL which is limited to fitting Gaussians of equal bandwidth. It is evident from the poor fit in some regions of Figure 4.21, Figure 4.22 and Figures B.12 to B.23 in Appendix B, that the spectra actually consist of several Gaussian curves of different bandwidths. It appears that if Curve 2 in Figure 4.21 was replaced by two Gaussian curves with a smaller bandwidth than the ones shown, a better fit could be obtained. Similarly the maximum in Figure 4.22 could be better fitted if Curves 2 and 3 were of a narrower bandwidth. All of the spectra studied had regions where a substitution of this type could produce a better fit. Hence, the values for both wavelength and intensity of Gaussian curves

arising from these fits must be regarded with caution due to their extremely approximate nature. Nevertheless, an approximate comparison can be made if it is assumed that the narrower Gaussian curves have been approximated in the same way in the fitting of each spectrum. It can been seen from Table 4.12, and the figures in Appendix B, that with the exception of $[Zn(TEA)ZQA.H_{-1}]^-$, which was too noisy to obtain a good fit for all Gaussian curves expected, the wavelengths obtained are fairly independent of the ligand in the ternary complex. In contrast, the relative intensities seem to vary more from complex to complex than for the fluorescence spectra. To help illustrate this, the averages of both the wavelengths and relative intensities obtained are shown in Table 7.13 along with their standard deviations. It can be seen that the standard deviations associated with the average wavelength values are reasonable, being a maximum of 1.7% of the associated wavelength, however, those associated with the average relative intensity vary from 10% to 52%, indicating a large variation in intensity with a change in the ligand used in the ternary complex for many of the Gaussian curves.

Gaussian Curve	Average Wavelength (nm)	Standard Deviation	Average Relative Intensity	Standard Deviation
1	298.9	3.91	0.695	0.160
2	325.4	1.69	0.852	0.087
3	349.6	5.78	1.000	0.000
4	375.1	2.08	0.631	0.234
5	397.9	2.17	0.164	0.024
6	433.0	4.21	0.041	0.021

Table 4.13 : The average wavelengths and relative intensities, and their standard deviations, are shown for each Gaussian curve in Table 4.12. The values obtained for the $[Zn(TEA)ZQA.H_{-1}]^-$ spectrum are omitted from the calculations.

A larger standard deviation is expected for Curve 6 as this is a low intensity curve and is therefore subject to greater baseline errors. A reasonably large variation in Curve 1 is also expected as the maximum of this curve lies outside, or close to, the limit of experimental points in most cases and may in fact be due to a different electronic transition. The larger variation in Curve 3 is due to the gradual change from '$[ZQA.H]^-$ like' to '[Zn(ZQA)] like' observed in the spectra. The more '[Zn(ZQA)] like' the spectrum, the greater the absorbance near 360 nm and the closer to 355 nm Curve 3 is fitted to take this into account. Some spectra could not be fitted for the higher wavelength Gaussian curves due to low absorbance in this region.

The similarity of the shape of the [Zn(ZQA)], $[Zn(ZQA)_2]^{2-}$ and [Zn(tacdo)ZQA] spectra, as well as the similarity of the $[ZQA.H]^-$ and $[Zn(NTA)ZQA.H]^{2-}$ spectra, are evident upon comparing the wavelengths and relative intensities of the Gaussian curves fitted to the relevant spectra in Table 4.12.

The fact that the wavelengths of the component Gaussian curves remain relatively constant upon changing the ligand in the ternary complex, tends to suggest that upon coordinating to Zn^{2+} that is already bound by a ligand, the relative energies of the ground electronic state, and the vibrational levels of the excited electronic state, remain relatively unchanged. This supports the similar results obtained for the fluorescence spectra shown above. However, these absorption results vary from the fluorescence results in the fact that the relative intensities of the component Gaussian curves, and therefore transition dipole moments of the transitions involved, seem to vary with a change in ternary complex. This is undoubtedly due to the poor quality of fitting in this case and the complicated nature of molecular absorption spectra arising from the presence of low energy excited electronic states which contribute to the spectrum observed in some cases. These extra electronic levels, however, often do not contribute to the observed fluorescence spectra. A significant change in the relative positions of the potential energy curves involved in an electronic transition would be expected to change which Gaussian curve would have the maximum intensity, as in Figure A.3. Thus, the fact that the same Gaussian curve, Curve 3, has the maximum intensity in the majority of the absorption spectra studied supports the fluorescence results as it suggests that there is no shift in the relative positions of the ground and excited state potential energy curves.

Although the true nature of the transitions in the observed molar absorbance spectra can not be identified, the highest wavelength, and therefore lowest energy, Gaussian curve, Curve 6, is most likely the (0,0) transition from the ground vibrational level of the ground electronic state to the ground vibrational level of the excited electronic state because it is coincident with the lowest wavelength, and therefore highest energy, Gaussian curve, Curve 1, fitted to the fluorescence spectra. The wavelength of this transition should correspond to the energy difference, a), in Figure 4.20 above. An approximate value for this energy difference is 4.6×10^{-19} Joules, obtained from the average wavelength for this transition in both forms of spectra, 430.8 ± 6.3 nm. The fact that approximately the same wavelength, and therefore energy, was obtained for the (0,0) transition in both the excitation and emission spectra implies that the ground and excited states of each complex exist in a similar solvation environment and little, if any, relaxation of the excited state takes place due to solvent rearrangement.

In conclusion, it is plain that the environment imposed about a Zn^{2+} by the ligands in the ternary complexes studied, does affect the amount of fluorescence or absorbance observed. It is therefore reasonable to assume that in a biological cell, the fluorescence observed due to Zinquin-A is not directly proportional to the amount of Zn^{2+} present. It is also possible that there may be environments in the cell that cause a total quenching of the fluorescence due to Zinquin-A bound to Zn^{2+}.

4.5 : Preliminary Force Field Molecular Modelling of the Ternary Complexes, [Zn(L)ZQA]

In order to determine whether a correlation exists between the fluorescence intensities observed and the structures of the [Zn(L)ZQA] complexes, force field molecular modelling was attempted using the package, INSIGHT II in conjunction with the minimisation package, DISCOVER 3, using the extended systematic force field, ESFF, as described in Section 5.5. Force field modelling is different to *ab initio* or semi-empirical molecular modelling because it does not deal with separate wave equations for each electron. Rather, it approximates the forces within a molecule by considering the forces between the atoms in that molecule. An example of a simple force field would define the steric energy of the molecule as the sum of all individual bond-stretching, angle-bending, bond torsion and van der Waals interactions,

with the optimum geometry exhibiting the lowest steric energy. Terms to describe other interactions, such as hydrogen bonding and electrostatic interactions, can also be included. The advantage of this method is that relatively rapid molecular modelling becomes possible for very large molecules for which the more complex *ab initio* modelling is not practical due to the large amount of time and computing power required. The complexes studied here are not overly large, and it is possible to use *ab initio* methods such as Gaussian 94 to minimise their structures, however, due to time and resource constraints, it was necessary to use the much more rapid force field method. This resulted in the added advantage of being able to use a greater number of starting points in the available time to give a greater chance of finding a global minimum rather than a local one. At least 15 starting points, with variations mainly in the positioning of the toluene and acid group of Zinquin-A, were used for each ternary complex studied. The structures of the $[Zn(L)(H_2O)_n]^{2+}$ complexes of the ligands in Figure 4.1 were minimised first and the lowest energy ligand (L) conformation obtained was used for all starting points in the ternary minimisation. It is important to keep in mind that these do not represent the best possible conditions. To have higher confidence in the results obtained, many more starting points including changes in the ligand (L) conformation would be preferable as it is possible that Zinquin-A could force conformations on the other ligand (L) which differ from those in $[Zn(L)(H_2O)_n]^{2+}$, leading to a change in the lowest energy conformation for the ternary complex. The minimisation process was found to be very dependant upon starting point, with most different starting points giving a minimised structure characterised by a different energy. The structure with the lowest energy was accepted as the best approximation of the global minimum in each case. As changing the potential parameter of an atom can change the minimised energy obtained with little change in structure, care was taken to ensure the same set of potential parameters was used for all starting points of the same complex.

The complexes studied in addition to $[Zn(L)(H_2O)_n]^{2+}$ for the ligands (L) in Figure 4.1 are listed in Table 4.14 along with the lowest total steric energy determined for each ternary complex. All of the ternary complexes studied showed distorted octahedral coordination geometry about the central Zn^{2+}, with the toluene moiety of the Zinquin-A dianion bent up towards the quinoline moiety. The quinoline moiety was slightly distorted from planar in all minimised structures. Where partially positive protons were present on the ligand (L = cyclen, cyclam, tacn, tacdo, tren, TEA), hydrogen bonding between them and the carboxylic acid group of Zinquin-A was observed, increasing the amount of twist in the quinoline moiety.

Hydrogen bonding was also observed between the oxygens of the sulphonamide group and these partially positive protons. Examples of minimised structures are shown for [Zn(tacdo)ZQA(H_2O)] and [Zn(cyclen)ZQA] in Figures 4.23 and 4.24 respectively, where two views which are perpendicular to each other are shown for each complex. The octahedral complex of [Zn(ZQA)(H_2O)$_4$] was also studied, with similar results to those discussed above.

Complex	Steric Energy (kcal mol^{-1})	Complex	Steric Energy (kcal mol^{-1})
[Zn(cyclam)ZQA]	-15.92	[Zn(TEA)ZQA.H$_{-1}$]$^{-}$	-65.07
[Zn(cyclen)ZQA]	-8.11	[Zn(TEA)ZQA.H$_{-2}$]$^{2-}$	+33.48
[Zn(NTA)ZQA]$^{3-}$	-90.90	[Zn(tacn)ZQA(H_2O)]	-143.59
[Zn(NTA)ZQA.H]$^{2-}$	-343.36	[Zn(tacdo)ZQA(H_2O)]	-151.33
[Zn(tren)ZQA]	-102.93	[Zn(tacdo)ZQA(H_2O)H]$^{+}$	-266.88
[Zn(TEA)ZQA]	-130.56	[Zn(ZQA)(H_2O)$_4$]	-648.44

Table 4.14 : The ternary complexes studied using force field molecular modelling and the total steric energy, in kcal mol^{-1}, for the lowest energy structure of each.

Unfortunately, no correlation between structural parameters and observed fluorescence intensity was found. Parameters measured included those that describe the Zn^{2+} coordination geometry (D-Zn^{2+}-D angles and Zn^{2+}-D bond lengths where D represents donor atoms), the extent of electron delocalisation (the angle between the approximate planes of the two rings in the quinoline moiety and the sulphonamide nitrogen-quinoline ring bond length), the location of the toluene moiety relative to the quinoline moiety (the torsion angle about the sulphonamide sulphur-toluene bond, the distance of the center of the toluene ring from the center of each ring in the quinoline moiety and the angle made by the three ring centers) and the extent of hydrogen bonding of the sulphonamide group and carboxylic acid moieties of Zinquin-A to the ligand (L). These results indicated that the fluorescence intensity was not dependent upon any single parameter examined. It is sensible to assume that several different influences, working in either a positive or negative way, combine to produce the fluorescence intensity observed, and it is therefore unsurprising that no correlation with a single influence could be found. There is also the additional complication that this type of molecular modelling representing the gaseous state, rather than the solution state, and the complexes may adopt different conformations in either state.

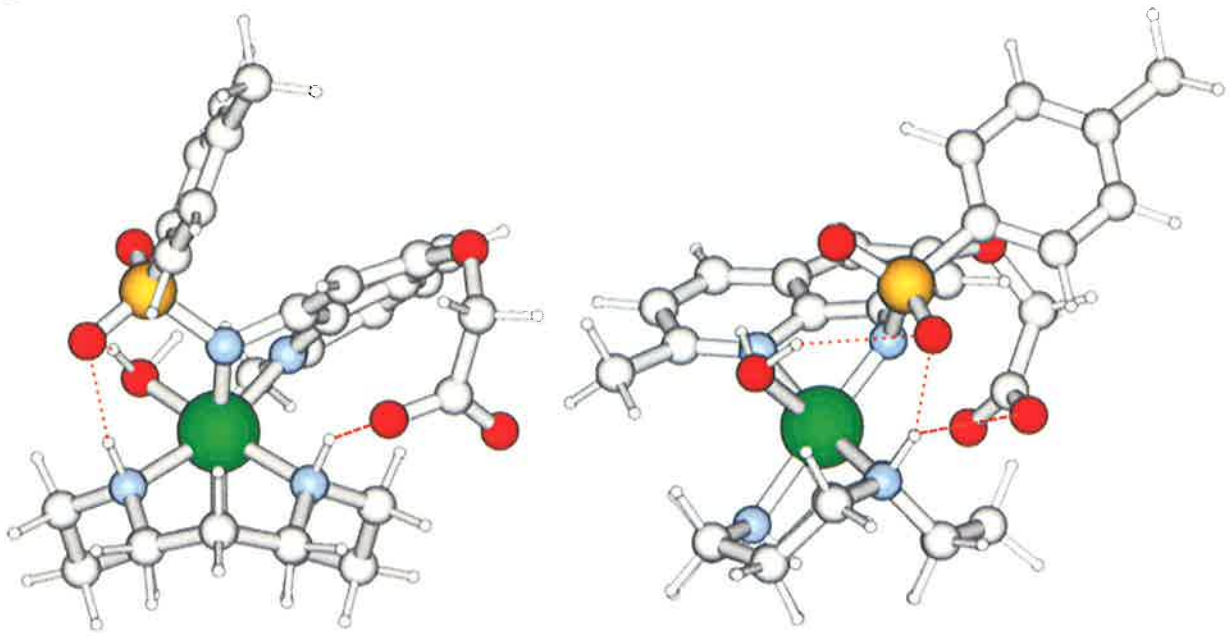

Figure 4.23 : The DISCOVER 3 minimised structure of [Zn(tacdo)ZQA(H_2O)]. The right view is equivalent to the left view rotated to the right by 90 degrees. Due to the symmetry in the tacdo ligand, some of its atoms are not visible. Hydrogen bonding is indicated by red dashed lines, the Zn^{2+} is green and the carbon, oxygen, nitrogen, sulphur and hydrogen atoms are shown in grey, red, blue, yellow and white, respectively.

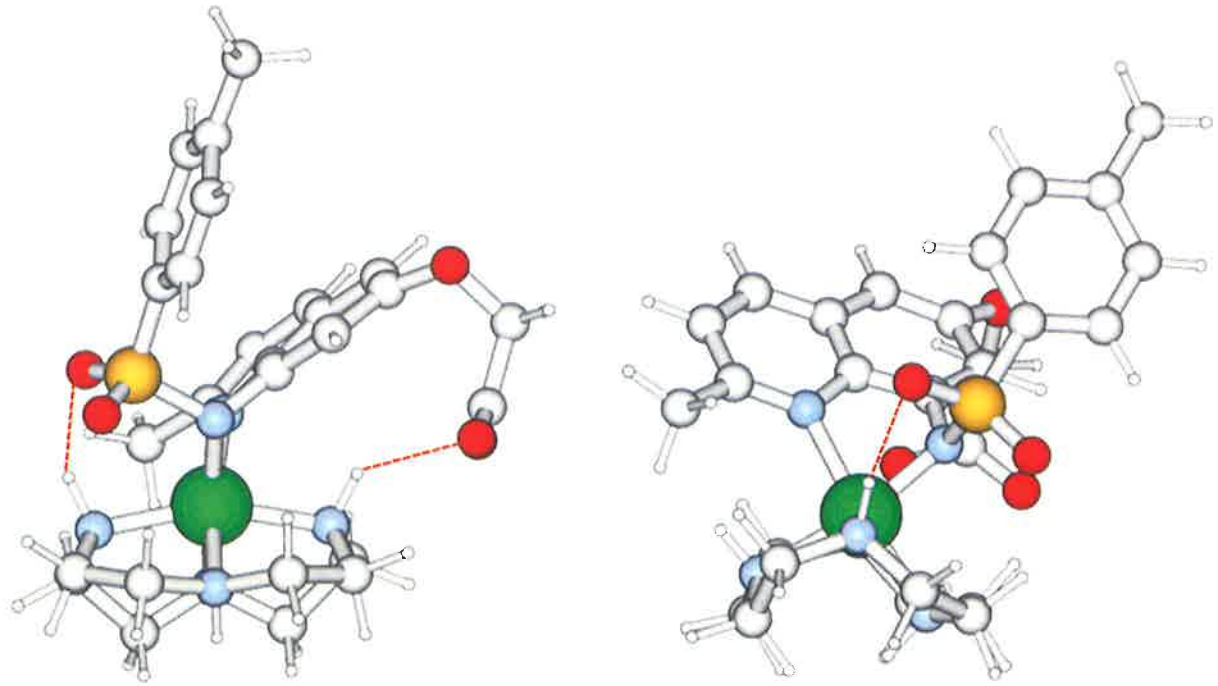

Figure 4.24 : The DISCOVER 3 minimised structure of [Zn(cyclen)ZQA]. The right view is equivalent to the left view rotated to the right by 90 degrees. Due to the symmetry in the cyclen ligand, some of its atoms are not visible. Hydrogen bonding is indicated by red dashed lines, the Zn^{2+} is green and the carbon, oxygen, nitrogen, sulphur and hydrogen atoms are shown in grey, red, blue, yellow and white, respectively.

4.6 : The Fluorescence of Zinquin-A with Carbonic Anhydrase

After modelling the environment about a Zn^{2+} that Zinquin-A could be bound to in a cell using convenient ligands, such as those in Figure 4.1, the next step is to use a Zn^{2+} containing bioinorganic molecule that is known to be found in cells. An ideal choice of bioinorganic molecule for this purpose would;

(a) be well characterised, preferably by X-Ray diffraction
(b) contain Zn^{2+} in a site accessible to Zinquin-A
(c) be commercially available at a reasonable cost

The zinc(II) metalloenzyme, carbonic anhydrase meets all of the above criteria to varying degrees. As discussed in Section 1.1.1, the carbonic anhydrase active site is well characterised and a crystal structure has been determined, indicating that the active site Zn^{2+} is bound by three histidyl residues at the base of a deep crevice in the protein structure.[17] A water or hydroxide ion is also bound to the Zn^{2+} which is in a distorted tetrahedral geometry and other water molecules are thought to be present in the active site area. Studies have shown that sulphonamides are able to coordinate to the Zn^{2+} in the active site and therefore inhibit the activity of carbonic anhydrase and displace the active site waters.[66-69] This suggests that Zinquin-A may also be able to access the Zn^{2+} due to its sulphonamide functional group. Finally, carbonic anhydrase is commercially available. Hence, carbonic anhydrase was chosen as the metalloenzyme used in this preliminary study of Zinquin-A-enzyme complexes.

Due to the low solubility of carbonic anhydrase in 50% aqueous ethanol, and the low solubility of Zinquin-A in water, it was necessary to use an aqueous solution of the enzyme in 0.1 mol dm^{-3} NaPIPES buffer at pH 6.6 to which was added a small amount of Zinquin-A in 50% aqueous ethanol, pH 6.6 (0.1 mol dm^{-3} NaPIPES), giving 95% aqueous ethanol after mixing as described in Section 5.4.4. This resulted in a sufficiently low Zinquin-A concentration to allow solubility in such a high percentage of water. It was also necessary to exclude all CO_2 from the samples to prevent the carbonic anhydrase from catalysing its hydration and producing acid (see Section 1.1.1) which would alter the pH of the solution and perhaps exceed the capability of the buffer. This was achieved by boiling the water and ethanol used before making up any solutions and working under a constant flow of nitrogen. As an added precaution, samples were measured as soon as practical after preparation.

The fluorescence spectrum obtained at 298.2 K for the carbonic anhydrase and Zinquin-A sample is compared with the spectra obtained under the same conditions for $Zn(ClO_4)_2$ and Zinquin-A, and Zinquin-A alone as shown in Figure 4.25 below. The wavelengths and intensities for the maxima are listed in Table 4.15. An excitation wavelength of 358 nm, slit widths of 2.5 nm and averages of four spectra were used for each solution measured.

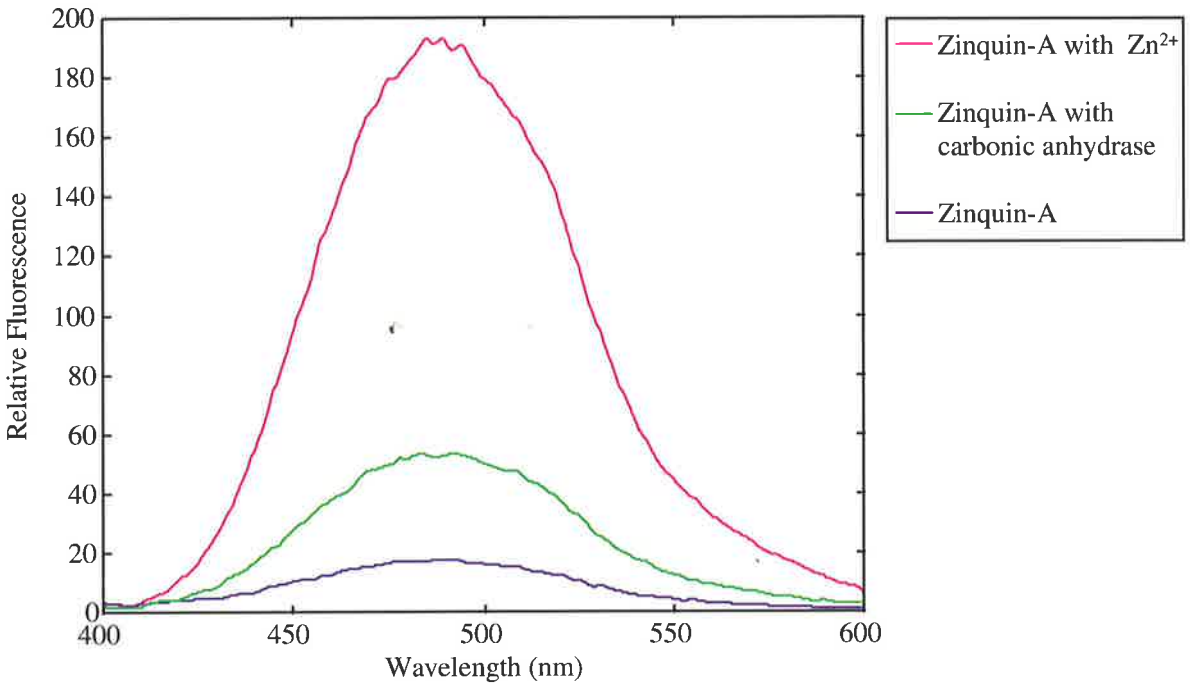

Figure 4.25 : Fluorescence spectra obtained in 95% aqueous ethanol for Zinquin-A (9.63×10^{-5} mol dm^{-3}); alone, with carbonic anhydrase (9.143×10^{-6} mol dm^{-3}), and with $Zn(ClO_4)_2$ (9.02×10^{-6} mol dm^{-3}). All solutions also contained 0.1 mol dm^{-3} NaPIPES at pH 6.6. T = 298.2 K, slits = 2.5 nm, Ex λ = 358 nm.

Solution	Wavelength (nm)	Intensity
Zinquin-A	490	17.7
Zinquin-A with carbonic anhydrase	490	53.4
Zinquin-A with Zn^{2+}	490	193

Table 4.15 : The fluorescence maxima observed for the spectra shown in Figure 4.25.

The low level of fluorescence in the Zinquin-A alone spectrum in Figure 4.25 is due to adventitious Zn^{2+} present in the buffer (see Section 2.2). The concentration of this adventitious Zn^{2+} could not be determined in the same way used previously (Sections 2.2.1 to 2.2.3) as no stability constants are known in this solvent system. The value can be approximated, however, if it is assumed that all the Zn^{2+} present in the Zinquin-A alone sample and Zinquin-A with Zn^{2+} sample is present as $[Zn(ZQA)_2]^{2-}$. This assumption is reasonable as the Zinquin-A is at least ten times the concentration of the Zn^{2+} in these solutions. As fluorescence is proportional to the concentration of the fluorescing species, $[Zn(ZQA)_2]^{2-}$ in this case, the ratio of fluorescence observed should be equal to the ratio of concentrations of $[Zn(ZQA)_2]^{2-}$ in the solutions measured, as in Equation 4.29.

$$\frac{fl(Zinquin - A)}{fl(Zinquin - A + Zn^{2+})} = \frac{[Zn(ZQA)_2^{2-}]'}{[Zn(ZQA)_2^{2-}]''} \tag{4.29}$$

Where fl(Zinquin-A) is the maximum fluorescence of the Zinquin-A alone spectrum,

fl(Zinquin-A + Zn^{2+}) is the maximum fluorescence of the Zinquin-A with Zn^{2+} spectrum,

$[Zn(ZQA)_2^{2-}]'$ is the concentration of $[Zn(ZQA)_2]^{2-}$ producing fl(Zinquin-A),

$[Zn(ZQA)_2^{2-}]''$ is the concentration of $[Zn(ZQA)_2]^{2-}$ producing fl(Zinquin-A + Zn^{2+}),

Assuming all the Zn^{2+} present is bound as $[Zn(ZQA)_2]^{2-}$;

$$[Zn(ZQA)_2^{2-}]' = [Adv\ Zn^{2+}] \tag{4.30}$$

and

$$[Zn(ZQA)_2^{2-}]'' = [Adv\ Zn^{2+}] + [Added\ Zn^{2+}] \tag{4.31}$$

Where $[Adv\ Zn^{2+}]$ is the concentration of adventitious Zn^{2+} present in all solutions,

$[Added\ Zn^{2+}]$ is the concentration of added Zn^{2+} in the Zinquin-A with Zn^{2+} solution.

so;

$$\frac{fl(Zinquin - A)}{fl(Zinquin - A + Zn^{2+})} = \frac{[Adv\ Zn^{2+}]}{[Adv\ Zn^{2+}] + [Added\ Zn^{2+}]} \tag{4.32}$$

and by rearranging;

$$[\text{Adv } Zn^{2+}] = \frac{\text{fl(Zinquin - A)} \times [\text{Added } Zn^{2+}]}{\text{fl(Zinquin - A + } Zn^{2+}\text{)} - \text{fl(Zinquin - A)}} \qquad (4.33)$$

Substituting in the values for maximum fluorescence given in Table 4.15 with a concentration of 9.02×10^{-6} mol dm^{-3} for the added Zn^{2+}, a value of 9.11×10^{-7} mol dm^{-3} is obtained for the concentration of adventitious Zn^{2+} present. Bearing in mind the assumptions involved in this method, the value obtained is in good agreement with the value of 8.41×10^{-7} mol dm^{-3} obtained for 0.1 mol dm^{-3} NaPIPES in 50% aqueous ethanol (Section 2.2.3).

No attempt was made to remove the adventitious Zn^{2+} in this case, however, as the amount originating from the buffer should be constant for all three spectra shown above and it is the change in fluorescence upon adding carbonic anhydrase that is of interest. From the preliminary results in Figure 4.25 above, it appears that the Zinquin-A anion is coordinating to the Zn^{2+} in the carbonic anhydrase as a greater fluorescence is observed for the spectrum containing both Zinquin-A and carbonic anhydrase as compared with the spectrum containing Zinquin-A alone. If the Zinquin-A was able to remove all of the Zn^{2+} from the active site of carbonic anhydrase, forming [Zn(ZQA)] or $[Zn(ZQA)_2]^{2-}$, it could be expected the spectrum observed would be similar to that obtained by replacing carbonic anhydrase with $Zn(ClO_4)_2$ at the same concentration. As can be seen from Figure 4.25, this is not the case as the spectrum of Zinquin-A with Zn^{2+} is much higher in intensity than the spectrum of Zinquin-A with carbonic anhydrase. It therefore appears that Zinquin-A is coordinating to the Zn^{2+} in carbonic anhydrase, forming a Zinquin-A-enzyme complex with a lower fluorescence than observed for $[Zn(ZQA)_2]^{2-}$ which, although stability constants are not known in this solvent system, should be the predominant Zinquin-A complex in the Zinquin-A with Zn^{2+} spectrum as mentioned previously. Such a decrease in fluorescence could be expected due to the considerably large size of the enzyme which would have more modes of relaxation, and therefore greater quenching, than the simpler [Zn(ZQA)] and $[Zn(ZQA)_2]^{2-}$ complexes.

So, in summary, the above preliminary results suggest that Zinquin-A is able to coordinate to carbonic anhydrase, forming a ternary complex with a lower fluorescence intensity than $[Zn(ZQA)_2]^{2-}$. This would indicate that Zinquin-A can coordinate to already bound Zn^{2+} in the cell, and that the fluorescence observed in such a case is different from that observed when Zinquin-A is bound to Zn^{2+} alone.

However, there are other possible interpretations of the preliminary results in Figure 4.25. The fact that an increase in fluorescence is observed upon adding carbonic anhydrase to Zinquin-A can also be interpreted as an increase in adventitious Zn^{2+} present in the sample. This would also occur if the solid carbonic anhydrase contained additional Zn^{2+} to that already present in the active site. Similarly, the observation that the fluorescence of Zinquin-A with carbonic anhydrase is lower than that of Zinquin-A with Zn^{2+} can have the alternative inference that Zinquin-A removes some of the Zn^{2+} in the active site of carbonic anhydrase, forming a small amount of $[Zn(ZQA)_2]^{2-}$ which results in the spectrum observed, with the remaining Zinquin-A either unattached to any Zn^{2+} or bound in a non-fluorescent Zinquin-A-enzyme complex. Another possibility is that the Zinquin-A-enzyme complex is of low stability and therefore only forms to a small extent. In this case, the fluorescence of the Zinquin-A-enzyme complex would be somewhat larger once it has been adjusted for concentration, and may even be greater than that observed for $[Zn(ZQA)_2]^{2-}$.

It is also somewhat uncertain that the Zinquin-A anion can enter the active site of carbonic anhydrase. Although, as stated previously, sulphonamides, such as sulphanilamide (Figure 4.26), have been shown to inhibit carbonic anhydrase activity and are therefore likely to be included in the active site region, sulphonamides such as sulphapyridine and sulphathiazole (Figure 4.26) that are substituted at the sulphonamide nitrogen do not act as inhibitors and therefore may not enter the active site.[66] As Zinquin-A is closer in structure to the substituted sulphonamides, it is possible that it too may not be readily included in the active site.

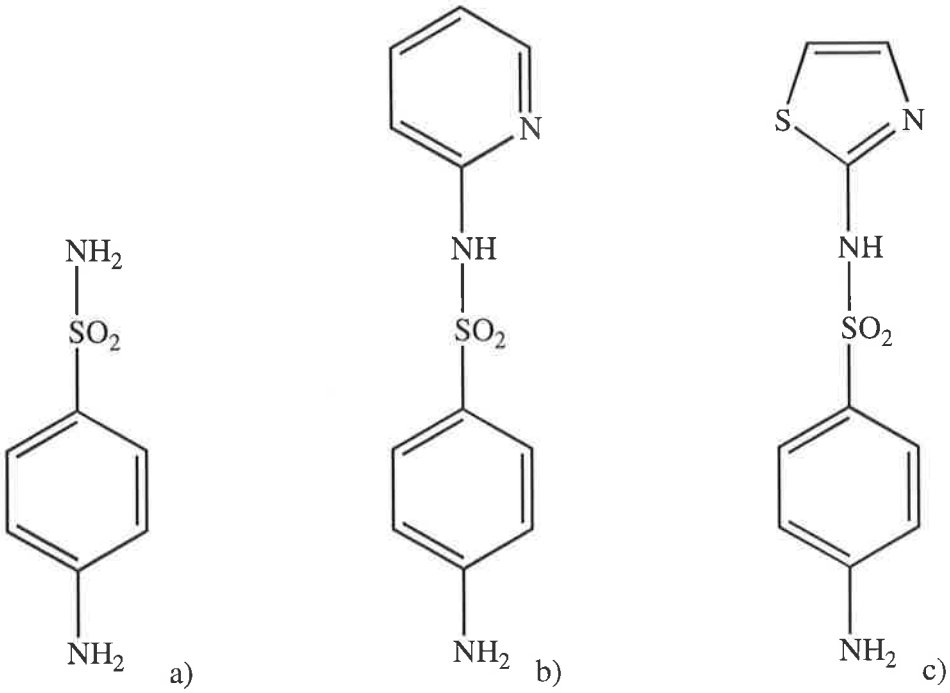

Figure 4.26 : A carbonic anhydrase inhibitor, a) sulphanilamide (*p*-aminobenzene-sulphonamide) and two *N*-substituted sulphonamides that do not show carbonic anhydrase inhibition. b) sulphapyridine (4-amino-*N*-(2-pyridyl)benzene-sulphonamide) and c) sulphathiazole (4-amino-*N*-(2-thiazolyl)benzene-sulphonamide).[66]

Hence, the results presented here are not fully conclusive that a Zinquin-A-enzyme complex is formed with carbonic anhydrase or fully conclusive that the fluorescence for Zinquin-A with carbonic anhydrase in Figure 4.25 can be attributed to such a complex. Further study of this matter, such as that suggested in Section 6.1, is required to arrive at a firm conclusion.

4.7 : References

1. K. E. Koike, *Chem. Soc. Rev.*, **27 (3)**, 179, 1998.

2. J. W. Kleineke and I. A. Brand, *J. Pharmacol. Toxicol. Methods*, **38 (4)**, 181, 1997.

3. K. M. Hendrickson, T. Rodopoulos, P. A. Pittet, I. Mahadevan, S. F. Lincoln, A. D. Ward, T. Kurucsev, P. A. Duckworth, I. J. Forbes, P. D. Zalewski and W. H. Betts, *J. Chem. Soc., Dalton Trans.*, 3879, 1997.

4. N. Wellinghausen, M. Martin and L. Rink, *Eur. J. Immunol.*, **27 (10)**, 2529, 1997.

5. M. Tsuda, K. Imaizumi, T. Katayama, K. Kitagawa, A. Wanaka, M. Tohyama, T. Takagi, *J. Neurosci.*, **17 (17)**, 6678, 1997.

6. D. Berendji, V. Kolbbachofen, K. L. Meyer, O. Grapenthin, H. Weber, V. Wahn and K. D. Kroncke, *FEBS Lett.*, **405 (1)**, 37, 1997.

7. P. D. Zalewski, X. Jian, L. L. L. Soon, W. G. Breed, R. F. Seamark, S. F. Lincoln, A. D. Ward and F. Z. Sun, *Reprod. Fertil. Dev.*, **8 (7)**, 1097, 1996.

8. N. Wellinghausen, A. Fischer, H. Kirchner and L. Rink, *Cell. Immunol.*, **171 (2)**, 255, 1996.

9. I. B. Mahadevan, M. C. Kimber, S. F. Lincoln, E. R. T. Tiekink, A. D. Ward, W. H. Betts, I. J. Forbes and P. D. Zalewski, *Aus. J. Chem.*, **49 (5)**, 561, 1996.

10. R. D. Palmiter, T. B. Cole and S. D. Findley, *EMBO J.*, **15 (8)**, 1784, 1996.

11. I. A. Brand and J. Kleineke, *J. Biol. Chem.*, **271 (4)**, 1941, 1996.

12. P. D. Zalewski, I. J. Forbes R. F. Seamark, R. Borlinghaus, W. H. Betts, S. F. Lincoln and A. D. Ward, *Chem. Biol.*, **1**, 153, 1994.

13. P. D. Zalewski, S. H. Millard, I. J. Forbes, O. Kapaniris, A. Slavotinek, W. H. Betts, A. D. Ward, S. F. Lincoln and I. Mahadevan, *J. Histochem. Cytochem.*, **42 (7)**, 877, 1994.

14. P. Coyle, P. D. Zalewski, J. C. Philcox, I. J. Forbes, A. D. Ward, S. F. Lincoln, I. Mahadevan and A. M. Rofe, *Biochem. J.*, **303**, 781, 1994.

15. P. D. Zalewski, I. J. Forbes and W. H. Betts, *Biochem. J.*, **296 (2)**, 403, 1993.

16. W. J. Bettger and B. L. O'Dell, *Life Sci.*, **28**, 1425, 1981.

17. A. Liljas, K. K. Kannan, P.-C. Bergstén, I. Waara, K. Fridborg, B. Strandberg, U. Carlbom, L. Järup, S. Lövgren and M. Petef, *Nature New Biology*, **235**, 131, 1972.

18. D. N. Silverman and S. Lindskog, *Acc. Chem. Res.*, **21**, 30, 1988.

19. A. E. Eriksson, T. A. Jones and A. Liljas, *Proteins*, **4**, 274, 1988.

20. Y. Pocker in "*Metal Ions in Biological Systems*", H. Sigel, *Ed.*, **25**, Marcel Deckker, New York, 1989.

21. H. Eklund, A. Jones and G. Schneider in "Zinc Enzymes", I. Bertini, C. Luchinat, M. Maret and M. Zeppezauer, *Eds.*, Birkhäuser, Boston, MA, 1986.

22. C. F. Springgate, A. S. Mildvan, R. Abrahamson and J. L. Engle, *J. Biol. Chem.*, **248**, 5987, 1973.

23. F. Y-H. Wu in "*Zinc Enzymes*", I. Bertini, C. Luchinat, M. Maret and M. Zeppezauer, *Eds.*, Birkhäuser, Boston, MA, 1986.

24. E. E. Kim and H. W. Wyckoff, *J. Mol. Biol.*, **218**, 449, 1991.

25. J. E. Butler-Ransohoff, D. A. Kendall and E. T. Kaiser in "*Metal Ions in Biological Systems*", H. Sigel, *Ed.*, **25**, Marcel Deckker, New York, 1989.

26. D. W. Christianson and W. N. Lipscomb, *Acc. Chem. Res.*, **22**, 62, 1989.

27. S. Mangani and P. Orioli, *Inorg. Chem.*, **31**, 365, 1992.

28. D. S. Auld, J. F. Riordan and B. L. Vallee in "*Metal Ions in Biological Systems*", H. Sigel, *Ed.*, **Vol. 25**, Marcel Deckker, New York, 1989.

29. S. K. Burley, P. R. David, A. Taylor and W. N. Lipscomb, *Proc. Natl. Acad. Sci. USA*, **87**, 6878, 1990.

30. K. H. Röhm in "*Zinc Enzymes*", I. Bertini, C. Luchinat, M. Maret and M. Zeppezauer, *Eds.*, Birkhäuser, Boston, MA, 1986.

31. B. W. Matthews, J. N. Jansonius, P. M. Colman, B. P. Schoenborn and D. Dupourque, *Nature New Biology*, **238**, 37, 1972.

32. B. W. Matthews, *Acc. Chem. Res.*, **21**, 33, 1988.

33. A. Fontana, G. Fassina, C. Vita, D. Dalzoppo, M. Zamai and M. Zambonin in "*Zinc Enzymes*", I. Bertini, C. Luchinat, M. Maret and M. Zeppezauer, *Eds.*, Birkhäuser, Boston, MA, 1986.

34. R. B. Davies and E. P. Abraham, *Biochem. J.*, **143**, 129, 1974.

35. B. L. Vallee, J. E. Coleman and D. S. Auld, *Proc. Natl. Acad. Sci. USA*, **88**, 999, 1991.

36. H. Takatsuji, *Cellular & Molecular Life Sciences*, **54 (6),** 582, 1998.

37. R. J. P. Williams, *Endeavour (New Ser.)*, **8**, 65, 1984.

38. R. D. Palmiter, *Toxicol. Appl. Pharmacol.*, **135**, 139, 1995.

39. M. Ebadi, P. L. Iversen, R. Hao, D. R. Cerutis, P. Rojas, H. K. Happe, L. C. Murrin and R. F. Pfeiffer, *Neurochem. Int.*, **27**, 1, 1995.

40. S. Saito and Y. Kojima, *Res. Comm. in Molec. Pathol. Pharmacol.*, **89**, 365, 1995.

41. H-P. Roth and M. Kirrchgessner, *Biol. Trace Elem. Res.*, **3**, 13, 1981.

42. E. Kimura and T. Koike, *Comm. Inorg. Chem.*, **11**, 285, 1991.

43. E. Kimura, *Prog. Inorg. Chem.*, **41**, 443, 1994.

44. T. Koike, S. Kajitani, I. Nakamura and M. Shiro, *J. Am. Chem. Soc.*, **117**, 1210, 1995.

45. E. Kimura, Y. Kodama, T. Koike and M. Shiro, *J. Am. Chem. Soc.*, **117**, 8304, 1995.

46. E. Kimura, I. Nakamura, T. Koike M. Shionoya, Y. Kodama, T. Ikeda and M. Shiro, *J. Am. Chem. Soc.*, **116**, 4764, 1994.

47. E. Kimura, H. Hashimoto and T. Koike, *J. Am. Chem. Soc.*, **118**, 10963, 1996.

48. E. Kimura and M. Shionoya in "*Transition Metals in Supramolecular Chemistry*", L. Fabbrizzi and A. Poggi, *Eds.*, Kluwer Academic Publishers, London, 1994.

49. T. Koike, M. Takamura and E. Kimura, *J. Am. Chem. Soc.*, **116**, 8443, 1994.

50. T. Koike and E. Kimura, *J. Am. Chem. Soc*, **113**, 8935, 1991.

51. E. Kimura, T. Shiota, T. Koike, M. Shiro and M. Kodama, *J. Am. Chem. Soc.*, **112**, 5805, 1990.

52. M. Shionoya, E. Kimura and M. Shiro, *J. Am. Chem. Soc.*, **115**, 6730, 1993.

53. M. Shionoya, T. Ikeda, E. Kimura and M. Shiro, *J. Am. Chem. Soc.*, **116**, 38489, 1994.

54. M. Shionoya, E. Kimura, H. Hayashida, G. Petho and L. G. Marzilli, *Adv. Supramol. Chem.*, **2**, 173, 1993.

55. M. Shionoya, M. Sugiyama and E. Kimura, *J. Chem. Soc., Chem. Commun.*, 147, 1994.

56. R. M. Smith and A. E. Martell, "*Critical Stability Constants*", Plenum Press, New York, **2**, 1975.

57. R. M. Smith and A. E. Martell, "*Critical Stability Constants*", Plenum Press, New York, **1**, 1975.

58. L. J. Zompa, *Inorg. Chem.*, **17**, 2531, 1978.

59. P. Gans, A. Sabatini and A. Vacca, *J. Chem. Soc., Dalton Trans.*, 1195, 1985.

60. R. M. Smith and A. E. Martell, "*Critical Stability Constants*", Plenum Press, New York, **5**, 1975.

61. V. J. Thöm, G. D. Hosken and R. D. Hancock, *Inorg. Chem.*, **24**, 3378, 1985.

62. M. Kato, T. Ito, *Inorg. Chem.*, **24**, 509, 1985.

63. A Macintosh version (P. A. Duckworth) of the Fortran program SPE, A. E. Martell and R. J. Motekaitis, "*Determination and use of Stability constants*", Appendix III, VCH, 1990.

64. A MATLAB program, T. Kurucsev, University of Adelaide, South Australia, Australia. Refer to Appendix E.

65. M. A. Snoswell and T. Kurucsev, *J. Cryst. and Spec. Res.*, **22**, 679, 1992.

66. T. Mann and D. Keilin, *Nature*, **146**, 164, 1940.

67. J. McD. Armstrong, D. V. Myers, J. A. Verpoorte and J. T. Edsall, *J. Biol. Chem.*, **241**, 5137, 1966.

68. K. Hakansson and A. Liljas, *FEBS Lett.*, **350 (2-3)**, 319, 1994.

69. C. T. Supuran and M. D. Banciu, *Revue Roumaine de Chimie*, **36**, 1345, 1991.

70. J. F. Desreux, E. Merciny, N. F. Loucin, *Inorg. Chem.*, **20**, 987, 1981.

71. M. Micheloni, A. Sabatini, P. Paolett, *J. Chem. Soc., Perkin Trans.*, **2**, 828, 1978.

72. R. Yang and L. J. Zompa, *Inorg. Chem.*, **15 (7)**, 1500, 1976.

73. J. J. Christensen, R. M. Izatt, D. P. Wrathall and L. D. Hansen, *J. Chem. Soc. (A)*, 1212, 1969.

74. M. Kodama, E. J. Kimura, *J. Chem. Soc., Dalton Trans.*, 2269, 1977.

75. T. Arishima, K. Hamada and S. Takamoto, *Nippon Kagaku Kaishi*, 1119, 1973.

76. J. H. Coates, G. J. Gentle and S. F. Lincoln, *Nature*, **249 (5459)**, 773, 1974.

CHAPTER 5

EXPERIMENTAL

5.1 : Properties of Free and Zinc(II) Bound Zinquin-A in 25% and 50% Aqueous Ethanol

5.1.1 : Materials

Zinquin-A (2-methyl-8-*p*-toluenesulphonamido-6-quinolyloxyacetic acid, ZQA.H_2),[1] NaOH (ConvoL, BDH), perchloric acid (70% in water, Ajax), ethylenediaminetetraacetic acid disodium salt (Na_2EDTA.H_2, Ajax) and sodium piperazine-*N*,*N*′-bis(2-ethane-sulphonate) buffer (NaPIPES, Calbiochem) were used as received. Potassium hydrogen phthalate (KHphthalate, BDH), $NaClO_4$ (Fluka) and $Zn(ClO_4)_2$ (Fluka) were used as received after drying under vacuum to constant weight and then stored over P_2O_5 in an evacuated desiccator. An aqueous $Zn(ClO_4)_2$ solution was standardised in triplicate using a cation exchange column, and this was used to prepare all Zn^{2+} containing solutions. Deionised water was ultrapurified with a Milli-Q Reagent system to produce water with a specific resistance of > 15 MΩ cm and boiled to remove any CO_2. Analytical grade ethanol (BDH) was further purified by distillation. HTL micropipettes were used for all volume measurements under 2 cm^3.

5.1.2 : Adventitious Zinc(II)

At the concentration levels used in this study, the levels of contaminant, or adventitious, Zn^{2+} (Adv. Zn^{2+}) present, even in analytical grade chemicals, generates a significant background fluorescence which must be determined (see Section 2.2). The methods used to determine the adventitious Zn^{2+} concentrations in various solvent systems are described below (Sections 5.1.2.1 to 5.1.2.3).

5.1.2.1 : EDTA Fluorescence Titration

The fluorescence of six solutions containing 0.000, 0.204, 0.408, 0.613, 0.817 or 1.02×10^{-6} mol dm^{-3} EDTA and either 5.18×10^{-6} mol dm^{-3} Zinquin-A, 0.10 mol dm^{-3} $NaClO_4$, 1.00×10^{-3} mol dm^{-3} NaPIPES buffer in 25% aqueous ethanol or 5.44×10^{-6} mol dm^{-3} Zinquin-A, 0.10 mol dm^{-3} NaPIPES buffer in 50% aqueous ethanol at pH 6.6 were measured using a Perkin Elmer LS50-B Luminescence Spectrophotometer. An excitation wavelength of 358 nm was used to measure the emission spectra, as an average of two scans, between 400 and 600 nm. Excitation and emission slit widths of 5 nm and a scan rate of 240 nm min^{-1} were used. Solutions were pre-equilibrated to 298.2 ± 0.1 K and maintained at this temperature during measurement in a 1 cm quartz cuvette by means of a thermostatted block. Fluorescence due to buffer alone was measured and subtracted from each spectrum. The maximum fluorescence for each spectrum was plotted against EDTA concentration giving an x-intercept equal to the minimum amount of EDTA required to complex all the adventitious Zn^{2+} and therefore its concentration.

5.1.2.2 : Zinquin-A Ultraviolet-Visible Titration

The ultraviolet-visible spectra of solutions containing 7.25×10^{-5}, 8.29×10^{-5}, 9.33×10^{-5}, 1.04×10^{-4} and 1.14×10^{-4} mol dm^{-3} Zinquin-A with 1.00×10^{-3} mol dm^{-3} NaPIPES buffer, 0.10 mol dm^{-3} $NaClO_4$ in 25% aqueous ethanol and 1.06×10^{-5}, 2.12×10^{-5}, 3.19×10^{-5}, 4.25×10^{-5} and 5.31×10^{-5} mol dm^{-3} Zinquin-A with 0.10 mol dm^{-3} NaPIPES buffer in 50% aqueous ethanol, all at pH 6.6, were determined in 1 cm quartz cells using a dual beam Cary 2200 spectrophotometer. A spectral band width of 1 nm, a response time of 0.5 s and a scan rate of 2 nm s^{-1} over a range of 220 to 300 nm were used. Each solution was run against a blank containing everything in that solution except Zinquin-A. Solutions were pre-equilibrated to 298.2 ± 0.1 K and maintained at this temperature during measurement by means of a thermostatted block. A baseline spectrum, with the same solution in both cells, was run and subtracted from all spectra using the MATLAB program KSPEC[2]. This removed any effect due to imperfectly matched cells. The experiment was then repeated with an excess of EDTA (approximately 7×10^{-4} mol dm^{-3}) added to each Zinquin-A solution.

As is described in detail in Section 2.2.3, the amount of adventitious Zn^{2+} common to all solutions can be determined from the intercept of a plot of absorbance at the maximum wavelength for $[Zn(ZQA)_2]^{2-}$, 264 and 263 nm for 25% and 50% aqueous ethanol, respectively, against Zinquin-A concentration. Comparing the line for the solutions with EDTA to the one for the solutions without EDTA gives an indication of the contribution of Zn^{2+} from the Zinquin-A solid alone.

5.1.2.3 : Zinquin-A Fluorescence Titration Fitting

Fluorescence spectra for Zinquin-A with increasing concentrations of added Zn^{2+} were determined as stated in Section 5.1.5. The MATLAB program SPECFIT,[3] which is normally used to determine formation constants and then either molar fluorescence or molar absorbance from fluorescence or absorbance titrations, respectively, was modified to keep the formation constants fixed while varying the adventitious Zn^{2+} concentration and molar fluorescences to obtain values for these parameters that most closely matched the experimental results. This is explained in more detail in Section 2.2.1.

5.1.3 : Potentiometric Titrations

The potentiometric titrations were performed using a Metrohm E665 Dosimat equipped with a 5 cm^3 burette and an Orion Ross Sureflow 81-72BN combination electrode which contained 0.10 mol dm^{-3} $NaClO_4$ in 25% aqueous ethanol. Data collection was controlled by the program AUTOTIT7[4] running on a Laser XT/3-8086 IBM compatible personal computer interfaced to the pH electrode through an Orion Research SA 720 potentiometer. All titrations were thermostatted at 298.2 ± 0.1 K in a water jacketted titration vessel which was closed to the atmosphere apart from a small exit to allow the egress of a fine stream of nitrogen. Nitrogen was bubbled through 0.10 mol dm^{-3} $NaClO_4$ to saturate it with solvent (25% aqueous ethanol) before passing it through the titration solution both during, and for 15 minutes prior to, the titration. This expelled any CO_2, preventing it from decreasing the pH of the solution. The titration solution was stirred by a magnetic stirrer bar throughout the titration.

All solutions were prepared in 25% aqueous ethanol (v/v) and were maintained at a constant ionic strength of 0.10 mol dm^{-3} using $NaClO_4$. A drying tube containing "Carbosorb" soda lime (10-16 mesh, BDH) was fitted to the bottle containing 0.0974 mol dm^{-3} NaOH (standardised by titration with 10 cm^3 aliquots of 5.00×10^{-3} mol dm^{-3} KHphthalate) to both prevent and indicate (by colour change) the presence of carbon dioxide in the titration vessel. The pK_as of Zinquin-A were determined by titration of 10 cm^3 aliquots of a solution containing 8.40×10^{-4} mol dm^{-3} Zinquin-A, 5.39×10^{-3} mol dm^{-3} $HClO_4$ and 0.10 mol dm^{-3} $NaClO_4$ with standardised NaOH (0.0974 mol dm^{-3}). The stability constants of [Zn(ZQA)] and $[Zn(ZQA)_2]^{2-}$ were determined by titrating similar solutions to which 27.9 µl of 0.10 mol dm^{-3} $Zn(ClO_4)_2$ solution had been added, giving a Zn^{2+} to Zinquin-A ratio of 1:3. This metal to ligand ratio was chosen as it showed a good formation of both [Zn(ZQA)] and $[Zn(ZQA)_2]^{2-}$. The protonation and formation constants were determined in triplicate using the FORTRAN program SUPERQUAD,[5] which minimised an error-square sum based on the differences between the measured and calculated electrode potentials. Where possible, the fitting regions were chosen to contain data points where SUPERQUAD indicated that between 10% and 90% of the ligand was present as the species of interest, this avoided the large error associated with very large or very small concentration ratios of the species in equilibrium. The fit of a single experimental run was considered to be statistically acceptable if χ^2 was less than 12.60 at the 95% confidence level. The graphical fit and the relative errors associated with the calculated constants were also taken into consideration when deciding on final values. The resultant constants were averaged using the MATLAB program ERRORS which calculates a weighted average (See Appendix E).

The electrode was calibrated every second day by titrating 10 cm^3 of a solution containing 5.21×10^{-3} mol dm^{-3} $HClO_4$ and 0.10 mol dm^{-3} $NaClO_4$ with standardised NaOH (1 cm^3, 0.0974 mol dm^{-3}) to determine E_0 and pK_w. E_0 was obtained from fitting the resulting data to the Nernst equation:

$$E = E_0 + \frac{RT}{F}\ln[H^+] \qquad (5.1)$$

where E is the observed potential (Volts);

E_0 is the standard potential for the electrode (Volts);

R is the gas constant, 8.314 J K^{-1} mol^{-1};

T is the temperature (Kelvin);

F is Faraday's constant, 9.6487×10^4 Coulombs mol^{-1}, and

$[H^+]$ is the hydrogen ion concentration.

By measuring the e.m.f. in millivolts rather than volts, converting to logarithm to the base 10 and considering only the experimental temperature of 298.2 K, the Nernst equation becomes:

$$\mathrm{pH} = \frac{E_0 - E}{59.15} \qquad (5.2)$$

where pH = -log[H+].

An experimental value for pK_w was determined from:

$$\mathrm{p}K_w = \frac{E_0 - E}{59.15} + \mathrm{pOH} \qquad (5.3)$$

where pK_w = pH + pOH and pOH = -log[OH^-]. Under the conditions used in these studies, the average pK_w = 14.6 in 25% aqueous ethanol. Diffusion correction terms for 0.10 mol dm^{-3} $NaClO_4$ in water, E_0 corr = 2.53 and pK_w corr = 1.116, were used as a best approximation in the calculation of the calibration parameters, E_0 and pK_w.

5.1.4 : Ultraviolet-Visible Spectroscopy

The ultraviolet-visible spectra of ZQA^{2-}, $[ZQA.H]^-$, $ZQA.H_2$, $[ZQA.H_3]^+$, [Zn(ZQA)] and $[Zn(ZQA)_2]^{2-}$ were determined in both 25% and 50% aqueous ethanol in 1 cm quartz cells using a dual beam Cary 2200 spectrophotometer. A spectral band width of 1 nm, a response time of 0.5 s and a scan rate of 2 nm s^{-1} were used. Each solution was run against a blank containing everything in that solution except Zinquin-A and Zn^{2+}. Solutions were pre-equilibrated to 298.2 ± 0.1 K and maintained at this temperature during measurement by means of a thermostatted block. A baseline spectrum, with the same solution in both cells, was run and subtracted from all spectra using the MATLAB program KSPEC[2]. This removed any effect due to imperfectly matched cells or the change in excitation lamp at 340 nm.

It was necessary to use weaker solutions to determine the absorbance between 220 and 300 nm than between 300 and 450 nm due to greater molar absorbances in the lower wavelength region. The pH of these solutions was chosen to give a high percentage formation of the species of interest. Various concentrations of $HClO_4$, NaPIPES and NaOH were used to give pHs in the range 1.50 to >12 and $NaClO_4$ was used to keep the ionic strength constant at I = 0.10 where necessary (See Table 5.1). The pH of all solutions was recorded before measurement of the spectra and the concentrations of each species present calculated using the program MACSPECIES.[6]

All the solutions for the unbound Zinquin-A species ZQA^{2-}, $[ZQA.H]^{-}$, $ZQA.H_2$ and $[ZQA.H_3]^{+}$ in both solvent systems contained 1.00×10^{-6} mol dm^{-3} EDTA which was added to remove any adventitious Zn^{2+} and ensure no contribution from Zinquin-A bound to Zn^{2+}. These solutions also contained approximately 1×10^{-4} mol dm^{-3} Zinquin-A for the high wavelengths and approximately 2×10^{-5} mol dm^{-3} or 1.2×10^{-5} mol dm^{-3} Zinquin-A for the lower wavelengths. The exact concentrations of Zinquin-A used are shown in Tables 5.2 and 5.3 along with the concentration in solution of the species of interest.

Species of Interest	pH	Supporting Electrolyte Used
ZQA^{2-}	>12	0.10 mol dm^{-3} NaOH
$[ZQA.H]^{-}$	6.6 [a]	1.00×10^{-3} mol dm^{-3} NaPIPES, 0.10 mol dm^{-3} $NaClO_4$
	6. 6 [b]	0.10 mol dm^{-3} NaPIPES
$ZQA.H_2$	4.3 [a]	1.04×10^{-4} mol dm^{-3} $HClO_4$, 0.10 mol dm^{-3} $NaClO_4$
	2.5 [b]	5.12×10^{-3} mol dm^{-3} $HClO_4$, 0.10 mol dm^{-3} $NaClO_4$
$[ZQA.H_3]^{+}$	1.5	0.10 mol dm^{-3} $HClO_4$
[Zn(ZQA)]	6.6 [a]	1.00×10^{-3} mol dm^{-3} NaPIPES, 0.10 mol dm^{-3} $NaClO_4$
	6.6 [b]	0.10 mol dm^{-3} NaPIPES
$[Zn(ZQA)_2]^{2-}$	6.6 [a]	1.00×10^{-3} mol dm^{-3} NaPIPES, 0.10 mol dm^{-3} $NaClO_4$
	6.6 [b]	0.10 mol dm^{-3} NaPIPES

a : 25% aqueous ethanol; **b**: 50% aqueous ethanol

Table 5.1 : pHs required for each species of interest and the supporting electrolyte used to obtain them. Solutions were made in both 25% aqueous ethanol and 50% aqueous ethanol unless indicated otherwise.

Species of Interest	pH	220 to 300 nm		300 to 450 nm	
		$[Zinquin\text{-}A]_{total}$ (mol dm^{-3})	[Species of Interest] (mol dm^{-3})	$[Zinquin\text{-}A]_{total}$ (mol dm^{-3})	[Species of Interest] (mol dm^{-3})
ZQA^{2-}	>12	2.12×10^{-5}	2.12×10^{-5}	1.06×10^{-4}	1.06×10^{-4}
$[ZQA.H]^{-}$	6.6	2.12×10^{-5}	2.12×10^{-5}	1.06×10^{-4}	1.06×10^{-4}
$ZQA.H_2$	4.3	1.68×10^{-5}	8.71×10^{-6}	1.06×10^{-4}	5.68×10^{-5}
$[ZQA.H_3]^{+}$	1.5	2.12×10^{-5}	2.07×10^{-5}	1.06×10^{-4}	1.04×10^{-4}

Table 5.2 : Concentrations used to determine the spectra of unbound Zinquin-A in various states of protonation. All solutions were in 25% aqueous ethanol and contain 1.00×10^{-5} mol dm^{-3} EDTA and supporting electrolytes as listed in Table 5.1 to give the correct pH.

Species of Interest	pH	220 to 300 nm		300 to 450 nm	
		$[Zinquin\text{-}A]_{total}$ (mol dm^{-3})	[Species of Interest] (mol dm^{-3})	$[Zinquin\text{-}A]_{total}$ (mol dm^{-3})	[Species of Interest] (mol dm^{-3})
ZQA^{2-}	>12	2.12×10^{-5}	2.12×10^{-5}	1.06×10^{-4}	1.06×10^{-4}
$[ZQA.H]^{-}$	6.6	1.28×10^{-5}	1.28×10^{-5}	1.06×10^{-4}	1.06×10^{-4}
$ZQA.H_2$	2.5	1.68×10^{-5}	1.32×10^{-5}	8.39×10^{-5}	6.50×10^{-5}
$[ZQA.H_3]^{+}$	1.5	2.12×10^{-5}	1.44×10^{-5}	1.06×10^{-4}	7.22×10^{-5}

Table 5.3 : Concentrations used to determine the spectra of unbound Zinquin-A in various states of protonation. All solutions are 50% aqueous ethanol and contain 1.00×10^{-5} mol dm^{-3} EDTA and supporting electrolytes as listed in Table 5.1 to give the correct pH.

The solutions for [Zn(ZQA)] at the high wavelengths contained 1.06×10^{-4} mol dm^{-3} Zinquin-A and 1.00×10^{-2} mol dm^{-3} or 2.00×10^{-3} mol dm^{-3} $Zn(ClO_4)_2$, for 25% and 50% aqueous ethanol solutions, respectively. The solutions for [Zn(ZQA)] at the lower wavelengths contained 2.12×10^{-5} or 1.28×10^{-5} mol dm^{-3} Zinquin-A and 2.00×10^{-3} or 2.41×10^{-4} mol dm^{-3} $Zn(ClO_4)_2$, for 25% and 50% aqueous ethanol solutions, respectively. All solutions were maintained at pH 6.6 by either 1.00×10^{-3} mol dm^{-3} NaPIPES and 0.10 mol dm^{-3} $NaClO_4$ or 0.10 mol dm^{-3} NaPIPES, for 25% and 50% aqueous ethanol solutions, respectively. An excess of Zn^{2+} was necessary to ensure the formation of predominantly [Zn(ZQA)]. Under the experimental conditions used for the solutions run at high wavelengths,

100.0% or 93.6% of the total ligand was in the [Zn(ZQA)] form, giving a concentration in solution of 1.06×10^{-4} or 9.95×10^{-5} for 25% and 50% aqueous ethanol solutions, respectively. Under the conditions used for the solutions run at the lower wavelengths, 100.0% or 93.5% of the total ligand was in the [Zn(ZQA)] form, giving a concentration in solution of 2.12×10^{-5} or 1.19×10^{-5} for 25% and 50% aqueous ethanol solutions, respectively.

The solutions for $[Zn(ZQA)_2]^{2-}$ at the high wavelengths contained 2.12×10^{-4} mol dm^{-3} Zinquin-A and 1.01×10^{-4} mol dm^{-3} $Zn(ClO_4)_2$, for both 25% and 50% aqueous ethanol solutions. The solutions for $[Zn(ZQA)_2]^{2-}$ at the lower wavelengths contained 4.25×10^{-5} or 2.55×10^{-5} mol dm^{-3} Zinquin-A and 2.06×10^{-5} or 1.28×10^{-5} mol dm^{-3} $Zn(ClO_4)_2$, for 25% and 50% aqueous ethanol solutions, respectively. All solutions were maintained at pH 6.6 by either 1.00×10^{-3} mol dm^{-3} NaPIPES and 0.10 mol dm^{-3} $NaClO_4$ or 0.10 mol dm^{-3} NaPIPES, for 25% and 50% aqueous ethanol solutions, respectively. In this case, an excess of ligand was required to ensure the formation of predominantly $[Zn(ZQA)_2]^{2-}$. Under the experimental conditions used for the solutions run at high wavelengths, 83.6% or 94.7% of the total zinc was in the $[Zn(ZQA)_2]^{2-}$ form, giving a concentration in solution of 8.41×10^{-5} or 9.54×10^{-5} for 25% and 50% aqueous ethanol solutions, respectively. Under the conditions used for the solutions run at the lower wavelengths, 62.3% or 76.9% of the total zinc was in the $[Zn(ZQA)_2]^{2-}$ form, giving a concentration in solution of 1.28×10^{-5} or 9.76×10^{-6} for 25% and 50% aqueous ethanol solutions, respectively.

The MATLAB programs AB12[7] and MABS12[8] were used to calculate and remove any contributions from species other than the one of interest in each solution to obtain the molar absorbances for Zinquin-A in its various protonated and bound states alone. Adventitious Zn^{2+} values of 6×10^{-7} and 8×10^{-7} mol dm^{-3} for 25% and 50% aqueous ethanol systems, respectively were included in the Zn^{2+} concentration of the solutions used to determine the spectra of [Zn(ZQA)] and $[Zn(ZQA)_2]^{2-}$.

5.1.5 : Fluorescence Spectroscopy

Fluorescence spectra of ZQA^{2-}, $[ZQA.H]^{-}$, $ZQA.H_2$, $[ZQA.H_3]^{+}$, $[Zn(ZQA)]$ and $[Zn(ZQA)_2]^{2-}$ were determined in both 25% and 50% aqueous ethanol using a Perkin Elmer LS50-B Luminescence Spectrophotometer. An excitation wavelength of 358 nm was used to measure the emission spectra, as an average of four scans, between 400 and 600 nm. Excitation and emission slit widths of 2.5 nm and a scan rate of 240 nm min^{-1} were used. Solutions were pre-equilibrated at 298.2 ± 0.1 K and maintained at this temperature during measurement in a 1 cm quartz cuvette by means of a thermostatted block. Fluorescence due to supporting electrolyte alone was measured and subtracted from each spectrum. Due to low absorption at 358 nm, the solutions for $[ZQA.H]^{-}$ and $ZQA.H_2$ were also excited at 336 nm.

The pH of the solutions was chosen to give a high percentage of formation with respect to the species of interest. Various concentrations of $HClO_4$, NaPIPES and NaOH were used to give pHs in the range 1.50 to >12 and $NaClO_4$ was used to keep the ionic strength constant at I = 0.10 mol dm^{-3} where necessary. (See Table 5.1) The pH of all solutions was recorded before measurement of the spectra and the concentrations of each species present calculated using the program MACSPECIES.[6]

All the solutions for the unbound Zinquin-A species ZQA^{2-}, $[ZQA.H]^{-}$, $ZQA.H_2$ and $[ZQA.H_3]^{+}$ in both solvent systems contained 1.00×10^{-6} mol dm^{-3} EDTA which was added to remove any adventitious Zn^{2+} and ensure no contribution from Zinquin-A bound to Zn^{2+}. These solutions also contained approximately 1×10^{-5} or 5×10^{-6} mol dm^{-3} Zinquin-A, with the exact concentrations of Zinquin-A used shown in Tables 5.4 along with the concentration in solution of the species of interest.

The MATLAB program AB12[7] was used to determine the molar fluorescence for $[Zn(ZQA)]$ and $[Zn(ZQA)_2]^{2-}$ from six solutions containing ratios of $Zn(ClO_4)_2$ to Zinquin-A from 0.25:1 up to 1000:1 or 0.3:1 up to 40:1, in 25% or 50% aqueous ethanol, respectively, giving differing amounts of $[Zn(ZQA)]$ and $[Zn(ZQA)_2]^{2-}$ in each solution. The ratios and exact concentrations used are given in Tables 5.5 and 5.6 below. Adventitious Zn^{2+} values of 6×10^{-7} and 8×10^{-7} mol dm^{-3} have been added to the total $[Zn^{2+}]$ for the 25% and 50% aqueous ethanol solutions, respectively.

		25% Aqueous Ethanol		50% Aqueous Ethanol	
Species of Interest	pH	$[Zinquin\text{-}A]_{total}$ (mol dm^{-3})	[Species of Interest] (mol dm^{-3})	$[Zinquin\text{-}A]_{total}$ (mol dm^{-3})	[Species of Interest] (mol dm^{-3})
ZQA^{2-}	>12	1.06×10^{-5}	1.06×10^{-5}	1.06×10^{-5}	1.06×10^{-5}
$[ZQA.H]^{-}$	6.6	5.31×10^{-6}	5.31×10^{-6}	5.00×10^{-6}	5.00×10^{-6}
$ZQA.H_2$	4.3	1.06×10^{-5}	2.63×10^{-6}		
	2.5			1.06×10^{-5}	8.18×10^{-6}
$[ZQA.H_3]^{+}$	1.5	1.06×10^{-5}	1.03×10^{-5}	1.06×10^{-5}	7.48×10^{-6}

Table 5.4 : Concentrations used to determine the spectra of unbound Zinquin-A in various states of protonation. All solutions are either 25% or 50% aqueous ethanol and contain 1.00×10^{-5} mol dm^{-3} EDTA and supporting electrolytes as listed in Table 5.1 to give the correct pH.

Ratio of $[Zn^{2+}]$:[Zinquin-A]	$[Zn^{2+}]_{total}$ (mol dm^{-3})	$[Zinquin\text{-}A]_{total}$ (mol dm^{-3})
1000:1	5.00×10^{-3}	5.31×10^{-6}
40:1	2.01×10^{-4}	5.31×10^{-6}
10:1	5.06×10^{-5}	5.31×10^{-6}
1:1	5.60×10^{-6}	5.31×10^{-6}
1:2	5.60×10^{-6}	1.06×10^{-5}
1:4	5.60×10^{-6}	2.12×10^{-5}

Table 5.5 : The ratios and concentrations of Zn^{2+} and Zinquin-A in solutions used to determine the molar fluorescence of [Zn(ZQA)] and $[Zn(ZQA)_2]^{2-}$. All solutions are in 25% aqueous ethanol and contain 1.00×10^{-3} mol dm^{-3} NaPIPES buffer and 0.10 mol dm^{-3} $NaClO_4$ adjusted to pH 6.6.

Ratio of $[Zn^{2+}]$:[Zinquin-A]	$[Zn^{2+}]_{total}$ (mol dm^{-3})	$[Zinquin\text{-}A]_{total}$ (mol dm^{-3})
40:1	2.02×10^{-4}	4.92×10^{-6}
10:1	5.20×10^{-5}	4.92×10^{-6}
2:1	1.20×10^{-5}	4.92×10^{-6}
1:1	5.00×10^{-6}	4.92×10^{-6}
3:5	3.00×10^{-6}	4.92×10^{-6}
3:10	3.00×10^{-6}	9.84×10^{-6}

Table 5.6 : The ratios and concentrations of Zn^{2+} and Zinquin-A in solutions used to determine the molar fluorescence of [Zn(ZQA)] and $[Zn(ZQA)_2]^{2-}$. All solutions are in 50% aqueous ethanol and contain 0.10 mol dm^{-3} NaPIPES buffer adjusted to pH 6.6.

The complexes, [Zn(ZQA)] and $[Zn(ZQA)_2]^{2-}$ were also studied in 50% aqueous ethanol at 298.2 K using another Perkin Elmer LS50B Luminescence Spectrophotometer which had a less sensitive photomultiplier attached to it. For this experiment similar parameters were used as described above but slit widths of 5 nm were used and each spectrum consisted of an average of 2 runs. The concentration of Zinquin-A was held constant at 5.00×10^{-6} mol dm^{-3} while the $Zn(ClO_4)_2$ concentration was varied from 0 to 1.00×10^{-4} mol dm^{-3} as shown in Table 5.7. It was necessary to add an adventitious Zn^{2+} value of 1.03×10^{-6} mol dm^{-3} to the concentration of added Zn^{2+} (See Section 5.1.2.3). The MATLAB program SPECFIT[3] was used to fit this data to obtain formation constants for [Zn(ZQA)] and $[Zn(ZQA)_2]^{2-}$ and to calculate their molar fluorescence.

Solution No.	$[Zn^{2+}]$ (mol dm^{-3})	Solution No.	$[Zn^{2+}]$ (mol dm^{-3})	Solution No.	$[Zn^{2+}]$ (mol dm^{-3})
1	0.00	12	3.03×10^{-6}	23	8.03×10^{-6}
2	1.03×10^{-6}	13	3.28×10^{-6}	24	9.03×10^{-6}
3	1.23×10^{-6}	14	3.53×10^{-6}	25	10.03×10^{-6}
4	1.43×10^{-6}	15	3.78×10^{-6}	26	11.03×10^{-6}
5	1.63×10^{-6}	16	4.03×10^{-6}	27	16.03×10^{-6}
6	1.83×10^{-6}	17	4.28×10^{-6}	28	21.03×10^{-6}
7	2.03×10^{-6}	18	4.53×10^{-6}	29	41.03×10^{-6}
8	2.23×10^{-6}	19	4.78×10^{-6}	30	61.03×10^{-6}
9	2.43×10^{-6}	20	5.03×10^{-6}	31	81.03×10^{-6}
10	2.63×10^{-6}	21	6.03×10^{-6}	32	101.03×10^{-6}
11	2.83×10^{-6}	22	7.03×10^{-6}		

Table 5.7 : $Zn(ClO_4)_2$ concentrations added to 5×10^{-6} mol dm^{-3} Zinquin-A to obtain fluorescence spectra of varying concentrations of [Zn(ZQA)] and $[Zn(ZQA)_2]^{2-}$. All solutions are in 50% aqueous ethanol and contain 0.10 mol dm^{-3} NaPIPES buffer adjusted to pH 6.6.

5.2 : Comparative Spectroscopy of Various Analogues of Sulphonamide Fluorophores

5.2.1 : Materials

6-methoxy-2-methyl-8-(*p*-toluenesulphonamido)quinoline (MM-TSQ.H),[9] 8-(benzene-sulphonamido)quinoline (BSQ.H),[9] 8-(*p*-toluenesulphonamido)quinoline (*p*-TSQ.H),[9] 8-(methanesulphonamido)quinoline (MSQ.H),[9] 8-(benzenecarbonamido)quinoline (BCQ.H),[9] 8-(quinolinesulphonamido)benzene (QSB.H),[9] perchloric acid (70% in water, Ajax), ethylenediaminetetraacetic acid disodium salt ($Na_2EDTA.H_2$, Ajax) and sodium piperazine-*N*,*N*′-bis(2-ethane-sulphonate) buffer (NaPIPES, Calbiochem) were used as received. $NaClO_4$ (Fluka) and $Zn(ClO_4)_2$ (Fluka) were used as received after drying under vacuum to constant weight and then stored over P_2O_5 in an evacuated desiccator. An aqueous $Zn(ClO_4)_2$ solution was standardised in triplicate using a cation exchange column, and this was used to prepare all Zn^{2+} containing solutions. Deionised water was ultrapurified with a Milli-Q Reagent system to produce water with a specific resistance of > 15 MΩ cm and boiled to remove any CO_2. Analytical grade ethanol (BDH) was further purified by distillation. A solvent system of 25% aqueous ethanol (v/v) was chosen as this was the highest percentage of water in which all the sulphonamidoquinolines used were soluble.

5.2.2 : Ultraviolet-Visible Spectroscopy

The ultraviolet-visible spectra of the free ligand (L.H), $[Zn(L)]^+$ and $[Zn(L)_2]$ (if applicable) were determined against a blank of 1.00×10^{-3} mol dm^{-3} NaPIPES and 0.10 mol dm^{-3} $NaClO_4$ in 1 cm quartz cells using a dual beam Cary 2200 spectrophotometer. A spectral band width of 1 nm, a response time of 0.5 s and a scan rate of 2 nm s^{-1} were used. All solutions were made in 25% aqueous ethanol adjusted to pH 6.6 with 1.00×10^{-3} mol dm^{-3} NaPIPES buffer and the ionic strength maintained at I = 0.10 with $NaClO_4$. Solutions were pre-equilibrated to 298.2 ± 0.1 K and maintained at this temperature during measurement by means of a thermostatted block. A baseline spectrum, with the same solution in both cells, was run and subtracted from all spectra using the MATLAB program KSPEC[2]. This removed any effect due to imperfectly matched cells or the change in excitation lamp at 340 nm.

The solutions for the free ligands contained approximately 1×10^{-4} mol dm^{-3} ligand (L.H), 1.00×10^{-3} mol dm^{-3} NaPIPES, 0.10 mol dm^{-3} $NaClO_4$ and 1.00×10^{-7} mol dm^{-3} EDTA which was added to remove any adventitious Zn^{2+} and ensure no contribution from ligand bound to Zn^{2+}. At pH 6.6, all of the ligands were entirely monoprotonated. The solutions for the $[Zn(L)]^+$ complexes contained approximately 1×10^{-4} mol dm^{-3} ligand (L.H), 1.00×10^{-2} mol dm^{-3} $Zn(ClO_4)_2$, 1.00×10^{-3} mol dm^{-3} NaPIPES and 0.10 mol dm^{-3} $NaClO_4$. An excess of Zn^{2+} was necessary to ensure the formation of predominantly $[Zn(L)]^+$. Under these experimental conditions, between 38.6% and 100.0% of the total ligand was in the $[Zn(L)]^+$ form, giving a concentration in solution of between 3.94×10^{-5} and 1.17×10^{-4} mol dm^{-3}. In the case of L = BSQ^- and QSB^-, the upper limit determined for the formation constant[10] was used in the calculation of percentage formation. The solutions for the $[Zn(L)_2]$ complexes contained approximately 2×10^{-4} mol dm^{-3} ligand (L.H), 1.01×10^{-4} mol dm^{-3} $Zn(ClO_4)_2$, 1.00×10^{-3} mol dm^{-3} NaPIPES and 0.10 mol dm^{-3} $NaClO_4$. In this case, an excess of ligand was required to ensure the formation of predominantly $[Zn(L)_2]$. Under these experimental conditions, between 83.9% and 99.2% of the total Zn^{2+} was in the $[Zn(L)_2]$ form, giving a concentration in solution of between 8.41×10^{-5} and 9.94×10^{-5} mol dm^{-3}. Only BSQ^-, *p*-TSQ^- and MM-TSQ^- form $[Zn(L)_2]$ species.[10] The exact concentrations used for each ligand are shown below in Tables 5.8 to 5.10. Tables 5.9 and 5.10 also indicate the concentration of $[Zn(L)]^+$ or $[Zn(L)_2]$ in solution.

Ligand (L)	[Ligand] (mol dm^{-3})	[EDTA] (mol dm^{-3})
BSQ^-	9.86×10^{-5}	1.00×10^{-5}
p-TSQ^-	1.11×10^{-4}	1.00×10^{-5}
MSQ^-	1.17×10^{-4}	1.00×10^{-5}
BCQ^-	9.68×10^{-5}	1.00×10^{-5}
QSB^-	1.02×10^{-4}	1.00×10^{-5}
MM-TSQ^-	1.08×10^{-4}	1.00×10^{-5}

Table 5.8 : Concentrations used to determine free ligand spectra. All the above solutions are at pH 6.6 in 25% aqueous ethanol with 1.00×10^{-3} mol dm^{-3} NaPIPES and $I = 0.10$ ($NaClO_4$).

Ligand (L)	$[Ligand]_{total}$ (mol dm^{-3})	$[Zn(ClO_4)_2]_{total}$ (mol dm^{-3})	$[Zn(L)^+]$ (mol dm^{-3})
BSQ^-	9.86×10^{-5}	1.00×10^{-2}	8.86×10^{-5}
p-TSQ^-	1.11×10^{-4}	1.00×10^{-2}	1.06×10^{-4}
MSQ^-	1.17×10^{-4}	1.00×10^{-2}	1.17×10^{-4}
BCQ^-	9.68×10^{-5}	1.00×10^{-2}	7.34×10^{-5}
QSB^-	1.02×10^{-4}	1.00×10^{-2}	3.94×10^{-5}
MM-TSQ^-	1.08×10^{-4}	1.00×10^{-2}	1.04×10^{-4}

Table 5.9 : Concentrations used to determine $[Zn(L)]^+$ spectra. All the above solutions are at pH 6.6 in 25% aqueous ethanol with 1.00×10^{-3} mol dm^{-3} NaPIPES and $I = 0.10$ ($NaClO_4$).

Ligand (L)	$[Ligand]_{total}$ (mol dm^{-3})	$[Zn(ClO_4)_2]_{total}$ (mol dm^{-3})	$[Zn(L)_2]$ (mol dm^{-3})
BSQ^-	1.97×10^{-4}	1.00×10^{-4}	9.10×10^{-5}
p-TSQ^-	2.22×10^{-4}	1.00×10^{-4}	9.36×10^{-5}
MSQ^-			
BCQ^-			
QSB^-			
MM-TSQ^-	2.16×10^{-4}	1.00×10^{-4}	9.94×10^{-5}

Table 5.10 : Concentrations used to determine $[Zn(L)_2]$ spectra. All the above solutions are at pH 6.6 in 25% aqueous ethanol with 1.00×10^{-3} mol dm^{-3} NaPIPES and $I = 0.10$ ($NaClO_4$). $[Zn(L)_2]$ does not form for MSQ^-, BCQ^- or QSB^-.[10]

The MATLAB program AB12[7] was used to obtain molar absorbances for $[Zn(L)]^+$ and $[Zn(L)_2]$ alone using the raw absorbance for these solutions and the free ligand molar absorbance. An adventitious Zn^{2+} concentration of 6×10^{-7} mol dm^{-3} was included in the total Zn^{2+} concentrations.

5.2.3 : Fluorescence Spectroscopy

Fluorescence spectra were collected using a Perkin Elmer LS50B Luminescence Spectrophotometer. An excitation wavelength of 358 nm was used to measure the emission spectra, as an average of four scans, between 400 and 600 nm. Excitation and emission slit widths of 2.5 nm and a scan rate of 240 nm min^{-1} were used. Solutions were pre-equilibrated to 298.2 ± 0.1 K and maintained at this temperature during measurement in a 1 cm quartz cuvette by means of a thermostatted block. Fluorescence due to buffer alone was measured and subtracted from each spectrum. Due to low absorption at 358 nm, the free ligand solutions were also excited at their absorption maxima, see Table 5.11 below. Due to the negligible concentration of $[Zn(L)]^+$ present in the ultraviolet-visible solutions when L = BCQ^- or BSQ^-, the fluorescence spectra of these complexes were not determined.

Species of Interest	Excitation λ	Species of Interest	Excitation λ
BSQ.H	358 nm and 304 nm	$[Zn(BSQ)]^+/[Zn(BSQ)_2]$	358 nm
p-TSQ.H	358 nm and 304 nm	$[Zn(p\text{-}TSQ)]^+/[Zn(p\text{-}TSQ)_2]$	358 nm
MSQ.H	358 nm and 304 nm	$[Zn(MSQ)]^+$	358 nm
BCQ.H	358 nm and 320 nm	$[Zn(MM\text{-}TSQ)]^+$/ $[Zn(MM\text{-}TSQ)_2]$	358 nm
QSB.H	358 nm and 301 nm		
MM-TSQ.H	358 nm and 340 nm		

Table 5.11 : Excitation wavelengths used for various species of interest.

All solutions were 25% aqueous ethanol, maintained at pH 6.6 with 1.00×10^{-3} mol dm^{-3} NaPIPES buffer and the ionic strength was maintained at $I = 0.10$ with $NaClO_4$. The solutions for the free ligands contained approximately 5×10^{-6} mol dm^{-3} ligand (L.H), 1.00×10^{-3} mol dm^{-3} NaPIPES, 0.10 mol dm^{-3} $NaClO_4$ and 1.00×10^{-7} mol dm^{-3} EDTA, which was added to remove any adventitious Zn^{2+} and ensure no contribution from ligand bound to Zn^{2+}. At pH 6.6, all of the ligands were entirely monoprotonated. The solutions for the $[Zn(L)]^+$ complexes contained approximately 5×10^{-6} mol dm^{-3} ligand (L.H), 5.00×10^{-3} mol dm^{-3} $Zn(ClO_4)_2$, 1.00×10^{-3} mol dm^{-3} NaPIPES and 0.10 mol dm^{-3} $NaClO_4$. An excess of Zn^{2+} was necessary to ensure the formation of predominantly $[Zn(L)]^+$. Under these experimental conditions, between 98.8% and 100.0% of the total ligand was in the $[Zn(L)]^+$ form, giving a concentration in solution of between 4.87×10^{-6} and 5.86×10^{-6} mol dm^{-3}. The solutions for

$[Zn(L)_2]$ contained approximately 2×10^{-5} mol dm^{-3} ligand (L.H), 5.60×10^{-6} mol dm^{-3} $Zn(ClO_4)_2$, 1.00×10^{-3} mol dm^{-3} NaPIPES and 0.10 mol dm^{-3} $NaClO_4$. In this case, an excess of ligand was required to ensure the formation of predominantly $[Zn(L)_2]$. Under these experimental conditions, between 83.1% and 98.1% of the total Zn^{2+} was in the $[Zn(L)_2]$ form, giving a concentration in solution of between 4.65×10^{-6} and 5.50×10^{-6} mol dm^{-3}. Only BSQ^-, *p*-TSQ^- and MM-TSQ^- form $[Zn(L)_2]$.[10] The exact concentrations used for each ligand are shown below in Tables 5.12 to 5.14. Tables 5.13 and 5.14 also indicate the concentration of $[Zn(L)]^+$ or $[Zn(L)_2]$ in solution.

Ligand (L)	[Ligand] (mol dm^{-3})	[EDTA] (mol dm^{-3})
BSQ^-	4.93×10^{-6}	1.00×10^{-5}
p-TSQ^-	5.54×10^{-6}	1.00×10^{-5}
MSQ^-	5.86×10^{-6}	1.00×10^{-5}
BCQ^-	4.84×10^{-6}	1.00×10^{-5}
QSB^-	5.11×10^{-6}	1.00×10^{-5}
MM-TSQ^-	5.41×10^{-6}	1.00×10^{-5}

Table 5.12 : Concentrations used to determine free ligand, L.H, spectra. All the above solutions are at pH 6.6 in 25% aqueous ethanol with 1.00×10^{-3} mol dm^{-3} NaPIPES and $I = 0.10$ ($NaClO_4$).

Ligand (L)	$[Ligand]_{total}$ (mol dm^{-3})	$[Zn(ClO_4)_2]_{total}$ (mol dm^{-3})	$[Zn(L)^+]$ (mol dm^{-3})
BSQ^-	4.93×10^{-6}	5.00×10^{-3}	4.87×10^{-6}
p-TSQ^-	5.54×10^{-6}	5.00×10^{-3}	5.51×10^{-6}
MSQ^-	5.86×10^{-6}	5.00×10^{-3}	5.86×10^{-6}
BCQ^-			
QSB^-			
MM-TSQ^-	5.41×10^{-6}	5.00×10^{-3}	5.39×10^{-6}

Table 5.13 : Concentrations used to determine $[Zn(L)]^+$ spectra. All the above solutions are at pH 6.6 in 25% aqueous ethanol with 1.00×10^{-3} mol dm^{-3} NaPIPES and I = 0.10 ($NaClO_4$).

Ligand (L)	$[Ligand]_{total}$ (mol dm^{-3})	$[Zn(ClO_4)_2]_{total}$ (mol dm^{-3})	$[Zn(L)_2]$ (mol dm^{-3})
BSQ^-	1.97×10^{-5}	5.60×10^{-6}	5.10×10^{-6}
p-TSQ^-	2.22×10^{-5}	5.60×10^{-6}	4.65×10^{-6}
MSQ^-			
BCQ^-			
QSB^-			
MM-TSQ^-	2.16×10^{-5}	5.60×10^{-6}	5.50×10^{-6}

Table 5.14 : Concentrations used to determine $[Zn(L)_2]$ spectra. All the above solutions are at pH 6.6 in 25% aqueous ethanol with 1.00×10^{-3} mol dm^{-3} NaPIPES and $I = 0.10$ ($NaClO_4$). $[Zn(L)_2]$ species do not form for MSQ, BCQ or QSB.[10]

The MATLAB program AB12[7] was used to obtain molar fluorescence for $[Zn(L)]^+$ and $[Zn(L)_2]$ alone using the raw fluorescence for these solutions and the free ligand molar fluorescence. An adventitious Zn^{2+} concentration of 6×10^{-7} mol dm^{-3} was included in the total Zn^{2+} concentrations.

5.3 : The Study of Zinc(II) in Cells and Nuclei with Zinquin-A and Zinquin-E

5.3.1 : Materials

LIM 1215 colon cancer cells were used as received as were sodium 1-hydroxy pyridine-2-thione (pyrithione, Sigma), sucrose (Sigma), ethylenediaminetetraacetic acid disodium salt ($Na_2EDTA.H_2$, Sigma), ethylenebis(oxyethylenenitrilo)tetraacetic acid (EGTA, ICN), Tris(hydroxymethyl)aminomethane (Tris, Sigma), 2-mercaptoethanol (Sigma), 10% NP40 detergent (Sigma), zinc sulphate ($ZnSO_4$, BDH), 'complete protease inhibitor cocktail' (Boehringer Mannheim), bulk Hank's Balanced Salt Solution (HBSS, Gibco), 0.05% Trypsin-EDTA (ICN), Dulbecco's phosphate buffered saline (PBS, pH 7.4, ICN), fetal calf serum (FCS, Biosciences), Zinquin-A (2-methyl-8-*p*-toluenesulphonamido-6-quinolyloxyacetic acid, $ZQA.H_2$)[1] and Zinquin-E (ethyl-[2-methyl-8-*p*-toluenesulphonamido-6-quinolyloxy]acetate, ZQE.H)[1]. The culture medium used was RPMI 1640 which was buffered using HEPES to pH 7.4 (ICN) and was supplemented with glutamine (2 mM), penicillin (100 $IUml^{-1}$), streptomycin (100 $\mu g\ ml^{-1}$), gentamicin (160 $\mu g\ ml^{-1}$) and 10% foetal bovine serum. All solutions were prepared using deionised water which was ultrapurified with a Milli-Q Reagent system to produce water with a specific resistance of > 15 MΩ cm except for the Zinquin-E and Zinquin-A bulks which were prepared using AR grade DMSO.

5.3.2 : Cell and Nuclei Preparation and Visualisation

For the study of whole cells, dead cells and cell growth medium were decanted from the LIM 1215 colon cancer cells which were then washed 4 times with PBS. The cells were cleaved from a 25 cm^2 vented culture flask by adding 2 cm^3 0.05% Trypsin-EDTA followed by incubation at 37°C until the cells flowed freely (approximately 5 minutes). Approximately 16 cm^3 of culture medium was then added to deactivate the trypsin, and after careful shaking, the contents of the flask were then divided into four aliquots of equal volume (4 cm^3). The aliquots were centrifuged at 1500 rpm for 5 minutes at 277 K using an IEC Centra-7R refrigerated centrifuge and the cells were washed with culture medium twice and then resuspended in 900 µl of culture medium. To half of the aliquots, 9 µl each of 4.00×10^{-4} mol dm^{-3} pyrithione and 2.57×10^{-3} mol dm^{-3} $ZnSO_4$ were added to give final concentrations of 3.92×10^{-6} mol dm^{-3} pyrithione and 2.52×10^{-5} mol dm^{-3} $ZnSO_4$. To the other aliquots, 18 µl

of water was added and they were then incubated for 35 minutes at 37°C. The cells were then washed 3 times with HBSS at pH 7.4 containing 4.164×10^{-3} mol dm^{-3} $NaHCO_3$ and resuspended in 1 cm^3 of this buffer. Zinquin-A, 5 µl of 5.13×10^{-3} mol dm^{-3}, or Zinquin-E, 5 µl of 5.12×10^{-3} mol dm^{-3}, in DMSO was then added to the aliquots to give solutions of the ester and the acid with and without added Zn^{2+} and pyrithione. The cells were viewed after an incubation of 20 minutes without further washing.

The nuclei were prepared as above, up to the HBSS wash, except 2 flasks of cells were combined before dividing into 4 aliquots (6 cm^3). Instead of resuspending the cells in 1 cm^3 of HBSS buffer, they were resuspended in 500 µl of a lysis buffer[11] consisting of 1.83×10^{-3} mol dm^{-3} EDTA, 9.15×10^{-3} mol dm^{-3} EGTA, 4.58×10^{-2} mol dm^{-3} 2-mercaptoethanol, 5% sucrose, 0.1% NP40, a complete protease inhibitor cocktail pellet and 1.83×10^{-2} mol dm^{-3} Tris-HCl at pH 7.5 and left at 0°C for 5 minutes. The aliquots were then centrifuged at 1500 rpm for 10 minutes and the pellets resuspended in 917 µl of HBSS buffer and 83 µl of 60% sucrose to which 5 µl of 5.13×10^{-3} mol dm^{-3} Zinquin-A or 5.12×10^{-3} mol dm^{-3} Zinquin-E in DMSO was added to give solutions of the ester and the acid with and without added Zn^{2+} and pyrithione. The nuclei were concentrated and viewed after an incubation of 20 minutes without further washing.

Both the cells and nuclei were viewed using an Olympus microscope equipped with a UVB dichroic mirror (Olympus, Tokyo) for low wavelength excitation and connected to a CCTV video colour camera and Multi Sync 3FG computer work station. Several images were captured and mean fluorescence intensity of individual cells, nuclei and backgrounds were computed using the Video Pro Image Analysis System (Leading Edge Pty Ltd, S. Australia). Care was taken to capture the fluorescence images rapidly to avoid quenching, which occurs after excessive ultraviolet excitation.

5.4 : Properties of Ternary Zinquin-A Complexes, [Zn(L)ZQA]

5.4.1 : Materials

Zinquin-A (2-methyl-8-*p*-toluenesulphonamido-6-quinolyloxyacetic acid, $ZQA.H_2$),[1] 2,2′,2″-triaminotriethylamine (tren, Strem), NaOH (ConvoL, BDH), perchloric acid (70% in water, Ajax), ethylenediaminetetraacetic acid disodium salt ($Na_2EDTA.H_2$, Ajax), boric acid (H_3BO_3, Ajax) and sodium piperazine-*N*,*N*′-bis(2-ethane-sulphonate) buffer (NaPIPES, Calbiochem) were used as received. 1,4,8,11-tetraazacyclotetradecane (cyclam, Strem), 1,4,7,10-tetraazacyclododecane (cyclen),[12] 1,4,7-triazacyclononane trihydrogen bromide (tacn.3HBr),[13] 1,5,9-triazacyclododecane trihydrogen chloride (tacdo.3HCl),[14] nitrilotriacetic acid trisodium salt (Na_3NTA, Fluka), Triethanolamine (TEA, BDH), bovine carbonic anhydrase (Sigma), Potassium hydrogen phthalate (KHphthalate, BDH), $NaClO_4$ (Fluka) and $Zn(ClO_4)_2$ (Fluka) were used as received after drying under vacuum to constant weight and then stored over P_2O_5 in an evacuated desiccator. An aqueous $Zn(ClO_4)_2$ solution was standardised in triplicate using a cation exchange column, and this was used to prepare all Zn^{2+} containing solutions. Deionised water was ultrapurified with a Milli-Q Reagent system to produce water with a specific resistance of > 15 MΩ cm and boiled to remove any CO_2. Analytical grade ethanol (BDH) was further purified by distillation. A solvent system of 50% aqueous ethanol (v/v) was chosen as this was the highest percentage of water in which Zinquin-A was soluble over the entire concentration range required. Due to the insolubility of carbonic anhydrase in ethanol, 95% aqueous ethanol was used for the carbonic anhydrase study and all solutions were made under N_2 to minimise contact with CO_2 which reacts rapidly with carbonic anhydrase to lower the pH of the solution by the formation of carbonic acid.

5.4.2 : Potentiometric Titrations

The potentiometric titrations were performed using a Metrohm E665 Dosimat equipped with a 5 cm^3 burette and an Orion Ross Sureflow 81-72BN combination electrode which contained 0.10 mol dm^{-3} $NaClO_4$ in 50% aqueous ethanol. Data collection was controlled by the program AUTOTIT7[4] running on a Laser XT/3-8086 IBM compatible personal computer interfaced to the electrode through an Orion Research SA 720 potentiometer. All titrations were thermostatted at 298.2 ± 0.1 K in a water jacketted titration vessel which was closed to the atmosphere apart from a small exit to allow the egress of a fine stream of nitrogen. Nitrogen was bubbled through 0.10 mol dm^{-3} $NaClO_4$ to saturate it with solvent (50% aqueous ethanol) before passing it through the titration solution both during, and for 15 minutes prior to, the titration. This expelled any CO_2, preventing it from decreasing the pH of the solution. The titration solution was stirred by a magnetic stirrer bar throughout the titration. Except for the solvent mixture, this is the same experimental set up as described in Section 5.1.3.

All solutions were in 50% aqueous ethanol (v/v) and were maintained at a constant ionic strength of 0.10 by $NaClO_4$. A drying tube containing "Carbosorb" soda lime (10-16 mesh, BDH) was fitted to the bottle containing 0.0997 mol dm^{-3} NaOH (standardised by titration with 10 cm^3 aliquots of 5.19×10^{-3} mol dm^{-3} KHphthalate) to both prevent and indicate (by colour change) the presence of carbon dioxide in the titration vessel. The pK_as of protonated cyclam, cyclen, tacdo, tacn, TEA, tren and $NTA.H_3$ were determined by titration of 10 cm^3 aliquots of solutions containing approximately 2×10^{-3} mol dm^{-3} ligand (L), between 0.10 and 0.0900 mol dm^{-3} $NaClO_4$ (to keep the ionic strength constant) and various concentrations of $HClO_4$ (to ensure total protonation of all nitrogen and oxygen donors) with standardised NaOH (0.0997 mol dm^{-3}). Table 5.15 shows the actual concentrations of ligand (L), acid and $NaClO_4$ used. The formation constants of $[Zn(L)]^{2+}$ and several other relevant species (see Section 4.2.2) were determined by titrating similar solutions to which approximately 100 or 200 µl of 0.10 mol dm^{-3} $Zn(ClO_4)_2$ solution had been added, resulting in Zn^{2+} to ligand (L) ratios of 1:2 and 1:1, respectively. The ternary formation constants of species such as [Zn(L)ZQA] were determined by combining 5 cm^3 of approximately 4×10^{-3} mol dm^{-3} ligand (L) solution with 5 cm^3 of 2.00×10^{-3} mol dm^{-3} Zinquin-A in the cell. All these solutions had concentrations of $HClO_4$ and $NaClO_4$ as listed in Table 5.16 which also gives the actual ligand concentrations used. Approximately 100 µl of 0.10 mol dm^{-3} $Zn(ClO_4)_2$ was then added to give a final ratio of $L:Zn^{2+}:ZQA^{2-}$ of 2:1:1. This ratio was chosen to minimise the formation of

both [Zn(ZQA)] and $Zn(OH)_2$ during the titration. The protonation and formation constants were determined in at least triplicate and the resultant constants determined using the FORTRAN program SUPERQUAD,[5] which minimised an error-square sum based on the differences between the measured and calculated electrode potentials. Where possible, the fitting regions were chosen to contain data points where SUPERQUAD indicated that between 10% and 90% of the ligand was present as the species of interest as this avoided the large error associated with very large or very small concentration ratios of the species in equilibrium. The fit of a single experimental run was considered to be statistically acceptable if χ^2 was less than 12.60 at the 95% confidence level. The graphical fit and the relative errors associated with the calculated constants were also taken into consideration when deciding on final values. The resultant constants were averaged using the MATLAB program ERRORS which calculates a weighted average (See Appendix E).

Ligand (L)	[Ligand] (mol dm^{-3})	[$HClO_4$] (mol dm^{-3})	[$NaClO_4$] (mol dm^{-3})
cyclen	2.14×10^{-3}	1.00×10^{-2}	0.0900
cyclam	2.03×10^{-3}	1.00×10^{-2}	0.0900
tacn	2.09×10^{-3}	2.00×10^{-3}	0.0980
tacdo	2.94×10^{-3}	2.00×10^{-3}	0.0980
tren	2.03×10^{-3}	1.00×10^{-2}	0.0900
NTA^{3-}	2.00×10^{-3}	1.00×10^{-2}	0.0900
TEA	2.03×10^{-3}	4.01×10^{-3}	0.0960

Table 5.15 : Concentrations used to determine protonation and binary formation constants of the ligands with Zn^{2+}. All solutions are 50% aqueous ethanol.

Ligand (L)	[Ligand] (mol dm^{-3})	[$HClO_4$] (mol dm^{-3})	[$NaClO_4$] (mol dm^{-3})
cyclen	4.11×10^{-3}	1.00×10^{-2}	0.0900
cyclam	4.05×10^{-3}	1.00×10^{-2}	0.0900
tacn	4.04×10^{-3}	4.01×10^{-3}	0.0960
tacdo	4.03×10^{-3}	4.01×10^{-3}	0.0960
tren	3.91×10^{-3}	1.00×10^{-2}	0.0900
NTA^{3-}	3.98×10^{-3}	1.00×10^{-2}	0.0900
TEA	4.13×10^{-3}	8.01×10^{-3}	0.0920
Zinquin-A	2.00×10^{-3}	4.06×10^{-3}	0.0960

Table 5.16 : Concentrations of ligand solutions used to determine ternary formation constants of [Zn(L)ZQA]. All solutions are 50% aqueous ethanol.

The electrode was calibrated every second day by titrating 10 cm^3 of a solution containing 1.00×10^{-2} mol dm^{-3} $HClO_4$ and 0.0900 mol dm^{-3} $NaClO_4$ with standardised NaOH (2 cm^3, 0.0997 mol dm^{-3}) to determine E_0 and pK_w from fitting the resulting data to the Nernst equation as described in Section 5.1.3. Under the conditions used, the average pK_w = 14.4 in 50% aqueous ethanol. Diffusion correction terms for 0.10 mol dm^{-3} $NaClO_4$ in water, E_0 corr = 2.53 and pK_w corr = 1.116, were used as a best approximation in the calculation of the calibration parameters, E_0 and pK_w.

5.4.2.1 : The Treatment of Hydroxy Species in Potentiometric Titration Analysis.

As is described in Chapter 4, many Zn^{2+} complexes form hydroxy species due to the greater acidity of water molecules attached to the Zn^{2+} in these complexes. This can be described by Equations 5.4 and 5.5 below;

$$[Zn(L)]^{2+} + OH^- \overset{K_{OH}}{\rightleftharpoons} [Zn(L)OH]^+ \qquad (5.4)$$

$$K_{OH} = \frac{[Zn(L)OH^+]}{[Zn(L)^{2+}][OH^-]} \qquad (5.5)$$

or by the cumulative Equations 5.6 and 5.7 below;

$$L + Zn^{2+} + OH^- \overset{K_{1OH}}{\rightleftharpoons} [Zn(L)OH]^+ \quad (5.6)$$

$$K_{1OH} = \frac{[Zn(L)OH^+]}{[L][Zn^{2+}][OH^-]} \quad (5.7)$$

However, SUPERQUAD can not fit for OH^- directly as it requires an equation involving H^+. The equations used by SUPERQUAD are given below in Equations 5.8 and 5.9.

$$L + Zn^{2+} \overset{K_{-1}}{\rightleftharpoons} [Zn(L)OH]^+ + H^+ \quad (5.8)$$

$$K_{-1} = \frac{[Zn(L)OH^+][H^+]}{[L][Zn^{2+}]} = \frac{[Zn(L)OH^+]}{[L][Zn^{2+}][H^+]^{-1}} \quad (5.9)$$

For this study, it is quite reasonable to represent the formation of the hydroxy species with an acid dissociation expression similar to Equation 5.8, rather than an OH^- association expression as in Equations 5.4 to 5.7, as it is believed that in this case the hydroxide originates from the water bound to the Zn^{2+} and not from the bulk solvent. The general expressions used in this study are shown in Equations 5.10 and 5.11. The term $[Zn(L)OH]^+$ has been replaced in favour of the term $[Zn(L)H_{-1}]^+$ as SUPERQUAD does not differentiate between a proton lost from a bound water and a proton lost from the ligand itself, and the results discussed in Chapter 4 indicate that the latter may occur for the Zn^{2+} complexes of TEA.

$$[Zn(L)]^{2+} \overset{K_{aL}'}{\rightleftharpoons} [Zn(L)H_{-1}]^+ + H^+ \quad (5.10)$$

$$K_{aL}' = \frac{[Zn(L)H_{-1}^+][H^+]}{[Zn(L)^{2+}]} = \frac{[Zn(L)H_{-1}^+]}{[Zn(L)^{2+}][H^+]^{-1}} \quad (5.11)$$

The constant, K_{aL}' can be derived from the K_{-1} obtained from SUPERQUAD simply by dividing by the formation constant of $[Zn(L)]^{2+}$, K_1 (defined in Section 4.2.2). Converting K_{aL}' to K_{OH} or K_{1OH}, which may be used in the literature, is slightly more complicated and makes use of the relationship $K_w = [OH^-] \times [H^+]$ which describes the dissociation of water in the bulk solvent. Equation 5.12 shows the derivation of the conversion of K_{aL}' to $K_{OH} = K_{aL}' / K_w$ and K_{1OH} can then be obtained by multiplying K_{OH} by the formation constant of $[Zn(L)]^{2+}$, K_1.

$$
\begin{aligned}
K_{OH} &= \frac{[Zn(L)OH^+]}{[Zn(L)^{2+}][OH^-]} \\
&= \frac{[Zn(L)OH^+]}{[Zn(L)^{2+}] K_w / [H^+]} \\
&= \frac{[Zn(L)OH^+]}{[Zn(L)^{2+}] K_w [H^+]^{-1}} \\
&= \frac{[Zn(L)OH^+]}{[Zn(L)^{2+}][H^+]^{-1}} \times \frac{1}{K_w} \\
&= K_{aL}' \times \frac{1}{K_w} \\
&= \frac{K_{aL}'}{K_w}
\end{aligned}
\qquad (5.12)
$$

5.4.3 : Ultraviolet-Visible Spectroscopy

The ultraviolet-visible spectra of the [Zn(L)ZQA] ternary species were determined in 1 cm quartz cells using a dual beam Cary 2200 spectrophotometer. A spectral band width of 1 nm, a response time of 0.5 s and a scan rate of 2 nm s^{-1} were used. Each solution was run against a blank containing everything in that solution except Zinquin-A. All solutions were 50% aqueous ethanol, maintained at pH 6.6 or pH 10 and I = 0.10 with 0.10 mol dm^{-3} NaPIPES or 0.10 mol dm^{-3} borate buffer respectively. Solutions were pre-equilibrated to 298.2 ± 0.1 K and maintained at this temperature during measurement by means of a thermostatted block. A baseline spectrum, with the same solution in both cells, was run and subtracted from all spectra using the MATLAB program KSPEC[2]. This removed any effect due to imperfectly matched cells or the change in excitation lamp at 340 nm.

It was necessary to use weaker solutions to determine the absorbance between 220 and 300 nm than between 300 and 450 nm due to greater molar absorbances in the lower wavelength region. The solutions used for the higher wavelength region contained approximately 1×10^{-3} or 5×10^{-3} mol dm^{-3} ligand, 1×10^{-4} mol dm^{-3} Zinquin-A, 4×10^{-4} or 3×10^{-3} mol dm^{-3} $Zn(ClO_4)_2$ and 0.10 mol dm^{-3} NaPIPES (pH 6.6) or borate buffer (pH 10). Those for the lower wavelength region contained approximately 2×10^{-4} or 5×10^{-3} mol dm^{-3} ligand, 2×10^{-5} mol dm^{-3} Zinquin-A, 9×10^{-5} or 3×10^{-3} mol dm^{-3} $Zn(ClO_4)_2$ and 0.10 mol dm^{-3} NaPIPES (pH 6.6) or borate buffer (pH 10). The concentrations used, shown in Tables 5.17 and 5.18, were chosen to give the maximum formation of the ternary species at the pH of interest. The NTA^{3-} and tacdo systems were run at both pH 6.6 and 10 as a mixture of ternary complexes were obtained at pH 6.6 for these systems. The cyclam system was determined at pH 10 alone as insufficient ternary complex formed at pH 6.6. An adventitious Zn^{2+} value of 8×10^{-7} mol dm^{-3} was included in the total Zn^{2+} concentrations for those at pH 6.6. No correction was required for those at pH 10 due to the larger concentrations of Zn^{2+} used. The concentrations of all species present were calculated using the program MACSPECIES[6] and the contribution to the spectra due to non-ternary species, such as [Zn(ZQA)], was calculated and removed before calculating the molar absorbance of the ternary complexes on their own.

Ligand (L)	pH	$[Ligand]_{Total}$ (mol dm^{-3})	$[Zn(ClO_4)_2]_{Total}$ (mol dm^{-3})	[Ternary Complex] (mol dm^{-3})
cyclen	6.6	1.03×10^{-3}	4.51×10^{-4}	9.41×10^{-5} **a**
cyclam	10	4.99×10^{-3}	3.01×10^{-3}	9.21×10^{-5} **a**
tacn	6.6	1.01×10^{-3}	4.51×10^{-4}	5.57×10^{-5} **a**
tacdo	6.6	5.00×10^{-3}	4.51×10^{-4}	6.15×10^{-5} **a**; 3.08×10^{-5} **b**
	10	5.05×10^{-3}	4.51×10^{-4}	1.04×10^{-4} **a**
tren	6.6	1.00×10^{-3}	4.51×10^{-4}	9.84×10^{-5} **a**
NTA^{3-}	6.6	4.98×10^{-3}	4.01×10^{-4}	4.24×10^{-6} **a**; 4.84×10^{-5} **b**
	10	5.03×10^{-3}	3.01×10^{-3}	8.70×10^{-5} **a**
TEA	6.6	5.20×10^{-3}	4.51×10^{-4}	1.26×10^{-5} **c**

Table 5.17 : Concentrations used to determine the absorbance of the ternary complexes in the 300 to 450 nm region. All solutions also contained Zinquin-A at 9.84×10^{-5} or 1.04×10^{-4} mol dm^{-3} for solutions at pH 6.6 (0.10 mol dm^{-3} NaPIPES) and pH 10 (0.10 mol dm^{-3} borate) respectively. The ternary complexes studied are; **a** : [Zn(L)ZQA], **b** : $[Zn(L)ZQA.H]^{+}$, and **c** : $[Zn(L)ZQA.H_{-1}]^{-}$.

Ligand (L)	pH	$[Ligand]_{Total}$ (mol dm^{-3})	$[Zn(ClO_4)_2]_{Total}$ (mol dm^{-3})	[Ternary Complex] (mol dm^{-3})
cyclen	6.6	2.07×10^{-4}	9.08×10^{-5}	1.61×10^{-5} **a**
cyclam	10	4.99×10^{-3}	3.01×10^{-3}	1.97×10^{-5} **a**
tacn	6.6	2.01×10^{-4}	9.08×10^{-5}	1.00×10^{-5} **a**
tacdo	6.6	4.92×10^{-3}	8.08×10^{-5}	1.23×10^{-5} **a**; 6.15×10^{-6} **b**
	10	5.05×10^{-3}	4.51×10^{-4}	2.07×10^{-5} **a**
tren	6.6	2.00×10^{-3}	9.08×10^{-5}	1.97×10^{-5} **a**
NTA^{3-}	6.6	4.98×10^{-3}	3.01×10^{-3}	1.44×10^{-6} **a**; 1.64×10^{-5} **b**
	10	5.03×10^{-3}	3.01×10^{-3}	1.98×10^{-5} **a**
TEA	6.6	5.20×10^{-3}	3.01×10^{-3}	2.93×10^{-6} **c**

Table 5.18 : Concentrations used to determine the absorbance of the ternary complexes in the 220 to 300 nm region. All solutions also contained Zinquin-A at 1.97×10^{-5} or 2.07×10^{-5} mol dm^{-3} for solutions at pH 6.6 (0.10 mol dm^{-3} NaPIPES) and pH 10 (0.10 mol dm^{-3} borate) respectively. The ternary complexes studied are; **a** : [Zn(L)ZQA], **b** : $[Zn(L)ZQA.H]^{+}$, and **c** : $[Zn(L)ZQA.H_{-1}]^{-}$.

5.4.4 : Fluorescence Spectroscopy

Fluorescence spectra of the ternary complexes were collected using a Perkin Elmer LS50B Luminescence Spectrophotometer. An excitation wavelength of 358 nm was used to measure the emission spectra, as an average of four scans, between 400 and 600 nm. Excitation and emission slit widths of 2.5 nm and a scan rate of 240 nm min^{-1} were used. Solutions were pre-equilibrated to 298.2 ± 0.1 K and maintained at this temperature during measurement in 1 cm quartz cuvettes by means of a thermostatted block. Fluorescence due to buffer alone was measured and subtracted from each spectrum.

Solutions contained approximately 1×10^{-4} or 5×10^{-3} mol dm^{-3} ligand (L), 1×10^{-5} mol dm^{-3} Zinquin-A, 4×10^{-4} or 3×10^{-3} mol dm^{-3} $Zn(ClO_4)_2$ and 0.10 mol dm^{-3} NaPIPES (pH 6.6) or borate buffer (pH 10) as shown in Table 5.19 below. As for the ultraviolet-visible spectra above, the concentrations used were chosen to give the maximum formation of the ternary species at the pH of interest. The NTA^{3-} and tacdo systems were run at both pH 6.6 and 10 as a mixture of ternary complexes were obtained at pH 6.6 for these systems. The cyclam system was determined at pH 10 alone as insufficient ternary complex formed at pH 6.6. An

adventitious Zn^{2+} value of 8×10^{-7} mol dm^{-3} was included in the total Zn^{2+} concentrations for solutions at pH 6.6. No correction was required for the solutions at pH 10 due to the high concentrations of Zn^{2+} used. The concentrations of all species present were calculated using the program MACSPECIES[6] and the contribution to the spectra due to non-ternary species, such as [Zn(ZQA)], was calculated and removed before calculating the molar absorbance of the ternary complexes on their own.

Ligand (L)	pH	$[Ligand]_{Total}$ (mol dm^{-3})	$[Zn(ClO_4)_2]_{Total}$ (mol dm^{-3})	[Ternary Complex] (mol dm^{-3})
cyclen	6.6	1.03×10^{-4}	4.58×10^{-5}	6.90×10^{-6} **a**
cyclam	10	4.99×10^{-3}	3.01×10^{-3}	9.91×10^{-6} **a**
tacn	6.6	1.01×10^{-4}	4.58×10^{-5}	4.52×10^{-6} **a**
tacdo	6.6	4.99×10^{-3}	4.08×10^{-5}	6.12×10^{-6} **a**; 3.07×10^{-6} **b**
	10	5.05×10^{-3}	4.51×10^{-4}	1.04×10^{-5} **a**
tren	6.6	1.00×10^{-4}	4.58×10^{-5}	9.84×10^{-6} **a**
NTA^{3-}	6.6	4.98×10^{-3}	3.50×10^{-3}	7.31×10^{-7} **a**; 8.34×10^{-6} **b**
	10	5.03×10^{-3}	3.01×10^{-3}	1.01×10^{-5} **a**
TEA	6.6	5.20×10^{-3}	1.50×10^{-3}	1.50×10^{-6} **c**

Table 5.19 : Concentrations used to determine the fluorescence of the ternary complexes in the 400 to 600 nm region. All solutions also contained Zinquin-A at 9.84×10^{-6} or 1.04×10^{-5} mol dm^{-3} for solutions at pH 6.6 (0.10 mol dm^{-3} NaPIPES) and pH 10 (0.10 mol dm^{-3} borate) respectively. The ternary complexes studied are; **a** : [Zn(L)ZQA], **b** : $[Zn(L)ZQA.H]^{+}$, and **c** : $[Zn(L)ZQA.H_{-1}]^{-}$.

For the Carbonic Anhydrase study, three solutions were prepared *in situ* by adding 325 µl of a 50% aqueous ethanol solution of 9.84×10^{-4} mol dm^{-3} Zinquin-A at pH 6.6 (0.10 mol dm^{-3} PIPES buffer) to 3 cm^3 of an aqueous solution of either 1.01×10^{-5} mol dm^{-3} carbonic anhydrase at pH 6.6 (0.10 mol dm^{-3} PIPES buffer), 1.00×10^{-5} mol dm^{-3} $Zn(ClO_4)_2$ at pH 6.6 (0.10 mol dm^{-3} PIPES buffer) or 0.10 mol dm^{-3} PIPES buffer at pH 6.6. This gave final concentrations of 9.63×10^{-5} mol dm^{-3} Zinquin-A, 9.143×10^{-6} mol dm^{-3} carbonic anhydrase and 9.02×10^{-6} mol dm^{-3} $Zn(ClO_4)_2$ and a 95% aqueous ethanol solvent after mixing in the cuvette.

5.5 : Preliminary Force Field Molecular Modelling of the Ternary Complexes, [Zn(L)ZQA]

Force field modelling was run on a Silicon Graphics Irix5r3 Indigo computer using the program INSIGHT II version 97.0, build 970914 IRIX and the optimisation package DISCOVER 3. The extended systematic force field, ESFF, was used to minimise the total potential energy of the complexes with a maximum derivative of 0.01. A maximum of 1000 iterations was set, however in some instances it was necessary to modify this to 2000 iterations before convergence. Atom based summation methods, with no cutoffs, were used to calculate vdW and coulomb interactions. The dielectric constant was set to 1.00. The molecular charge was assigned using the macro initialize_charge.bcl and the partial charges this produced were accepted. The discover parameters were set so that the potential type of atoms were automatically modified to the most appropriate before minimisation and care was taken to ensure that the same potentials were used each time a complex was refined so the resultant energies could be compared. The minimisation process used up to three algorithms depending on the amount of minimisation required.

5.6 : References

1. As provided by M. Kimber, University of Adelaide, South Australia, Australia.

2. A MATLAB program, K. M. Hendrickson, University of Adelaide, South Australia, Australia. Refer to Appendix E.

3. A MATLAB program, T. Kurucsev, University of Adelaide, South Australia, Australia, Refer to Appendix E.

4. A FORTRAN program for the control of automated titrations, P. A. Duckworth, University of Adelaide, South Australia, Australia.

5. P. Gans, A. Sabatini and A. Vacca, *J. Chem. Soc., Dalton Trans.*, 1195, 1985.

6. A Macintosh version (P. A. Duckworth) of the FORTRAN program SPE, A. E. Martell and R. J. Motekaitis, "*Determination and use of Stability constants*", Appendix III, VCH, 1990.

7. AB12 is a subroutine in the MATLAB program SPECFIT, T. Kurucsev, University of Adelaide, South Australia, Australia. Refer to Appendix E.

8. A modified version (K. Hendrickson) of the MATLAB program AB12 which is a subroutine in the MATLAB program SPECFIT, T. Kurucsev, University of Adelaide, South Australia, Australia. Refer to Appendix E.

9. As provided by I. Mahadevan, University of Adelaide, South Australia, Australia.

10. C. Haskard, Honours Thesis, University of Adelaide, South Australia, Australia.

11. Z. Z. Chen, J. C. McGuire, K. L. Leach and J. C. Cambier, *J. Immunol.*, **138 (7)**, 2345, 1987.

12. As provided by O. Wyness, University of Adelaide, South Australia, Australia.

13. As provided by B. May, University of Adelaide, South Australia, Australia.

14. As provided by S. Creaser, University of Adelaide, South Australia, Australia.

CHAPTER 6

SUGGESTED FUTURE WORK

6.1 : Future work

To fully understand how Zinquin works and to use it to elucidate the vital roles Zn^{2+} plays in the body, much additional research needs to be carried out. For example the speed at which the intracellular esterases hydrolyse Zinquin-E (Figure 2.2), if indeed they do, is still unknown. Hydrolysis experiments could be carried out, perhaps using HPLC, to determine the relative rates of hydrolysis of Zinquin-E with cytoplasm derived from a variety of cells and with sodium hydroxide.

Zinquin distribution in the cell could also be further studied using techniques such as confocal microscopy which gives a three dimensional view of a fluorescing cell by illuminating and detecting in a confined, focused area with the aid of a laser. As all parts of the cell that are not in focus appear black, it is possible to visualise various planes through the specimen and store the individual images which can then be shown as a composite picture or as a rotatable three dimensional structure. This method has already been used with Zinquin-E[1] and could prove whether the Zinquin-A and Zinquin-E are binding to the cellular or nuclear membranes or not in the case of extracted nuclei (Section 3.2) and give additional information about the location of Zn^{2+} in cells. Radioactive labelling of the Zinquin-E could also be used to locate it in the cell even if its fluorescence is being quenched, indicating if it is in the darkened areas of a cell or if it is excluded from these areas.

Since the coordination environment about a Zn^{2+} effects the fluorescence of a Zinquin-A molecule bound to it, it is reasonable to expect that the fluorescence lifetime of the excited Zinquin-A molecule would also be dependent on the immediate coordination environment. Thus it may be possible to 'map' the various environments Zn^{2+} is found in throughout the cell using lifetime fluorescence spectroscopy.[2] This method is often combined with confocal microscopy and measures the lifetime of the excited state by one of two methods. The simplest is to illuminate the sample with a narrow pulse of light and capture the resulting fluorescence decay (time domain), however this requires a very rapid detector. A more

advanced method depends upon the sinusoidal oscillation of fluorescence arising from excitation by light with a sinusoidally modulated intensity. The lifetime of the fluorescence can then be determined from the demodulation and phase shift of the emitted light relative to the excitation beam by using equations derived from the Fourier Transform of a summation of exponential decays. Comparison to known environments such as the ternary complexes studied in this work and the Zn^{2+} metalloenzymes with well characterised active site structures could identify varying environments within the cell.

Further research into the formation of Zinquin-A-enzyme complexes would be of benefit as mentioned in Section 4.6. Several things also need clarification in the preliminary carbonic anhydrase study. First it is necessary to determine the concentration of adventitious Zn^{2+} present in the solid carbonic anhydrase used and therefore determine the if this is the cause of the spectrum shown for Zinquin-A with carbonic anhydrase in Figure 4.25. This could possibly be achieved via atomic absorption spectroscopy in this case, as the Zn^{2+} naturally present in the carbonic anhydrase active site would cause the Zn^{2+} concentration to be within the range measurable by this method. As each carbonic anhydrase molecule has one Zn^{2+}, the difference between the concentrations of carbonic anhydrase and Zn^{2+} determined by atomic absorption spectroscopy would give a value for the adventitious Zn^{2+} concentration. For this method to be effective, however, an accurate concentration of carbonic anhydrase is required.

To determine if Zinquin-A is able to enter the carbonic anhydrase active site, the enzymatic activity of carbonic anhydrase could be assayed in the presence of Zinquin-A. If the enzymatic activity is inhibited to some degree, it is likely that Zinquin-A can enter the active site despite being a *N*-substituted sulphonamide. Of course, other methods such as three dimensional NMR and maybe even mass spectrometry could also be used to identify the formation of a Zinquin-A-enzyme complex. One method that could prove effective is to separate the components of the Zinquin-A with carbonic anhydrase solution by their size using Sephadex gel filtration in a similar manner to that used by P. Coyle *et al* to study the binding of Zinquin-A to metallothionein.[3] The fluorescence due to Zinquin-A could then be measured for each fraction, indicating the relative concentrations of the large Zinquin-A-enzyme complex and the smaller [Zn(ZQA)] and $[Zn(ZQA)_2]^{2-}$ complexes which should have been separated due to their large size difference.

The molecular modelling carried out for this work, Section 4.5, could be expanded further. The number of starting points used for the ternary complexes could be increased, testing the assumption that the ligand forming the ternary complex with Zn^{2+} and Zinquin-A has the lowest energy conformation found for the ligand with Zn^{2+} and water. It is also possible to 'solvate' the complex, or surround it with solvent molecules, before minimisation to give a better idea of the solution state rather than the gaseous state. The next step would be to use INSIGHT II and DISCOVER 3 to model Zinquin-A binding to the Zn^{2+} in the active site of metalloenzymes with known structure such as carbonic anhydrase. This could indicate if the Zinquin-A does bind to the Zn^{2+}, if it is included in the active site, if it distorts or denatures the enzyme, if it binds with both nitrogen donors and even if it extracts the Zn^{2+} from the active site.

Unfortunately, due to time and resource limitations, it has not been possible to follow these avenues of research into Zinquin-A at this stage. As can be seen, there are many more interesting aspects of this useful intracellular Zn^{2+} probe to be investigated in the future.

6.2 : References

1. P. D. Zalewski, I. J. Forbes R. F. Seamark, R. Borlinghaus, W. H. Betts, S. F. Lincoln and A. D. Ward, *Chem. Biol.*, **1**, 153, 1994.

2. T. French, P. T. C. So, C. Y. Dong, K. M. Berland and E. Gratton, *Methods Cell Biol.*, **56**, 277, 1997.

3. P. Coyle, P. D. Zalewski, J. C. Philcox, I. J. Forbes, A. D. Ward, S. F. Lincoln, I. Mahadevan and A. M. Rofe, *Biochem. J.*, **303**, 781, 1994.

APPENDIX A

THE THEORY OF ELECTRONIC SPECTROSCOPY

The basis of all spectroscopy is the interaction of electromagnetic radiation with matter. The electromagnetic spectrum which is used for various types of spectroscopy is extremely large and encompasses energies between 10^{-3} and 10^{9} J mol^{-1} which can cause different changes in molecules including change in nuclear or electron spin, orientation, configuration, electron distribution or nuclear configuration. Due to the large range, usually only small regions of the spectrum are studied at one time, for example the ultraviolet and visible region, approximately 100 to 800 nm, which can cause changes in the electronic distribution of atoms and molecules as discussed below. The energy and wavelength of electromagnetic radiation are related by Equation A.1, and different units are used in different regions of the spectrum. As suggested above, the units typically used in the ultraviolet-visible region are nanometers (nm) or 10^{-9} m as this gives convenient axis numbers.

$$E = \frac{hc}{\lambda} = h\nu \qquad (A.1)$$

Where E is energy in Joules

h is Planck's constant = 6.63×10^{-34} Joules s

c is the speed of light = 3×10^{8} m s^{-1}

λ is the wavelength in m

and ν is the frequency in s^{-1}.

Every molecule has many electronic energy levels, with the lowest energy levels occupied by electrons. When irradiated with electromagnetic radiation (light), if the energy of that radiation ($h\nu$) corresponds exactly to the energy difference between an occupied and a higher energy, unoccupied electronic state ($E'' - E'$), the energy is absorbed, causing the promotion of an electron to the higher energy, or excited, electronic state. This is shown schematically in Figure A.1. As can be seen in Figure A.1, each electronic level (S_n or T_n) has a fine structure of vibrational energy levels ($v = n$) and upon electronic excitation, the molecule is usually vibrationally excited. As the vibrational energy levels are close together, a single electronic transition can show vibrational fine structure arising from excitation to different vibrational

levels in the same electronic level. This fine structure is normally only seen clearly in spectra determined in the gas phase, with the slower rotation of the molecules tending to mask the fine structure in pure liquids or in solution. It is possible, however, to use resolution enhancement techniques to determine the vibrational fine structure from solution and liquid spectra.[1]

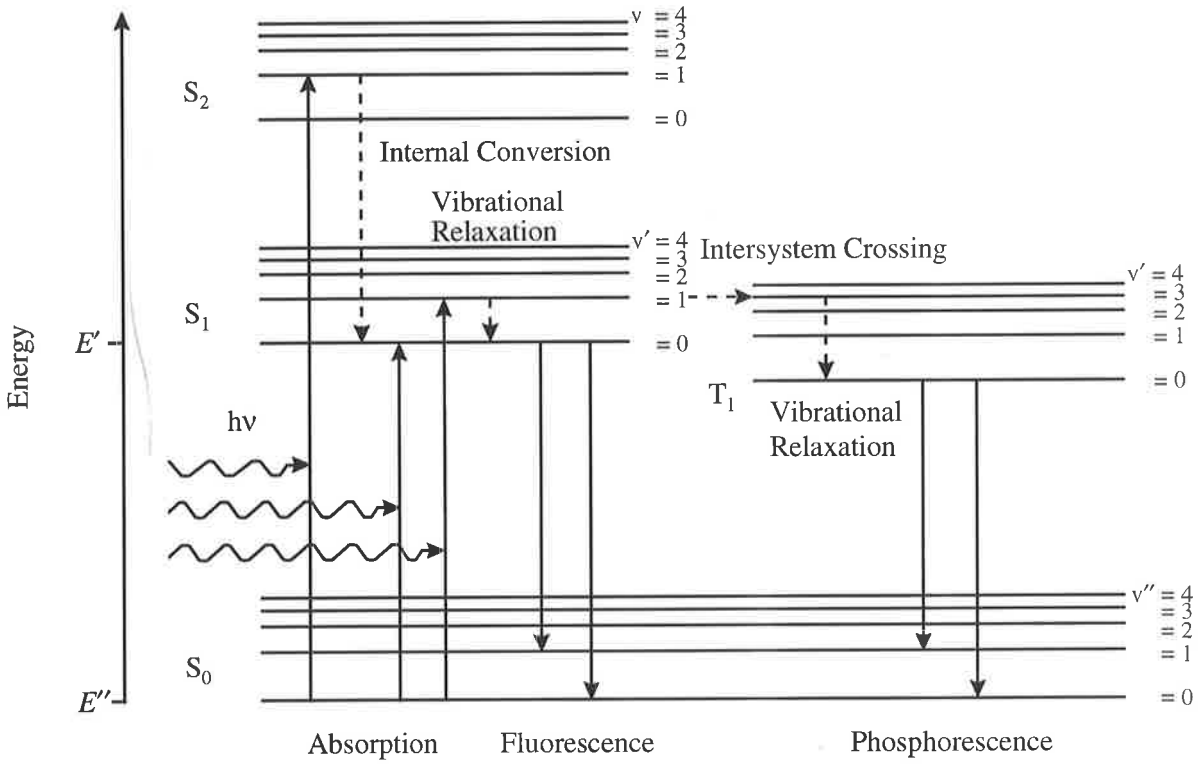

Figure A.1 : A schematic energy level diagram that illustrates the electronic transitions that occur for some molecules.

After absorbing electromagnetic radiation (hν), the molecule is in a less stable, excited state and will therefore tend to return to the ground electronic state (S_0). This can occur by several pathways. The energy can be re-emitted as light with the same energy (hν) as the incident electromagnetic radiation, causing no net effect on the molecule, or non-radiative decay (loss of energy without emission of light) can occur, followed by emission of light with an energy less than the incident electromagnetic radiation. Within an excited electronic state, vibrational relaxation (energy loss through inelastic collisions) occurs rapidly in most molecules, and hence, although it is theoretically possible for emission to occur from any excited vibrational level, it usually occurs from the ground vibrational level of the excited electronic state. Emissions of this type are called fluorescence, as shown in Figure A.1, and the light produced is of a longer wavelength (lower energy) than the light absorbed due to the vibrational

relaxation. It is possible for emission to occur to excited vibrational levels of the ground electronic state, which gives fluorescence a similar vibrational fine structure to absorbance, however it is the vibronic structure of the ground electronic state that is probed in this case, rather than that of the excited electronic state.

If a very large amount of energy is absorbed, it is possible to excite the molecule to an even higher excited electronic state as shown in Figure A.1. Emission can then occur from a vibrational level in this electronic state, or internal conversion can occur followed by emission from a lower energy excited electronic state. Internal conversion is the non-radiative transfer between electronic states of the same multiplicity, for example, the transition from S_2 to S_1 shown in Figure A.1, where both states are singlet electronic states. This can be caused by the loss of energy through collisions (as in the example shown) or by the overlapping of a low energy vibrational level in the higher energy electronic state and a high energy vibrational level in the lower energy electronic state. Intersystem crossing is more common between two excited electronic states rather than an excited electronic state and the ground electronic state as the energies of electronic states become closer with an increase in energy.

Phosphorescence is also depicted schematically in Figure A.1. This is similar to fluorescence in that it is an emission of light which occurs from the ground vibrational level of an excited electronic state, however it has a much longer lifetime. For phosphorescence to occur, there must be a triplet excited electronic state with a vibrational energy level that corresponds in energy to a vibrational energy level in the singlet excited electronic state. It is then possible for intersystem crossing to occur which involves a transition from the singlet to triplet state which is only weakly allowed due to the change in spin state. Once in the triplet state, vibrational relaxation occurs rapidly, leaving the molecule in the ground vibrational level of the excited triplet electronic state. As the relaxation to the ground electronic state is also spin-forbidden, it occurs very slowly, and hence phosphorescence has a long lifetime.

Not all absorption or emission transitions to different vibrational states occur with the same intensity. The intensity of light resulting from a transition depends upon the probability of that transition occurring. This probability is called the transition moment of a molecule and is described by Equation A.2 below.

$$TM = \int \Psi_a \hat{M} \Psi_b \, d\tau \qquad (A.2)$$

Where TM is the transition moment

Ψ_a and Ψ_b are the wave equations describing the energy levels between which the transition occurs

$\hat{M}$ is the dipole moment operator

and τ is lifetime.

This can be visualised for a simple, diatomic molecule by considering the shapes of the squared wave equations for each vibrational energy level as these give the probability function, or distribution. This is shown schematically in Figure A.2 where the electronic energy level is represented as a potential energy surface or Morse curve which describes the change in energy with a change in internuclear distance and the probability functions of the vibrational levels are shown within these. The nuclei are most likely to be found at separations given by the maxima of the curve for each vibrational state, *ie*, at the turning points.

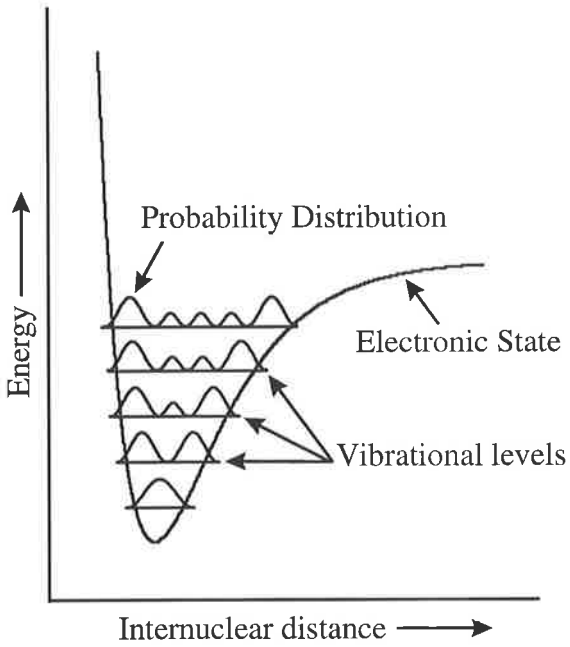

Figure A.2 : A schematic diagram of the probability distribution for a diatomic molecule according to quantum theory.

The Franck-Condon principle states that electronic transitions are very rapid (~10^{-15}s) and therefore internuclear distances in a vibrating molecule do not change appreciably during an electronic transition. This means that when depicting electronic transitions on diagrams similar to Figure A.2, the transition is drawn as a vertical line, indicating no change in internuclear distance. Within a vibrational level, the transition will originate from a maximum in the probability function as shown in Figure A.3 and may terminate in any of the vibrational levels that exist at that internuclear distance. The greater the probability function of a vibrational level at that distance, the greater the overlap of the two wave equations and therefore the greater the transition moment and the intensity of the transition. Hence the series of transitions observed will increase in intensity to a maximum and then decrease as the probability function overlaps differ. A change in the relative positions of the ground and excited electronic states will result in a change in the relative intensities of the observed transitions as shown in Figure A.3. Significant broadening of the vibrational transitions is shown in Figure A.3, which would result in the more featureless spectra characteristic of solutions. The case for absorption is shown, however the same principle applies for emission, with the emission originating from the maximum of the probability function of the ground vibrational level in the excited electronic state.

Although these concepts pertain to diatomic molecules, it is possible to expand them, to some extent, to polyatomic molecules. Even though the diagrams increase in the number of dimensions and the squared wave functions increase in complexity, the concepts of probability function overlaps, and the Franck-Condon principle remain relevant.

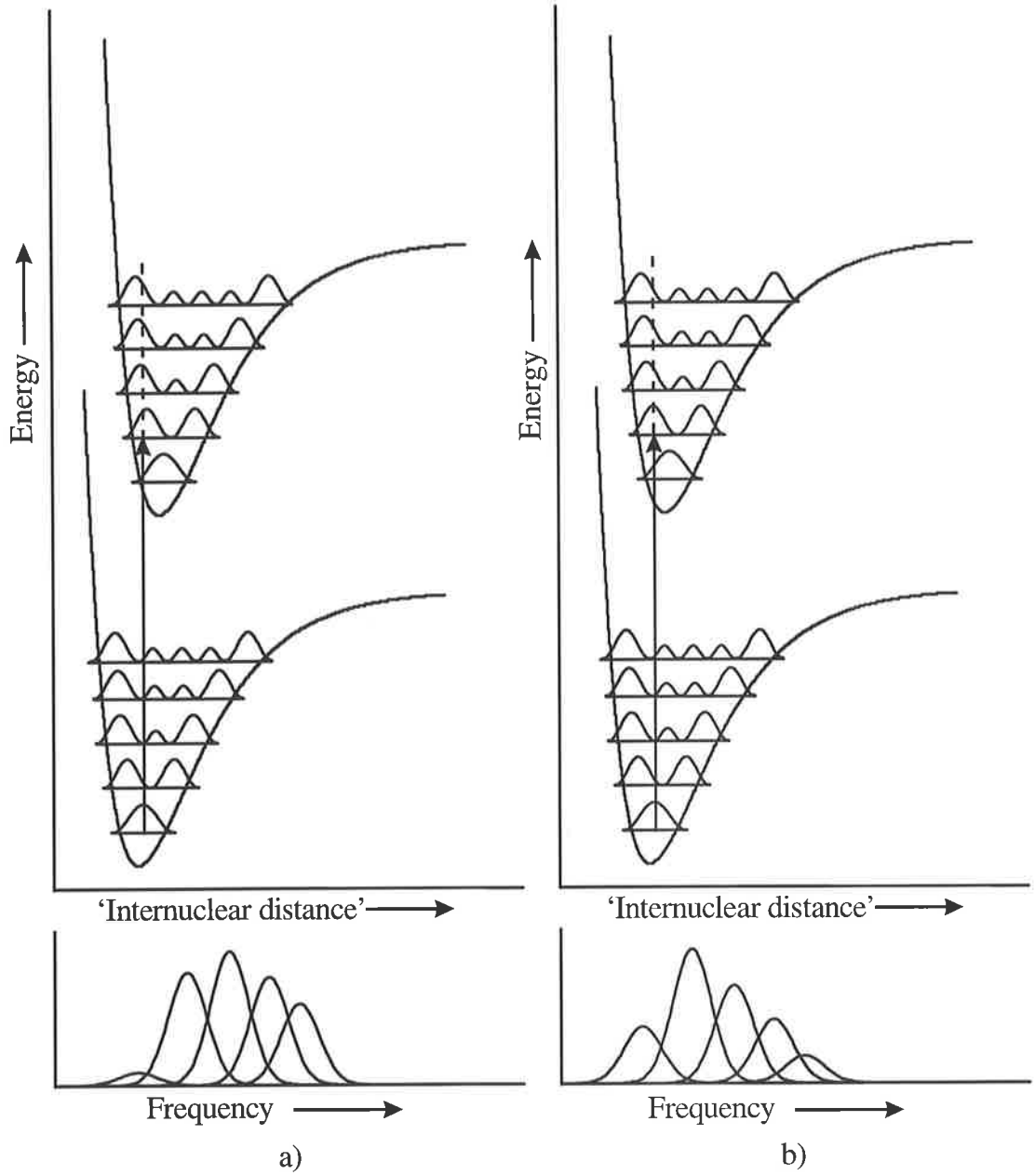

Figure A.3 : A schematic diagram showing the change in probability function overlap, and therefore spectrum, upon moving the excited electronic state relative to the ground electronic state. The excited electronic state is shifted towards slightly shorter internuclear distances in b).

Reference

1. M. A. Snoswell and T. Kurucsev, *J. Cryst. and Spec. Res.*, **22**, 679, 1992.

APPENDIX B

THE FITTING OF GAUSSIAN CURVES TO TERNARY COMPLEX SPECTRA

As mentioned in section 4.4, the molar absorbance and adjusted molar fluorescence spectra obtained for the ternary and Zn^{2+} complexes of Zinquin-A were analysed with a resolution enhancement algorithm and were subsequently fitted for Gaussian curves which are likely to represent the individual transitions that produce the observed absorbance or fluorescence.[1] The complete results obtained from using the MATLAB program BANDANAL[2] are included here. The experimental data is represented as points, the spectrum fitted to these points is a line passing near to them and the remaining curves represent the Gaussian curves which add up to give the fitted spectrum. It is interesting to note the similarity in the number and position of these Gaussian curves especially for the fluorescence spectra, as discussed in section 4.4. The wavelength and intensity at the maximum of each Gaussian curve is listed in the table to the right of each spectrum studied. The curves are labelled in each table from the left to the right of the associated figure. The half band width of the fitted Gaussian curves and the sum of the squared deviations (ssd) for the fit are also shown for each spectrum.

1. M. A. Snoswell and T. Kurucsev, *J.Cryst. and Spec. Res.*, **22**, 679, 1992.

2. A MATLAB program, T. Kurucsev, University of Adelaide, South Australia, Australia. Refer to Appendix E.

B.1 : Fluorescence Spectra

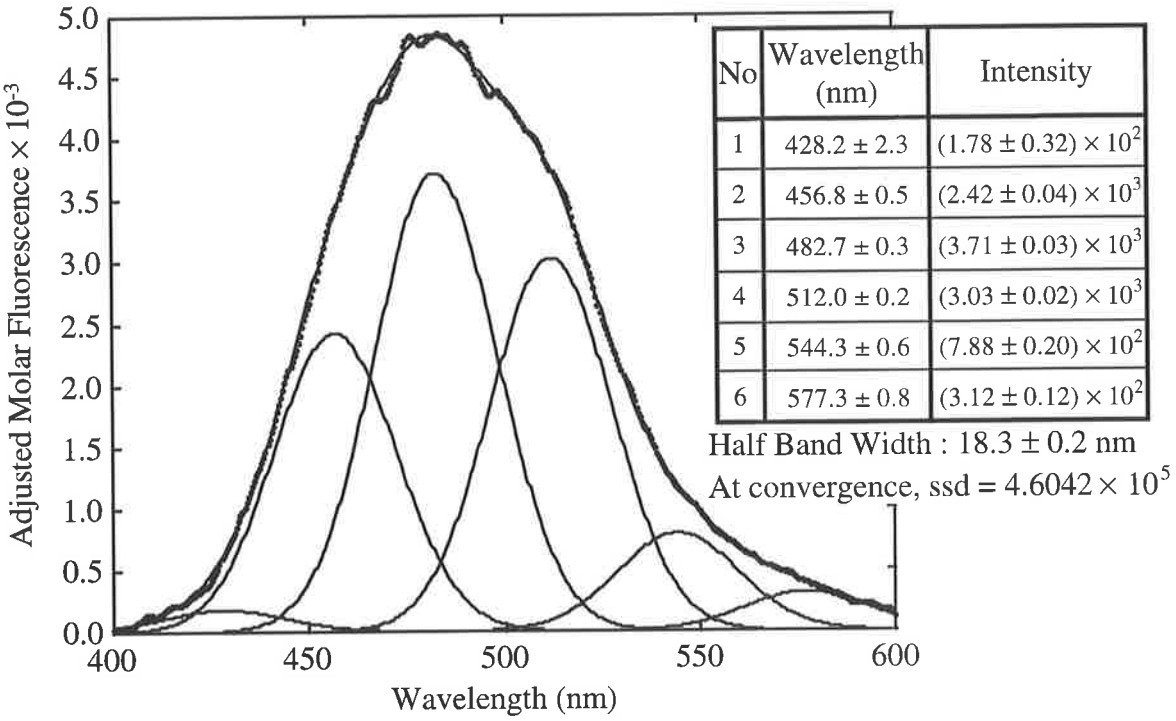

No	Wavelength (nm)	Intensity
1	428.2 ± 2.3	(1.78 ± 0.32) × 10^2
2	456.8 ± 0.5	(2.42 ± 0.04) × 10^3
3	482.7 ± 0.3	(3.71 ± 0.03) × 10^3
4	512.0 ± 0.2	(3.03 ± 0.02) × 10^3
5	544.3 ± 0.6	(7.88 ± 0.20) × 10^2
6	577.3 ± 0.8	(3.12 ± 0.12) × 10^2

Half Band Width : 18.3 ± 0.2 nm

At convergence, ssd = 4.6042 × 10^5

Figure B.1 : The fitting of Gaussian curves to the adjusted molar fluorescence spectrum of [Zn(cyclen)ZQA].

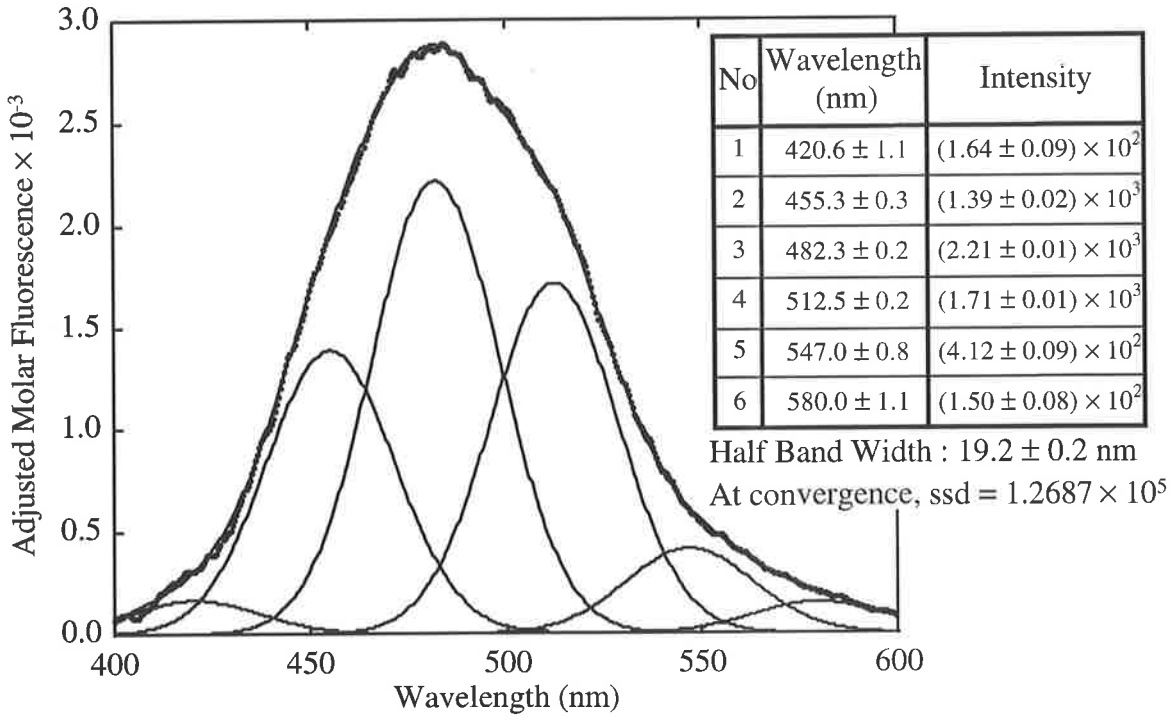

No	Wavelength (nm)	Intensity
1	420.6 ± 1.1	(1.64 ± 0.09) × 10^2
2	455.3 ± 0.3	(1.39 ± 0.02) × 10^3
3	482.3 ± 0.2	(2.21 ± 0.01) × 10^3
4	512.5 ± 0.2	(1.71 ± 0.01) × 10^3
5	547.0 ± 0.8	(4.12 ± 0.09) × 10^2
6	580.0 ± 1.1	(1.50 ± 0.08) × 10^2

Half Band Width : 19.2 ± 0.2 nm

At convergence, ssd = 1.2687 × 10^5

Figure B.2 : The fitting of Gaussian curves to the adjusted molar fluorescence spectrum of [Zn(cyclam)ZQA].

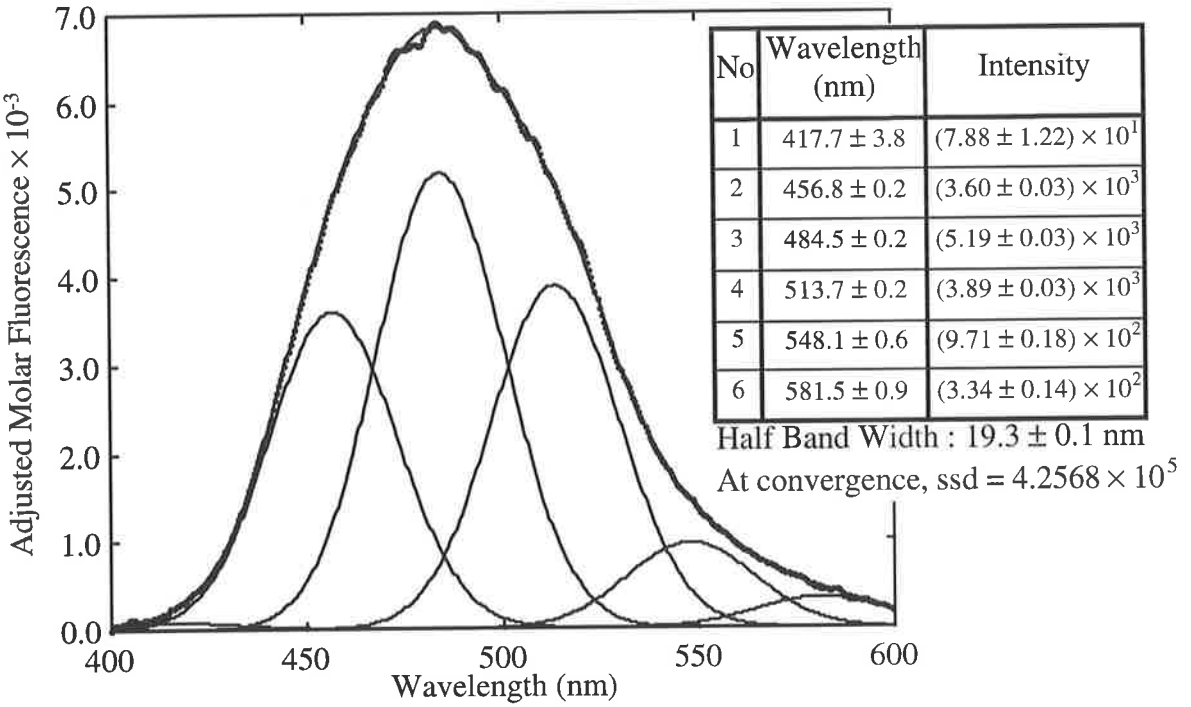

No	Wavelength (nm)	Intensity
1	417.7 ± 3.8	(7.88 ± 1.22) × 10¹
2	456.8 ± 0.2	(3.60 ± 0.03) × 10³
3	484.5 ± 0.2	(5.19 ± 0.03) × 10³
4	513.7 ± 0.2	(3.89 ± 0.03) × 10³
5	548.1 ± 0.6	(9.71 ± 0.18) × 10²
6	581.5 ± 0.9	(3.34 ± 0.14) × 10²

Figure B.3 : The fitting of Gaussian curves to the adjusted molar fluorescence spectrum of [Zn(tacn)ZQA].

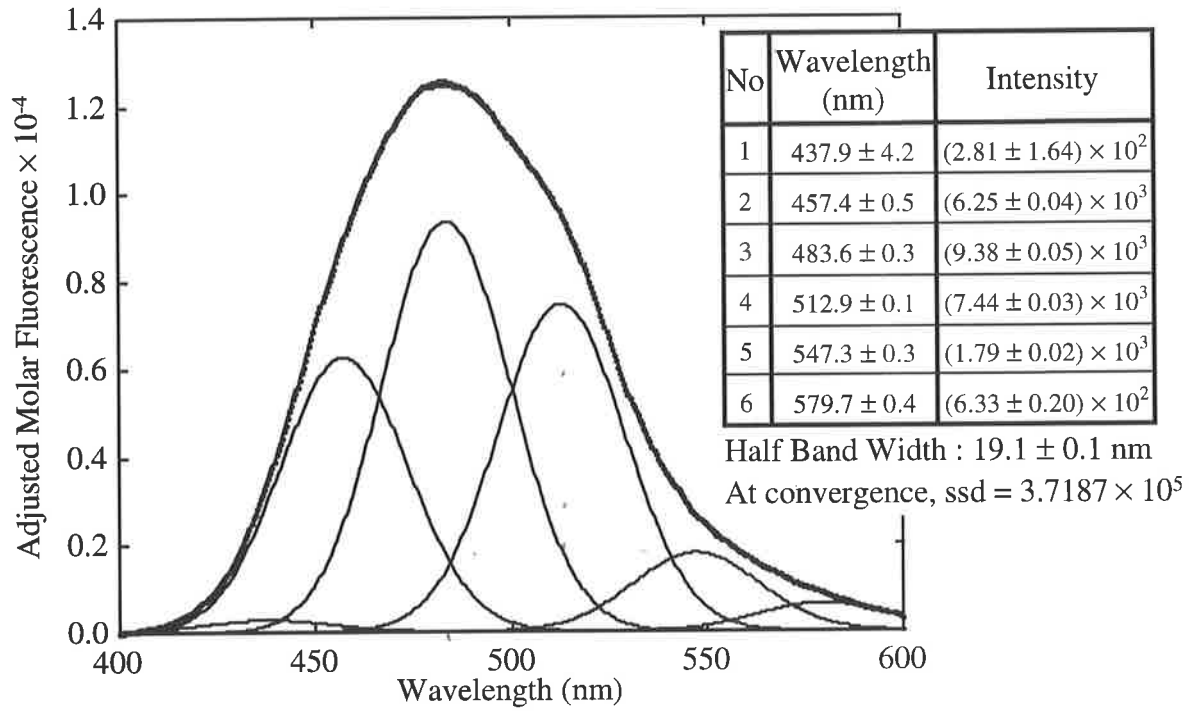

No	Wavelength (nm)	Intensity
1	437.9 ± 4.2	(2.81 ± 1.64) × 10²
2	457.4 ± 0.5	(6.25 ± 0.04) × 10³
3	483.6 ± 0.3	(9.38 ± 0.05) × 10³
4	512.9 ± 0.1	(7.44 ± 0.03) × 10³
5	547.3 ± 0.3	(1.79 ± 0.02) × 10³
6	579.7 ± 0.4	(6.33 ± 0.20) × 10²

Figure B.4 : The fitting of Gaussian curves to the adjusted molar fluorescence spectrum of [Zn(tacdo)ZQA].

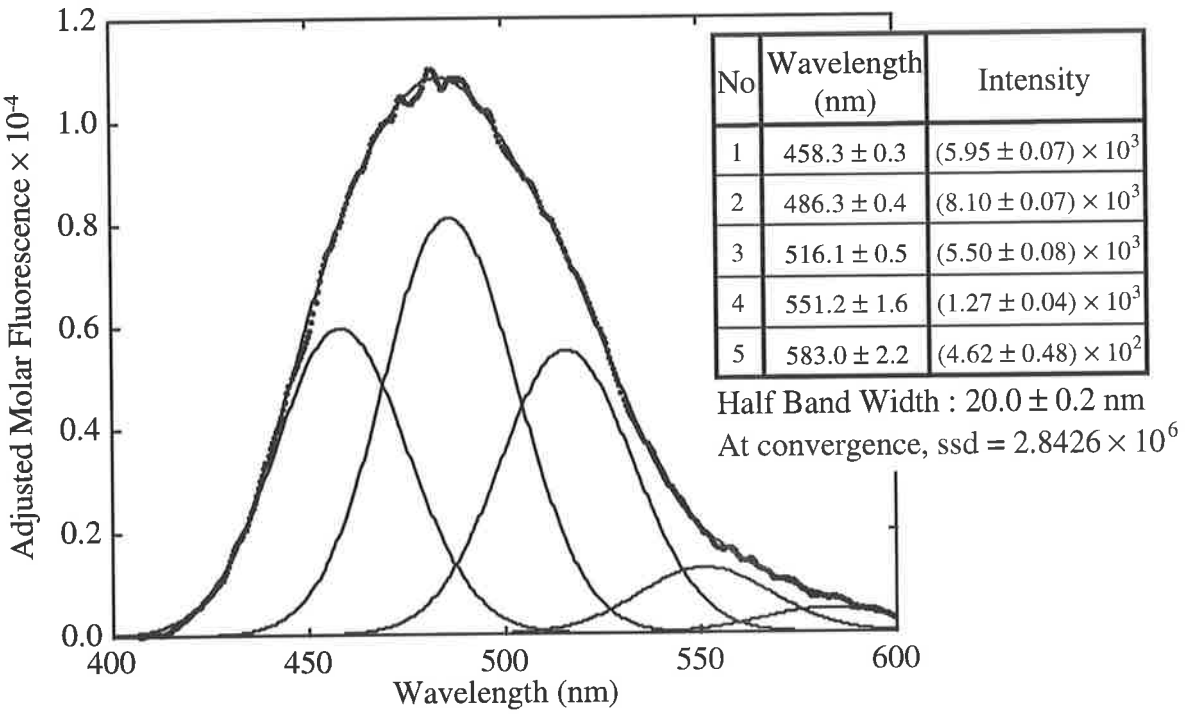

No	Wavelength (nm)	Intensity
1	458.3 ± 0.3	(5.95 ± 0.07) × 10³
2	486.3 ± 0.4	(8.10 ± 0.07) × 10³
3	516.1 ± 0.5	(5.50 ± 0.08) × 10³
4	551.2 ± 1.6	(1.27 ± 0.04) × 10³
5	583.0 ± 2.2	(4.62 ± 0.48) × 10²

Figure B.5 : The fitting of Gaussian curves to the adjusted molar fluorescence spectrum of $[Zn(tacdo)ZQA.H]^+$.

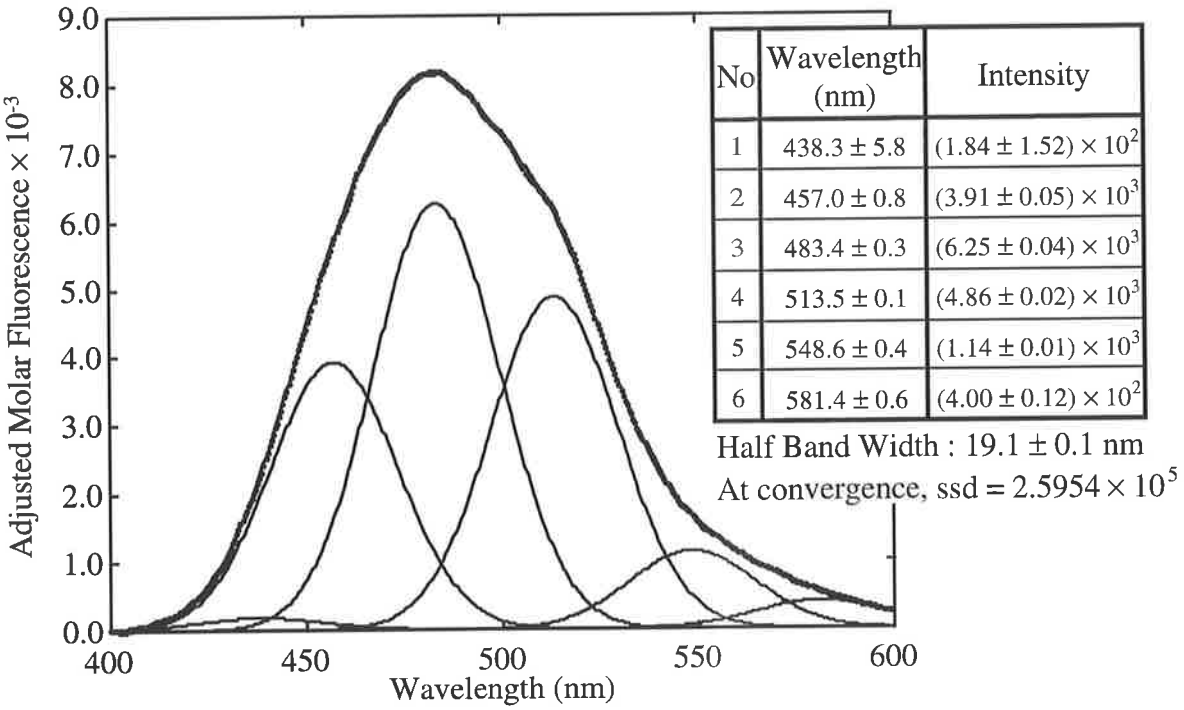

No	Wavelength (nm)	Intensity
1	438.3 ± 5.8	(1.84 ± 1.52) × 10²
2	457.0 ± 0.8	(3.91 ± 0.05) × 10³
3	483.4 ± 0.3	(6.25 ± 0.04) × 10³
4	513.5 ± 0.1	(4.86 ± 0.02) × 10³
5	548.6 ± 0.4	(1.14 ± 0.01) × 10³
6	581.4 ± 0.6	(4.00 ± 0.12) × 10²

Figure B.6 : The fitting of Gaussian curves to the adjusted molar fluorescence spectrum of [Zn(tren)ZQA].

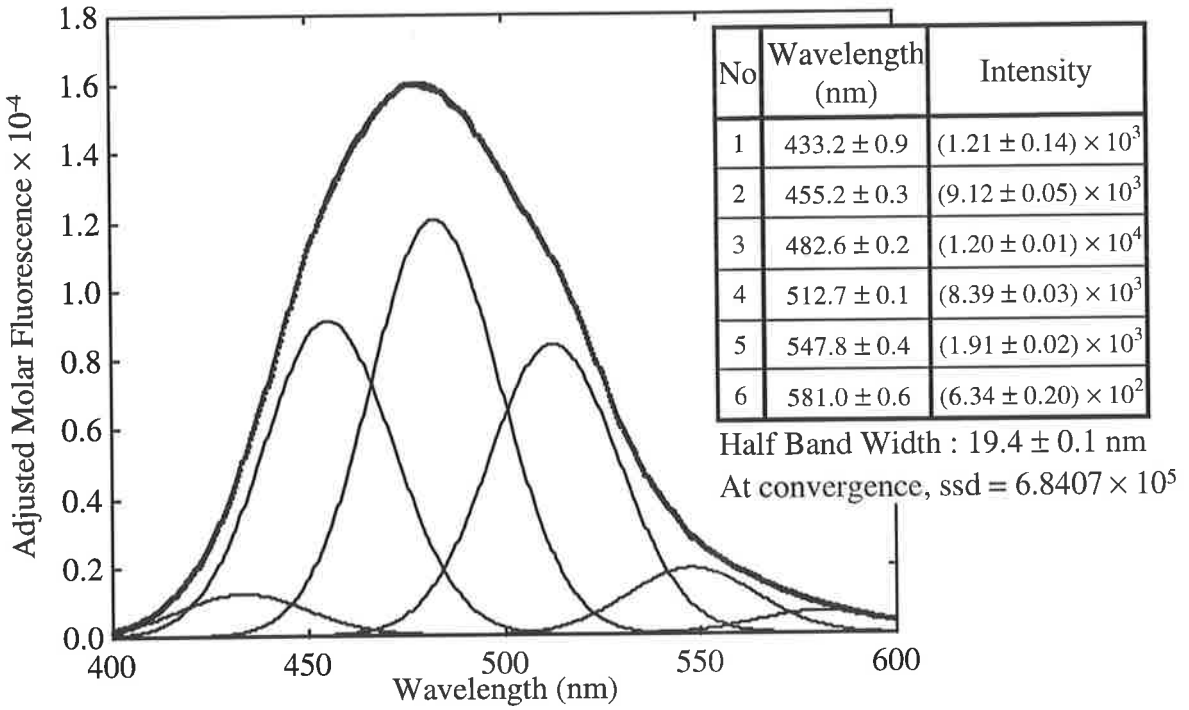

No	Wavelength (nm)	Intensity
1	433.2 ± 0.9	(1.21 ± 0.14) × 10^3
2	455.2 ± 0.3	(9.12 ± 0.05) × 10^3
3	482.6 ± 0.2	(1.20 ± 0.01) × 10^4
4	512.7 ± 0.1	(8.39 ± 0.03) × 10^3
5	547.8 ± 0.4	(1.91 ± 0.02) × 10^3
6	581.0 ± 0.6	(6.34 ± 0.20) × 10^2

Half Band Width : 19.4 ± 0.1 nm

At convergence, ssd = 6.8407 × 10^5

Figure B.7 : The fitting of Gaussian curves to the adjusted molar fluorescence spectrum of $[Zn(NTA)ZQA]^{3-}$.

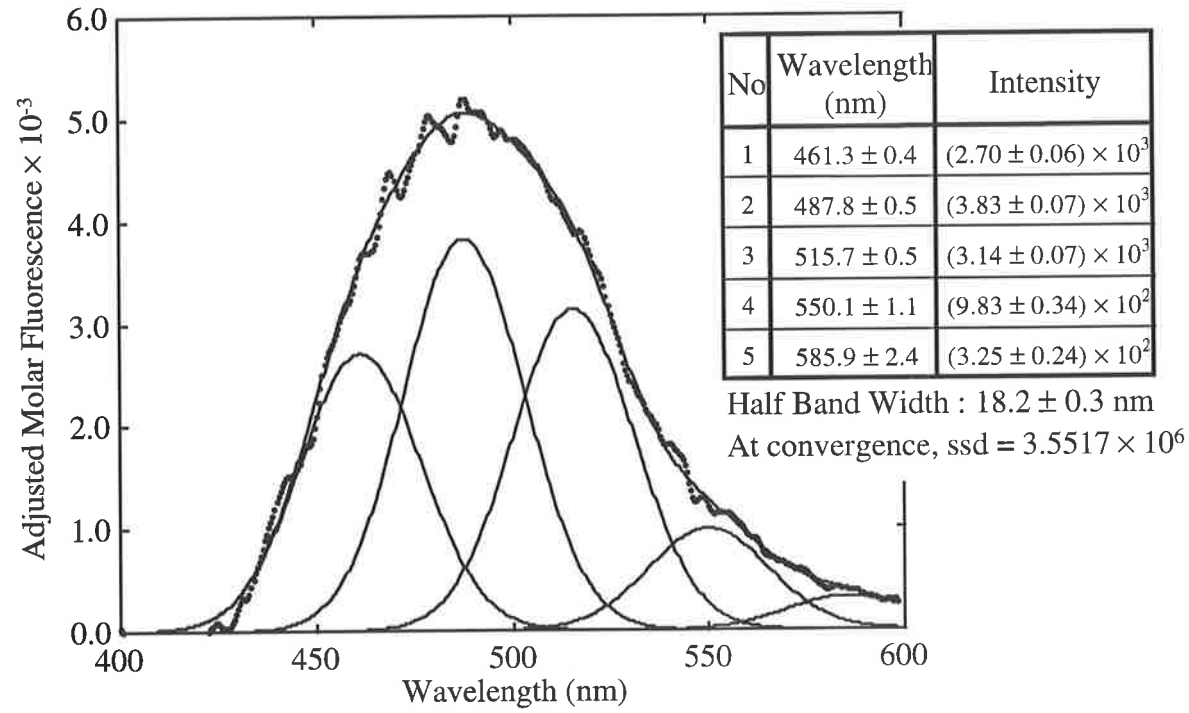

No	Wavelength (nm)	Intensity
1	461.3 ± 0.4	(2.70 ± 0.06) × 10^3
2	487.8 ± 0.5	(3.83 ± 0.07) × 10^3
3	515.7 ± 0.5	(3.14 ± 0.07) × 10^3
4	550.1 ± 1.1	(9.83 ± 0.34) × 10^2
5	585.9 ± 2.4	(3.25 ± 0.24) × 10^2

Half Band Width : 18.2 ± 0.3 nm

At convergence, ssd = 3.5517 × 10^6

Figure B.8 : The fitting of Gaussian curves to the adjusted molar fluorescence spectrum of $[Zn(NTA)ZQA.H]^{2-}$.

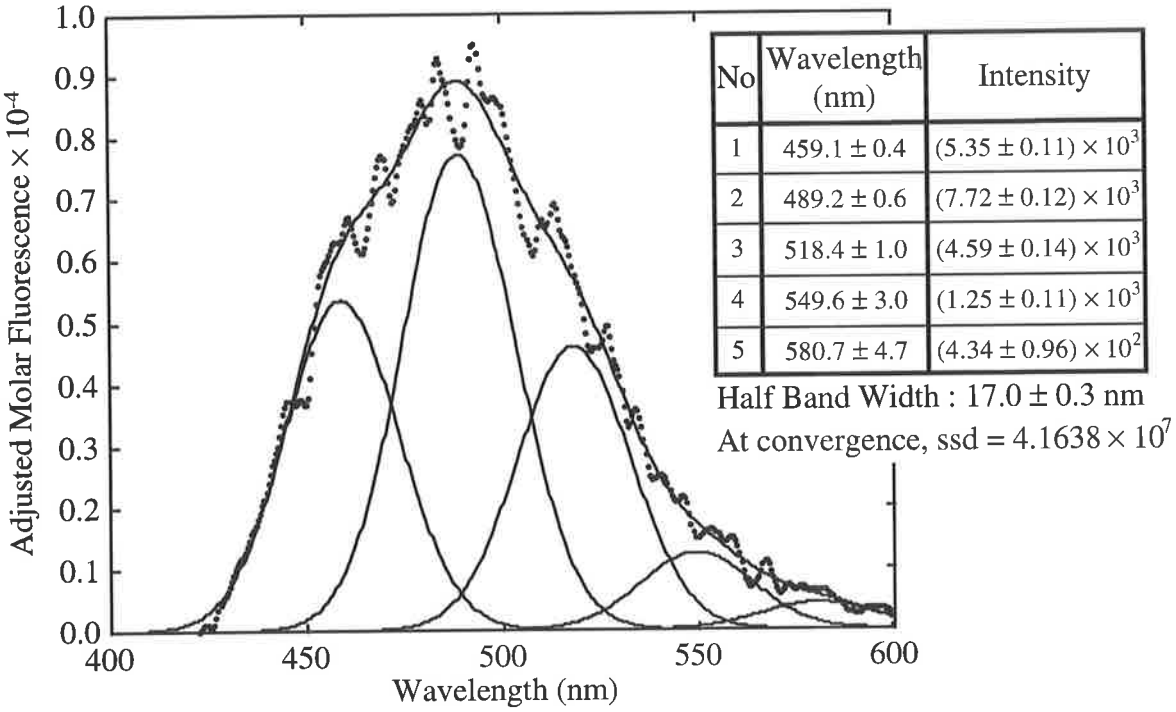

No	Wavelength (nm)	Intensity
1	459.1 ± 0.4	(5.35 ± 0.11) × 10^3
2	489.2 ± 0.6	(7.72 ± 0.12) × 10^3
3	518.4 ± 1.0	(4.59 ± 0.14) × 10^3
4	549.6 ± 3.0	(1.25 ± 0.11) × 10^3
5	580.7 ± 4.7	(4.34 ± 0.96) × 10^2

Half Band Width : 17.0 ± 0.3 nm

At convergence, ssd = 4.1638 × 10^7

Figure B.9 : The fitting of Gaussian curves to the adjusted molar fluorescence spectrum of $[Zn(TEA)ZQA.H_{-1}]^-$.

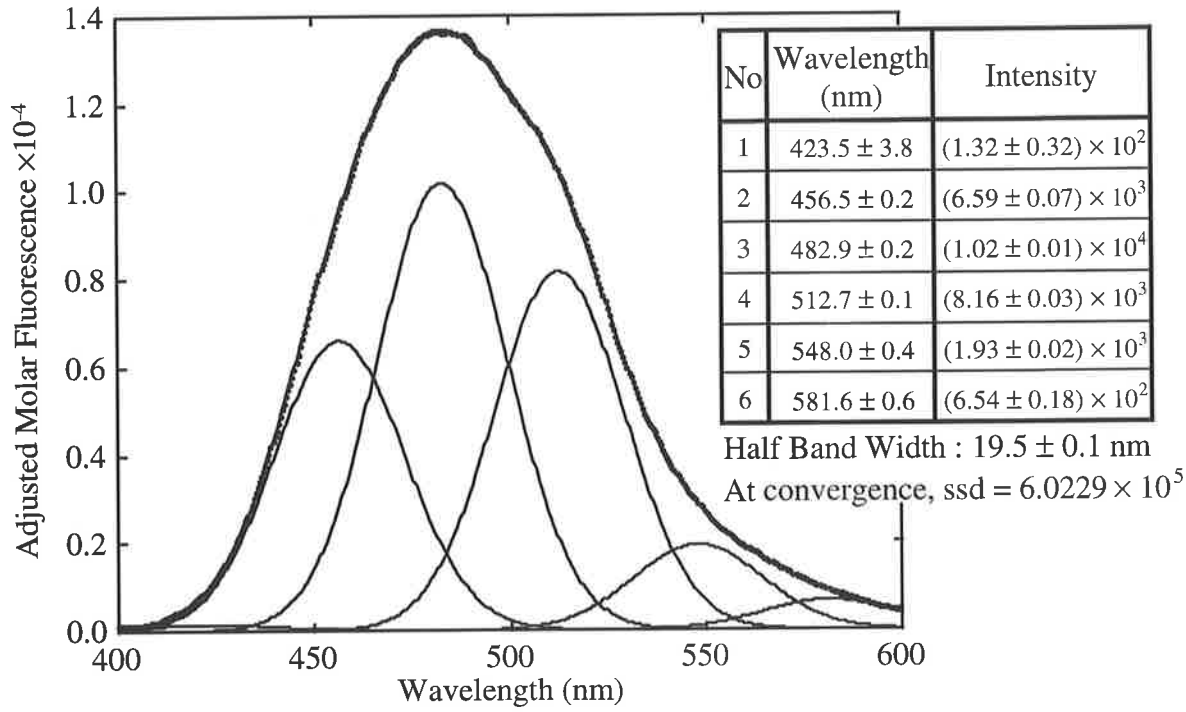

No	Wavelength (nm)	Intensity
1	423.5 ± 3.8	(1.32 ± 0.32) × 10^2
2	456.5 ± 0.2	(6.59 ± 0.07) × 10^3
3	482.9 ± 0.2	(1.02 ± 0.01) × 10^4
4	512.7 ± 0.1	(8.16 ± 0.03) × 10^3
5	548.0 ± 0.4	(1.93 ± 0.02) × 10^3
6	581.6 ± 0.6	(6.54 ± 0.18) × 10^2

Half Band Width : 19.5 ± 0.1 nm

At convergence, ssd = 6.0229 × 10^5

Figure B.10 : The fitting of Gaussian curves to the adjusted molar fluorescence spectrum of [Zn(ZQA)].

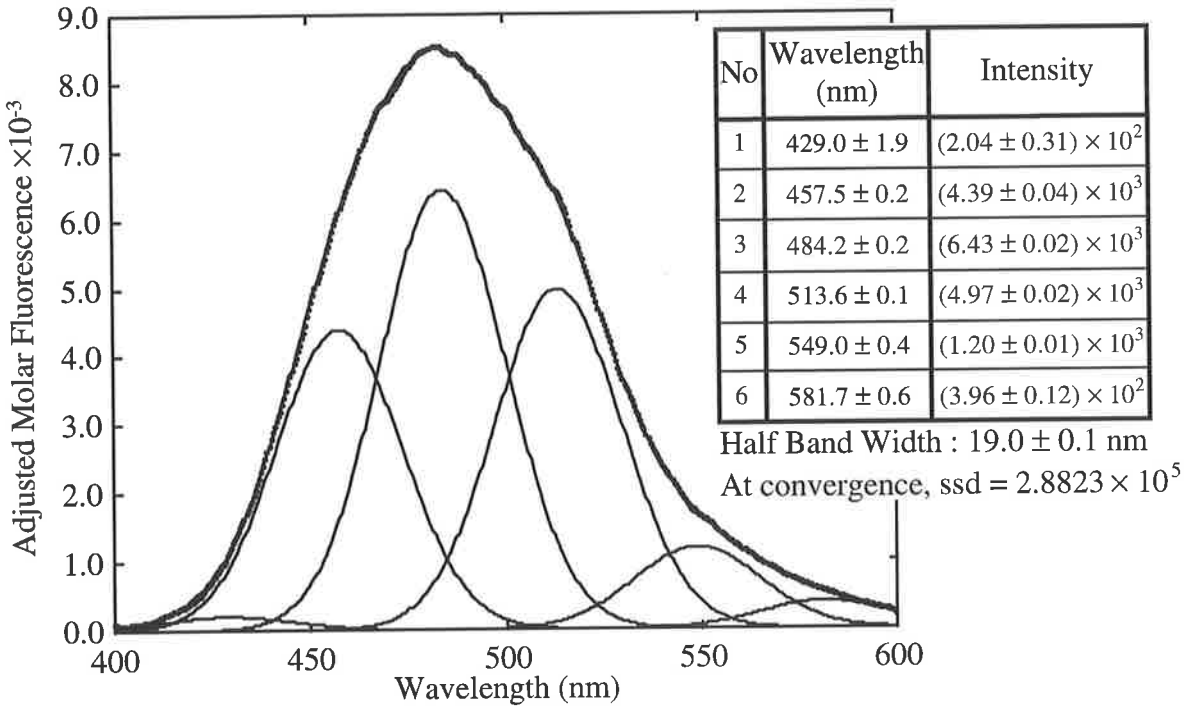

No	Wavelength (nm)	Intensity
1	429.0 ± 1.9	(2.04 ± 0.31) × 10^2
2	457.5 ± 0.2	(4.39 ± 0.04) × 10^3
3	484.2 ± 0.2	(6.43 ± 0.02) × 10^3
4	513.6 ± 0.1	(4.97 ± 0.02) × 10^3
5	549.0 ± 0.4	(1.20 ± 0.01) × 10^3
6	581.7 ± 0.6	(3.96 ± 0.12) × 10^2

Figure B.11 : The fitting of Gaussian curves to the adjusted molar fluorescence spectrum of $[Zn(ZQA)_2]^{2-}$.

B.2 : Ultraviolet-Visible Absorption Spectra

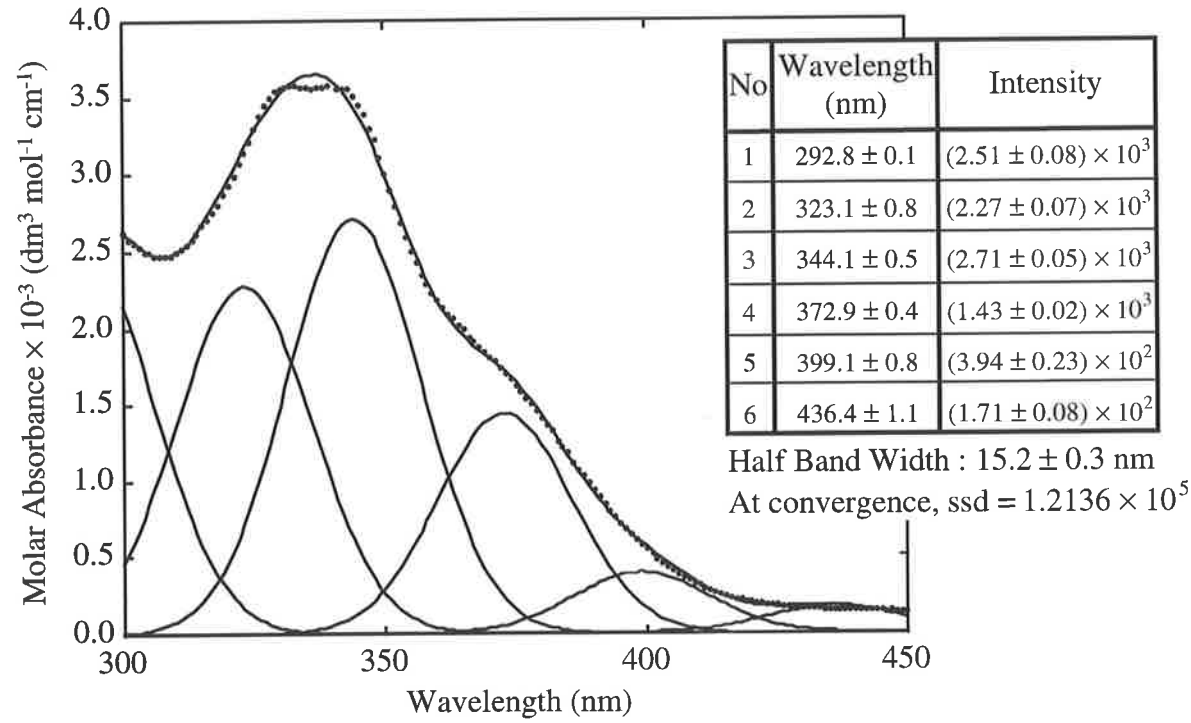

No	Wavelength (nm)	Intensity
1	292.8 ± 0.1	(2.51 ± 0.08) × 10^3
2	323.1 ± 0.8	(2.27 ± 0.07) × 10^3
3	344.1 ± 0.5	(2.71 ± 0.05) × 10^3
4	372.9 ± 0.4	(1.43 ± 0.02) × 10^3
5	399.1 ± 0.8	(3.94 ± 0.23) × 10^2
6	436.4 ± 1.1	(1.71 ± 0.08) × 10^2

Figure B.12 : The fitting of Gaussian curves to the molar absorbance spectrum of [Zn(cyclen)ZQA] in the 300 to 450 nm region.

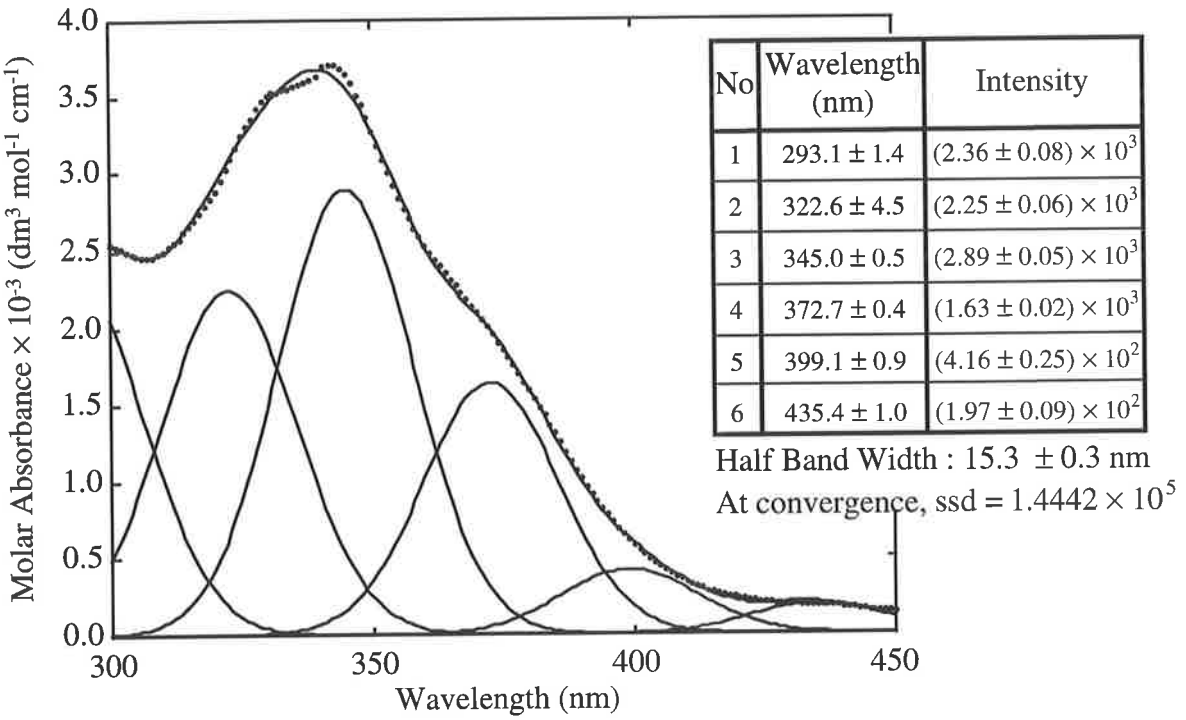

Figure B.13 : The fitting of Gaussian curves to the molar absorbance spectrum of [Zn(cyclam)ZQA] in the 300 to 450 nm region.

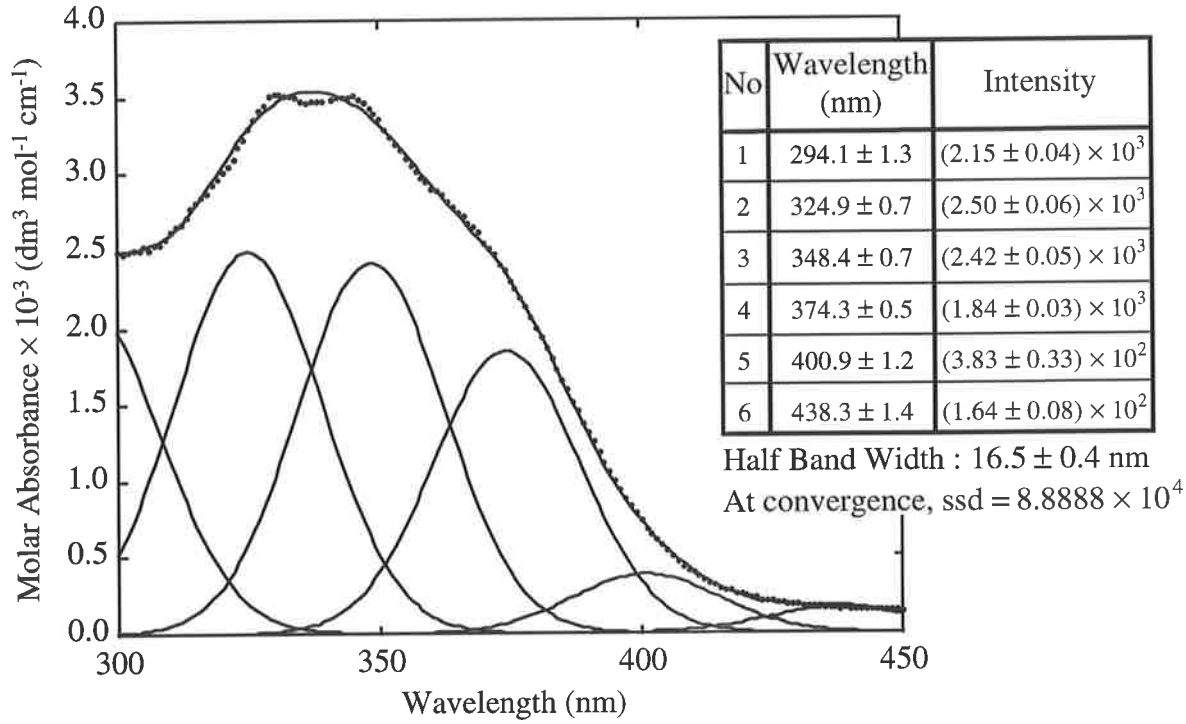

Figure B.14 : The fitting of Gaussian curves to the molar absorbance spectrum of [Zn(tacn)ZQA] in the 300 to 450 nm region.

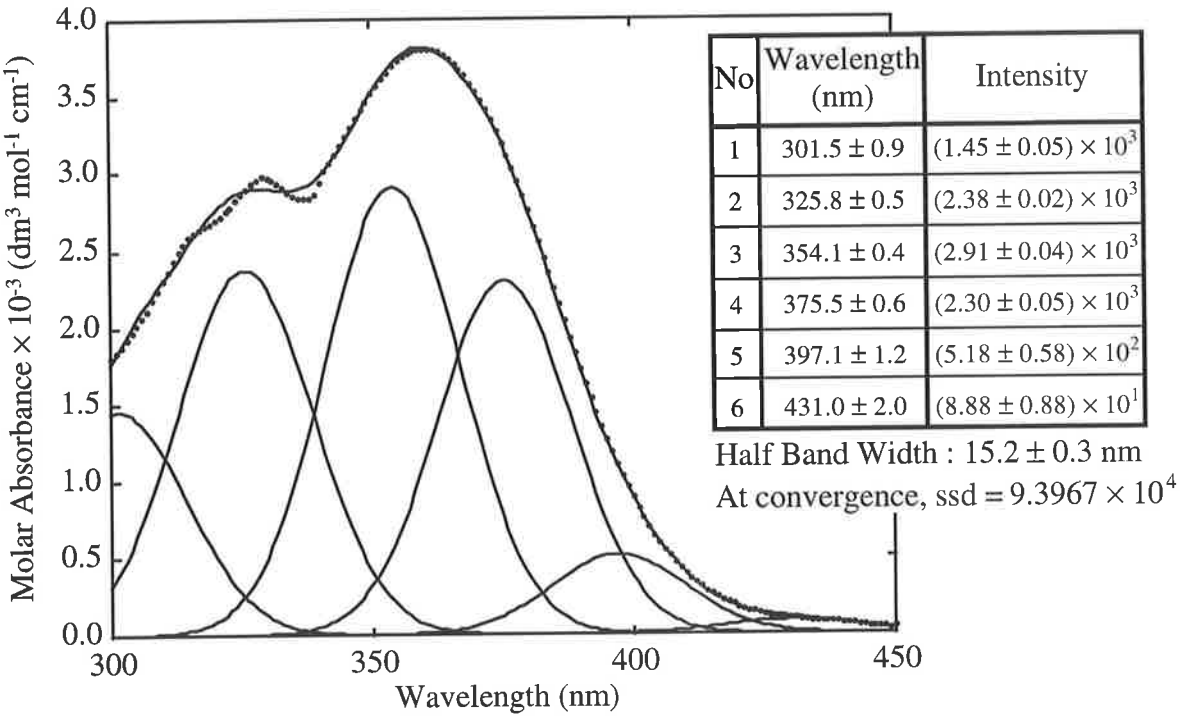

Figure B.15 : The fitting of Gaussian curves to the molar absorbance spectrum of [Zn(tacdo)ZQA] in the 300 to 450 nm region.

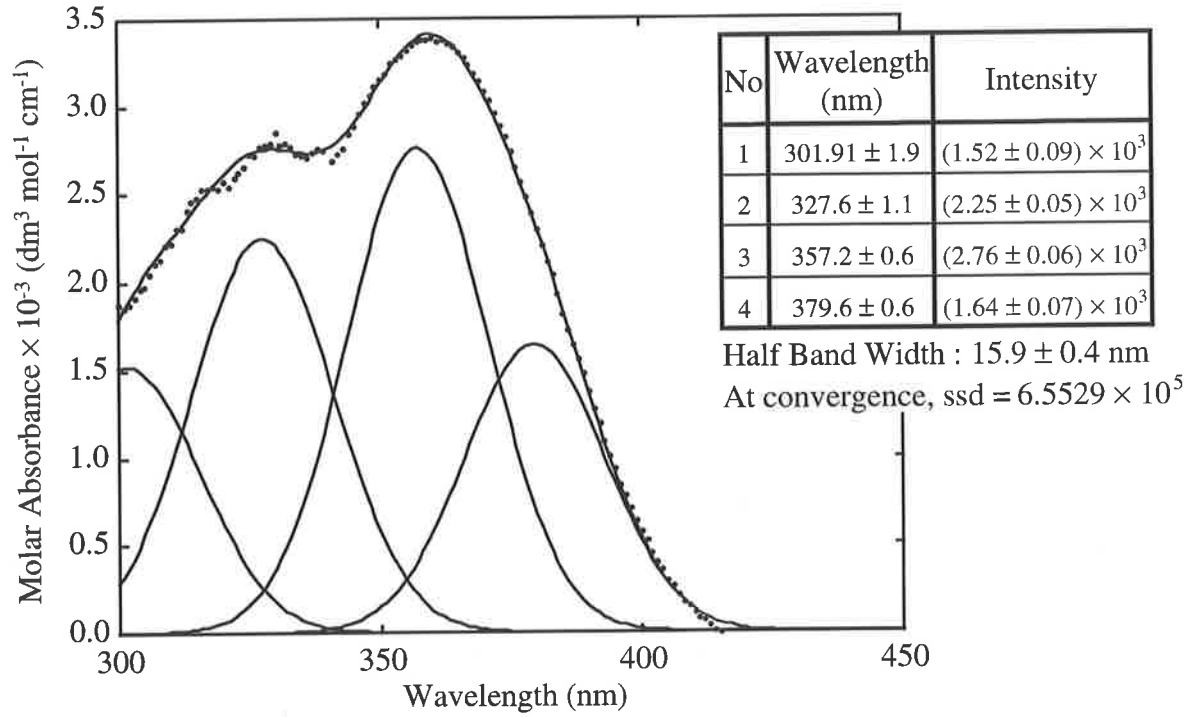

Figure B.16 : The fitting of Gaussian curves to the molar absorbance spectrum of $[Zn(tacdo)ZQA.H]^+$ in the 300 to 450 nm region.

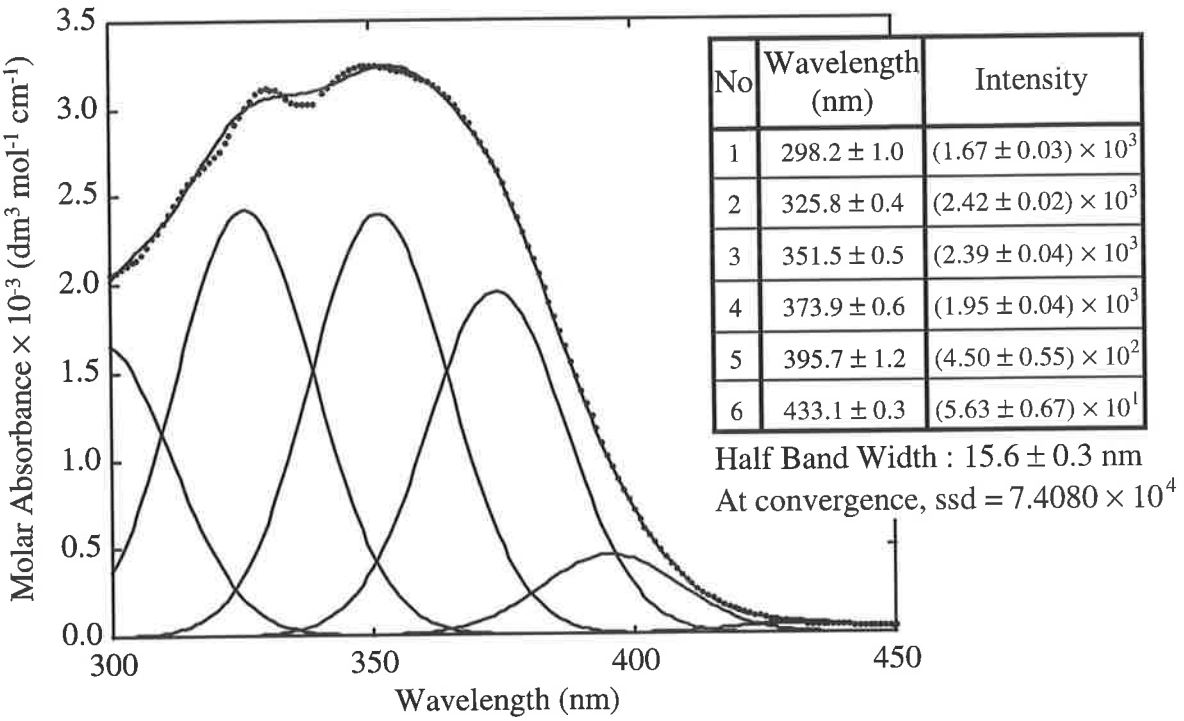

No	Wavelength (nm)	Intensity
1	298.2 ± 1.0	(1.67 ± 0.03) × 10^3
2	325.8 ± 0.4	(2.42 ± 0.02) × 10^3
3	351.5 ± 0.5	(2.39 ± 0.04) × 10^3
4	373.9 ± 0.6	(1.95 ± 0.04) × 10^3
5	395.7 ± 1.2	(4.50 ± 0.55) × 10^2
6	433.1 ± 0.3	(5.63 ± 0.67) × 10^1

Figure B.17 : The fitting of Gaussian curves to the molar absorbance spectrum of [Zn(tren)ZQA] in the 300 to 450 nm region.

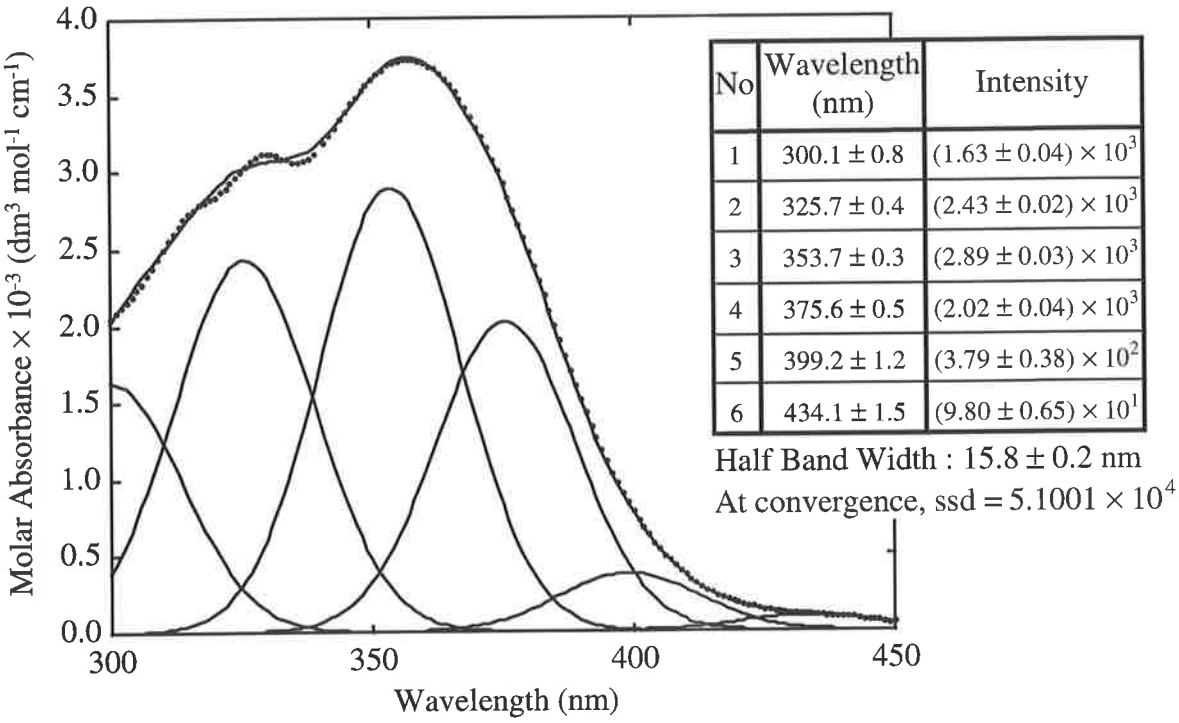

No	Wavelength (nm)	Intensity
1	300.1 ± 0.8	(1.63 ± 0.04) × 10^3
2	325.7 ± 0.4	(2.43 ± 0.02) × 10^3
3	353.7 ± 0.3	(2.89 ± 0.03) × 10^3
4	375.6 ± 0.5	(2.02 ± 0.04) × 10^3
5	399.2 ± 1.2	(3.79 ± 0.38) × 10^2
6	434.1 ± 1.5	(9.80 ± 0.65) × 10^1

Figure B.18 : The fitting of Gaussian curves to the molar absorbance spectrum of $[Zn(NTA)ZQA]^{3-}$ in the 300 to 450 nm region.

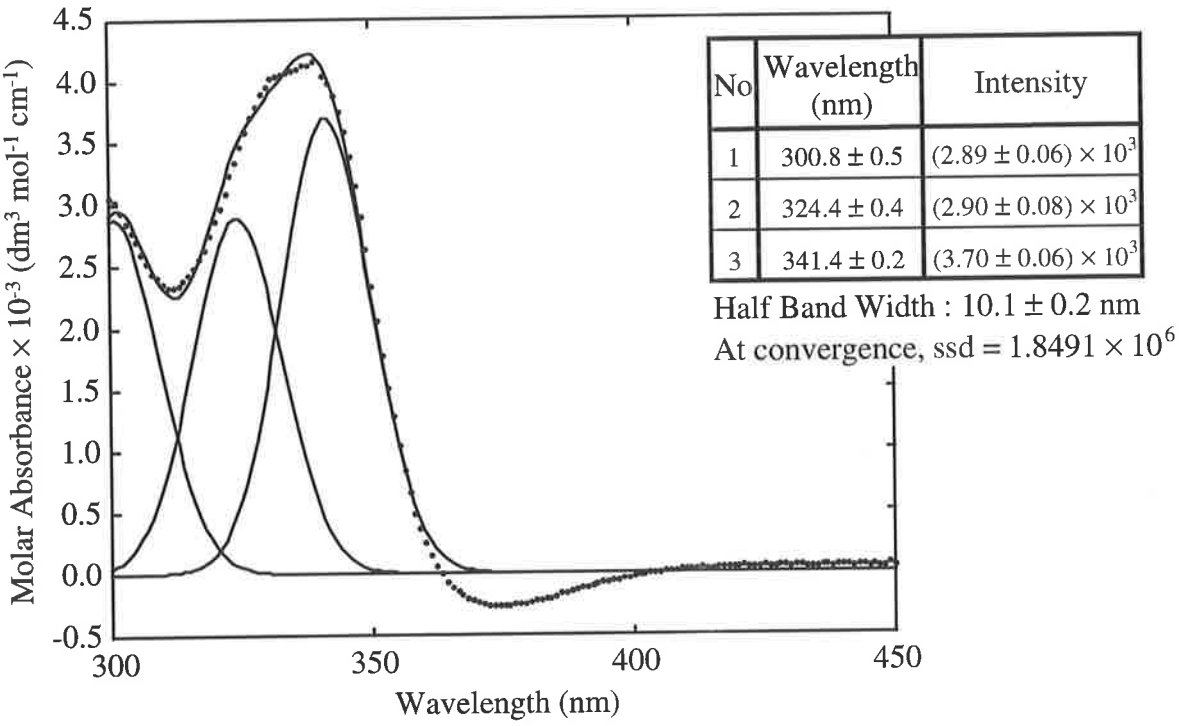

Figure B.19 : The fitting of Gaussian curves to the molar absorbance spectrum of $[Zn(NTA)ZQA.H]^{2-}$ in the 300 to 450 nm region.

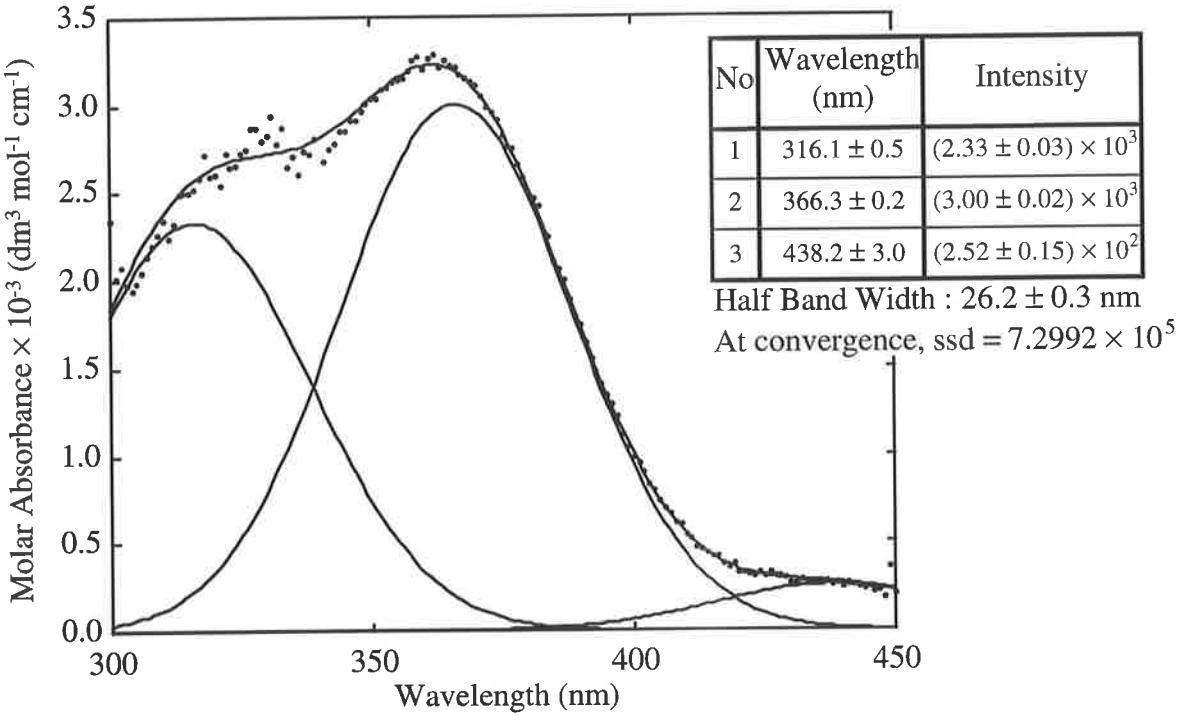

Figure B.20 : The fitting of Gaussian curves to the molar absorbance spectrum of $[Zn(TEA)ZQA.H_1]^-$ in the 300 to 450 nm region.

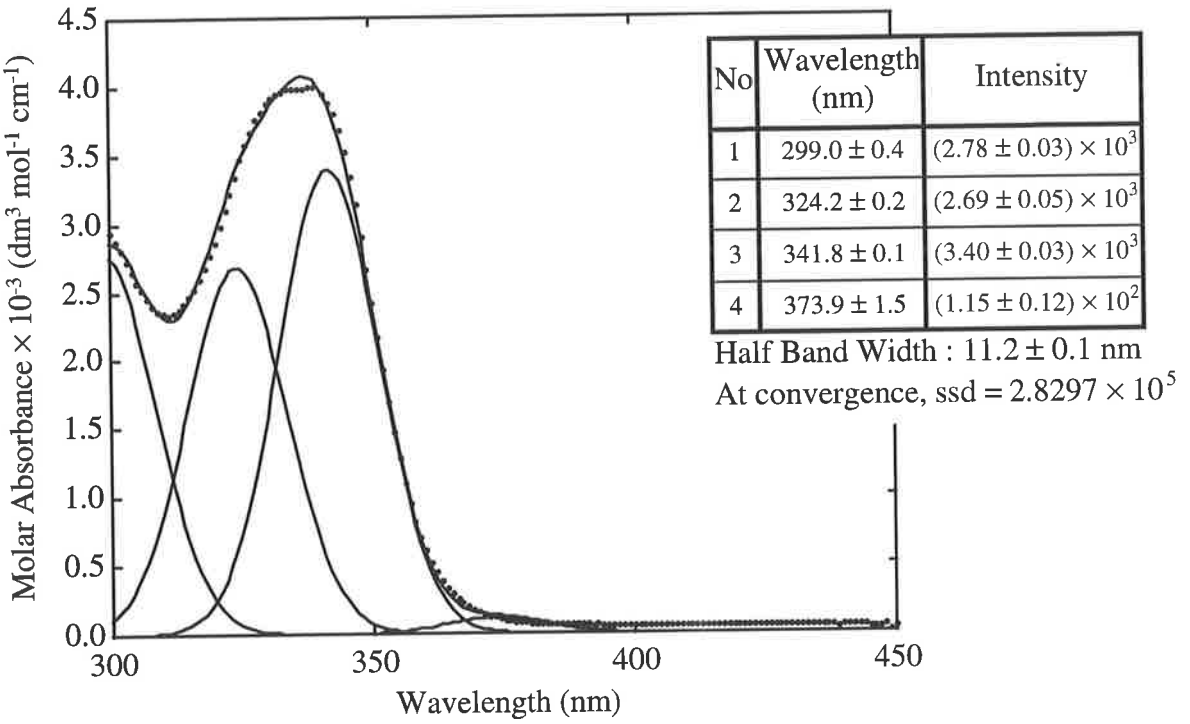

No	Wavelength (nm)	Intensity
1	299.0 ± 0.4	(2.78 ± 0.03) × 10^3
2	324.2 ± 0.2	(2.69 ± 0.05) × 10^3
3	341.8 ± 0.1	(3.40 ± 0.03) × 10^3
4	373.9 ± 1.5	(1.15 ± 0.12) × 10^2

Half Band Width : 11.2 ± 0.1 nm

At convergence, ssd = 2.8297 × 10^5

Figure B.21 : The fitting of Gaussian curves to the molar absorbance spectrum of $[ZQA.H]^-$ in the 300 to 450 nm region.

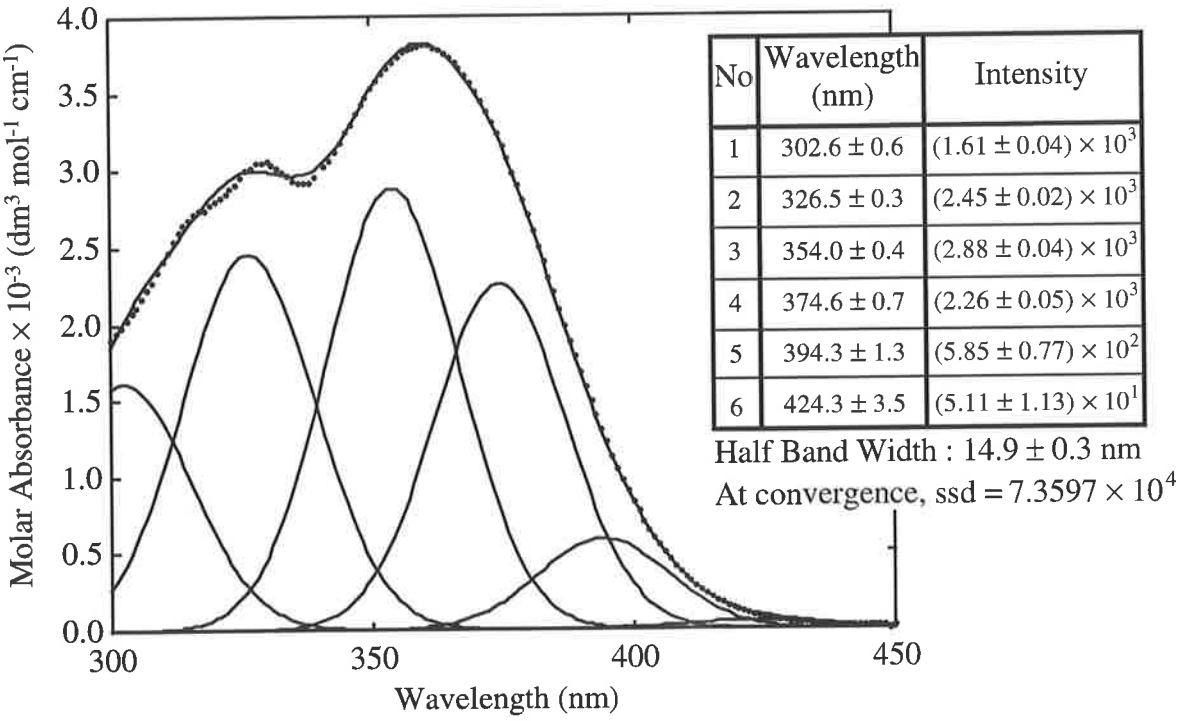

No	Wavelength (nm)	Intensity
1	302.6 ± 0.6	(1.61 ± 0.04) × 10^3
2	326.5 ± 0.3	(2.45 ± 0.02) × 10^3
3	354.0 ± 0.4	(2.88 ± 0.04) × 10^3
4	374.6 ± 0.7	(2.26 ± 0.05) × 10^3
5	394.3 ± 1.3	(5.85 ± 0.77) × 10^2
6	424.3 ± 3.5	(5.11 ± 1.13) × 10^1

Half Band Width : 14.9 ± 0.3 nm

At convergence, ssd = 7.3597 × 10^4

Figure B.22 : The fitting of Gaussian curves to the molar absorbance spectrum of [Zn(ZQA)] in the 300 to 450 nm region.

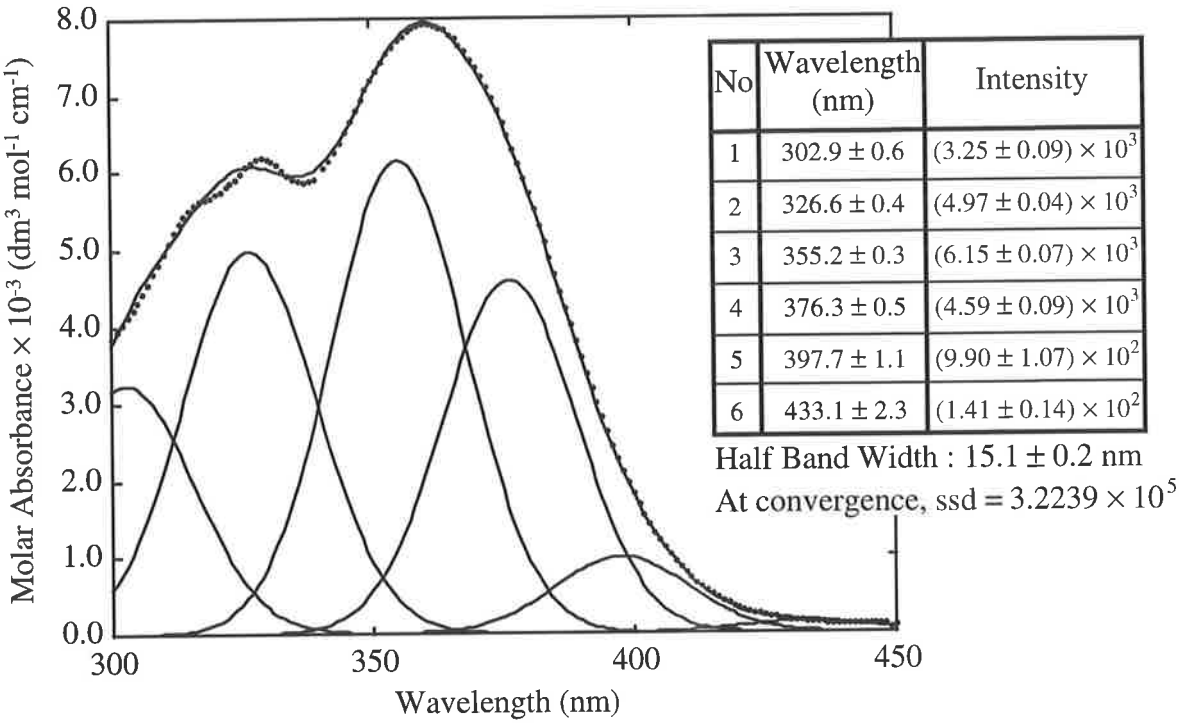

No	Wavelength (nm)	Intensity
1	302.9 ± 0.6	(3.25 ± 0.09) × 10^3
2	326.6 ± 0.4	(4.97 ± 0.04) × 10^3
3	355.2 ± 0.3	(6.15 ± 0.07) × 10^3
4	376.3 ± 0.5	(4.59 ± 0.09) × 10^3
5	397.7 ± 1.1	(9.90 ± 1.07) × 10^2
6	433.1 ± 2.3	(1.41 ± 0.14) × 10^2

Half Band Width : 15.1 ± 0.2 nm

At convergence, ssd = 3.2239 × 10^5

Figure B.23 : The fitting of Gaussian curves to the molar absorbance spectrum of $[Zn.(ZQA)_2]^{2-}$ in the 300 to 450 nm region.

APPENDIX C

SPECIATION PLOTS FOR THE LIGAND SYSTEMS USED TO OBTAIN TERNARY COMPLEX FLUORESCENCE SPECTRA

As mentioned in section 4.2.3, the stability and protonation constants derived from the potentiometric titrations can be used in the program MACSPECIES[1] to calculate the percentage formation of all species over a range of pH's. The actual concentration of each species present at a given pH can then be calculated. In all the speciation plots below, the concentration represented by 100% formation is defined as the total concentration of Zinquin-A, 1.04×10^{-5} mol dm^{-3} for the cyclam system and 9.84×10^{-6} mol dm^{-3} for all others. T = 298.2 K, I = 0.1 ($NaClO_4$) and all concentrations are as chosen for the fluorescence spectra of the ternary species at pH 6.6, with the exception of the cyclam system which was only determined at pH 10 (Section 4.4). Although the plots are most accurate near the fitting regions used for the titrations, they have been extended to a larger range (pH 2 to 12) to show the speciation expected if the determined stability constants were valid over the entire pH range.

1. A Macintosh version (P. A. Duckworth) of the Fortran program SPE, A. E. Martell and R. J. Motekaitis, *"Determination and use of Stability constants"*, Appendix III, VCH, 1990.

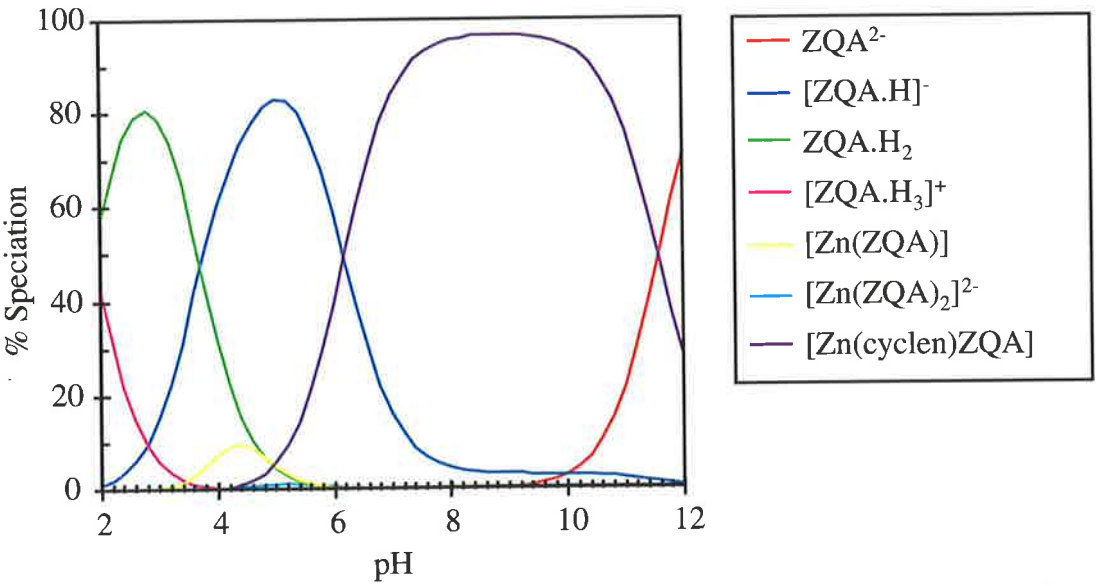

Figure C.1 : Speciation plot for a solution containing 9.84×10^{-6} mol dm^{-3} Zinquin-A, 1.03×10^{-4} mol dm^{-3} cyclen and 4.58×10^{-5} mol dm^{-3} $Zn(ClO_4)_2$, showing the species present in 50% aqueous ethanol at various pH. % Speciation is shown relative to the total concentration of Zinquin-A, I = 0.1 ($NaClO_4$) and T = 298.2 K.

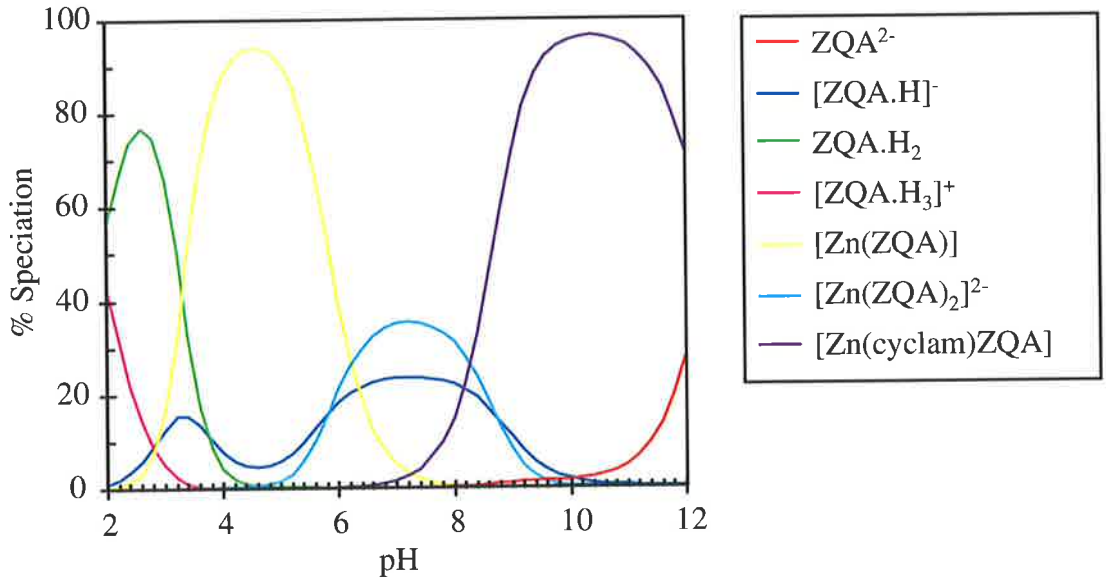

Figure C.2 : Speciation plot for a solution containing 1.04×10^{-5} mol dm^{-3} Zinquin-A, 4.99×10^{-3} mol dm^{-3} cyclam and 3.01×10^{-3} mol dm^{-3} $Zn(ClO_4)_2$, showing the species present in 50% aqueous ethanol at various pH. % Speciation is shown relative to the total concentration of Zinquin-A, I = 0.1 ($NaClO_4$) and T = 298.2 K.

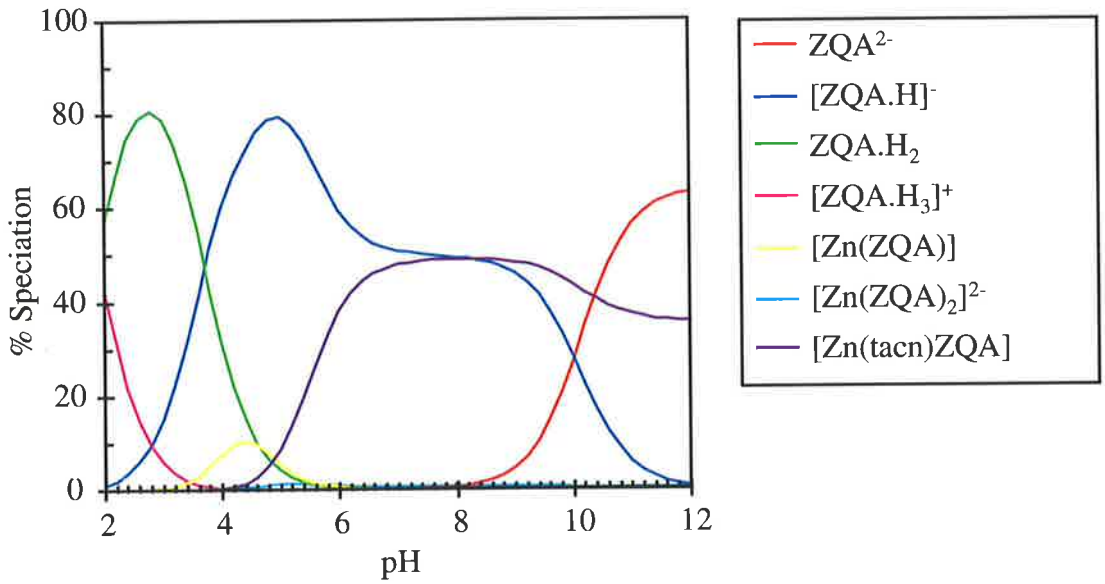

Figure C.3 : Speciation plot for a solution containing 9.84×10^{-6} mol dm^{-3} Zinquin-A, 1.01×10^{-4} mol dm^{-3} tacn and 4.58×10^{-5} mol dm^{-3} $Zn(ClO_4)_2$, showing the species present in 50% aqueous ethanol at various pH. % Speciation is shown relative to the total concentration of Zinquin-A, I = 0.1 ($NaClO_4$) and T = 298.2 K.

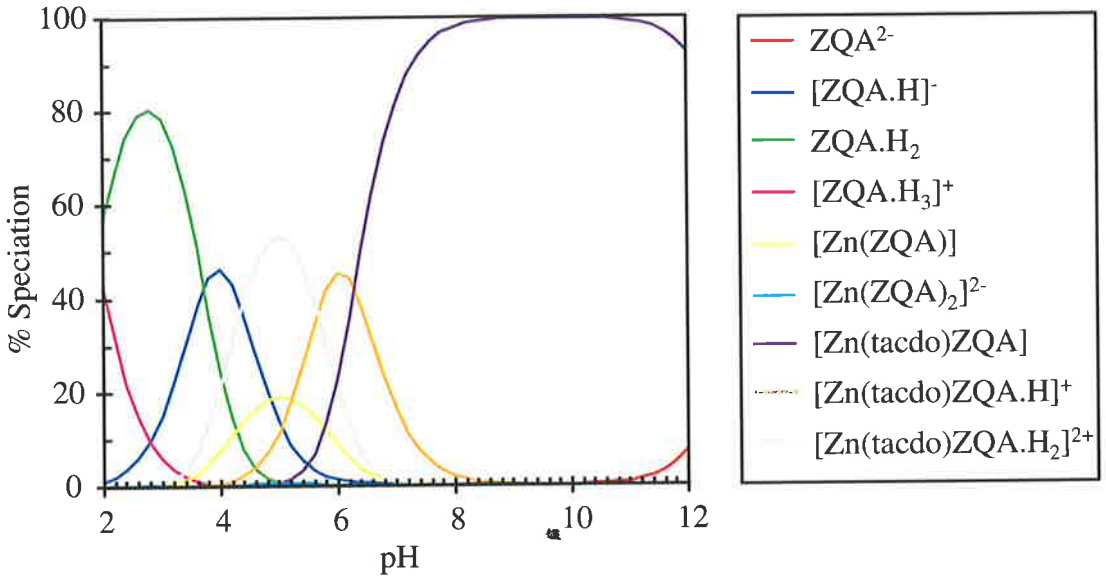

Figure C.4 : Speciation plot for a solution containing 9.84×10^{-6} mol dm^{-3} Zinquin-A, 4.99×10^{-3} mol dm^{-3} tacdo and 4.08×10^{-5} mol dm^{-3} $Zn(ClO_4)_2$, showing the species present in 50% aqueous ethanol at various pH. % Speciation is shown relative to the total concentration of Zinquin-A, I = 0.1 ($NaClO_4$) and T = 298.2 K.

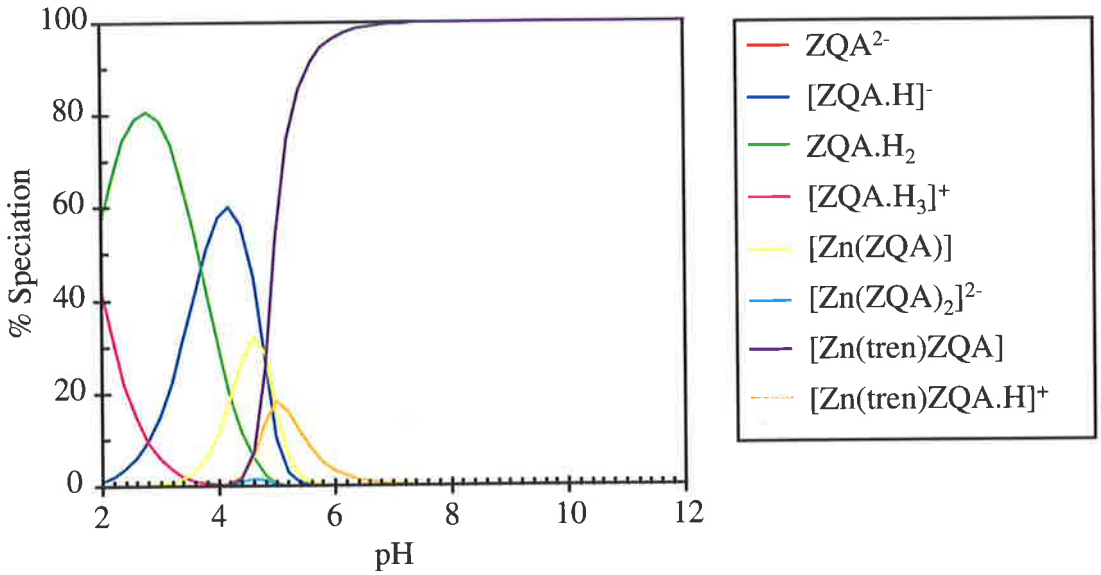

Figure C.5 : Speciation plot for a solution containing 9.84×10^{-6} mol dm^{-3} Zinquin-A, 1.00×10^{-4} mol dm^{-3} tren and 4.58×10^{-5} mol dm^{-3} $Zn(ClO_4)_2$, showing the species present in 50% aqueous ethanol at various pH. % Speciation is shown relative to the total concentration of Zinquin-A, I = 0.1 ($NaClO_4$) and T = 298.2 K.

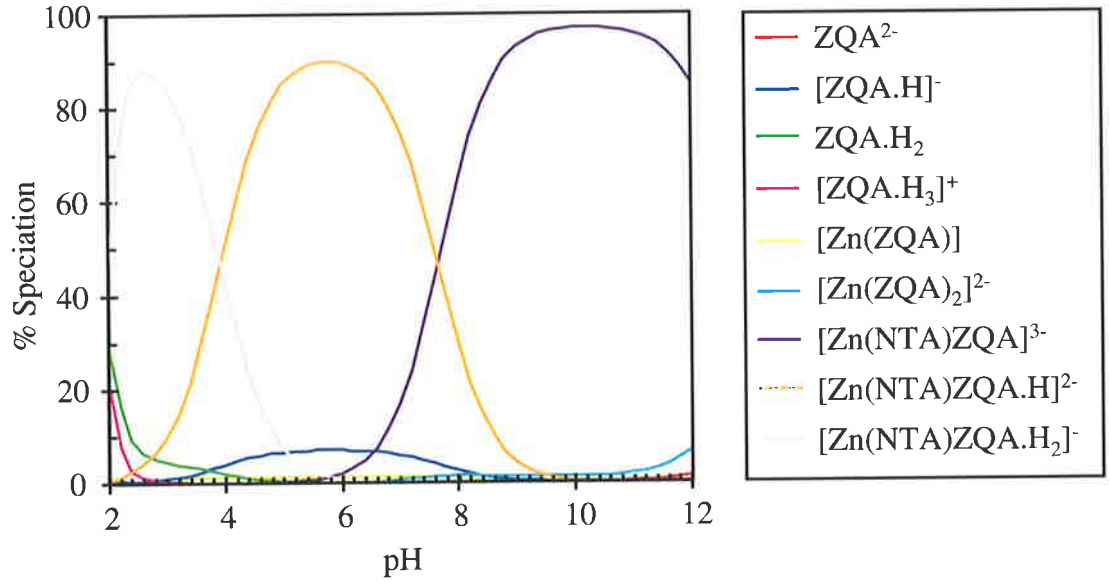

Figure C.6 : Speciation plot for a solution containing 9.84×10^{-6} mol dm^{-3} Zinquin-A, 4.98×10^{-3} mol dm^{-3} $NTA.H_3$ and 3.50×10^{-3} mol dm^{-3} $Zn(ClO_4)_2$, showing the species present in 50% aqueous ethanol at various pH. % Speciation is shown relative to the total concentration of Zinquin-A, I = 0.1 ($NaClO_4$) and T = 298.2 K.

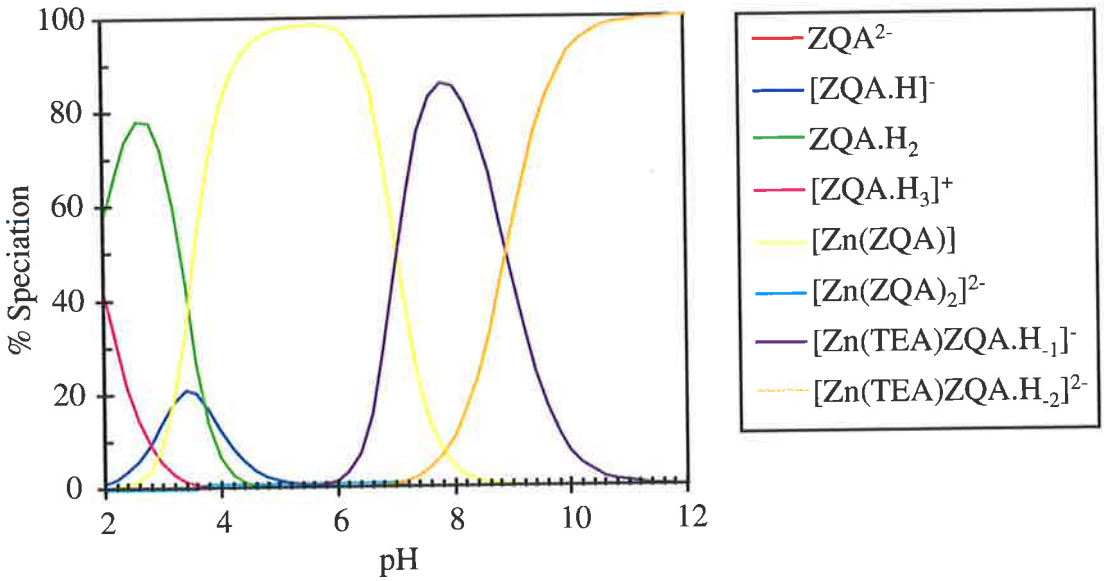

Figure C.7 : Speciation plot for a solution containing 9.84×10^{-6} mol dm^{-3} Zinquin-A, 5.20×10^{-3} mol dm^{-3} TEA and 1.50×10^{-3} mol dm^{-3} $Zn(ClO_4)_2$, showing the species present in 50% aqueous ethanol at various pH. % Speciation is shown relative to the total concentration of Zinquin-A, I = 0.1 ($NaClO_4$) and T = 298.2 K.

APPENDIX D

CONCENTRATIONS OF SPECIES IN THE SOLUTIONS USED TO DETERMINE THE SPECTRA OF [Zn(L)ZQA]

As mentioned in greater detail in Sections 5.4.3 and 5.4.4, to obtain the ultraviolet-visible and fluorescence spectra for the ternary complexes of the form [Zn(L)ZQA], it was necessary to identify the other Zinquin-A containing species present in the solutions used to obtain the spectra, and their concentration. This was achieved using the program MACSPECIES[1] with the stability constants determined in 50% aqueous ethanol (Section 4.2) and the total concentrations of the ligand (L), Zinquin-A and Zn^{2+} in each solution (Tables 5.16 to 5.18). MACSPECIES outputs the percentage formation relative to the total Zinquin-A concentration for all species at any given pH and this can be converted to a concentration by multiplying the percentage formation by the total Zinquin-A concentration. Both of these values are shown in Tables D.1 to D.3 for all Zinquin-A containing species that were present in the solutions at greater than 2% formation.

As can be seen from Tables D.1 to D.3, the tacdo solutions contained a small amount (3.7%) of $[Zn(tacdo).H_2]^{2+}$. As this concentration is less than 5% of the total Zinquin-A concentration, the contribution of this species to the spectra was considered sufficiently small to omit from the calculations.

1. A Macintosh version (P. A. Duckworth) of the Fortran program SPE, A. E. Martell and R. J. Motekaitis, *"Determination and use of Stability constants"*, Appendix III, VCH, 1990.

Ligand (L)	pH	Total [Ligand] (mol dm^{-3})	Total [$Zn(ClO_4)_2$] (mol dm^{-3})	[Zn(L)ZQA] (mol dm^{-3}) (% of Zinquin-A)	[Zn(L)ZQA.H^+] (mol dm^{-3}) (% of Zinquin-A)	[Zn(L)ZQA.H_2^{2+}] (mol dm^{-3}) (% of Zinquin-A)	[ZQA.H^-] (mol dm^{-3}) (% of Zinquin-A)	[Zn(ZQA)] (mol dm^{-3}) (% of Zinquin-A)	[$Zn(ZQA)_2^{2-}$] (mol dm^{-3}) (% of Zinquin-A)
cyclen	6.6	1.03×10^{-3}	4.51×10^{-4}	9.41×10^{-5} (95.6%)			4.31×10^{-6} (4.4%)		
cyclam	10	4.99×10^{-3}	3.01×10^{-3}	9.21×10^{-5} (88.9%)					4.00×10^{-6} (3.9%)
tacn	6.6	1.01×10^{-3}	4.51×10^{-4}	5.57×10^{-5} (56.6%)			4.10×10^{-5} (41.6%)		
tacdo	6.6	5.00×10^{-3}	4.51×10^{-4}	6.15×10^{-5} (62.4%)	3.08×10^{-5} (31.3%)	3.62×10^{-6} (3.7%)		2.24×10^{-6} (2.3%)	
	10	5.05×10^{-3}	4.51×10^{-4}	1.04×10^{-4} (100.0%)					
tren	6.6	1.00×10^{-3}	4.51×10^{-4}	9.84×10^{-5} (99.1%)					
NTA^{3-}	6.6	4.98×10^{-3}	4.01×10^{-4}	4.24×10^{-6} (4.3%)	4.84×10^{-5} (49.2%)		3.87×10^{-5} (39.3%)		3.44×10^{-6} (3.5%)
	10	5.03×10^{-3}	3.01×10^{-3}	8.70×10^{-5} (84.0%)					8.00×10^{-6} (7.7%)
TEA	6.6	5.20×10^{-3}	4.51×10^{-4}	1.26×10^{-5} (12.8%)				6.74×10^{-5} (68.4%)	9.14×10^{-6} (9.3%)

Table D.1 : Concentrations used to determine the absorbance of the ternary complexes in the 300 to 450 nm region. All solutions also contained Zinquin-A at 9.84×10^{-5} or 1.04×10^{-4} mol dm^{-3} for solutions at pH 6.6 (0.100 mol dm^{-3} NaPIPES) and pH 10 (0.100 mol dm^{-3} borate) respectively. All percentage formations below 2% were omitted.

Ligand (L)	pH	Total [Ligand] (mol dm^{-3})	Total $[Zn(ClO_4)_2]$ (mol dm^{-3})	[Zn(L)ZQA] (mol dm^{-3}) (% of Zinquin-A)	$[Zn(L)ZQA.H^+]$ (mol dm^{-3}) (% of Zinquin-A)	$[Zn(L)ZQA.H_2^{2+}]$ (mol dm^{-3}) (% of Zinquin-A)	$[ZQA.H^-]$ (mol dm^{-3}) (% of Zinquin-A)	[Zn(ZQA)] (mol dm^{-3}) (% of Zinquin-A)	$[Zn(ZQA)_2^{2-}]$ (mol dm^{-3}) (% of Zinquin-A)
cyclen	6.6	2.07×10^{-4}	9.08×10^{-5}	1.61×10^{-5} (81.9%)			3.53×10^{-6} (17.9%)		
cyclam	10	4.99×10^{-3}	3.01×10^{-3}	1.97×10^{-5} (94.8%)					
tacn	6.6	2.01×10^{-4}	9.08×10^{-5}	1.00×10^{-5} (50.8%)			9.37×10^{-6} (47.6%)		
tacdo	6.6	4.92×10^{-3}	8.08×10^{-5}	1.23×10^{-5} (62.3%)	6.15×10^{-6} (31.2%)	7.19×10^{-7} (3.7%)		4.21×10^{-7} (2.2%)	
	10	5.05×10^{-3}	4.51×10^{-4}	2.07×10^{-5} (100.0%)					
tren	6.6	2.00×10^{-3}	9.08×10^{-5}	1.97×10^{-5} (99.1%)					
NTA^{3-}	6.6	4.98×10^{-3}	3.01×10^{-3}	1.44×10^{-6} (7.3%)	1.64×10^{-5} (83.5%)		1.50×10^{-6} (7.6%)		
	10	5.03×10^{-3}	3.01×10^{-3}	1.98×10^{-5} (95.4%)					4.08×10^{-7} (2.0%)
TEA	6.6	5.20×10^{-3}	3.01×10^{-3}	2.93×10^{-6} (14.9%)				1.65×10^{-5} (84.3%)	

Table D.2 : Concentrations used to determine the absorbance of the ternary complexes in the 220 to 300 nm region. All solutions also contained Zinquin-A at 1.97×10^{-5} or 2.07×10^{-5} mol dm^{-3} for solutions at pH 6.6 (0.10 mol dm^{-3} NaPIPES) and pH 10 (0.10 mol dm^{-3} borate) respectively. All percentage formations below 2% were omitted.

Ligand (L)	pH	Total [Ligand] (mol dm^{-3})	Total $[Zn(ClO_4)_2]$ (mol dm^{-3})	[Zn(L)ZQA] (mol dm^{-3}) (% of Zinquin-A)	$[Zn(L)ZQA.H^+]$ (mol dm^{-3}) (% of Zinquin-A)	$[Zn(L)ZQA.H_2^{2+}]$ (mol dm^{-3}) (% of Zinquin-A)	$[ZQA.H^-]$ (mol dm^{-3}) (% of Zinquin-A)	[Zn(ZQA)] (mol dm^{-3}) (% of Zinquin-A)	$[Zn(ZQA)_2^{2-}]$ (mol dm^{-3}) (% of Zinquin-A)
cyclen	6.6	1.03×10^{-4}	4.58×10^{-5}	6.90×10^{-5} (70.1%)			2.91×10^{-6} (29.5%)		
cyclam	10	4.99×10^{-3}	3.01×10^{-3}	9.91×10^{-6} (95.6%)					
tacn	6.6	1.01×10^{-4}	4.58×10^{-5}	4.52×10^{-6} (45.9%)			5.17×10^{-6} (52.6%)		
tacdo	6.6	4.99×10^{-3}	4.08×10^{-5}	6.12×10^{-6} (62.2%)	3.07×10^{-6} (31.2%)	3.59×10^{-7} (3.7%)		2.05×10^{-7} (2.1%)	
	10	5.05×10^{-3}	4.51×10^{-4}	1.04×10^{-5} (100.0%)					
tren	6.6	1.00×10^{-4}	4.58×10^{-5}	9.84×10^{-6} (99.1%)					
NTA^{3-}	6.6	4.98×10^{-3}	3.50×10^{-3}	7.31×10^{-7} (7.4%)	8.34×10^{-6} (84.7%)		6.47×10^{-7} (6.6%)		
	10	5.03×10^{-3}	3.01×10^{-3}	1.01×10^{-5} (97.3%)					
TEA	6.6	5.20×10^{-3}	1.50×10^{-3}	1.50×10^{-6} (15.3%)				8.22×10^{-6} (83.9%)	

Table D.3 : Concentrations used to determine the fluorescence of the ternary complexes in the 400 to 600 nm region. All solutions also contained Zinquin-A at 9.84×10^{-6} or 1.04×10^{-5} mol dm^{-3} for solutions at pH 6.6 (0.100 mol dm^{-3} NaPIPES) and pH 10 (0.100 mol dm^{-3} borate) respectively. All percentage formations below 2% were omitted.

APPENDIX E

MATLAB PROGRAMS

MATLAB (The MathWorks, Inc., Natick, MA) is an interactive application designed for numeric computation and data visualisation. Fundamentally, MATLAB is built upon a foundation of sophisticated matrix software for analysing linear systems of equations and thus it proves extremely useful in analysing and manipulating spectra. Some of the MATLAB programs used throughout this work are mentioned in this appendix and others are available in the optimisation toolbox of MATLAB.

E.1 : SPECFIT

Tom Kurucsev 1995

SPECFIT is a program that is designed to calculate stability constants from fluorescence or ultraviolet-visible spectra followed by the molar fluorescence or absorbance for each complex alone. It achieves this by using non-linear least squares fitting of the concentration dependence of the spectra to specific association models of metal and ligand, or host and guest. The program allows the user a choice of three fitting algorithms, DATAFIT, FMINS or LEAST2 which are all found in the optimisation toolbox of MATLAB. To allow the fixing of stability constants at a predetermined value, DATAFIT was modified so that the default minima and maxima of the parameters could be altered. There are many subroutines in SPECFIT, and only those relevant to this work are included here. Although the routine SPECFIT.M starts the program, the bulk of the instructions are in SPECTRY.M.

SPECTFIT.M

```
% SPECFIT
% T Kurucsev  version 950217
clc
if exist('oldset.mat')
      delete oldset.mat;
end
disp('Change to your MATLABsubdirectory')
disp(' ')
```

```
disp('When ready to continue type return')
keyboard
temp=input('Do you have a .mat file for this set of data? (y/n) ','s');
if temp ~= 'y'
        disp(' ')
        disp('          Welcome to')
        disp('          S P E C F I T ')
        disp('          ~~~~~~~~~~~~~~~')
        disp('Non-linear least squares fitting of the concentration')
        disp('dependence of solution spectra to specific association models')
        disp('between ligands and a host (cyclodextrin or metal ion)')
        disp(' ')
        disp('hit any key if you want to proceed')
        pause
        clc
        disp('You will need the following text files (*.txt):')
        disp('absorbances (emissivities) of the solutions of dimension nw x ns')
        disp('molar absorptivities (emissivities) of ligand and host or metal (nw x 2)')
        disp('concentrations of ligand and host or metal (ns x 2)')
        disp('              where')
        disp('nw is the number of wavelengths')
        disp('ns is the number of solutions')
        disp(' Note that it is assumed that the baselines have been subtracted')
        disp(' from the spectra')
        disp(' ')
        disp('If the directory containing these files is not in the')
        disp('matlab\startup.m file quit now and add the path')
        disp(' ')
        disp('If you are ready to proceed hit any key')
        pause
        clc
        for i=1:3
                temp=input('name of absorbance (emission) file? ','s');
                if exist(temp), break, end
                if i ~= 3
                        disp(' try again')
                else
                        eval(temp)
                end
        end
        eval(['load ',temp]);
        aname=temp(1:length(temp)-4);
        for i=1:3
                temp=input('name of molar absorptivity (emissivity) file? ','s');
                if exist(temp), break, end
                if i ~= 3
                        disp(' try again')
                else
                        eval(temp)
                end
        end
```

```
    eval(['load ',temp]);
    lname=temp(1:length(temp)-4);
    for i=1:3
        temp=input('name of concentrations file? ','s');
        if exist(temp), break, end
        if i ~= 3
            disp(' try again')
        else
            eval(temp)
        end
    end
    eval(['load ',temp]);
    cname=temp(1:length(temp)-4);
    clear temp temp1 i
    [nw ns]=size(eval(aname));
    w1=input('first wavelength? ');
    wi=input('wavelength increment? ');
    wl=(w1:wi:w1+wi*(nw-1))';
    a=eval(aname);
    l=eval(lname);
    c=eval(cname);
    save oldset w1 wi aname lname cname wl a l c
    clear nw ns wi w1 a l c
    clc
    whos
    disp('This list of 7 current variables consists of the 3 input')
    disp('matrices, of their names and of the wavelength vector.')
    disp('You should save these to a .mat file by typing :')
    disp('      save filename')
    disp('so that for future work with this set of data you may')
    disp('start the fitting directly.')
    disp('      When ready to continue type return')
    keyboard
    clc
end
spectry
```

E.1.1 : SPECTRY.M

```
% SPECTRY
% T Kurucsev version 950425

% Modified by Kym Hendrickson to fit two regions simultaneously

repeat=1;
resout=1;
fitout=1;
specout=1;
while repeat
    close
```

```
temp='oldset.mat';
if exist(temp)
      eval(['load ',temp]);
else
      for i=1:3
            temp=input('name of .mat file? ','s');
            if exist(temp), break, end

            if i ~= 3
                  disp(' try again')
            else
                  eval(temp)
            end

      end

      eval(['load ',temp]);
      w1=wl(1);
      wi=wl(2)-wl(1);
      winc=wi;
      a=eval(aname);
      l=eval(lname);
      c=eval(cname);
end

nregion=0;
wfirst=w1;
temp=input('are you fitting two separate regions? (y/n) ','s');

if temp=='y'
      nregion=1;
      spr=zeros(1,4);
      spr=input(' type the 4 limits starting at the uv end as [ ] ');
      nr1=1 + (spr(1)-w1)/wi;
      nr2=1 + (spr(2)-w1)/wi;
      nr3=1 + (spr(3)-w1)/wi;
      nr4=1 + (spr(4)-w1)/wi;
      a1=[a(nr1:nr2,:); a(nr3:nr4,:)];
      l1=[l(nr1:nr2,:); l(nr3:nr4,:)];
      ar1=a(nr1:nr4,:);
      lr1=l(nr1:nr4,:);
else
      clear ar1 lr1 spr
      disp([' The first wavelength for the fit is ',num2str(wfirst)])
      temp=input(' type in a new value or hit return ');

      if temp ~=[]
            wfirst=temp;
      end

      winc=wi;
```

```
        disp([' The wavelength increment is ',num2str(winc)])
        temp=input(' type in a new value (multiple of original) or hit return ');

        if temp ~=[]
            winc=temp;
        end

        nw=length(wl);
        disp([' The total number of points are ',num2str(nw)])
        temp=input(' type in a new value or hit return ');

        if temp ~=[]
            nw=temp;
        end

        clear temp i
        nfirst=1 + (wfirst-w1)/wi;
        ninc=winc/wi;
        nlast=nfirst+ninc*(nw-1);
        wlast=wl(nlast);
        a1=a(nfirst:ninc:nlast,:);
        l1=l(nfirst:ninc:nlast,:);
        ww=wfirst:winc:wlast;
    end
    save oldset wfirst winc nw nfirst ninc nlast aname lname cname wl a l c
    clc
    model=str2mat('1:1 host/ligand',...
'1:2 host/ligand',...
'2:1 host/ligand',...
'1:3 host/ligand',...
'1:2 h/l in one step',...
'1:4 h/l in two steps');
    mod=menu('Choose equilibrium model',model(1,:),...
model(2,:),model(3,:),model(4,:),model(5,:),model(6,:));
    clc
    k0=input(' Initial estimates of the k values: [k1 ....] ');
    clc
    method=str2mat('fmins','least2','datafit');
    min=menu('Choose method',method(1,:),method(2,:),method(3,:));
    nw=length(l1(:,1));
    ns=length(c);
    nvars=length(k0);
    nfun=length(a1(:));
        nc=3;

    if mod==1
        fun1='mod1';
        fun2='ab1';
    elseif mod==5
        fun1='mod5';
        fun2='ab5';
```

```
else
        nc=4;

        if mod==2
                fun1='mod12';
                fun2='ab12';
        else

                if mod==3
                        fun1='mod21';
                        fun2='ab21';
                elseif mod ==6
                        fun1='mod24';
                        fun2='ab24';
                else
                        nc=5;
                        fun1='mod123';
                        fun2='ab123';
                end

        end

end

% Bill Venables' suggestion to "smooth" input matrix first
%     by singular value decomposition
%
%[u s v]=svd(a1);
%WNV=u(:,1:nc)*s(1:nc,1:nc)*v(:,1:nc)';
%a1=WNV;

evalstr1=[fun1,'(k,1,a1,l1,c,ns,nw)'];

if min==1
        k=fmins(fun1,k0,[1 0.1 1],[],0,a1,l1,c,ns,nw);
        f=eval(evalstr1);
        f=f(:);
        KOUT=k(:);
        J=zeros(nfun,nvars);
        CHG=1e-3*abs(KOUT);
        OLDF=f;

        for i=1:nvars
                temp=KOUT(i);
                KOUT(i)=temp+CHG(i);
                k(:)=KOUT;
                f=eval(evalstr1);
                f=f(:);
                J(:,i)=(f-OLDF)/CHG(i);
                KOUT(i)=temp;
        end
```

```
        f=OLDF;
else
        if min==2
                [k,options,f,J]=least2(fun1,k0,[12e-6],[],1,a1,l1,c,ns,nw);
        else
                [k,f,J]=datafit(fun1,k0,1,a1,l1,c,ns,nw);
        end
end

q=f'*f;
HESS=J'*J;
covar=q*inv(HESS)/(nfun-nvars);
var=diag(covar);
sd=sqrt(var);
fid=fopen('result','w');
fprintf(fid,'Fitting of data from file %s\n\n',aname);

if nregion==1
        fprintf(fid,'the limits of the two regions are %5.1d %5.1d %5.1d %5.1d\n',spr);
else
        fprintf(fid,'starting wavelength %5.1d\n',wfirst);
        fprintf(fid,'increments %4.1d\n',winc);
        fprintf(fid,'number of wavelengths %4.0d\n\n',nw);
        fprintf(fid,'ending wavelength %5.1d\n',wlast);

end

fprintf(fid,'Model %s\n',model(mod,:));
fprintf(fid,'Method %s\n',method(min,:));
fprintf(fid,'\n');
fprintf(fid,'At convergence thessd was %12.4e\n',q);
fprintf(fid,'The equilibrium constants and their standard deviationsare:\n');

for i=1:nvars
        fprintf(fid,'%12.3e  +/-%12.3e\n',k(i),sd(i));
end

type result
fclose(fid);
disp('hit any key to see plot of spectra')
pause

if nregion==1
        a1=ar1;
        l1=lr1;
        nw=length(a1(:,1));
        ww=wl(nr1:nr4);
end

evalstr2=[fun2,'(k,a1,l1,c,ns,nw)'];
[E,C]=eval(evalstr2);
```

```
    subplot(2,1,1)
    plot(ww,E,'-',ww,l1(:,1),':');
    title(['Fitting of data from file ',aname,', Model ',model(mod,:)]);
    set(gcf,'PaperType','a4letter','PaperPosition',[1 3 6 7]);
    disp(' ')
%   disp('hit any key to see fit at the maximum');
%   pause
    temp=input(' type wavelength for fit ');

    if temp ~=[]
        wselect=temp;
    end

%   pause
    c2=c(:,2);
    A=abcalc(mod,k,a1,l1,c,ns,nw);
%   [y i]=max(A(:,ns));

    if nregion == 1
        i=1+(wselect-spr(1))/winc;
    else
        i=1 + (wselect-wfirst)/winc;
    end

% I think below was a bug, changed to above -KMH 18.4.96
%   i=1 + (wselect-w1)/wi;
    subplot(2,1,2)
% Carolyn Haskard 11/95
    cav=mean(c(:,1));
    plot(c2,cav*(A(i,:)-c2'*l1(i,2))./(c(:,1))','-',c2,cav*(al(i,:)-c2'*l1(i,2))./(c(:,1))','o')
%   plot(c2,A(i,:)./(c(:,1))','-',c2,al(i,:)./(c(:,1))','o')
    title(['Fit at wavelength ',num2str(wselect)])
    disp(' ')
    disp('hit any key to continue')
    pause
    temp=input('save the results? (y/n) ','s');

    if temp=='y'

        if resout==1
            res=input('filename? ','s');
            fid2=fopen(res,'w');
        else
            fid2=fopen(res,'a');
        end

        fid=fopen('result','r+');
        fprintf(fid2,'\n');

        while 1
            line=fgetl(fid);
```

```
            if ~isstr(line), break,end
            fprintf(fid2,'%s\n',line);
        end

        fclose('all');
        resout = resout+1;
    end

    temp=input('save the fit? (y/n) ','s');

    if temp=='y'

        if fitout==1
            fit=input('filename? ','s');
            fid3=fopen(fit,'w');
        else
            fid3=fopen(fit,'a');
        end

        fprintf(fid3,'Fitting of data from file %s\n\n',aname);
        fprintf(fid3,'starting wavelength %5.1d\n',wfirst);
        fprintf(fid3,'increments %4.1d\n',winc);
        fprintf(fid3,'number of wavelengths %4.0d\n\n',nw);
        fprintf(fid3,'Model %s\n',model(mod,:));
        fprintf(fid3,'Method %s\n',method(min,:));
        fprintf(fid3,'\n');
% CAH 11/95
        out=[c2 cav*((A(i,:)-c2'*l1(i,2))./c(:,1)')'cav*((a1(i,:)-c2'*l1(i,2))./c(:,1)')'];
%       fprintf(fid3,'%12.4e%12.4e%12.4e\n',out);
        save out.txt out -ascii -tabs;
        fclose('all');
        fitout = fitout+1;
    end

    temp=input('print the figure? (y/n) ','s');

    if temp=='y'
        print -dsetup
    end

    temp=input('save the spectra? (y/n) ','s');

    if temp=='y'

        if specout==1
            spec=input('filename? ','s');
            fid=fopen(spec,'w');
        else
            fid=fopen(spec,'a');
        end
```

```
            fprintf(fid,'Fitting of data from file %s\n',aname);
            fprintf(fid,'Model %s\n',model(mod,:));
            fprintf(fid,'Method %s\n',method(min,:));
            fprintf(fid,'\n');
            Elig=[l1(:,1) E];
            out=[ww' Elig]';

            if mod==1
                  fprintf(fid,'%6.1f  %12.0f%12.0f\n',out);
            else
                  if mod~=4
                        fprintf(fid,'%6.1f  %12.0f%12.0f%12.0f\n',out);
                  else
                        fprintf(fid,'%6.1f  %12.0f%12.0f%12.0f%12.0f\n',out);
                  end
            end

            fprintf(fid,'\n\n');
            specout = specout+1;
            fclose('all');
      end

      delete result
      temp=input('continue with this set of data? (y/n) ','s');

      if temp =='n'
            repeat=0;
      end

end

delete oldset.mat;
close
clear
disp(' ')
disp('END OF SPECFIT SESSION')
```

E.1.1.1 : AB12.M

```
function [E,C] = ab12(k,a,l,c,ns,nw)
%
% Calculation of the molar absorptivity/emissivity matrix of the 1:1 and 1:2
%  metal/ligand complexes
% Calls function k1k2
%
% Usage  [E,C] = ab12(k,a,l,c,ns,nw);
%
% Input:    k, the vector of the equilibrium constants
%           a, the experimental absorbance/fluorescence matrix (nw x ns)
%           l, the ligand and metal molar absorptivity/emissivity matrix (nw x 2)
```

```
%           c = [l0 m0] the matrix of ligand and metal concentrations (ns x 2)
%           ns, the number of solutions
%           nw, the number of wavelengths
%
% Output:  E, molar absorptivities/emissivities of 1:1 and 1:2 species
%           C concentrations of the 1:1 and 1:2 species
%
% Advantitious host concentration as last parameter
lk=length(k);
if lk > 2
      adhost=k(lk)*1e-12;
      k=k(1:lk-1);
      c=c+[zeros(ns,1) ones(ns,1)*adhost];
end
%
E=zeros(nw,2);
c1=zeros(ns,4);
for i=1:ns
      p=[k c(i,:)];
      c1(i,:)=k1k2(p);
end
L=l*(c1(:,1:2))';
A=a-L;
C=c1(:,3:4);
E=A*pinv(C');
e1=E(:,1); e2=E(:,2)/2;
E=[e1,e2];
%note that these molar values are 'per ligand'
```

E.1.1.2 : MOD12.M

```
function q = mod12(k,flag,a,l,c,ns,nw)
%
% Calculation of the deviations of the molar absorptivities/emissivities
%  in the fit of the 1:1 and 1:2 ligand/metal complex spectra
% Calls function k1k2
%
% Usage  q = mod12(k,flag,a,l,c,ns,nw)
%
% Input:   k = the initial estimate of the equilibrium constants
%          flag, if zero, gives the ssd, else the deviation matrix is calculated
%          a, the experimental absorbance/fluorescence matrix (nw x ns)
%          l, the ligand and cd absorptivity/emissivity matrix (nw x 2)
%          c, the matrix of stoichiometric ligand and metal concentrations
%          ns, the number of solutions
%          nw, the number of wavelengths
%
% Adventitious host concentration as last parameter
lk=length(k);
if lk > 2
```

```
        adhost=k(lk)*1e-12;
        k=k(1:lk-1);
        c=c+[zeros(ns,1) ones(ns,1)*adhost];
end
%
c1=zeros(ns,4);
for i=1:ns
        p=[k c(i,:)];
        c1(i,:)=k1k2(p);
end
L=l*(c1(:,1:2))';
A=a-L;
C=c1(:,3:4);
E=A*pinv(C');
eneg=E<0;
f=abs(A-E*C');% + 1e5*abs(E.*eneg*C');
if flag==0
        f=f(:);
        q=f'*f;
else
        q=f;
end
```

E.1.1.3 : ABCALC.M

```
function A = cabcalc(mod,k,a,l,c,ns,nw)
%
% Calculation of the absorption/fluorescence matrix
%
% Calls function k1 or k1k2 or k2k1 or k123 or k2k4
%
% Usage  A = abcalc(mod,k,a,l,c,ns,nw)
%
%Input:     mod, the equilibrium model used
%           k, the vector of the equilibrium constants
%           a, the experimental absorbance/fluorescence matrix (nw x ns)
%           l, the ligand and host molar absorptivity/emissivity matrix (nw x 2)
%           c = [l0 m0] the matrix of ligand and host concentrations (ns x 2)
%           ns, the number of solutions
%           nw, the number of wavelengths
%
% Output:  E, molar absorptivities/emissivities of 1:1 and 1:2 species
%           C concentrations of the 1:1 and 1:2 species
%
lk=length(k);
% Advantitious host concentration as last parameter
if mod == 1
        if lk > 1
                adhost=k(lk)*1e-12;
                k=k(1:lk-1);
```

```
            c=c+[zeros(ns,1) ones(ns,1)*adhost];
            lk=lk-1;
        end
end
if mod == 2
        if lk > 2
            adhost=k(lk)*1e-12;
            k=k(1:lk-1);
            c=c+[zeros(ns,1) ones(ns,1)*adhost];
            lk=lk-1;
        end
end
%
if lk == 1
        E=zeros(nw,1);
        c1=zeros(ns,3);
elseif lk == 2
        E=zeros(nw,2);
        c1=zeros(ns,4);
elseif lk==3
        E=zeros(nw,3);
        c1=zeros(ns,5);
end
for i=1:ns
        p=[k c(i,:)];
        if mod == 1
            c1(i,:)=k1(p);
        elseif mod == 2
            c1(i,:)=k1k2(p);
        elseif mod == 3
            c1(i,:)=k2k1(p);
        elseif mod == 4
            c1(i,:)=k123(p);
        elseif mod == 5
            c1(i,:)=k5(p);
        elseif mod == 6
            c1(i,:)=k2k4(p);
        end
end
L=l*(c1(:,1:2))';
A=a-L;
if lk==1
        C=c1(:,3);
elseif lk==2
        C=c1(:,3:4);
elseif lk==3
        C=c1(:,3:5);
end
E=A*pinv(C');
all=[l E];
A=all*c1';
```

E.1.1.4 : K1K2.M

```
function q = k1k2(p)
%
% Calculation of the species concentrations at a given point for
%  1:1 and 2:1 ligand/metal complex equilibria
%
% Usage  q = k1k2(k1 k2 l0 m0)
%
k1=p(1); k2=p(2); l0=p(3); m0=p(4);
q=zeros(1,4);
t1=k1*k2; t2=k1*(1+k2*(2*m0-l0)); t3=1+k1*(m0-l0); t4=-l0;
t=[t1 t2 t3 t4];
r=roots(t);
ni=size(r);
for i=1:ni
        if r(i) ~=conj(r(i))
                r(i) = 0;
        end
end
rr=r>0;
l1=r'*rr;
m1=m0/(t1*l1*l1+k1*l1+1);
ml=k1*l1*m1;
ml2=k2*l1*ml;
q(1)=l1; q(2)=m1; q(3)=ml; q(4)=ml2;
```

E.2 : MABS12

Kym Hendrickson 1997

MABS12 is a modified version of AB12 which calculates the molar fluorescence or absorbance using pre-determined equilibrium concentrations rather than calculating them from the stability constants. The equilibrium concentrations were calculated first using MACSPECIES in most cases.

MABS12.M

```
function E = mabs12(a,l,c,ns,nw)
%
% Calculation of the molar absorptivity/emissivity matrix of the 1:1 and 1:2
%  metal/ligand complexes
%
%
% Usage  E = mabs12(a,l,c,ns,nw);
%
% Input:    a, the experimental absorbance/fluorescence matrix (nw x ns)
%           l, the ligand and metal molar absorptivity/emissivity matrix (nw x 2)
%           c = [l m ml ml2] the matrix of equilibrium concentrations (ns x 4)
%           ns, the number of solutions
%           nw, the number of wavelengths
%
% Output:  E, molar absorptivities/emissivities of 1:1 and 1:2 species
%
%
E=zeros(nw,2);
L=l*(c(:,1:2))';
A=a-L;
C=c(:,3:4);
E=A*pinv(C');
```

E.3 : KSPEC

Kym Hendrickson 1995

The instrument used to collect the ultraviolet-visible spectra, the Cary 2200, did not measure absorbance at fixed wavelength intervals, but at a fixed rate. This resulted in the spectra and baseline having points at slightly different wavelengths, which meant that the baseline could not be removed from the spectra using a simple subtraction. Hence, this simple program was developed. The MATLAB SPLINE function is used to interpolate the absorbance values for given wavelength values and create spectra and a baseline with the same wavelength values. A simple subtraction is then used by the program to remove the baseline from all of the spectra.

KSPEC.M

```
function [xi,newspec] = kspec(base,spectra)

%
%  'Splines' Cary spectra and subtracts base line.
%
%  Input:  [xi,newspec] = kspec(base,spectra);
%
%  Spectra must be columns in the matrix 'spectra' (Wavelength and absorbance
%  column pairs) with all columns made the same length by adding zeros to the
%  base of  shorter columns.
%  The baseline is in a different file, 'base' ([wl abs]).
%  All spectra in 'spectra' must have the same baseline.
%
%  The program returns xi = new wavelength range
%            newspec = new set of spectra (baseline removed)
%
%  There is an option for molar absorptivity, but this can only be used if all
%  the absorbance can be attributed to one species of known concentration. If
%  there is significant absorbance from more than one species, alternative
%  programs (such as ab12) should be used on the 'newspec' matrix produced.
%
%     There is also a plotting option.
%
%            KMH 9/95
%

xb = base(:,1);
yb = base(:,2);

a = input('Please enter the lower wavelength limit : ');
b = input('Please enter the higher wavelength limit : ');
c = input('Please enter the wavelength interval : ');
```

```
xi = a:c:b;
lx = length(xi);
xi = xi';

yb = spline(xb,yb,xi);

s = size(spectra);
l = s(2);
d = s(1);

for i = 1:2:l
        count = 0;
        wl = spectra(:,i);
        abs = spectra(:,i+1);
        for I = 1:d
                if wl(I,:)~=0
                        count = count + 1;
                end
        end
        y = spline(wl(1:count,:),abs(1:count,:),xi);
        y = y - yb;
        if i==1
                newspec = [y];
        else
                newspec = [newspec y];
        end
end

ans = input('Would you like molar absorptivity? (y/n) : ','s');
if ans == 'y'
        disp('   ');
        disp('Please note that this program assumes all the absorbance from');
        disp('spectra(1) is due to concentration(1). If there are significant');
        disp('amounts of species(2) in with species(1), then programs such as');
        disp('ab12 must be used to obtain a realistic molar absorptivity.');
        disp('   ');
        disp('If you wish not to calculate the molar absorptivity,');
        disp('please enter 0 at the prompt in place of a matrix.');
        conc = input('Please give the concentration matrix [c1 c2...] : ');
        if conc ~= 0
                lc = length(conc);
                for i = 1:lc
                        newspec(:,i) = newspec(:,i)./conc(i);
                end
                ylab = 'Molar Absorptivity';
        else
                ylab = 'Absorbance';
        end
else
        ylab = 'Absorbance';
end
```

```
temp =input('Would you like to plot the spectra? (y/n) : ','s');
if temp=='y'
        ti = input('Please enter a title : ','s');
        figure
        plot(xi,newspec)
        title(ti);
        xlabel('Wavelength');
        ylabel(ylab);
end

disp(' ');
disp('To save the new spectra with the wavelengths, type');
disp('      temp = [xi newspec]; (return)');
disp('      save filename.txt temp -ascii -tabs');
disp('at the matlab prompt.');
```

E.4 : ERRORS

Carolyn Haskard, Kym Hendrickson, Tom Kurucsev and Ari Verbyla

The error program supplied in MATLAB was modified so that it was suitable for the calculation of errors associated with stability constants (Carolyn Haskard 1993). At first there were two options for the averaging program, AV, depending upon whether the difference between runs, or the errors provided from SUPERQUAD, were greater. This was modified (Kym Hendrickson 1995) with the help of Ari Verbyla (Department of Statistics, The University of Adelaide) and Tom Kuruscev (Chemistry Department, The University of Adelaide) to calculate an error that considered both of these factors.

ERRORS.M

```
function errors
%   Presents a menu of options for error calculations.

labels = str2mat(...
        'Average values without any calculations', ...
        'Divide and average 2 values from the same run', ...
        'Average and divide 2 values from different runs', ...
        'k2/(k1**2), where k2 and k1 come from the same run', ...
        'k3/(k2*k1), where k3 and k2 come from the same run', ...
        'k3/(k2*k1), where k3, k2 and k1 come from different runs');

% Callbacks
callbacks = [ ...
        'nocalc     '
        'samediv2   '
        'div2       '
        'samediv3   '
        'partdiv3   '
        'div3       '];

mymenu('errors', 'Error Calculations', labels,callbacks);
```

E.4.1 : NOCALC.M

```
function out = nocalc
%
% Averages values without any calculations
%
% k1  = matrices of stability constants (or other values)
% e1  = matrices of corresponding RELATIVE errors
%
```

```
% Carolyn Haskard December 1993
%
k1=input('Please enter the matrix ofk''s ([...]) : ');
e1=input('Please enter the matrix of relative errors ([...]) : ');
e1=k1.*e1;
% converts relative to absolute errors
[k,err,logk,logerr]=av(k1,e1)
```

E.4.1.1 : AV.M

```
function [avr,std,lav,lsd] = av(k,err)
%
%Calculation of weighted average following an iterative method
%     suggested by Ari Verbyla from the Department of Statistics
%
%            T Kurucsev and K Hendrickson 1995
%
%usage:     [avr,std,lav,lsd] = av(k,err)
%
%     input:        k, vector of results to average
%                   err, vector of errors of k
%     output:       avr, weighted average of k
%                   std, corresponding standard deviation
%                   lav, log10 of avr
%                   lsd, error of lav
%
n=length(k);
if n > 1
        sig2=err.^2;
        rsig2=1./sig2;
        avr=sum(k.*rsig2)/sum(rsig2);
        kik2=(k-avr).^2;
        bold=sum(kik2)/(n-1);
        repeat=1;
        while repeat
                sig2=err.^2+bold;
                rsig2=1./sig2;
                rsig22=rsig2.^2;
                rsig23=rsig2.^3;
                sum1=sum(rsig2);
                sum2=sum(rsig22);
                sum3=sum(rsig23);
                avr=sum(k.*rsig2)/sum(rsig2);
                kik2=(k-avr).^2;
                sb=0.5*((sum2/sum1)-sum1+sum(kik2.*rsig22));
                ib=0.5*(sum2-2*sum3/sum1+sum2/(sum1^2));
                std2=bold+sb/ib;
                diff=abs(std2-bold);
                if (diff/bold)<0.0001
                        repeat=0;
```

```
            end
            bold=std2;
        end
        %std=sqrt(std2);
        errbtw=sqrt(std2)
        abserr=err
        std=sqrt(1/sum1);
        v1=avr+std;
        v2=avr-std;
        vlog1=log10(v1);
        vlog2=log10(v2);
        lav=log10(avr);
        diff1=vlog1-lav;
        diff2=lav-vlog2;
        if(diff1>diff2)
            lsd=diff1;
        else
            lsd=diff2;
        end
else
        avr=k(1);
        std=err(1);
        v1=avr+std;
        v2=avr-std;
        vlog1=log10(v1);
        vlog2=log10(v2);
        lav=log10(avr);
        diff1=vlog1-lav;
        diff2=lav-vlog2;
        if(diff1>diff2)
            lsd=diff1;
        else
            lsd=diff2;
        end
end
```

E.4.2 : SAMEDIV2.M

```
function out = samediv2
%
% Use when need to divide values from the same run before averaging.
% Divides corresponding elements of the entered matrices, propagating
% their errors, and then averages the values.
%
% (k2 +/- e2)
% ---------- = k +/- err
% (k1 +/- e1)
%
% Calculates k and err for the above division of two values, each with
%  an associated error.
```

```
%
% k2, k1  = matrices of stability constants (or other values)
% e2, e1  = matrices of corresponding relative errors
%
% Carolyn Haskard December 1993
%
k2=input('Please enter the matrix ofk''s for the numerator ([...]) : ');
e2=input('Please enter the matrix of relative errors for the numerator ([...]) : ');
k1=input('Please enter the matrix ofk''s for the denominator ([...]) : ');
e1=input('Please enter the matrix of relative errors for the denominator ([...]) : ');
e2=k2.*e2;
e1=k1.*e1;
% converts relative to absolute errors
ka=k2./k1;
a=sqrt(ka.^2.*(((e2./k2).^2) + ((e1./k1).^2)));
[k,err,logk,logerr]=av(ka,a)
```

E.4.3 : DIV2.M

```
function out = div2
%
% Averages the values in each matrix first and then divides
% Use when dividing values from TWO different types of runs
%
% (k2 +/- e2)
% ----------  = k +/- err
% (k1 +/- e1)
%
% Calculate k and err for the above division of two values, each with
%  an associated error
%
% k2, k1  = matrices of stability constants (or other values)
% e2, e1  = matrices of corresponding RELATIVE errors
%
% Carolyn Haskard December 1993
%
k2=input('Please enter the matrix ofk''s for the numerator ([...]) : ');
e2=input('Please enter the matrix of relative errors for the numerator ([...]) : ');
k1=input('Please enter the matrix ofk''s for the denominator ([...]) : ');
e1=input('Please enter the matrix of relative errors for the denominator ([...]) : ');
e2=k2.*e2;
e1=k1.*e1;
% converts relative to absolute errors
[ka,a]=av(k2,e2);
[kb,b]=av(k1,e1);
k=ka./kb
err=sqrt(k.^2.*(((a./ka).^2) + ((b./kb).^2)))
v1 = k + err;
v2 = k - err;
vlog1 = log10(v1);
```

```
vlog2 = log10(v2);
logk = log10(k)
diff1 = vlog1 - logk;
diff2 = logk - vlog2;
if (diff1 > diff2)
        logerr = diff1
        else logerr = diff2
end
```

E.4.4 : SAMEDIV3.M

```
function out = samediv3
% Use when need to divide values which are all from the same run before averaging
% Divides corresponding elements of the matrices, propagating their errors, and
%   then averages the values.
% In the expression both k2 and k1 come from the same run.
%
%       (k2 +/- e2)
% ---------------------- = k +/- err
% (k1 +/- e1)(k1 +/- e1)
%
% Calculates k and err for the above division, where each component has
%  an associated error.
%
% k2, k1  = matrices of stability constants (or other values)
% e2, e1  = matrices of corresponding RELATIVE errors
%
% Carolyn Haskard December 1993
%
k2=input('Please enter the matrix for the denominator, k2 ([...]) : ');
e2=input('Please enter the matrix for the relative errors, e2 ([...]) : ');
k1=input('Please enter the matrix for the denominator, k1 ([...]) : ');
e1=input('Please enter the matrix for the relative errors, e1 ([...]) : ');
e2=k2.*e2;
e1=k1.*e1;
% converts relative to absolute errors
ka=k2./(k1.^2);
a=sqrt(ka.^2.*(((e2./k2).^2) + ((e1./k1).^2)  +  ((e1./k1).^2)));
[k,err]=av(ka,a)
v1 = k + err;
v2 = k - err;
vlog1 = log10(v1);
vlog2 = log10(v2);
logk = log10(k)
diff1 = vlog1 - logk;
diff2 = logk - vlog2;
if (diff1 > diff2)
        logerr = diff1
        else logerr = diff2
end
```

E.4.5 : PARTDIV3.M

```
function out = partdiv3
%
% Use when need to divide values from the same run before averaging and
%  completing the calculation.
% Divides corresponding elements of the k3 and k2 matrices, propagating
%  their errors. Then averages the values and divides by the average k1,
%  once again propagating the errors.
% In the expression ONLY k3 and k2 come from the same run.
%
%      (k3 +/- e3)
% ---------------------- = k +/- err
% (k2 +/- e2)(k1 +/- e1)
%
% Calculates k and err for the above division, where each component has
% an associated error.
%
% k3, k2, k1  = matrices of stability constants (or other values)
% e3, e2, e1  = matrices of corresponding RELATIVE errors
%
% Carolyn Haskard December 1993
%
k3=input('Please enter the matrix for the numerator, k3 ([...]) : ');
e3=input('Please enter the matrix for the relative errors, e3 ([...]) : ');
k2=input('Please enter the matrix for the denominator, k2 ([...]) : ');
e2=input('Please enter the matrix for the relative errors, e2 ([...]) : ');
k1=input('Please enter the matrix for the denominator, k1 ([...]) : ');
e1=input('Please enter the matrix for the relative errors, e1 ([...]) : ');
e3=k3.*e3;
e2=k2.*e2;
e1=k1.*e1;
% converts relative to absolute errors
ka=k3./k2;
a=sqrt(ka.^2.*(((e3./k3).^2) + ((e2./k2).^2)));
[kb,b]=av(ka,a);
[kc,c]=av(k1,e1);
k=(kb./kc)
err=sqrt(sqrt((k.^2.*(((b./kb).^2) + ((c./kc).^2))).^2))
v1 = k + err;
v2 = k - err;
vlog1 = log10(v1);
vlog2 = log10(v2);
logk = log10(k)
diff1 = vlog1 - logk;
diff2 = logk - vlog2;
if (diff1 > diff2)
        logerr = diff1
        else logerr = diff2
end
```

E.4.6 : DIV3.M

```
function out = div3
%
% Averages the values in each matrix first and then divides
% Use when dividing values from THREE different types of runs
%
%     (k3 +/- e3)
% ---------------------- = k +/- err
% (k2 +/- e2)(k1 +/- e1)
%
% Calculate k and err for the above division, where each component has
% an associated error
%
% k3, k2, k1  = matrices of stability constants (or other values)
% e3, e2, e1  = matrices of corresponding RELATIVE errors
%
% Carolyn Haskard December 1993
%
k3=input('Please enter the matrix for the numerator, k3 ([...]) : ');
e3=input('Please enter the matrix for the relative errors, e3 ([...]) : ');
k2=input('Please enter the matrix for the denominator, k2 ([...]) : ');
e2=input('Please enter the matrix for the relative errors, e2 ([...]) : ');
k1=input('Please enter the matrix for the denominator, k1 ([...]) : ');
e1=input('Please enter the matrix for the relative errors, e1 ([...]) : ');
e3=k3.*e3;
e2=k2.*e2;
e1=k1.*e1;
% converts relative to absolute errors
[ka,a]=av(k3,e3);
[kb,b]=av(k2,e2);
[kc,c]=av(k1,e1);
k=(ka./(kb.*kc))
err=sqrt(sqrt((k.^2.*(((a./ka).^2) + ((b./kb).^2) + ((c./kc).^2))).^2))
v1 = k + err;
v2 = k - err;
vlog1 = log10(v1);
vlog2 = log10(v2);
logk = log10(k)
diff1 = vlog1 - logk;
diff2 = logk - vlog2;
if (diff1 > diff2)
        logerr = diff1
        else logerr = diff2
end
```

E.5 : BANDANAL

Tom Kurucsev 1995

The vibrational fine structure of electronic transitions is often broadened in solution, and therefore only a broad envelope is observed for the spectrum. Resolution enhancement is one method that can be used to locate the maxima of vibronic transitions within an electronic spectrum. In BANDANAL, this approach is followed by least squares fitting of the spectrum to Gaussian bands at the wavelengths of the various vibronic transitions located. The program is somewhat limited in the fact that it assumes all of the transitions result in Gaussian curves of the same bandwidth, but it has been proven to work effectively under conditions in which this assumption is true. For examples, and more details, see M. A. Snoswell and T. Kurucsev, *J.Cryst. and Spec. Res.*, **22**, 679, 1992.

BANDANAL.M

```
function [Q,P,S] = bandanal(x,y)
%
% Resolution enhancement
%     followed by
% least squares fitting of to Gaussian bands
%
% Usage  [Q,P,S] = bandanal(x,y)
% Input: x, the wavelength vector
%         y, the spectrum
%
% Output: Q, the matrix of wavelength and calculated spectra [w q q1 q2 q3]
%           S, the sum square deviation
%           P, the fitted set of parameters
set(0,'Format','shortE','FormatSpacing','compact');
temp=input(' Enhance the resolution? (y/n) ','s');
if temp=='y'
      renpol(x,y);
end
temp=input(' Fit to Gaussians? (y/n) ','s');
if temp=='y'
      bc=input(' vector of band centres? [...]');
      bi=input(' vector of band intensities? [...] ');
      bw=input(' value of half band width? ');
      nb=length(bc);
      if nb~=length(bi)
            disp(' error in input; must terminate');
            break
      end
      for i=1:nb
```

```
            j=2*i-1;
            p(j)=bi(i); p(j+1)=bc(i);
        end
        p(2*nb+1)=bw;
        key=1;
%if key==1
        datafit('gaussfit',p,key,x,y);
%else
%       fmins('gaussfit',p,[0 0.1 1],[],key,x,y);
%end
        P=ans;
        f=gaussfit(P,1,x,y);
        f=f(:);
        nfun=length(y);
        nvars=length(P);
        POLD=P;
        POUT=P(:);
        J=zeros(nfun,nvars);
        CHG=1e-3*abs(POUT);
        OLDF=f;
        for i=1:nvars
              temp=POUT(i);
              POUT(i)=temp+CHG(i);
              P(:)=POUT;
              f=gaussfit(P,1,x,y);;
              f=f(:);
              J(:,i)=(f-OLDF)/CHG(i);
              POUT(i)=temp;
        end
        f=OLDF;
        P=POLD;
        S=f'*f;
        HESS=J'*J;
        covar=S*inv(HESS)/(nfun-nvars);
        var=diag(covar);
        sd=sqrt(var);
        fid=fopen('result','w');
        fprintf(fid,'Fitting of data to Gaussians');
        fprintf(fid,'\n');
        fprintf(fid,'At convergence thessd was %12.4e\n',S);
        fprintf(fid,'The parameters and their standard deviationsare:\n');
        for i=1:nvars
              fprintf(fid,'%12.3e  +/-%12.3e\n',P(i),sd(i));
        end
        type result
        fclose(fid);
        [Qs,Qi]=gaussall(x,P);
        tit=input('Please enter a title : ','s');
        figure
        plot(x,y,'.',x,Qs,x,Qi);
        title(tit)
```

```
        scalex(300,450)

        temp=input('save the results? (y/n) ','s');
        if temp=='y'
                temp=input('filename? ','s');
                fid2=fopen(temp,'w');
                fid=fopen('result','r+');
                fprintf(fid2,'\n');
                while 1
                        line=fgetl(fid);
                        if ~isstr(line), break,end
                        fprintf(fid2,'%s\n',line);
                end
        end
        fclose('all');
        Q=[x Qs Qi];
        delete result;
end
```

E.5.1 : RENPOL.M

```
function Y=renpol(w,y)
%function Y=renpol(w,y,gam,beta)
%w=wavelength vector
%y=response (absorbance) vector
%use of "exponential" filter (Snoswell & Kurucsev)
%gam=filter bandwidth
%beta=filter power
%

%close all;
n=length(y);
m=2.^ceil(log(n)/log(2));
yf=zeros(1,m);
px=[1:3,n-2:n]';
py=y(px);
cc=polyfit(px,py,3);
fit=polyval(cc,1:n)';
yf(1:n)=y-fit;
mo2=m/2;
Y=realft(yf,mo2,1);
figure('Position',[400 120 400 420]);
plot(Y(1:20));
repeat=1;
while repeat
        gam=input(' filter bandwidth? ');
        beta=input(' filter power? ');
        if gam==[] | beta==[]
        repeat==0;, break, end;
        %
```

```
    %filt=expfilt(20,beta,gam);
    %plot(filt);
    %pause;
    %
    Y=realft(yf,mo2,1);
    Y(1)=0;
    for j=1:mo2-1
        k=2*j+1;
        zz=(j/gam)^2;
        x2=beta*zz*(zz-1);
        fac=exp(-x2)/(mo2^2);
        Y(k)=fac*Y(k);
        Y(k+1)=fac*Y(k+1);
    end
    Y(2)=0;
    Y=realft(Y,mo2,-1);
    Y=Y(1:n);
    factor=max(yf)/abs(max(Y)-Y(1));
    Y=factor*(Y-ones(1,n)*Y(1))+polyval(cc,1:n);
    clf reset;
    if w(1) < w(n)
        plot(w,y,':',w,Y,'g'),set(gca,'XLim',[w(1) w(n)]);
    else
        plot(w,y,':',w,Y,'g'),set(gca,'XLim',[w(n) w(1)]);
    end
    title(['gamma and beta are ',num2str(gam),' and ',num2str(beta)]);
    temp=input(' continue with new set? (y/n) ','s');
    if temp ~='y'
        repeat=0;
    end
end
```

E.5.1.1 : REALFT.M

```
function Y=realft(data,n,isign)
%function Y=realft(data,n,isign)
theta=6.28318530717959/2/n;
c1=0.5;
if isign==1
        c2=-0.5;
        data=four1(data,n,+1);
else
        c2=0.5;
        theta=-theta;
end
th2=theta/2;
ds=sin(th2);
wpr=-2*ds^2;
wpi=sin(theta);
wr=1+wpr;
wi=wpi;
n2p3=2*n+3;
for i=2:n/2+1
        i1=2*i-1;
        i2=i1+1;
        i3=n2p3-i2;
        i4=i3+1;
        h1r=c1*(data(i1)+data(i3));
        h1i=c1*(data(i2)-data(i4));
        h2r=-c2*(data(i2)+data(i4));
        h2i=c2*(data(i1)-data(i3));
        data(i1)=h1r+wr*h2r-wi*h2i;
        data(i2)=h1i+wr*h2i+wi*h2r;
        data(i3)=h1r-wr*h2r+wi*h2i;
        data(i4)=-h1i+wr*h2i+wi*h2r;
        wtemp=wr;
        wr=wr*wpr-wi*wpi+wr;
        wi=wi*wpr+wtemp*wpi+wi;
end
if isign==1
        h1r=data(1);
        data(1)=h1r+data(2);
        data(2)=h1r-data(2);
else
        h1r=data(1);
        data(1)=c1*(h1r+data(2));
        data(2)=c1*(h1r-data(2));
        data=four1(data,n,-1);
end
Y=data;
```

E.5.1.2 : FOUR1.M

```
function Y=four1(data,nn,isign)
%function Y=four1(data,nn,isign)
n=2*nn;
j=1;
for i=1:2:n
      if j>i
            tempr=data(j);
            tempi=data(j+1);
            data(j)=data(i);
            data(j+1)=data(i+1);
            data(i)=tempr;
            data(i+1)=tempi;
      end
      m=n/2;
      while m>=2 & j>m
            j=j-m;
            m=m/2;
      end
      j=j+m;
end
mmax=2;
while n>mmax
      istep=2*mmax;
      fim=isign*mmax;
      theta=6.28318530717959/fim;
      th2=theta/2;
      ds=sin(th2);
      wpr=-2.*ds^2;
      wpi=sin(theta);
      wr=1;
      wi=0;
      for m=1:2:mmax
            for i=m:istep:n
                  j=i+mmax;
                  tempr=wr*data(j)-wi*data(j+1);
                  tempi=wr*data(j+1)+wi*data(j);
                  data(j)=data(i)-tempr;
                  data(j+1)=data(i+1)-tempi;
                  data(i)=data(i)+tempr;
                  data(i+1)=data(i+1)+tempi;
            end
            wtemp=wr;
            wr=wr*wpr-wi*wpi+wr;
            wi=wi*wpr+wtemp*wpi+wi;
      end
      mmax=istep;
end
Y=data;
```

E.5.1.3 : EXPFILT.M

```
function y = expfilt(n,beta,gam,height)
%       y = expfilt(n,beta,gamma,height)
%Calculates the exponential filter for resolution enhancement
%The function accepts 3 parameters with height=1 as the default
if nargin < 4
        height=1;
end
%tr=n/2;
%x=((1:n)-tr)*sqrt(1/gam);
x=(1:n)*sqrt(1/gam);
x2=x.^2;
x4=x.^4;
y=height*exp(beta*(x2-x4));
plot(y);
```

E.5.2 : GAUSSFIT.M

```
function s = gaussfit(p,key,x,y)
%
% Calculation of the sum square deviation between a spectrum y, and three Gaussians
% over the range x. One bandwidth only
% Calls function gauss3
% Usage  s = gaussfit(p,key,x,y)
% Input: x, the wavelength vector
%        y, the spectrum
%        p, the parameter vector with
%        p(1) = band 1 maximum
%        p(2) = band 1 center
%        ...
%        p(last) = half band width
%
[q,qi] = gaussall(x,p);
f=y-q;
if key==0
        s = f'*f;
else
        s=f;
end
```

E.5.3 : GAUSSALL.M

```
function [q,qi] = gaussall(x,p)
%
% Calculation of Gaussians over the range x
%     using a single bandwidth
% Usage  [q,qi] = gaussall(x,p)
% Input:    x,  the wavelength vector
%           p,  the parameter vector with
%           p(1) = band 1 maximum
%           p(2) = band 1 centre
%           ...
%           p(last) = half bandwidth
%
n=length(x);
np=length(p);
nb=(np-1)/2;
x0=zeros(1,nb);
I0=zeros(1,nb);
qi=zeros(n,nb);
del=p(np);
ln2=log(2);
for i=1:nb
      j=2*i-1;
      I0=p(j);
      x0=p(j+1);
      qi(:,i)=I0*exp(-ln2*((x-ones(n,1)*x0)/del).^2);
end
q=sum(qi');
q=q';
```